UNIVERSITY OF LIVERPOOL

Investigating the Molecular Mechanism of Crosstalk Between NF-κB and Nrf2 Signalling Pathways

Thesis submitted in accordance with the requirements of the University of Liverpool for the degree of Doctor of Philosophy by

Joanna Dorota Wardyn

December 2015

Declaration

This thesis is the result of my own work, unless otherwise stated, and it is based upon the results from experimental work performed as a PhD student between October 2012 and September 2015 in the Department of Cellular and Molecular Physiology at University of Liverpool. Neither this thesis nor any part of it has been submitted in support of an application for another degree or qualification at this or any other university or institute of learning.

Joanna Dorota Wardyn

This research was carried out in the Department of Cellular and Molecular Physiology, Institute of Translational Medicine, at the University of Liverpool

Table of Contents

Declaration **2**

Abstract **8**

Acknowledgements **9**

Publications **10**

Abbreviations **11**

1. General Introduction **16**

1.1.1. The Introduction to the Nrf2 Pathway 16
1.1.2. The Regulation of the Nrf2 Protein Stability and Activity by Keap1 18
1.1.3. The Regulation of Nrf2 Protein Stability by GSK-3/β-TrCP/PI3K Axis 21
1.1.4. The RNF4-mediated Degradation 22
1.1.5. The Role of Post-translational Modifications in Regulating Nrf2 Activity 23
1.1.5.1. Phosphorylation 23
1.1.5.2. Dephosphorylation 24
1.1.5.3. Acetylation 25
1.1.6. Transcriptional Regulation of Nrf2 26
1.1.7. Function of Nrf2 Gene Targets 27
1.1.7.1. Iron Metabolism 27
1.1.7.2. The Antioxidant Properties of the Nrf2 Target Genes 28
1.1.7.3. Proteasomal Degradation and Autophagy 29
1.1.7.4. PPP pathway 30
1.1.7.5. Bach1 31
1.1.8. Intracellular Sources of ROS 31
1.1.9. Pharmacological Inducers and Inhibitors of Nrf2 32
1.1.9.1. Nrf2 Activating Compounds 32
1.1.10. Brusatol –the Nrf2 Inhibitor 34
1.1.11. Role of Nrf2 in Cancer 34
1.2. The Introduction to the NF-κB Pathway 35
1.2.1. The NF-κB Cellular Function and Regulation 35
1.2.2. The Regulation of NF-κB Signalling 36
1.2.3. Gene Targets 37
1.2.3.1. Inflammatory Factors 37
1.2.4. The Canonical Cascade 39
1.2.5. The Non-canonical Cascade 41
1.2.6. NF-κB and ROS 41
1.2.6.1. SOD 43
1.2.6.2. iNOS 44
1.2.7. The NF-κB Dynamic Behaviour 44
1.3. The NF-κB and Nrf2 Pathways in the CNS 47
1.3.1. Cell Types in the Nervous System 47
1.3.1.1. Neurons 47
1.3.1.2. Astrocytes 47
1.3.1.3. Microglia 49
1.3.1.4. Oligodendrocytes 49
1.3.2. Neuroinflammation 50
1.3.3. The Role of NF-κB and Nrf2 in the CNS 51
1.3.3.1. NF-κB 51
1.3.3.2. The Nrf2 Pathway in the Nervous System 52
1.3.4. Conclusions 53
1.4. The Molecular Crosstalk Between NF-κB and Nrf2 53
1.4.1. Are the Protective Roles of p65 and Nrf2 Redundant? 53
1.4.2. Nrf2 Activity is Modulated by p65 54

1.4.3. The Proteins Linking the Nrf2 and NF-κB Pathways 56
1.5. Summary: 57
1.6. THESIS AIMS 58
2. METHODS 59
2.1. Generation of Fluorescent Expression Plasmids 59
2.1.1. Gateway Recombination Cloning 59
Table 2.1 The KOD PCR reaction conditions and cycling parameters 60
Table 2.2 PCR primers used for amplification of genes of interest and incorporation using Gateway cloning system. 60
2.1.2. Bacterial Transformation 61
Table 2.3 Bacterial strains and reaction conditions used for transformation of target constructs. 62
2.1.3. Bacterial Colony PCR (BCPCR) 62
Table 2.4 BIOTAQ PCR reaction conditions and cycling parameters. 62
2.1.4. Verification of Plasmid Quality 63
2.1.5. Sequencing 63
2.1.6. Preparation of Glycerol Stocks 63
2.1.7. LR Reaction 64
2.1.8. Bacterial Media 65
Table 2.5 Growth media used for bacterial culture 66
Table 2.6 The concentration of antibiotics used in selective bacterial growth media. 66
2.1.9. Genomic DNA Extraction 66
2.2. In-Fusion Cloning 67
2.2.1. Insert Amplification 67
2.2.2. Vector Linearization 68
2.2.3. The In-Fusion Reaction 68
2.3. List of Plasmids Used 69
Table 2.8 List of plasmid used for imaging and dual luciferase experiments 70
2.4. Primary Cell Culture 70
2.4.1. Preparing Glass Coverslips for Neuronal Culture 70
2.4.2. Neuron-Astrocyte Cultures 71
2.4.3. Culture of Primary Astrocytes 72
2.4.4. Viability Assay 73
2.4.5. Transfection of Primary Cells 73
Table 2.9 The quantity of plasmids used for imaging and dual luciferase studies on primary cells 74
2.4.6. Dual Luciferase Assay 74
2.4.6.1. Dual Luciferase Data Analysis 75
2.5. Immunocytochemistry 75
Table 2.10 The list of antibodies and their concentrations used in immunocytochemistry. 77
2.6. Production of Lentivial Particles 77
2.6.1. Transduction 78
2.7. Cell Culture Growth Media 79
Table 2.11 Cell culture media components used for maintenance of primary and immortalized cells (all components from Invitrogen) 80
2.8. Cell Culture of SK-N-AS and BAC$^{Nrf2\text{-}Venus}$ Neuroblastoma Cell Lines 80
Table 2.12 The BAC$^{Nrf2\text{-}Venus}$ cell seeding densities used for experiments 81
2.8.1. Transfections of Plasmids Encoding Fluorescent Fusion Proteins 81
2.8.2. Keap1 Gene Silencing Using siRNA 81
2.8.3. Cryogenic Storage of SK-N-AS and BAC$^{Nrf2\text{-}Venus}$ Cells 82
2.8.4. Thawing Cell Stocks 82
2.9. Q-PCR 83
2.9.1. Q-PCR Primer Preparation 83
Table 2.13 Primers used for Q-PCR expression measurements of selected, representative target genes 84
2.9.2. mRNA Extraction 84

2.9.3. Converting mRNA into cDNA 85
2.9.4. Setting up Q-PCR Reaction 85
Table 2.14 The Q-PCR cycling parameters. 86
2.9.5. Q-PCR Data Analysis 86
2.10. Preparation of Whole Cell Lysates for Western Blotting Analysis 86
2.10.1. Nuclear and Cytoplasmic Extraction 87
2.11. Western Immunoblotting 88
2.11.1. X-Ray Film for Western Blot Detection 88
Table 2.15 Primary antibodies used for Western blotting 89
2.11.2. Cytokine Stocks 89
2.12. Stock and Working Concentrations of Compounds Used 89
Table 2.16 List of compounds used in this project alongside their stock and working concentrations. 90
2.13. Live Cell Imaging 90
Table 2.17 List of fluorescent protein fusions imaged throughout this project alongside their excitation source and filter settings for collection of the emission signal 92
2.13.1. Lambda Scan 92
2.13.2. pDendra2 Imaging 92
2.13.3. Image Analysis 93
2.13.4. Fluorescence Cross Correlation Spectroscopy (FCCS) 94

RESULTS CHAPTER 1: 95

3. Construction and Characterisation of Expression Systems to Study Dynamic Nrf2 and NF-κB Responses in Primary Mouse Neurons, Astrocytes and Human SK-N-AS Neuroblastoma Cells 95

3.1. CHAPTER 1 AIMS: 95
3.2. Introduction 95
3.3. RESULTS 96
3.3.1. Characterisation of dynamic NF-κB responses in Murine Neurons and Astrocytes 96
3.3.1.1. Primary Cell Culture Characterisation 96
3.3.1.2. Measuring TNFα-induced NF-κB Responses in Neural Cells 98
3.3.1.3. Quantitative Analysis of Conditional NF-κB Transcriptional Activity in Primary Neurons, Astrocytes 100
3.3.1.4. Investigating Dynamic p65 Responses in Primary Mouse Neurons and Astrocytes 105
3.3.1.5. Astrocytes Exhibit Inherent Basal NF-κB Activity 109
3.3.2. Constructing Molecular Tools to Image Dynamic Nrf2 Responses in Primary Hippocampal Astrocytes and Neurons. 112
3.3.2.1. Characterisation of Nrf2 Responses in Astrocytes and Neurons 112
3.3.2.2. 2.2. Development of Lentiviral Expression System for Imaging of Dynamic Nrf2 Responses 116
3.3.3. Development of an Astrocyte Specific Nuclear Marker 119
3.3.4. Characterisation of Nrf2 Dynamic Responses Using a Stable Nrf2-Venus Expressing BACNrf2-Venus Neuroblastoma Model for Live Cell Imaging 121
3.3.4.1. Comparison of Endogenous Nrf2 and BAC-derived Nrf2-Venus Dynamic Responses 121
3.3.4.2. Measuring Keap1 and Nrf2 Interaction in Live Cells 126
3.3.4.3. Basal Nrf2 Dynamics 128
3.4. DISCUSSION 130
3.4.1. Astrocytes Exhibit Strong Basal and TNFα-Induced NF-κB Responses 130
3.4.2. The Autonomous NF-κB Activation 132
3.4.3. Low Expression Molecular Tools are Required for Optimal Imaging of Physiologically Relevant Nrf2 Dynamic Responses 134
3.4.4. *GFAP*-LaminB1-Cyan Drives Astrocyte-Specific Nuclear Marker Expression 137
3.4.5. Characterisation of BAC$^{Nrf2\text{-}Venus}$ 138

3.4.5.1. The BAC$^{Nrf2\text{-}Venus}$ is an Excellent Imaging Tool for Dissecting Nrf2 Pathway Regulation 138
3.4.5.2. The mCherry-Keap1 and Nrf2-Venus Form Stable Complexes in Live Cells 138
3.4.5.3. Nrf2 Protein Levels are Regulated in Cell-Cycle Dependent Manner 139

RESULTS CHAPTER 2 142

4. Investigating Dynamic Crosstalk Between Nrf2 and NF-κB Signalling Responses 142

4.1. CHAPTER 2 AIMS: 142
4.2. Introduction 142
4.3. RESULTS 143
4.3.1. Effects of TNFα Stimulation on the Nrf2 Pathway in SK-N-AS Neuroblastoma Cells 143
4.3.1.1. Measuring Expression of Nrf2 Target Genes 145
4.3.1.2. Imaging Nuclear Dynamics of p65 and Nrf2 Transcription Factors in Live Cells 148
4.3.2. Measuring the Consequences of Concerted Nrf2 and p65 Activation 152
4.3.3. Investigating The Effect of IL-1β on Nrf2 Signalling 155
4.3.4. Investigating The Role of Keap1 Regulation of Nuclear Nrf2 Dynamics Under Inflammatory Conditions 155
4.3.5. Investigating the GSK-3-mediated Nrf2 Regulation Following Cytokine Induced Inflammatory Stress 158
4.3.6. Effect of Prolonged TNFα Stimulation on Nrf2 Dynamics And Transcriptional Activity 160
4.3.7. Impact of Nrf2 Activation on NF-κB Pathway Dynamic Responses 162
4.4. DISCUSSION 165

RESULTS CHAPTER 3 176

5. Single-Cell Analysis of Nrf2 Dynamic Regulation in a Neuroblastoma Cell Model 176

5.1. CHAPTER 3 AIMS 176
5.2. Introduction 176
5.3. RESULTS 177
5.3.1. Analysis of Single-Cell Keap1 Dependent Nrf2 Regulation 177
5.3.2. The Effect of Keap1 Overexpression on Nrf2 Localisation in Response to CDDO-Me 179
5.3.3. Quantitative Live Cell Analysis of Nrf2 Nuclear Import and Export Dynamics 182
5.3.4. Comparing the Relative Effects of the Keap1 and GSK-3 on the Regulation of Nrf2 in Live SK-N-AS Neuroblastoma Cells 192
5.3.5. The PML-Dependent Nuclear Nrf2 Regulation 192
5.3.6. The Role of Acetylation in Modulating Nrf2 Activity 197
5.4. DISCUSSION 199

RESULTS CHAPTER 4 210

6. Investigating the Mechanism of Action of Brusatol 210

6.1. CHAPTER 4 AIMS: 210
6.2. Introduction 210
6.3. RESULTS 211
6.3.1. Brusatol Depletes Nrf2 Protein Levels and Transcriptional Activity in BAC$^{Nrf2\text{-}Venus}$ SK-N-AS Neuroblastoma cells 211
6.3.2. Brusatol Triggers p65 Nuclear Translocation 211
6.3.3. Brusatol Does Not Inhibit N*RF2* Gene Expression 216
6.3.4. Use of a Photoswitchable pDendra2-Nrf2 Fusion Protein to Investigate the Mechanism of Action of Brusatol on Nrf2. 216
6.3.5. Determination of brusatol target specificity 223
6.4. Discussion 225

CONCLUDING DISCUSSION **231**

CONCLUSIONS **239**

Bibliography **241**

Supplementary Information **260**

8. Supplementary Movies (attached) **260**

8.1. List of Movies (avi. format) 260

8.2. Viability Assays on BAC$^{Nrf2\text{-}Venus}$ 263

8.3. Vector Maps of Generated Constructs (Figure 8.3 and 8.4) 264

8.4. Quantification of Protein Levels from Western Blot Analysis 266

Abstract

Investigating the Molecular Mechanisms of Crosstalk Between NF-κB and Nrf2 Signalling Pathways

In order to maintain tissue homeostasis, cells must respond swiftly to inflammatory and oxidative challenges, ensuring appropriate processes are sequentially activated and repressed when stress conditions are normalised.
Nuclear factor (erythroid-derived 2)-like 2 (Nrf2) and Nuclear Factor-κB (NF-κB) are the key regulators of cellular antioxidant and inflammatory responses respectively. Imbalance between these processes is a contributing factor in many human diseases, including neurodegeneration, autoimmune disorders and cancers. Pharmacological and genetic studies suggest that there is functional crosstalk between these two pathways, however mechanistic details of conditional dominance between them remain unclear.
To address this, we have generated multiple, low expression, fluorescent molecular tools that allow monitoring of the distribution and activity of Nrf2 and NF-κB proteins in primary living neurons and astrocytes. This allowed us to characterise the cell-specific antioxidant and inflammatory signalling, as well as to understand the patterns in basal activity.

We also investigated patterns of crosstalk in a cancer-related context utilising a previously generated SK-N-AS neuroblastoma cell line, engineered to stably express Nrf2-Venus, from a bacterial artificial chromosome (BAC). This model cell-line was first extensively characterised in order to define conditional Nrf2 responses to antioxidant compounds in real-time. We then proceeded to investigate the effect of acute inflammation on the cellular antioxidant activity, in order to define the extent and nature of functional crosstalk between NF-κB and Nrf2. Data from these studies provide definitive proof of a self limiting reciprocal mechanism of interplay in neuroblastoma cells, in which NF-κB-mediated inflammatory signalling promotes an increase in Nrf2 transcription which then in turn supresses further NF-κB signalling. In addition, results from single cell imaging and population level studies show that Nrf2 responses are fine tuned, by either Keap1-mediated mechanism of repression.

To define the intricate mechanisms of basal Nrf2 activity, we utilised a photo-switchable fluorescent protein fusion, which provided the first direct measurements of Nrf2 nuclear import and export dynamics in live-cells.
Finally, we used the sophisticated live cell imaging approaches to define the mechanism of action of the Nrf2 inhibiting drug brusatol. Significantly, these results contradict published data and reveal a more general explanation for the potential therapeutic utility of brusatol.

Acknowledgements

The last 4 years were a rocky road but so many people contributed to make this PhD an enjoyable experience. First and foremost I would like to thank my supervisor Chris Sanderson for his support throughout my project and his trust in me. I am very grateful to the Wellcome Trust for their funding and support. My thanks goes to my secondary supervisors Christopher Goldring and Violaine See for their extremely valuable scientific discussions and the CCI imaging facility for letting me use their fantastic imaging equipment.

I was lucky to have many generous and supportive collaborators that I had the pleasure of working alongside. I would especially like to thank Mike White's group for many reagents, invaluable scientific dialogue and expertise, especially James Bagnall and James Boyd who helped with the FCCS experiments. I would also like to express my gratitude to Massimiliano Stagi, who sparked new scientific interest in me and has supported me in my future carrier choices.

Profound gratitude goes to the Sanderson lab that made my life in Liverpool so much fun and I am very grateful for being able to work in such an amazing team! I loved working alongside you Emily, Hania, Dave, Jen and Bronwyn and especially Amy Ponsford who was my partner in crime and made this time so entertaining. You guys made me go to work with a grin on my face every single day (unless it was raining). Thank you Dayani and Nesan for countless conversations and for the best flatmates I could have ever wished for!

I would like to express my wholehearted gratitude to Gosia, Marta, Staś and Wanda who always reminded me how important good friends are in life! My Mama and Babcia Ewa for their love and support and giving me the strength to make me feel that everything is attainable.
Last, but not least, I would like to express my gratitude and love to Mat, for his understanding, patience and support and making this PhD possible. Without you I would never have done this!

Publications

Wardyn J.D., Sanderson C.M., Swan, L.E., Stagi, M. (2015) Low cost production of 3D-printed devices and electrostimulation chambers for the culture of primary neurons. *Journal of Neuroscience Methods* **251:** 17-23

Wardyn J.D., Ponsford A.H., Sanderson C.M. (2015) Dissecting molecular cross-talk between Nrf2 and NF-κB response pathways. *Biochem Soc T* **43:** 621-626

McCue H.V.*, Wardyn J.D.*, Burgoyne R.D., Haynes L.P. (2013) Generation and characterization of a lysosomally targeted, genetically encoded Ca(2+)-sensor. *The Biochemical journal* **449:** 449-457

Manuscripts in preparation:

- "The Single Cell Imaging of Molecular Crosstalk Between Nrf2 and NF-κB Pathways"
- "Mechanism of Action of Brusatol"

Presentations and Conferences

- UK and Ireland NF-κB/IKK Workshop, Sir Charles Wilson Building, Glasgow, 8-10th of June 2015, poster presentation
- The Keap1/Nrf2 Pathway in Health and Disease, Robinson College, Cambridge 6-8 Jan 2015, presented talk and poster
- Centre for Imaging Facility Imaging Day, University of Liverpool, short talk 13-14th of November 2014
- Astrocyte in Health and Neurodegenerative Disease- 28-29th of April 2014, University College London, poster presentation
- The 4th International Conference on Environmental Response 28th of Feb-2nd of March 2014,Tohoku University, Sendai, Japan
- UK/Ireland NF-κB meeting, Liverpool, 23-25 April 2013, Liverpool

Abbreviations

A20	Tumor necrosis factor alpha-induced protein 3
AD	Alzheimer's disease
AHR	Aryl hydrocarbon receptor
ALS	Amyotrophic lateral sclerosis
AML	Acute Myeloid Leukemia
AP-1	Activator protein-1
ARE	Antioxidant Response Element
ATP	Adenosine Triphosphate
BAC	Bacterial Artificial Chromosome
Bach1	BTB And CNC Homology 1, Basic Leucine Zipper Transcription Factor 1
BBB	Brain blood barrier
BCA	Bicinchoninic acid
BFP	Blue Fluorescent Protein
BSA	Bovine Serum Albumin
BTB	Bric a Brac
bZIP	Basic Leucine Zipper
CBP	CREB Binding Protein
CD11b	Cluster of differentiation 11b
CDDO-Me	CDDO methyl ester
cDNA	Coding DNA
CFP	Cyan Flourescent Protein
cGMP	Cyclic guanosine monophosphate
CNC	Cap'n'Collar
CNS	Central nervous system
CO	Carbon Monoxide
CPM	Counts per minute
CSF	Cerebrospinal fluid
Cul	Cullin
Cys	Cysteine
ddH_2O	Double distilled water
DEPC	Diethylpyrocarbonate

DIV	Day *in vitro*
DMEM	Dulbecco's Modified Eagle's Medium
DMSO	Dimethyl Sulphoxide
DNA	Deoxyribonucleic acid
DNAse	Deoxyribonuclease
DPBS	Dulbecco's PBS
DsRedXP	*Discosoma sp*. Red (Express)
DTT	Dithiothreitol
E	Embryonic
ECL	Enhanced chemiluminescence
EGFP	Enhanced green fluorescent protein
EMSA	Electrophoretic mobility assay
FBS	Foetal Bovine Serum
FCCS	Fluorescence Cross-Correlation Spectroscopy
FCS	Fluorescence Correlation Spectroscopy
FISH	Fluorescence *in Situ* Hybridisation
FRAP	Fluorescence Recovery After Photobleaching
G6PD	Glucose-6-phosphate dehydrogenase
GABA	Gamma-aminobutyric acid
GCLM	Glutamate-Cysteine ligase modifier subunit
GFAP	Glial fibrillary acidic protein
GGT	Gamma-glytamyl transpeptidase
GP	Glycoprotein
GSH	Glutathione
GSK-3	Glycogen synthase kinase 3
GSR	Glutathione reductase
GSSG	Glutathione disulfide
GST	Glutathione S-Transferase
H	Hours
H_2O_2	Hydrogen Peroxide
HAT	Histone acetyltransferase
hCMV	Human cytomegalovirus
HD	Huntington's disease

HDACs	Histone deacetylases
HeBS	HEPES buffered saline
HEK293	Embryonic Kidney Cells 293
HIF	Hypoxia-inducible factor
HO-1	Heme Oxygenase-1 (gene/protein)
HRP	Horse radish peroxidase
IDH-1	Isocitrate dehydrogenase-1
IKBα	Inhibitor of NF-κB α
IKK	Inhibitory κB kinase
IKKβ	Inhibitory κB Kinase β
IL-6	Interleukin 6
IL-8	Interleukin 8
IL-1β	Interleukin 1β
iNOS	Inducible Nitric oxide synthase
JNK	c-Jun N-terminal kinases
Keap1	Kelch-like ECH-associated protein
KO	Knock out
KPNA6	Karyopherin alpha 6
LARII	Luciferase assay reagent II
LB	Luria-Bertani
LMB	Leptomycin B
LPS	Bacterial Lipopolysaccharide
Lys	Lysine
MAF	Musculo-Aponeurotic Fibrosarcoma
MAPK	Mitogen-Activated Protein Kinases
ME-1	Malic enzyme-1
MEM	Minimal Essential Medium
Min	Minutes
mRNA	Messenger Ribonucleic Acid
MS	Multiple sclerosis
NEAA	Non-essential amino acids
NEMO	NF- κB essential modulator

NES	Nuclear export signal
NF-κB	Nuclear Factor Kappa-light-chain-enhancer of activated B cells
NIK	NF-κB inducing kinase
NLS	Nuclear localisation signal
NNF	Normalised nuclear fluorescence
NO	Nitric oxide
NPC	Neural progenitor cells
NQO1	NAD(P)H dehydrogenase (quinone 1)
Nrf2	Nuclear factor (erythroid-derived 2)-like 2
NTC	No template control
P	Postnatal
PBS	Phosphate buffer solution
PBS-T	PBS-Tween
PCR	Polymerase Chain Reaction
PD	Parkinson's disease
PDL	Poly-D-Lysine
PGD	6-phosphogluconate dehydrogenase
PI3K	Phosphoinositide kinase 3
PKC	Protein kinase C
PKG	cGMP dependant kinase
PML NBs	Promyelocytic leukemia protein nuclear bodies
PPP	Pentose phosphate pathway
Prx1	Peroxiredoxin-1
PTEN	Phosphatase and tensin homologue deleted on chromosome 10
Q-PCR	Quantitative Polymerase Chain Reaction
Rbx1	Ring Box 1
RFP	Red fluorescent protein
RNAse	Ribonuclease
ROI	Region of interest
ROS	Reactive Oxygen Species
RT	Room temperature
S&G	Stop and Glo
SDS	Sodium Dodecyl Sulphate

Ser	Serine
SFN	Sulforaphane
SFXN	Sulfiredoxin
siRNA	Short interfering RNA
SK-N-AS	Human Neuroblastoma
SOC	Super Optimal Broth with Catabolite repression
SOD	Superoxide dismutase
SQSTM1	Sequestosome 1
Src	Proto-oncogene tyrosine-protein kinase
STAT	Signal Transducers and Activators of Transcription
TACE	Tumor necrosis factor alpha converting enzyme
tBHQ	Tert-butyl hydroxyquinone
TC	Tissue culture
TCA	Tricarboxylic acid
TD	Transactivation domain
TKT	Transketolase
TNF-α	Tumour necrosis factor-α
TRADD	Tumor necrosis factor receptor type 1-associated death
TRAF6	TNFα receptor associated factor6
TRXDN	Thioredoxin
UBC	Ubiquitin
UV	Ultraviolet
V/V	Volume per volume
W/V	Weight per volume
WT	Wild type
XRE	Xenobiotic response element
β-TrCP	β-transducin repeats-containing proteins
γ-GCS	γ-Glutamate-Cysteine

1. General Introduction

1.1.1. The Introduction to the Nrf2 Pathway

The emergence of oxygen in the early Earth's atmosphere produced by photosynthetic ancestors of Cyanobacteria over 2.4 billion years ago triggered the biggest step in animal evolution. The engulfment of aerobic mitochondria yielding higher energy through effective respiratory processes facilitated inception of more complex life forms. However, the cost of this 'upgrade' to the host cell was the requirement for an efficient detoxification system to deal with the constant production of reactive oxygen species, which are associated with normal mitochondrial activity (Embley & Martin, 2006).

There is increasing realisation that the effects of this symbiotic relationship, which is maintained in all eukaryotic cells, within all multicellular organisms, may significantly contribute to the process of aging and age-related diseases. The more effective production of energy through oxidative phosphorylation is paired with a constant battle against the resulting reactive oxygen species (ROS). The aerobic cell has evolved mechanisms to defend itself from these potentially harmful reactive oxygen and nitrogen species. In essence, eukaryotic cells encode sensor proteins that react to reactive oxygen or nitrogen species by turning on transcription of a collection of cytoprotective antioxidant genes (Pajares *et al,* 2015). The Nuclear factor (erythroid-derived 2)-like 2 (Nrf2) transcription factor performs a central role in this process, regulating around 1% of human gene expression, many of which perform powerful protective functions (Cuadrado *et al*, 2009).

The coding sequence of the Nrf2 gene was first characterised by Yuet Wai Kan, who discovered that the encoded protein was able to bind to the activator ptotein-1 (AP-1) and NEF-E2 tandem repeat consensus DNA sequence. The first evidence of the involvement of Nrf2 in the regulation of glutathione-S transferase (GST) and NAD(P)H dehydrogenase (quinone 1) (NQO1) antioxidant genes expression was demonstrated by Massayuki Yamamoto, and this observation initiated a global explosion in Nrf2 pathway research (Hayes & Dinkova-Kostova, 2014). The Nrf2 protein belongs to the Cap'n'Collar family of proteins (CNC) and to the subfamily of

basic leucine zipper (bZIP) proteins, which also include Jun, Fos and ATF4 transcription factors (Hirotsu *et al,* 2012*;* Jyrkkanen *et al,* 2011). The transcriptional activity of the Nrf2 protein requires the formation of a heterodimer complex with another member of the bZIP subfamily- the small MAF (sMaf) proteins, such as MafK, MafG or MafF. This interaction facilitates bind to a *cis* regulatory DNA element called the Antioxidant Response Element (ARE), which is contained within the promoters of Nrf2 target genes (Hirotsu *et al,* 2012; Bryan *et al,* 2013). The consensus ARE sequence is defined as 5'-TGACNNNGC-3' (N- unspecified nucleotide) and it is usually encoded downstream of the consensus sMaf binding site,

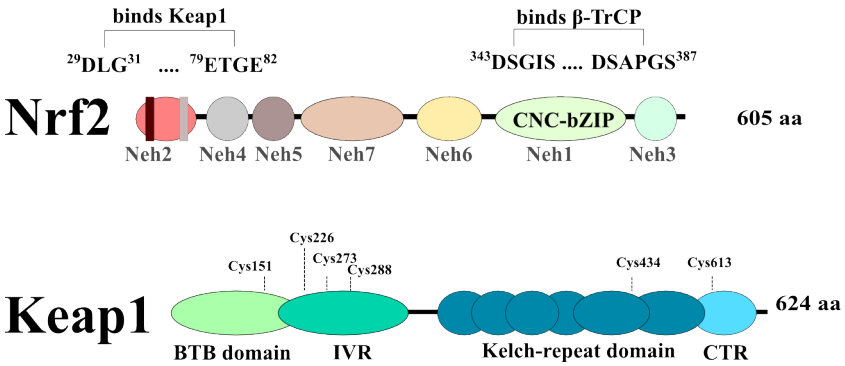

Figure 1.1 The domain topologies of Nrf2 and Keap1 proteins. Schematic representation of Nrf2 and Keap1 proteins showing the distribution of functional domains and binding sites/residues. (Adapted from Hayes & Dinkova-Kostova, 2014).

also termed the Maf Recognition Element (MARE) (5'-TGCTGAGCAGCA-3') (Hirotsu *et al*, 2012). Binding of the sMaf-Nrf2 dimer to target DNA sequences initiates recruitment of the RNA Polymerase II, promoting the subsequent assembly of the transcriptional apparatus (Belleza *et al,* 2010). The sMaf proteins are widely expressed in most tissues and are though to play redundant roles in transcription process, acting as DNA-binding enhancers for bZIP proteins such as Nrf2, Nrf1 and p45. sMaf are regulated predominantly though transcription and interestingly *smafG* variant contains an ARE sequence in its promoter, which can be modulated by Nrf2 (Blank, 2008). The Nrf2 protein contains a single nuclear localisation signal (NLS)

and two nuclear export signal (NES) motifs, which regulate its cellular localisation (Cuadrado *et al,* 2009). Nrf2 knockdown mice develop normally, but are highly susceptible to environmental stress and the toxic effects of compounds such as tobacco smoke and paracetamol; they are also prone to developing cancers and neurodegenerative or inflammatory diseases (Bryan *et al,* 2013; Neymotin *et al,* 2011*;* Vargas & Johnson, 2009*)*. This highlighted the protective role of Nrf2 and prompted extensive research, which validated its regulatory function in lipid oxidation, anabolic metabolism, protein degradation, responses to chemical stimuli, immune signalling, multidrug resistance, expression of molecular chaperones and wound healing (Papp *et al,* 2012; Wu *et al,* 2011*;* Mitsuishi *et al*, 2012a; Sporn & Liby, 2012*;* Wakabayashi *et al,* 2010).

Nrf2 is ubiquitously expressed in all cell types, with the highest levels being detected in lungs, brain, testis, spleen, skeletal and heart muscle and in the kidney (Chan *et al,* 1996). The key characteristic of this transcription factor is its very low basal activity and its stringent regulation, as the half-life of Nrf2 protein has been estimated to last only 10-30min (Belleza *et al,* 2010*)*. The stability of Nrf2 dramatically increases as a result of diverse stimuli including plant-derived phytochemicals and intracellular and extracellular stress factors, such as ultraviolet (UV) and gamma (or ionising) radiation, electrophiles, pollution, inflammation and reactive oxidant species (ROS) (Lee *et al,* 2005; Bryan *et al,* 2013).

The regulation of antioxidant pathway activity is very complex and is not yet fully understood, however, research into the antioxidant pathway is growing rapidly, as its protective properties show promise in the treatment of a wide array of diseases. The paradigm and complexity of Nrf2 protein regulation are described in the next paragraph.

1.1.2. The Regulation of the Nrf2 Protein Stability and Activity by Keap1

Expression levels of the Nrf2 protein are primarily controlled at a post-transcriptional level, through an interaction with proteins that trigger proteasome mediated degradation (Suzuki & Yamamoto, 2015; Cuadrado *et al,* 2009). The best understood negative regulator of Nrf2 is the Kelch-like ECH-associated protein

(Keap1), which is an actin-bound zinc metalloprotein that acts as an E3-ligase, facilitating the attachment of ubiquitin chain to Nrf2 (Ghosh *et al*, 2011). Keap1 binds as a dimer to the Neh2 domain within Nrf2 forming bonds with the high affinity ETGE and low affinity DLG amino acid sequences (**Figure 1.1**). This interaction brings the Nrf2 protein into proximity with Cullin3 and Ring Box 1 (Rbx1), which then catalyze the process of ubiquitin attachment (Baird *et al*, 2013). The domain topology of Nrf2 and Keap1 proteins are shown in **Figure 1.1**. Keap1 is located mainly in the cytosol where it constantly sequesters and ubiquitinates Nrf2, thereby restricting basal Nrf2 activity to very low levels. The Keap1 has been also reported to enter the nuclear space, however its nuclear function requires clarification. An unusually high number of reactive cysteine (Cys) residues are encoded within Keap1 (27 Cys residues), makes it an extremely sensitive sensor of oxidative stress, with C151, C257, C273, C288 and C297 being especially sensitive to oxidation (Bryan *et al*, 2013; Figiel, 2008).

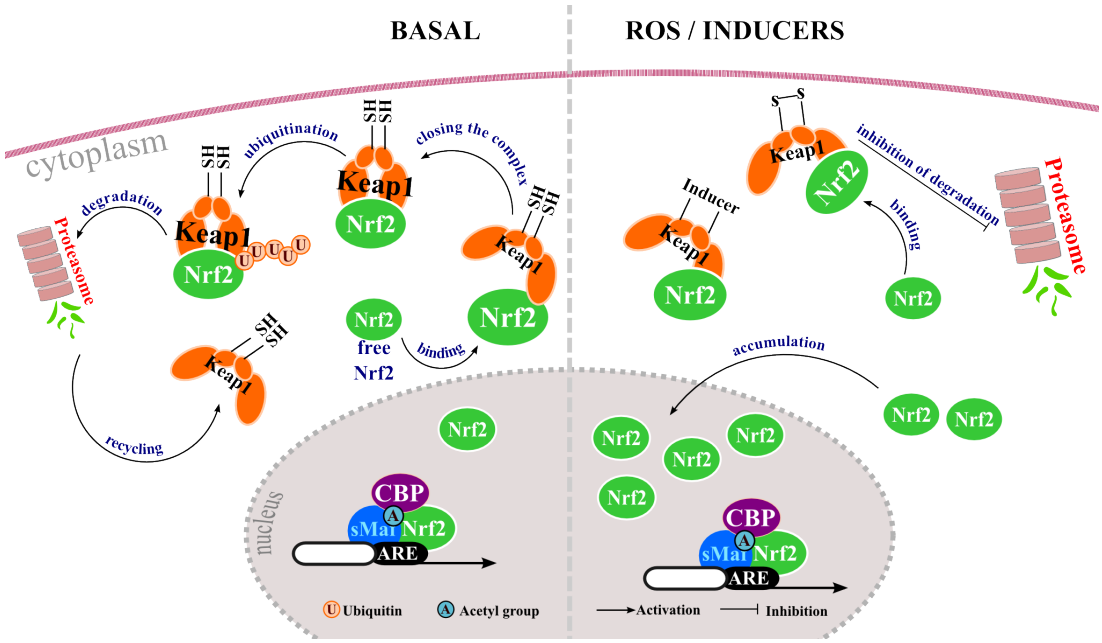

Figure 1.2 The Keap1-dependent Nrf2 regulation. The basal (left) and the ROS/pharmacological inducer (right) inflicted modes of Nrf2 regulation are represented. The Nrf2 becomes sequestered to Keap1 and the complex closes allowing attachment of the ubiquitin chain. The Keap1 is then recycled and binds to another Nrf2 molecule. Some basal activity is allowed (left). In the event of modification of cysteine residues on Keap1 by oxidation or attachment of electrophilic compounds the Keap1 is unable to form the closed complex and therefore catalyse the ubiquitin attachment. The newly made Nrf2 is then accumulated in the nuclear space and leads to ARE genes transcription. (Adapted from Baird *et al*, 2013).

The reactivity of Cys residues is characterised by the pKa value of its thiol residues, and this value can be lowered (rendered more reactive) by the presence of basic and aromatic amino acids, or metal centres located around it (Bryan *et al,* 2013). The oxidation of thiols within Cys residues leads to the formation of disulphide bridges between cysteines, resulting in a conformational change in Keap1 protein structure, which in turn prevents the effective ubiquitination and degradation of Nrf2 (Baird *et al*, 2013; Chiu & Dawes, 2012).

The Nrf2/Keap1 model of regulation has been described as the '*conformational cycling mechanism*' (Baird *et al*, 2013), in which the Nrf2 is constantly sequestered by Keap1 dimers and targeted for degradation through the formation of closed complex between the N-terminal BTB domain and C-terminal DC domain of Keap1 and the ETGE and DLG motifs in Nrf2 (see **Figure 1.1**) (Tanji *et al,* 2013). Following degradation of the Nrf2 protein, the Keap1 dimer is recycled and is able to bind newly made Nrf2 protein (Baird *et al,* 2014). In the event of oxidative stress, or pharmacological intervention, specific Cys residues on Keap1 become modified leading to the release of the DLG domain of Nrf2, thus forming an open complex that can no longer be ubiquitinated and degraded (**Figure 1.2**). Newly formed Nrf2 proteins will still bind to free Keap1 dimers, however as Keap1 becomes saturated, free Nrf2 is then allowed to enter the nucleus, where it will subsequently heterodimerise with sMaf and bind to ARE containing promoter sequences (Baird *et al,* 2013*)*. The additional consequence of the open complex formation is that it exposes the Nrf2 protein for competitive interactions with other partners such as p21, p62 and prothymyosin, as well as phosphorylation by various kinases, leading to the activation of ARE gene expression (Baird *et al,* 2014; Chen *et al,* 2012). Therefore, antioxidant pathway activation will rely on Nrf2 protein synthesis to overcome the levels of Keap1, which are usually present in cells at very low (near-saturated) levels (Suzuki *et al,* 2013). Covalent modification of Keap1 cysteines sensitises it to degradation by Sequestosome 1 (p62)-mediated autophagy. The Keap1-p62 interaction is possible due to change in the Keap1 conformation resulted from oxidative stress. This exposes it for binding to the STGE motif within the p62, which mimics the low affinity ETGE site present within the Nrf2 protein. This process initiates an assembly of autophagy machinery and depletion of Keap1, allowing Nrf2 to accumulate in the nuclear space (Bryan *et al,* 2013). Suzuki *et al* demonstrated that Nrf2 gene expression can be modulated by the relative abundance of Nrf2 and

Keap1, so the basal activity of Nrf2 will be dependent on both newly formed Nrf2 protein and the levels of Keap1 protein in the cytoplasm (Suzuki *et al*, 2013; Baird *et al*, 2014). This hypothesis has been reinforced by studies investigating the negative regulation of Keap1, which show that enhanced expression of micro RNAs miR27 and miR2000a, both of which target Keap1 mRNA, as well as an increase in Keap1 promoter methylation, lead to a rise in basal levels of Nrf2 activity (Bryan *et al,* 2013; Suzuki & Yamamoto, 2015). On the other hand, the ubiquitin specific peptidase 15 (USP15) deubiquitinating enzyme was shown to negatively regulate Nrf2 function as it enhances Keap1 activity and complex formation with Cul3/Rbx1, by catalysing the removal of the ubiquitin chains on Keap1 (Ashabi *et al,* 2013).
Efforts to generate Keap1$^{-/-}$ mice to investigate Keap1-mediated regulation of Nrf2 responses failed because the animals die shortly after birth, due to hyperkeratinosis of the upper digestive track (Suzuki & Yamamoto, 2015; Stepkowski *et al*, 2011). However, a liver specific Keap1 knockout has been generated, allowing the effects of high Nrf2 expression on hepatocyte physiology to be investigated (Suzuki & Yamamoto, 2015).

1.1.3. The Regulation of Nrf2 Protein Stability by GSK-3/β-TrCP/PI3K Axis

The Keap1/Cull3/Rbx1 complex is extremely robust and efficient in restricting Nrf2 protein expression, however, several other negative regulators of Nrf2 protein have been described. The recently described GSK-3/β-TrCP axis exhibits a notable difference to Keap1-mediated inhibition. Whereas, Keap1 acts as an extremely sensitive sensor of oxidative and chemical stress, the GSK-3 pathway acts by adjusting the antioxidant activity in tune with cellular signalling cascades and the metabolic status of the cell, as such its input varies greatly between tissues (Kim *et al,* 2013; Nisole *et al,* 2013). GSK-3 is a serine/threonine kinase characterised first through its role in the inhibition of glycogen synthase in low nutrient environments (Lee & Kim, 2007). However since its discovery, GSK-3 has been implicated in diabetes mellitus (DM) and in psychological and neurodegenerative disorders. GSK-3 is encoded by two isoforms (GSK-3α and GSK-3β), which share 86% sequence homology and have redundant biological functions (Guan *et al,* 2014; Lee & Kim, 2007). GSK-3 is active basally and requires priming phosphorylation of its targets, which then prompts further attachment of a phosphate group onto a serine or

threonine residue. In the presence of glucose the insulin/Akt/PI3K pathway leads to GSK-3 phosphorylation at Ser9 (β isoform) and Ser21 (α isoform), which terminates its activity. Therefore, high nutrient environments inhibit GSK-3 activity allowing glycogen re-synthesis (Lee & Kim, 2007). Nrf2 is also a target for GSK-3 phosphorylation, on the Neh6 domain (**Figure 1.1**), facilitating docking of the β-TrCP E3 ubiquitin ligase and formation of the β-TrCP/Skp1/Cull1/Rbx1 complex, which like Keap1/Cull3/Rbx1 catalyses ubiquitination of Nrf2 and subsequent degradation (Rojo *et al,* 2012; Chowdhry *et al,* 2013). While Keap1 dominates the control of cytoplasmic Nrf2 levels, the GSK-3/β-TrCP axis is thought to be predominantly active in the nucleus, directing Nrf2 protein for nuclear proteasomal degradation (Chowdhry *et al,* 2012). GSK-3 activity is regulated by insulin signalling and extracellular signals such as hormones and growth factors, consequently Nrf2 activity can be fine-tuned in line with glucose availability and growth signals (Clodfelder *et al,* 2005; Cuadrado, 2015).

1.1.4. The RNF4-mediated Degradation

There is at least one further alternative degradation pathway of Nrf2, which was described recently by Malloy *et al*. This mechanism involves the accumulation of Nrf2 into promyolytic leukaemia nuclear bodies (PML-NBs) and takes place independently of the Keap1 and GSK-3 activity. The PML-NBs are dynamic nuclear structures that perform multiple cellular roles, such as transcriptional regulation and protein degradation, however the exact mechanism of their action still remains to be elucidated (Lallemand-Breitenbach & Hugues, 2010). This route of Nrf2 degradation requires the SUMOylation of Nrf2 proteins, which are then recognised by the RNF4 E3 ubiquitin ligase, leading to the further modification of Nrf2 by the attachment of ubiquitin chains. The modified Nrf2 is then sequestered into mature PML-NBs, which contain the proteasome subunits that mediate Nrf2 degradation. The mechanisms that control this route of degradation and tissue specificity are not well defined and the environmental conditions that favour this mode of control remain to be further established (Malloy *et al,* 2013; Guo *et al,* 2014).

1.1.5. The Role of Post-translational Modifications in Regulating Nrf2 Activity

1.1.5.1. Phosphorylation

The regulation of Nrf2 can be fine-tuned by several post-translational modifications, such as, phosphorylation, which regulate antioxidant gene expression and facilitate rapid responses to subtle changes in the cellular environment. The best defined phosphorylation event is mediated by the Protein kinase C (PKC), which targets Ser40 within the Neh2 domain of Nrf2 that is located within the proximity to the Keap1 binding sites, leading to enhanced nuclear accumulation (Cuadrado *et al,* 2009; Bryan *et al,* 2013). Also, PKC is activated by PI3K signalling in response to growth factors and by catalysing the inhibitory phosphorylation of GSK-3 thereby indirectly augmenting Nrf2 activity (Belleza *et al*, 2010; Kim *et al,* 2013). Cellular antioxidant activity can also be modulated by nutrient availability, by the mammalian target of rapamycin (mTOR) pathway. In a nutrient rich environment, mTOR activation leads to the phosphorylation of serine on the STGE motif of p62/SQSTM1. This increases its competitive binding to Keap1 leading to Nrf2 nuclear shuttling, leading to an increase in antioxidant target gene expression (**Figure 1.3**) (Ichimura *et al,* 2013). Similarly, endoplasmic reticulum (ER) stress, resulting from the accumulation of misfolded proteins can activate the protein kinase RNA-like endoplasmic reticulum kinase (PERK), which subsequently mediates phosphorylation of Nrf2. This is thought to promote dissociation (or open complex formation) from Keap1, allowing Nrf2 nuclear localisation and the transcription of protective genes (Stepkowski *et al,* 2011*;* Mitsuishi *et al,* 2012a, Cullinan *et al;* 2003). Other kinases that have been reported to inhibit Keap1-mediated degradation include JNK, ERK1/2, p38 and MEK5. At this point it should be noted that Nrf2 is predicted to be involved in ~ 281 binary protein interactions, although a significant number of these interactions have yet to be verified. Nevertheless, it is highly probable that in the near future additional mechanisms of conditional Nrf2 regulation will be identified (Papp *et al,* 2012).

Phosphorylation of Nrf2 not only dictates its Keap1-regulated degradation, but also governs its cellular localisation. The Src family of proteins includes Fyn, Fgr, Yes and Src, promote the nuclear export of Nrf2 by modification the Tyr568 residue (Niture *et al,* 2011; Jain *et al,* 2006). Nuclear localisation of the Src proteins is also

regulated by GSK-3, which enhances their nuclear retention. Therefore, increased GSK-3 activity not only regulates the nuclear degradation of Nrf2 but also plays an important role in controlling its export into the cytoplasm for Keap1-mediated degradation, thus ensuring the efficient termination of antioxidant signalling (Cuadrado, 2015).

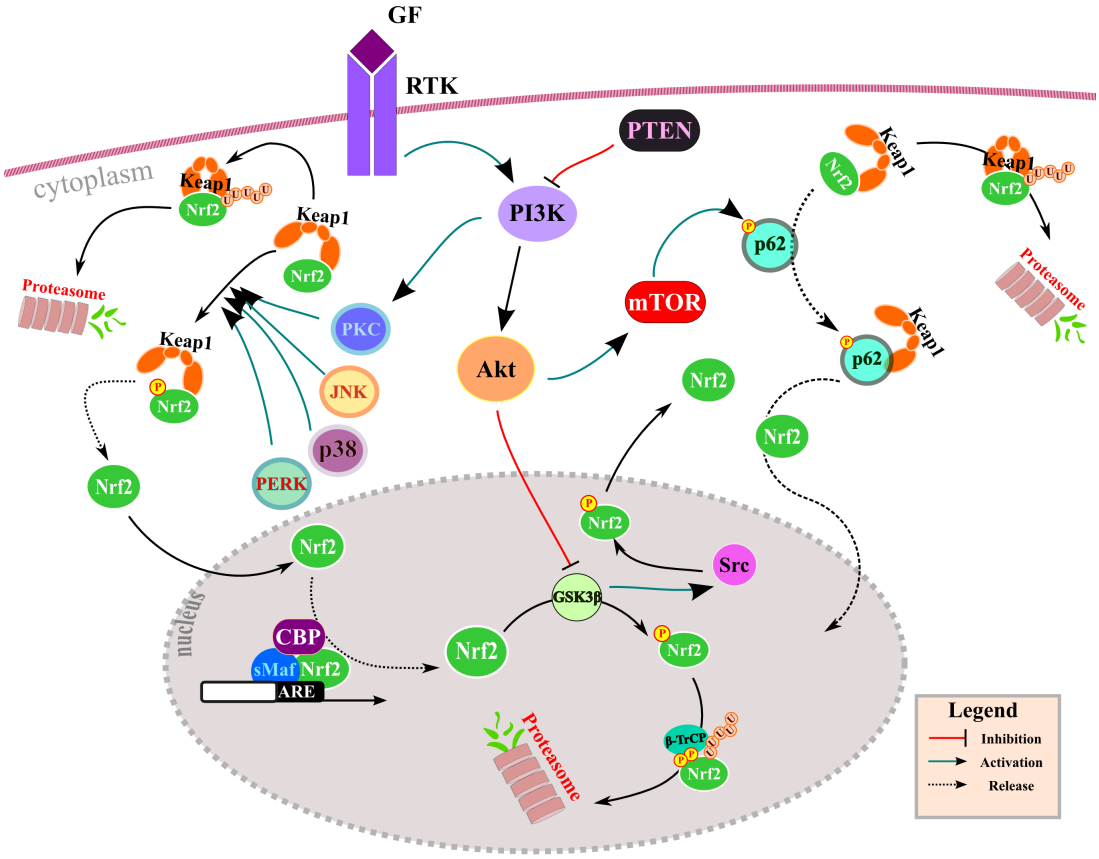

Figure 1.3 Regulation of Nrf2 by phosphorylation. Diagram depicting major modes of regulation of Nrf2 protein through phosphorylation including PI3K, Akt, mTOR, GSK-3 and PTEN. GF=growth factor, RTK=receptor tyrosine kinase (Adapted from Papp *et al*, 2012; Belleza *et al*, 2010; Stepkowski *et al*, 2011 and Carracedo *et al*, 2008).

1.1.5.2. Dephosphorylation

Antioxidant gene expression is also modulated by de-phosphorylation. The phosphatase and tensin homologue deleted on chromosome 10 (PTEN) has been identified as a negative regulator of Nrf2 function, as demonstrated by the fact that PTEN negative cancers display increased levels of Nrf2 transcriptional activity (Cuadrado, 2015; Mitsuishi *et al*, 2012b). Lack of PTEN was associated with

enhanced Nrf2 activation in response to antioxidant inducers such as tert-Butylhydroquinone (tBHQ) in Jurkat human leukaemia cells, suggesting that PTEN has an inhibitory effect on Nrf2 function (Sakamono *et al*, 2009). Overexpression of PTEN leads to inhibition of PI3K, thus affecting its downstream targets such as Akt/mTOR signalling and preventing the subsequent boost in Nrf2 target gene expression (**Figure 1.3**) (Carracedo *et al*, 2008). Furthermore, this triggers activation of GSK-3, which in turns enhances the degradation of Nrf2 through the GSK-3/β-TrCP axis (Rojo *et al*, 2014). Therefore, high activity of PTEN not only leads to functional repression of Nrf2 but also enhanced protein clearance. The summary of regulatory phosphorylation and de-phosphorylation events is depicted in diagram in **Figure 1.3**.

1.1.5.3. Acetylation

Together with many other transcription factors Nrf2 requires acetylation by the transcriptional co-factor the p300/CBP histone acetylase protein (HAT), which augments Nrf2 DNA binding and gene transcription (Sun *et al,* 2009). The Neh1 DNA binding domain within Nrf2 contains 18 lysine (Lys) residues, which can be modified by acetyl group attachment. This creates a positive charge on the surface of Neh1 and augments its interaction with negatively charged phosphate groups within the DNA backbone. Deletion of the individual Lys residues within Nrf2 did not have a significant effect on ARE-driven gene transcription, suggesting that they have redundant functions. However, deletion of all 18 residues was effective in reducing antioxidant activity (Sun *et al,* 2009). Besides, p300/CBP-mediated Nrf2 acetylation, the hMOF acetylase has also been identified as an enzyme that is capable of acetylating Lys588 of Nrf2, which also increases Nrf2 nuclear retention and gene transcription. The activity of hMOF is high in NSCLC tissue, and this increase in activity has been shown to be associated with the cancer resistance to drug treatment and poor patient prognosis (Chen *et al,* 2014).

Protein acetylation can be reversed by the action of histone deacetylase enzymes (HDACs), which are grouped into 4 classes accordingly to their homology with the yeast counterparts, which have been shown to have different substrate specificity (Lu *et al,* 2015).

HDACs inhibitors have been shown to have pleiotropic effects on the transcription of ARE response genes. For example, inhibition of the SirT1 deacetylase (HDAC class III) led to increased Nrf2 transcriptional activity and nuclear retention, coupled with increased acetylation of Lys558 and Lys591 residues (Kawai *et al,* 2011). Enhancement of acetylation by inhibition of HDAC enzymes, using the antibiotic trichostatin A (TSA), which targets classes I, II and IV HDACs, had a positive effect on Nrf2 transcriptional activity, by reducing Keap1 expression (Wang *et* al, 2012). Also, HDACs inhibitors were shown to improve neuronal viability during glucose starvation and ischemic damage in a mouse model of stroke. In addition, there are also reports of the positive effect of HDACs inhibitors on antioxidant expression in Parkinson's disease (Wang *et al,* 2012; Lu *et al,* 2015). In contrast to these studies, deletion of HDAC II by siRNA and pharmacological agents led to a decrease in H_2O_2 induced Nrf2 nuclear accumulation and an increase in oxidative stress (Mercado *et al,* 2011). Therefore, different classes of HDACs are involved in modulating the antioxidant gene expression and the outcome of their function may well be cell type specific and may also depend on the prevailing cell signalling signature.

1.1.6. Transcriptional Regulation of Nrf2

The fine balance between Keap1 and Nrf2 protein expression levels may dictate the basal expression of ARE-response genes. The importance of the transcriptional regulation of Nrf2 was highlighted by studies investigating single nucleotide polymorphisms (SNPs) within the *NRF2* gene promoter. Variations in SNPs in the upstream promoter sequence are associated with significantly decreased Nrf2 mRNA and protein expression. Population analysis of SNPs variations revealed profound increases in the risk of developing lung cancer, even in patients that have not smoked in the past (Hayes & Dinkova-Kostova, 2014). The *NRF2* gene has been predicted to be regulated by 34 transcription factors based on the consensus sequences encoded within its proximal promoter. So far the AhR, RXRα, SP-1, PPARγ, Myc, Pax, AP-1, NF-κB transcription factors and also Nrf2 itself have been shown to modulate the activity of the *NRF2* gene promoter region (Papp *et al,* 2012; Cuadrado *et al,* 2009; Wakabayashi *et al,* 2010; Hayes & Dinkova-Kostova, 2014; Rushoworth *et al,* 2012; Kwak *et al,* 2002; Pajares *et al,* 2015).

The transcriptional regulation of Nrf2 is achieved, in part, by the Aryl hydrocarbon receptor (AhR), which like Nrf2 is an inducible transcription factor that responds to xenobiotic stress, mediating the transcription of phase I and II metabolising enzymes (Wakabayashi *et al,* 2010, Tang *et al,* 2010). The AhR resides basally within the cytoplasm in complex with Hsp90 and 38-kDa immunophilin like protein and its nuclear translocation is initiated by the polycyclic hydrocarbons (*e.g*. dioxins). The AhR protein recognises the xenobiotic response element (XRE) in the promoter of gene targets including the *NRF2* promoter (Wakabayashi *et al,* 2010). In addition, the Nrf2 promoter contains 2xARE sequences, which means that it has the potential to modulate its own transcription, however, as yet it is unclear whether this mechanism of transcriptional regulation operates during either inducible or basal activity (Hayes & Dinkova-Kostova, 2014; Kwak *et al, 2002*). Interestingly, the κB transcriptional response sequence, was detected within the 1.2kb proximal promoter region, and experiments in AML cells have shown that high Nrf2 activity, resulting from inflammatory signalling, contributed to the resistance of cancer cells to bortezomib treatment (Rushworth *et al*, 2012).

1.1.7. Function of Nrf2 Gene Targets

Nrf2 controls the transcription of over 200 genes and depending on the tissue context, these genes have prominent roles in the maintenance of redox status and the generation of reducing equivalents, protein folding and degradation, cell metabolism, calcium homeostasis and drug metabolism (Thimmulappa *et al,* 2002; Hayes & Dinkova-Kostova, 2014). The main pathways regulated by Nrf2 response genes are described below.

1.1.7.1. Iron Metabolism

Heme oxidase (HO-1) is an inducible microsomal enzyme abundant in most tissues responsible for catalysing the cleavage of the porphyrin ring of heme to yield ferrous iron (Fe^{2+}), carbon monoxide (CO) and biliverdin, which is subsequently converted to bilirubin (Vargas & Johnson, 2009; Dorresteijn *et al,* 2015). The Fe^{2+} generated in this reaction triggers the activation of the iron ATPase pump, which then mediates the export of intracellular iron ions. Fe^{2+} ions can also trigger the expression of

ferritin iron storage protein, an Nrf2 target gene, which sequesters free intracellular ferrous iron (Soares *et al*, 2004). The concentration of free Fe^{2+} and heme is higher under oxidative stress and this significantly increases the concentration of free radical species, which are generated as a result of the Fenton reaction and can lead to cytokine induced programmed cell death. In contrast, bilirubin has a potent antioxidant activity, which prevents apoptotic cell death (Gozzelino *et al,* 2010). The Nrf2 is though to be the main regulator of inducible HO-1 expression, however other transcription factors have also been reported to bind to the *HMOX-1* promoter sequence, such as c-fos, c-jun and Ap-1 (Lu *et al,* 2014).

1.1.7.2. The Antioxidant Properties of the Nrf2 Target Genes

Many proteins equipped with reactive cysteine residues rely on transient ROS signals to modulate their activity. As a result, basal ROS concentration have the potential to effect multiple important cellular signalling events, thereby acting as a local, transient second messenger. The resulting increase in free radical species leads to the modification of thiol group in the cysteine residues and formation of sulfenic acid, disulfides, and mixed disulfides with glutathione or nitrosothiols. These are often necessary for appropriate protein function, however sometimes they may also hinder its activity (Bindoli *et al,* 2013).

Elevation of ROS levels triggers the oxidative stress responses, which involves global changes in gene transcription and cell growth. Furthermore, extreme levels of ROS can initiate apoptosis (Pajarez *et al,* 2015). Nrf2 mediates the transcription of genes involved in reversing oxidative cysteine modifications, thereby preventing toxic accumulation of free radicals. The key function of Nrf2 is to ensure the replenishment of the cellular redox potential, by ensuring *de novo* synthesis of glutathione (GSH) by controlling the expression of the glutamate-cysteine ligase, catalytic subunit (GCLC) and the glutamate cysteine ligase, modifier subunit (GCLM) (Hayes & Dinkova-Kostova, 2014; Mitsuishi *et al,* 2012a). GSH is a potent antioxidant tripeptide present in the cell at mM concentration, where it acts as an electron donor, forming disulphide-bridges (S-S) on oxidised cysteines (Findlay *et al,* 2005). This can be achieved either by reducing the S-S bridges back to the un-oxidised state, or by enabling protein glutathionylaiton (post-translational

modification), which protects it from further oxidation (Findlay *et al,* 2005). The oxidised form of GSH, glutathione disulfide (GSSG), can be restored by expression of ARE-driven glutathione reductase (GSR) (Gozzelino *et al,* 2010; Vargas & Johnson, 2009). The NAD(P)H dehydrogenase quinine 1 (NQO1) is another example of canonical Nrf2 gene target, which reduces the highly reactive quinines preventing the formation of reactive oxygen compounds (Hayes & Dinkova-Kostova, 2014; Thimmalappa *et al,* 2002).

The cysteines residues within the antioxidant proteins are effective electron acceptors and are therefore able to buffer cellular free radical concentration. The oxidation of reactive Cys residues takes place sequentially, from cysteine to sulfenic acid and then from sulfenic acid to sulfinic acid, each step leading to progressive alternations in protein structure and function (Findlay *et al,* 2005). Nrf2 regulates expression of the small redox protein sulfiredoxin (SFXN), which can reverse the oxidation of sulfinic acid Cys residues back to the more readily reversible sulfenic acid form, as well as thioredoxin (TRXDN), which then sequentially convert sulfenic acid back into the native thiol group (Winyard *et al,* 2005). In simple terms, the process of reducing involves an exchange of disulphide bonds between the cysteines and the reducing proteins. These are just a few examples of antioxidant proteins regulated by Nrf2 however there are several others such as catalase, prostaglandin reductase and peroxiredoxin-1 (Prx1) and all have significant roles in maintaining the intracellular redox balance protecting the sensitive structural building blocks of cells (Hayes & Dinkova-Kostova, 2014; Dowell & Johnson, 2013).

1.1.7.3. Proteasomal Degradation and Autophagy

The proteasome is a molecular "furnace" which clears away proteins within both the nuclear and cytoplasmic compartments. The proteasome displays selectivity for degradation of proteins depending on its subunit composition. The 20S proteasome primarily degrades unfolded proteins and does not require ubiquitin attachment to its targets, furthermore it can form the 26S proteasome by pairing with one or two 19S subunits, which changes its preference towards native-ubiquitinated proteins (Pajarez *et al,* 2015). Thomas Kensler and colleagues first reported that the structural and catalytic subunits of the 20S proteasome are regulated by Nrf2 activity, adding to the wide portfolio of Nrf2 inducible genes (Hayes & Dinkova-Kostova, 2014).

Proteasomal degradation targets individual proteins. Importantly, Nrf2 also modulates the expression of p62/SQSTR1 that plays a key role in autophagosome formation, which in assistance from lysosomal digestion leads to the disposal of unwanted cellular components, such as, damaged organelles and protein aggregates (Taguchi *et al,* 2012; Pajarez *et al,* 2015). The damaged cargo is usually extensively labelled by ubiquitin chain attachment and recognised by the p62/SQSTR1 adaptor protein, which marks it for loading into the autophagosome (Fujita *et al,* 2011). The autophagosome then fuses with the lysosome and the cargo is digested by the action of the proteolytic enzymes within the lysosomal lumen. This form of autophagosomal degradation is active during starvation, as the presence of nutrients effectively inhibits mTOR activity (Pajarez *et al,* 2015, Krejci, 2012). Therefore, Nrf2 regulates the clearance of unfolded and native proteins by increasing proteasome availability and augmenting the clearance of whole organelles through by autophagy.

1.1.7.4. PPP pathway

The Nrf2 transcriptional activity has been shown to play a pivotal role in redirection of glucose metabolism into pentose phosphate pathway (PPP) under sustained PI3K activity (Mitsuishi *et al*, 2012a; Wu *et al,* 2011). PPP is an alternative route for anaerobic glucose utilisation and around 2-3% of the brain glucose is being shunt into the PPP (Takahashi *et al, 2012*). The net product of PPP is the production of ribose-5 phosphate, for the synthesis of nucleotides and NADPH, which are key donors of reducing potential for GSH and TRXN enzymes that are essential for the recovery of oxidative stress and the reduction of oxidised cysteines (Mitsuishi *et el,* 2012a; Ludtmann *et al*, 2013; Heiss *et al,* 2013). This pathway is especially important in high glucose environments, which is also associated with increased levels of oxidative stress and the tumour microenvironment, where the production of nucleotides and reducing equivalents fuels anabolic tumour growth (Hajnoczky *et al*, 2015; Mitsuishi *et al,* 2012). The key rate-limiting enzymes in this process are glucose-6-phosphate dehydrogenase (G6PD), 6-phosphogluconate dehydrogenase (PGD), transketolase (TKT), malic enzyme-1 (ME-1) and isocitrate dehydrogenase-1

(IDH-1). All of which have are ubiquitous inducible Nrf2 gene-targets (Wu *et al,* 2011; Pajarez *et al*, 2015; Timmlappa *et al,* 2002).

1.1.7.5. Bach1

Significantly, Nrf2 nuclear translocation is not the sole determinant of ARE-driven gene transcription, as other factors may also limit access to the promoters of these target genes. For example, the availability of ARE binding sites may be restricted by the Bach1 protein, which like Nrf2, also belongs to the bZIP family of transcription factors and dimerises with sMaf proteins to bind to cis-acting sequences (Jyrkkanen *et al,* 2011). Unlike Nrf2, Bach1 lacks the leucine zipper transactivation domain (TD) necessary to initiate transcription, therefore its binding has a potent inhibitory role in ARE gene transcription, including NQO1 and HO-1 gene expression (Stepkowski *et al*, 2011; Kanezaki *et al,* 2001). Bach1 is also sensitive to increased levels of free radical species, which modulate oxidation of its reactive cysteine residues, thus promoting its nuclear export. Significantly, this process can also be triggered by the accumulation of free intracellular heme, thereby allowing Nrf2 to bind to previously occupied promoter ARE sequences. Interestingly, Bach1 contains an ARE site in its own promoter region and the application of Nrf2 inducing drugs leads to an increase in Bach1 mRNA, subsequently leading to dampening of Nrf2 target gene expression (Jyrkkanen *et al,* 2011).

1.1.8. Intracellular Sources of ROS

There are multiple oxygen and nitrogen species that act as redox signalling molecules, including hydrogen peroxide (H_2O_2), superoxide (O^-_2), singlet oxygen (O), hydroxyl radical (OH^-) and nitric oxide (NO) and its by-products. H_2O_2 can readily act as a second messenger and is present within tissues at low concentrations, where it is able to freely pass through lipid membranes. The main generator of H_2O_2 within cells is the NADPH oxidase enzyme, which is the main driver of intracellular oxidative stress (Bindoli *et al,* 2013). NADPH activity is vital in the generation of oxidative bursts in macrophages and neutrophils and serves as a potent weapon against phagocytised pathogens and therefore plays important roles in mediating inflammatory signalling (more on NADPH oxidase in Section 1.2.6).

Mitochondria are also a major source of cellular oxidative stress, due to the production of high levels of superoxide created during mitochondrial respiration. However, the net balance of ROS production is though to be smaller in healthy mitochondria than previously though (Bindoli *et al*, 2013; Pajarez *et al,* 2015). In addition, a considerable amount of redox stress is also generated as a response to unfolded proteins in the endoplasmic reticulum (Pajarez *et al,* 2015).

Lipids, DNA and proteins are all prone to ROS induced damage, creating a risk of harmful mutations and further exacerbation of oxidative stress by the accumulation of dysfunctional proteins (Vargas & Johnson, 2009). The biggest changes in oxygen radical levels occurs as a result of drastic variation in the cellular environment, as experienced under conditions of hyperglycaemia, inflammation and damage from UV and ionising radiation (Takahashi *et al,* 2012).

1.1.9. Pharmacological Inducers and Inhibitors of Nrf2

1.1.9.1. Nrf2 Activating Compounds

The induction of antioxidant genes by Nrf2 ameliorates the overproduction of ROS, however under conditions of persistently high levels of oxidative stress, as observed in chronic inflammatory disorders, pharmacological induction of Nrf2 could be necessary to boost protective responses. There are several well-characterised, plant derived and synthetic compounds that effectively trigger Nrf2 gene expression. In general, these act via electrophilic attack on the reactive thiol groups located in reactive cysteines in Keap1 (Baird *et al,* 2014; Suzuki & Yamamoto, 2015). The first described inducer of Nrf2 was an isothiocyanate molecule the sulforaphane (SFN), isolated from broccoli and described by Paul Talay's lab in 1992 (Zhang *et al*, 1992). SFN is present in broccoli as a precursor glucosinolate, which becomes hydrolysed to the biologically active form (the glucosinolate glucoraphanin by β-thioglucosidase enzyme) upon chewing or plant damage. SFN acts by targeting C51 within Keap1 thus blocking Nrf2 degradation, possibly by inducing the formation of the open complex, which then allows newly formed Nrf2 protein to enter the nucleus (Baird *et al,* 2014; Tufekci *et al,* 2011). The study by Clarke *et al,* demonstrated that within 3h

of ingesting 40g of broccoli sprouts, it was possible to detect a substantial increase in SFN concentration, reaching 2μmol/L in the blood plasma of study subjects (Clarke *et al,* 2011). Also, Zhou *et al,* demonstrated that broccoli soup made from 100g broccoli florets (cooked 90s at 700-W) yielded blood plasma concentrations between 3.8 to 10.7μmol/L of SFN within 1.5h of ingestion (Zhou *et al,* 2015; Gasper *et al,* 2015). SFN has also been shown to have potent anticancer properties and has also demonstrated promising neuroprotective action in a mouse model of Parkinson disease (Morroni *et al*, 2013; Clarke *et al,* 2011).

To date, the most potent Nrf2 inducer characterised is the CDDO-Me triterpenoid compound derived from oleanolic acid (found in olive oil), also known as Bardoxolone methyl and can induce antioxidant gene expression at nM concentrations (Suzuki & Yamamoto, 2015; Hayes & Dinkova-Kostova, 2014). The CDDO-Me also targets Keap1 Cys residues and exhibits potent neuroprotective properties and has been shown to delay the onset of ALS in a mouse model of this disease, extending the life of motor neurons by reducing inflammatory signalling (Danilov *et al,* 2009). Importantly, the neuroprotective effects of CDDO-Me are possible as it is able to pass the blood brain barrier (BBB) (Neymotin *et al,* 2011). CDDO-Me has been previously used in the clinics for the treatment of chronic kidney disease, however the trial was closed following the phase II stage due to the occurrence of deleterious adverse drug effects. Nevertheless, several other clinical trails have subsequently been initiated, focusing on pulmonary hypertension and diabetes associated chronic kidney disease (Suzuki & Yamamoto, 2015). Importantly the only available effective treatment accepted recently by the FDA for treatment of multiple sclerosis (MS) is dimethyl fumarate (DMF). Its neuroprotective activity has been attributed to the activation of the Nrf2 pathway possibly by modulating HDAC expression, although the exact mechanism of action of this drug is still unknown (Suzuki & Yamamoto, 2015; Sporn *et al*, 2012; Kalinin *et al,* 2013). Importantly many compounds that can activate Nrf2 signalling are present in dietary compounds, mostly plants and many inducers have been characterised, to date these include: reservatrol, from grapes; curcumin, from turmeric; SFN, from broccoli, cabbage, kale, broccoli sprouts; wasabi; honey; cinnamon; garlic; green tea and many more sources (Bryan *et al*, 2013; Tufekci *et al*, 2011; Pajares *et al,* 2015).

1.1.10. Brusatol –the Nrf2 Inhibitor

Induction of Nrf2 is expected to yield protective cellular responses, however there is also an urgent need for the development of selective inhibitors of the Nrf2 pathway, for the treatment of cancers that evade treatment by hijacking the antioxidant activity. Brusatol is a plant-derived quasinoid from *Brucea javanica,* which has been shown to rapidly deplete Nrf2 levels, by decreasing its stability possibly via poly-ubiquitination and clearance by an unidentified mechanism (Olayanju *et al*, 2015; Ren *et al,* 2011). Addition of the drug leads to reduced expression of Nrf2 target genes including γGCS, MRP1 and MRP2, without affecting Keap1 protein levels (Ren *et al,* 2011). Significantly, Ren *et al,* demonstrated that 40nM brusatol leads to the sensitisation of cancer xenographs to cisplatin, therefore showing promise in cancer treatment as an adjuvant to chemotherapy (Ren *et al,* 2011).

1.1.11. Role of Nrf2 in Cancer

The antioxidant activity of Nrf2 is though to play a very important role in disease prevention, as demonstrated by the phenotype of Nrf2 knockout animals, which are hypersensitive to toxicity, inflammation and neurodegenerative disorders (Suzuki & Yamamoto, 2015; Bryan *et al,* 2013; Vargas & Johnson, 2009). However, Nrf2 acts as a double edge sword conferring beneficial effects during health, although in the event of tumourgenesis, elevated levels of Nrf2 contribute cancer cells resistant to therapeutic drugs and radiation (Hayes *et al,* 2006). Multiple cancers have been found to exhibit low expression or activity of Keap1 *e.g*. gastric, gallbladder, breast, ovary and liver cancers, which are frequently associated with poor prognosis (Sporn *et al,* 2012). The loss of function has been attributed to mutations of Keap1, especially in Nrf2 binding domains, as well as a reduction in Keap1 expression, due to methylation mediated inactivation of the Keap1 promoter (Suzuki *et al,* 2013; Sporn *et al,* 2012; Belleza *et al,* 2012). Other frequently detected mutations associated with cancer also occur in the ETDGE and DLG binding motifs within the Nrf2 protein (**Figure 1.1**), thus rendering it insensitive to negative regulation by Keap1. In addition, oncogenic activation of KRas, Braf and Myc signalling pathways in cancers have also been linked to increased antioxidant gene expression (Sporn *et*

al, 2012). On the other hand Nrf2 KO mice were found to be susceptible to development of cancers and when injected with Lewis lung carcinoma these mice exhibited a significant increase in the number and size of tumour nodules (Suzuki & Yamamoto, 2015). An important consequence of high Nrf2 activity in cancers is the activation of a genetic program designed to detoxify and reduce oxidative stress in response to ionising and gamma irradiation and the increased expression of drug metabolising enzymes, and export pumps, which collectively confer protection against chemotherapy (Ren *et al,* 2011; Rushworth *et al,* 2012; Hayes & Dinkova-Kostova, 2013). Therefore, the status of Nrf2 activation should be determined prior to selection of optimal treatment regimes, in order to select an optimal therapeutic strategy, as the inhibition of Nrf2 could sensitise the cancer to the treatment routines.

1.2. The Introduction to the NF-κB Pathway

1.2.1. The NF-κB Cellular Function and Regulation

The NF-κB transcription factor mediates immune responses to bacterial and viral infections, as well as initiates gene expression supporting inflammation, cell development, proliferation, anti-apoptotic pathways, oxidative metabolism and protection against UV radiation (Smale *et al,* 2011; Mauro *et al,* 2011; Kaltschmidt *et al,* 2005). The NF-κB pathway is evolutionarily conserved from the ancient horseshoe crab *Carcinoscorpius rotindicauda* to humans, suggesting an indispensable protective role through the animal kingdom (Wang *et al,* 2006). The Nobel Prize winner David Baltimore, first proved that the DNA enhancer element of the immunoglobin heavy chain enhancer sequence in the B-cell lymphocytes is driven by the NF-κB transcription factor (Sen *et al,* 1986). We now know that NF-κB is actually a family of transcription factors including RelA (p65), RelB, c-rel, p50 (105) and p52 (p100) subunits, which act as homo- or heterodimers (Heyden & Ghosh, 2008). Only the p65, RelB and c-rel contain the transactivation domain required to drive transcription. The p50 and p52 subunits are detected basally in the nucleus of unstimulated cells and are thought to have an inhibitory effect on gene expression, by blocking DNA sequence availability (Hayden & Ghosh, 2008; Zhong *et al,* 2002). NF-κB expression is universal in cells with the exception of the RelB

subunit, which is selectively expressed in the thymus, lymph nodes and Peyer's patches (Li & Verma, 2002).

1.2.2. The Regulation of NF-κB Signalling

NF-κB signalling is mediated by a complex network of protein interactions usually initiated by en extracellular stimuli (Hayden & Ghosh, 2008). The NF-κB subunits form homo and heterodimers through their Rel homology domains (RHD), which are also necessary for their dimerization, DNA binding and association with the IKBα inhibitor (Perkins & Gilmore, 2006; Hayden & Ghosh, 2008). The p65/p50 heterodimer is sequestered in the cytoplasm by association with IKBα, which obscures one out of two NLS and limits its nuclear entry (Hayden & Ghosh, 2008; Mincheva-Tascheva & Soler, 2013; Li & Verma, 2002). Importantly, NF-κB gene transcription is inducible by variety of stress stimuli and over 150 different factors have been identified as activators of NF-κB mediated gene expression *e.g.* LPS, exotoxin B, muramyl peptide, viruses *e.g.* Hepatitis B, Adenovirus, Herpex Simplex Virus-1, HIV, cytokines, but also physical stress, UV radiation, shear stress, ischemia oxidative stress and environmental hazards (Glass *et al,* 2010; Pahl, 1999). The NF-κB homo- and hetero-dimers associate specifically with the κB regulatory DNA consensus sequences: 5'GGGRNYYYCC-3' (where "N" is unspecified nucleotide, "R" is an unspecified purine and "Y" is a pyrimidine residue) upstream of NF-κB target genes, (Chen *et al,* 1998; Sen *et al,* 1986). Even though the p50 homodimer is inhibitory on gene expression, heterodimer formation with p65 greatly enhances the affinity of the p50/p65 transcription factor for DNA, with binding affinity estimated to be approximately 10^{-13} to 10^{-10}M, stronger than a majority of other transcription factors (Chen *et al,* 1998). What is more, RelB, c-Rel, p50 and p52 also are regulated by the κB sequence and therefore the composition and quantity of NF-κB heterodimers can be adjusted to the inducing stimuli (Perkins & Gilmore, 2006).

1.2.3. Gene Targets

NF-κB plays a central role in the maintenance of the immune responses by initiating the genetic program designed to modulate the local environment and to attract the immune cells to the site of infection or injury. It mediates the expression of approx. 300 genes, including numerous cytokines and their receptors, anti-apoptotic genes and adhesion molecules (Pahl, 1999; Turner *et al,* 2010). For the purpose of this chapter only selected gene targets will be discussed in more detail.

1.2.3.1. Inflammatory Factors

Cytokines are small signalling proteins that are secreted into the extracellular space, mediating inter-cellular signalling in response to environmental threats and can have both pro-inflammatory and anti-inflammatory properties (Zhang & An, 2007). The pro-inflammatory cytokines are mainly secreted by activated macrophages, however, they have also been shown to be secreted by many other immune and non-immune cells and have redundant roles in inflammatory signalling (Zhang & An, 2007; Liu & Chan, 2014). The cytokines described below are commonly expressed in response to NF-κB activation, during inflammatory stress (Scheller *et al,* 2011).

IL-8 is a pro-inflammatory chemokine that conveys signalling through the CXRC2 receptor and plays important role in attracting neutrophils to the site of inflammation (Zhang & An, 2007). It is commonly secreted by immune cells such as phagocytes, microglia and leukocytes in response to inflammation, infection, ischemia and trauma. IL-8 is produced by many cell-types and its expression can be activated by TNFα, IL-1 and other inflammatory stimuli, such as endotoxins. Apart from its chemoattractant properties it can trigger the release of granzymes and initiate oxidative bursts by augmenting the NADPH oxidase activity in neutrophils (Baggiolini *et al,* 1992).

IL-1β and TNFα are other examples of inflammatory cytokines. Predominantly secreted by the monocytes and macrophages, but also by many other non-immune cells (Zhang & An, 2007). Interleukin-1β (IL-1β) is synthesised in an inactive form (pro-IL-1β) and it requires further cleavage by the multi-protein inflammasome

complex to yield mature, functional molecules. Its action depends largely on the cell type, but generally it leads to activation of the NF-κB pathway, thus amplifying inflammatory signals and driving production of other signalling molecules, such as IL-1β and IL-6. High IL-1β expression has been implicated in Alzheimer's disease (AD) and leads to aggravation of the disease pathology (Liu & Chan, 2014).

IL-6 has a very interesting function and mechanism of activation of downstream signalling pathways. It acts by binding to the IL-6 receptor, which then associates with the glycoprotein 130 (gp130) receptor associated protein. The membrane-bound IL-6R is present only on a handful of cells however most cells contain the type I signal transducer protein gp130 protein on their surface. Interestingly the IL-6 receptor can exist also in a soluble form, and can transduce signalling by associating with the gp130 present on cellular membrane, effectively leading to activation of downstream JAK/STAT, PI3K and ERK kinases (Scheller *et al,* 2011). Aside from its well-established pro-inflammatory roles, IL-6 also has anti-inflammatory and regenerative functions, which distinguishes it from other cytokines described above. It also acts by attracting neutrophils and monocytes into to the site of infection. It can also have cell specific pro- and anti-apoptotic properties designed to resolve the inflammatory signalling of neutrophils, which otherwise create considerable local damage. IL-6 is involved in the production of chemoattractant molecules designed to lure monocytes into the site of infection and modulate the expression of adhesion molecules on endothelial cells, allowing leukocyte transmigration and cell differentiation. IL-6 mediated signalling orchestrates the local inflammatory environment by directing the sequential signalling in multiple cell types (Scheller *et al,* 2011).

Tumour necrosis factor (TNFα) was first described over 40 years ago as an anti-tumourgenic factor by Carswell *et al,* (Carswell *et al,* 1975). Low basal TNFα concentrations are necessary to maintain normal physiological function and it is also thought to have neuroprotective properties (Figiel, 2008). TNFα is one of the best-studied cytokines and it is also a potent activator of the NF-κB-mediated gene expression, playing an important role in systemic inflammation and the induction of fever (Liu & Chan, 2014; Lee *et al,* 2014). It has pleiotropic effects as it can induce a

range of cellular responses such as proliferation, chemotaxis, apoptosis and inflammation, as its downstream signalling triggers several molecular cascades (Liu *et al,* 2014). TNFα is produced as a monotrimeric transmembrane molecule and becomes solubilised by the TNFα converting enzyme (TACE), which is anchored to the plasma membrane. This cleavage results in the formation of monomeric form of TNFα (mTNFα), which remain associated with the membrane and a monotrimeric soluble form with higher affinity for the target receptors. The TNFα binding to the TNFR1 and TNFR2 receptors triggers their trimerization (**Figure 1.4**) and downstream signalling relay (Figiel, 2008).

There are two receptors activated by the TNFα cytokine with TNFR1 (p55) and the TNFR2 (p75), which share extensive homology in their ligand binding, although the intracellular effector domains are largely unrelated (Baker & Reddy, 1998; Declerq *et al,* 1998). Despite that, they can both induce apoptosis and the NF-κB pathway by activating downstream signalling. The ligand-binding domain contains a cysteine rich domain (CRD), which serves as an anchor for receptor trimerisation by disulphide bonds between the individual monomers (Baker & Reddy, 1998).

1.2.4. The Canonical Cascade

Pro-inflammatory cytokines such as TNFα, IL-1β activate the canonical signalling cascade by engaging the extracellular receptors and initiating a relay of intracellular phosphorylation events, which co-ordinate signalling and conditional cell responses (Sakurai *et al*, 2003). Activation of the TNFR1 receptor initiates the TRADD/RIP signalling cascade, which removes the phosphate group from the IKK kinases complex, comprised of the IKKα and IKKβ catalytic subunits and IKKγ (NF-κB essential modifier, NEMO) (**Figure 1.4**). IKK activation results in the phosphorylation of IKBα on Ser32 and Ser36 and parallel activation of several kinases, such as MAPK p38, JNK (Liu *et al,* 2014; Hayden & Ghosh, 2008; Perkins & Gilmore, 2006). Phosphorylation primes IKBα for interaction with the β-TrCP/Skp1/Cullin1 complex, which drives IKBα ubiquitination and proteasomal degradation, finally releasing the NF-κB subunits to the nucleus (Winston *et al*,

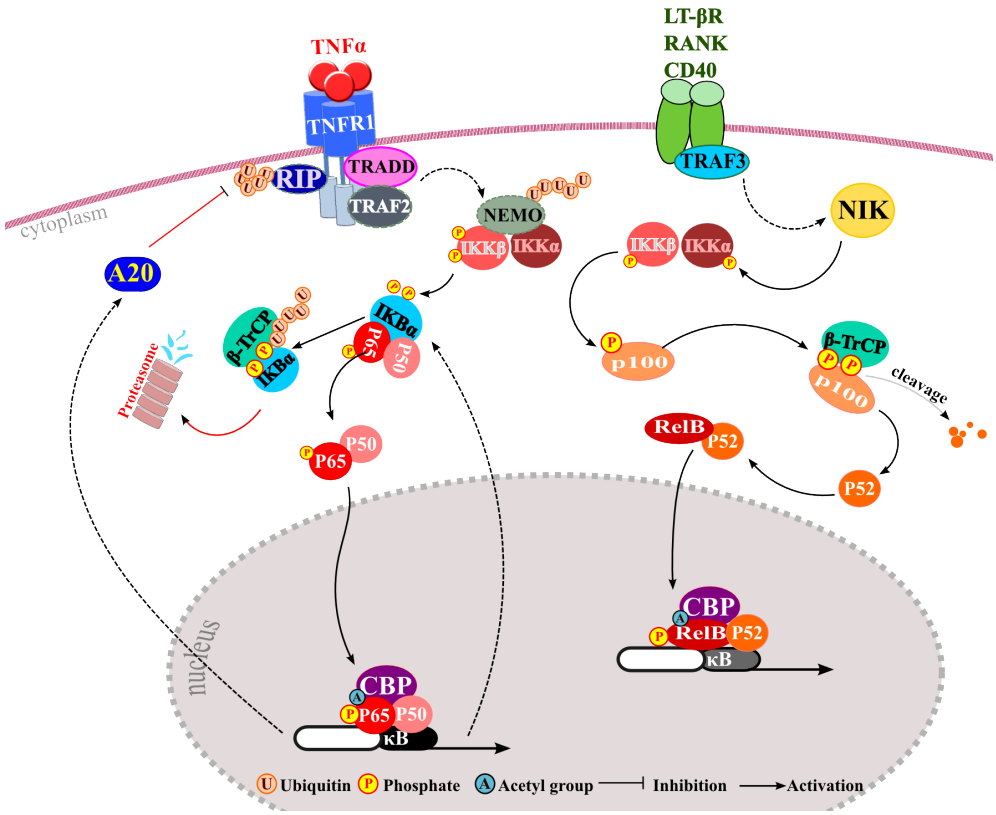

Figure 1.4 The Canonical and Non-Canonical NF-κB Pathways. The canonical/classical pathway of NF-κB activation involves TNFα that triggers a downstream cascade of TNFR1 ubiquitination and phosphorylation events leading to nuclear occupancy of p65/p50 heterodimers. The non-canocial pathway involves downstream NIK kinase signalling and activation of CD40, RANK or LT-βR receptors. The net result is processing of the p100 subunit precursor into functional p52 protein and association with RelB binding partner. The RelB/p52 then translocates to the nucleus and mediates transcription of κB driven genes. (Adapted from Kim *et al*, 2013; Buelna-Chontal & Zazueta, 2013; Kaltschmidt *et al*, 2005).

1999). It should be noted that the IKBα/p65/p50 complex is though to basally shuttle through the nucleus, but is persistently recovered to the cytoplasm as a result of a strong IKBα NES sequence, so its degradation skews subcellular distribution towards the nucleoplasm (Perkins & Gilmore, 2006; Kim *et al*, 2013). Several post-translational modifications are necessary to enhance NF-κB transcriptional activity including multiple phosphorylation events and acetylation by p300/CBP (Huang & Hung, 2013; Heyden & Ghosh, 2008; Zhong *et al*, 2002). The entire signalling

process from the TNFR1 activation to the κB transcription is very rapid, taking place within minutes (Perkins & Gilmore, 2006). The activation of inflammatory gene transcription also initiates multiple negative feedback loops, which keep the inflammatory signalling at bay. The IKBα protein is one of the earliest gene targets of NF-κB signalling, in response to TNFα cytokine. Shortly following translation it localises to the nucleus and removes p65 from the DNA, and sequesters it back into the cytoplasm (Bergquist *et al,* 2009). In addition, NF-κB also transcribes the de-ubiquitinating enzyme (DUB) A20, which terminates the signalling cascade upstream of the IKK complex by modification of the receptor interacting protein (RIP), which is essential for TNRF1 receptor signalling (**Figure 1.4**). The A20 protein removes Lys-63 chains from the RIP protein leading to Lys-48 ubiquitination and targeting for proteasomal degradation, leading to inactivation of the downstream phosphor-relay signalling (Chen & Chen, 2013*;* Wertz *et al,* 2004). Therefore, both IKBα and A20 create safety loops terminate the signalling from the inflammatory signalling.

1.2.5. The Non-canonical Cascade

Non-canonical NF-κB signalling involves distinct receptors and ligands, such as *e.g.* the CD40 and RANK receptors, which initiate distinct molecular cascades by activating the NF-κB inducing kinase (NIK) which phosphorylates the IKKα dimer leading to the processing of p100 precursor proteins into their mature p52 subunits. The most commonly detected partner for p52 interaction is RelB, and the p52/RelB complex detects slightly altered κB sequences to those recognised by canonical p50/p65 transcription factor (**Figure 1.4**) (Perkins & Gilmore, 2006).

1.2.6. NF-κB and ROS

The NF-κB activation triggers transcription of Manganese Superoxide Dismutase (MnSOD) enzyme, which swiftly reduces TNFα-induced ROS levels. In the absence of NF-κB activation the TNFα stimulus generates substantial intracellular ROS, which further triggers prolonged c-Jun N-terminal protein kinase (JNK) activation and finally apoptosis (Perkins & Gilmore, 2006; Liu *et al*, 2014). Therefore, the

activation of NF-κB gene transcription is critical to cell survival during prolonged TNFα signalling and its absence or malfunction can dramatically decrease cellular viability.

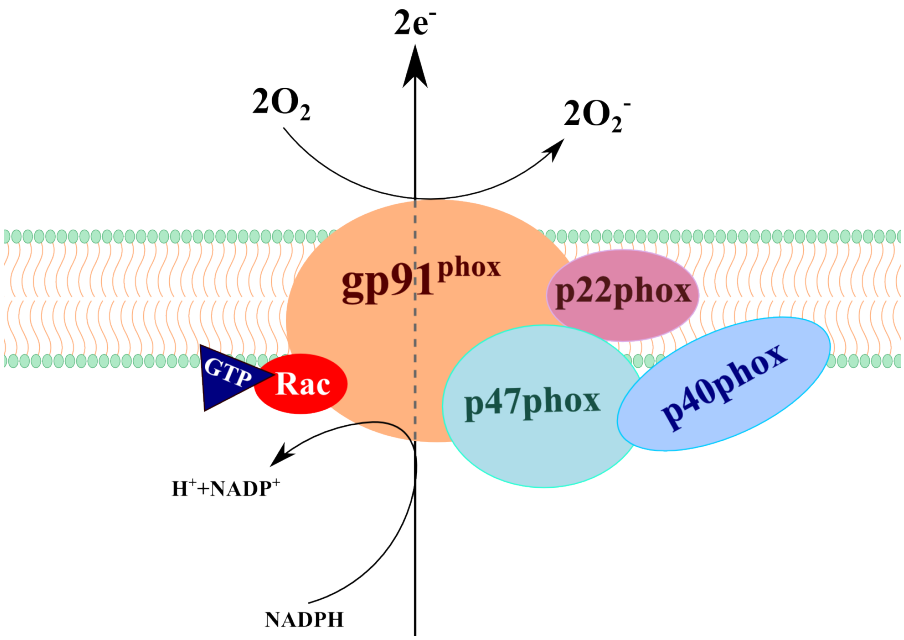

Figure 1.5 The NADPH oxidase enzyme. The Schematic representation of the activated NADPH oxidase enzyme showing the subunits necessary for the assembly of the functional enzyme. The reduction of one NADPH equivalent results in net production of 2 superoxide anions. (Adapted from Gardiner *et al*, 2013).

The NADPH oxidase is a major source of intracellular ROS. First described in phagocyte cells, it is now appreciated that NADPH subunits are distributed in nearly all tissues and play important roles in immunological defence, protein modification, cellular signalling and differentiation. However, high expression aggravates neurodegenerative and cardiovascular disorders (Bedard & Krause, 2007). The NADPH oxidase has several isoforms that differ in their subunit composition, but the

canonical enzyme is composed of five subunits: the $p22^{phox}$, the cytochrome b558 containing gp91phox (NOX2) and cytoplasmic part with $p40^{phox}$ (NCF4), $p47^{phox}$ (NCF1), $p67^{phox}$ (NCF2) and a small GTPase Rac (**Figure 1.5**) (Manea *et al,* 2007; Bedard & Krause, 2007). The $p22^{phox}$ subunit is expressed in response to NF-κB signalling and is essential for functioning of the NADPH oxidase. The complete enzyme coordinates the transport of electrons across the plasma membrane or within the plasma of intracellular vesicles, generating superoxide from reduced oxygen, which is rapidly converted to H_2O_2 at low pH (spontaneously) or cleared away by superoxide dismutase , or stress caused by mechanical forces (**Figure 1.5**). High NADPH oxidase activity may act as a positive feedback loop, reinforcing inflammatory signalling, as NF-κB transcriptional activity is redox sensitive (Manea *et al,* 2007).

1.2.6.1. SOD

NF-κB regulates expression of several superoxide dismutase (SOD) enzymes including SOD1, SOD2, MnSOD and Cu/ZnSOD (Saleh *et al,* 2013). The importance of the protective function of SOD enzymes is highlighted by the phenotype of the MnSOD knockout mice, which have a life span of only a few days. MnSOD is a redox-active metalloenzyme located within the mitochondrial membrane. The active MnSOD homotetramer scavenges the superoxide (*e.g.* created by the NADPH oxidase) to produce H_2O_2 and dioxygen by reaction presented below. (Sheng *et al,* 2014).

$$2O_2^{\bullet-} + 2H^+ \xrightarrow{SOD} O_2 + H_2O_2$$

With increasing expression of the SOD family of enzymes the half-life of superoxide dramatically changes. The half-life of $O_2^{\bullet-}$ at 10^{-9}M in the environment that does not contain SOD proteins can reach several hours. Whereas, the same concentration of superoxide in the presence of 10^{-9}M SOD is reduced extremely fast, with a half-life of only 175ms (Sheng *et al,* 2014). Therefore, NF-κB mediated gene expression contributes to the increase of oxidative environment by upregulating the NADPH

oxidase but also to the clearance of ROS by increasing the availability of the powerful antioxidant SOD enzymes.

1.2.6.2. iNOS

NF-κB regulates the expression of the inducible nitric oxide synthase (iNOS) enzyme, which synthesises the gaseous second messenger nitric oxide (NO) (Vannini *et al,* 2015). NO participates in multiple processes in the body and can act to modulate the vascular tone and participate in multiple signalling cascades. NO interacts with the guanylate synthase enzyme yielding the cyclic guanosine monophosphate (cGMP) molecule, which further activates the cGMP dependant kinase (PKG). This leads to a cascade of events regulating the vasodilation of blood vessels. Importantly, the NO allows a post-translational modification called S-nitrosilaiton, which alters the function of numerous proteins. The NO molecules also commonly participate in formation of free oxidative radicals, as interaction of NO with oxygen species yields peroxynitrites, which can damage lipids, nucleotides and proteins. The effect of NO depends on its concentration, with 100nM being protective and a threshold above 500nM leading to cytotoxicity and induction of apoptosis (Vannini *et al,* 2015; Bindoli & Rigobello, 2013).

1.2.7. The NF-κB Dynamic Behaviour

The spatio-temporal organisation of cellular networks fine-tunes the output of multiple signalling parameters into a functional response. A notable example of control of cell fate by the fluctuations in transcriptional activity has been shown during the differentiation of neural progenitor cells (NPCs) into astrocytes, neurons and oligodendrocytes in the brain. The frequency and persistence of oscillations of the Asc1/Mash1, Hes1 and Olig2 transcription factors drive the differentiation of NPCs by determining the temporal expression of the target genes, which commit the cells to the defined differentiation path (Imayoshi *et al,* 2013). Analogously, frequency in oscillations in intracellular Ca^{2+} concentration determines the strength of the cellular responses, therefore the temporal dynamics of protein and signalling molecules is fundamental in control of cellular function (Turner *et al,* 2010).

Computational simulation of NF-κB dynamics in response to inflammatory stimuli conducted by Hoffman *et al* was the first study to predict oscillatory nuclear shuttling of the NF-κB in cells. The mathematical modelling of NF-κB activity suggested that the rate of synthesis and degradation of IKBα/β and IKBε were likely to determine the oscillatory nuclear dynamics of p65. This hypothesis was partially confirmed by evidence of the fluctuations in NF-κB binding to target DNA sequences measured by electrophilic mobility assay (EMSA) in the IKBε$^{-/-}$ mouse fibroblasts (Hoffmann *et al,* 2002).

Single-cell imaging experiments performed by Nelson *et al,* reinforced the prediction introduced by Hoffman *et al,* providing evidence for oscillatory nuclear dynamics of fluorescently labelled p65 in live-cells (Nelson *et al,* 2004). Interestingly, this unusual temporal behaviour was shown to be triggered by a pro-inflammatory TNFα stimulus, which following the initial peak of p65 nuclear accumulation, led to asynchronous nuclear cytoplasmic shuttling between cells (Nelson *et al,* 2004). The fluorescently labelled p65-dsRedXP oscillations occurred every 100min for about 20hrs in the continuous presence of TNFα (10ng/ml), whereas a 5min pulse of TNFα cytokine led to a synchronous single peak in SK-N-AS and HELA cells. This phenotype is driven by the delayed feedback loop of IKBα gene transcription and with time the gradual increase in its expression dampens the temporal behaviour of NF-κB. The negative regulation initiated by fast IKBα expression (30min peak) leads to augmented temporal oscillatory dynamics, whereas expression of the IKBε subunit results in their dampening (120min peak expression) (Hoffmann *et al*, 2002; Nelson *et al,* 2004). IKBα is an excellent regulator of NF-κB as it is very sensitive to transcriptional activation, due to the unusually high number of 6xκB repeats in the *IKBA* promoter region (the average is 2-3) (Zambrano *et al,* 2014). The role of the IKB proteins is redundant in regulation of NF-κB but the timing of their subsequent expression is detrimental to the frequency and the amplitude of the NF-κB nuclear oscillations *e.g*. the IKBα$^{-/-}$ mice are prenatally lethal however the insertion of IKBα promoter upstream of the *IKBE* (encoding IKBε) rescued this phenotype (Hoffmann *et al,* 2002).

The NF-κB gene expression profile was monitored in response to varying durations of inflammatory signals by luciferase transcriptional reporter assays, demonstrating that a pulsatile stimulation results in a lower magnitude of induction and faster peak in transcription as compared to continuous application of TNFα. This suggested that the persistence of inflammatory stimulus greatly alters the expression pattern of target genes (Nelson *et al,* 2004). The tenacity of the NF-κB signalling is though to be maintained by the IKBβ activity, which is more resistant to degradation evoked by the inflammatory stimuli (Li & Verma, 2002).

Variations in the frequency of p65 oscillations have different effects on NF-κB target gene transcription, therefore the dynamic parameters of p65 cytoplasmic: nuclear shuttling act as a code, which enables calibration of the expression of genes necessary to handle the stress response (Turner *et al,* 2010). What is more, the duration of the inflammatory signalling has been shown to modulate the portfolio of activated gene targets, which can be divided into early, middle and late genes *e.g*. IKBα is an early gene, whereas RANTES is an example of a late gene target (Ashall *et al,* 2002).

The study by Ashall *et al,* demonstrated that synchronicity of NF-κB oscillations between cells is augmented by 5min pulsatile application of TNFα at 200min intervals, whereas shorter pulses (60-100min) diminished the magnitude of p65 nuclear translocation leading to a smaller number of cells responding to the stimuli. This result suggested that in order to allow subsequent NF-κB translocations, the system needs to be reinstated, before it can again be sensitive to the cytokine activation (Ashall *et al,* 2002). The heterogeneity of NF-κB oscillatory behaviour is determined by the levels of the IKBε expression, which is slightly delayed in comparison to IKBα, and knockdown of IKBε leads to synchronised nuclear shuttling of fluorescently labelled p65 in live cells. Heterogeneity is an important inherent characteristic of cellular behaviour, which ensures robustness of the signalling output. It minimises the risk of augmented synchronous pro-inflammatory gene expression, which could lead to uncontrolled tissue inflammation. Interestingly, the protective character of cellular heterogeneity is demonstrated by the asynchronous pattern of apoptosis and cell division processes (Paszek *et al,* 2010).

1.3. The NF-κB and Nrf2 Pathways in the CNS

Chronic oxidative stress has been associated with neurodegeneration and it is becoming increasingly recognized that a better understanding of the control of antioxidant and inflammatory response pathways in the CNS could improve patient outlook, as well as, reinforce disease prevention. The different cell-types that constitute the central nervous system are briefly described below, followed by a discussion of the role of NF-κB and Nrf2 signalling in the central nervous system in a cell specific context.

1.3.1. Cell Types in the Nervous System

1.3.1.1. Neurons

Neurons are unique cells that process information by electrical or chemical signalling. In the CNS there are about 100 billion neurons composed of subpopulations of cells specializing in secreting specific neurotransmitters, such as glutamate, dopamine, acetylcholine, gamma-aminobutyric acid (GABA) and others, which convey a specific message (Liu *et al,* 2014). They are highly complex cells that form thousands of neurite processes interconnecting with other neurons and glial cells. The neurons have a very high oxidative metabolic rate and therefore are highly susceptible to generated intracellular ROS, especially as they are required to withstand the environmental challenges in order to remain viable for many years (Bell *et al,* 2011). Due to their highly specialized role they rely largely on functional support from surrounding glial cells. This is especially evident as they depend on astrocyte cells to secrete metabolic compounds such as lactate, which is then used by neuronal cells as a primarily energy source to fuel the tricarboxylic acid (TCA) cycle (Tsacopoulos *et al,* 1996).

1.3.1.2. Astrocytes

Astrocytes (also called astroglia) are glial cells characterized by the formation of multiple star-like processes. The name glia means glue in Greek, the name originated from the assumption that they were playing solely a structural role in the brain.

However, research into astrocyte physiology has intensified recently, because they were recognised as playing a key role in protective cellular responses, cognitive behaviour, inflammatory and antioxidant signalling, learning, memory and brain metabolism (Wang *et al,* 2012b). Astrocyte end-feet processes wrap around synaptic connections forming a "tripartite synapse" allowing them to modulate the synaptic activity and ensuring the appropriate synapse maintenance and protection. The metabolism of these cells is tightly coupled with the neuronal activity, which has been shown to trigger an increase in astrocyte glucose uptake and aerobic glycolysis, and to enhance the lactate shuttle for neuronal consumption (Tsacopoulos *et al,* 1996*; Zonta et al,* 2002*; Pellerin et al,* 1994*)*. They also play a vital role in maintaining the ion balance and water content and in the clearance of glutamate neurotransmitter to prevent its excitotoxicity (Losi *et al,* 2012). Importantly, astrocyte processes are in direct contact with the arterioles and form the BBB therefore they are able to take up compounds from the blood and process them for secretion into neurons and the extracellular fluid. The interaction of astrocytes with the blood vessels can dynamically regulate vascular tone, depending on brain energy needs, coupling its function with increased oxygen and nutrient use (Zonta *et al,* 2002). Astrocytes are also an important energy source in the brain, as they are able to store and mobilise energy in the form of glycogen. It is thought that a single astrocyte cell is in contact with over 100,000 neuronal synapses and up to 600 dendrites forming a functional syncytium, which can reach up to 80,000μm^3 (Pfreiger & Slezak, 2012). What is more they can modulate inter-astrocyte signalling through connexins (gap junctions), which permit diffusion of ions and propagation of calcium waves, synchronizing their local signalling (Stobart & Anderson, 2013). Astrocyte cells, together with microglia (discussed below) play central role in modulating the immune signalling within the CNS and respond to multiple stress stimuli such as cytokines extracellular protein aggregates, lipopolysaccharide (LPS), extracellular ATP, glutamate and chemokines. They are also key players in maintaining the antioxidant protection of the brain as astrocytes secrete high quantity of the GSH for utilisation in neuronal cells that are unable to synthesize it and therefore rely exclusively on astrocyte specific production of this antioxidant (Vargas & Johnson, 2009). Due to the incredible multi-functionality and protective roles of

astrocytes they become increasingly important as pharmacological targets to tackle a range of brain disorders.

1.3.1.3. Microglia

Microglia are the brain's resident macrophages, modulating immune signalling processes and they constitute around 10% of cells in the CNS (Liu & Chan, 2014). They exist in the resting state when they secrete anti-inflammatory signals and neurotropic factors. They constantly inspect the surrounding environment and influence astrocyte and neuronal inflammatory signalling (Brown *et al,* 2010). The microglia abandon their resting status as a result of an injury or infection and switch to an activated mode, during which they secrete factors such as pro-inflammatory cytokines and chemokines in order to mobilize immune cells from the blood, which migrate to the site of injury (Hoing *et al,* 2012; Liu & Chan, 2014). This is especially relevant, as the immune cells from the circulation normally do not cross through the blood brain barrier, they can only enter as a result of astrocytic and microglial chemokine secretion and inflammatory cues (Glass *et al,* 2010). The microglia are also able to engulf bacteria, viruses and toxic protein aggregates, which are then destroyed by oxidative burst within the phagosome (Lee *et al,* 2003). Continuous activation of microglia causes significant damage from ROS and is associated with progression of neurodegenerative disorders (Bedard & Krause, 2007).

1.3.1.4. Oligodendrocytes

Oligodendrocytes are also a type of glial cells that form myelin sheets protecting the neuronal axons from environmental stress in the brain and in the spinal cord (Pfreiger & Slezak, 2012). They migrate towards electrically active neuronal processes and insulate them and have an important regulatory role in maintaining appropriate neuronal physiology. They are able to control the local environment of axons by secreting neurotrophic factors ultimately leading to an increase in neuronal viability and protection against the harmful effects of inflammation. The oligodendrocytes are particularly sensitive to ROS damage and TNFα induced apoptosis, but the restoration of myelin sheets can take place from oligodendrocyte

precursor cells, which can further differentiate into myelin forming oligodendrocyte (Bradl & Lassman, 2010).

1.3.2. Neuroinflammation

Lipids are the most sensitive cellular components to free-radical damage and since the brain is a very lipid rich tissue it is very prone to oxidative stress (Vargas & Johnson, 2009). With aging the balance between the oxidative stress and inflammation changes in favour of higher ROS production and altered metabolism, which supports the inflammatory signalling. For example, the antioxidant activity of Nrf2 is though to be diminished, leading to decreased GSH content, possibly caused by a parallel increase in GSK-3 activity (Vargas & Johnson, 2009; Suh *et al,* 2004). It is argued that aging is not directly caused by increased ROS but by the decline in mitochondrial function and oxidative metabolism. A further hallmark of the aging brain is an increased level of lactate, which indicates alterations in the brain's bioenergetics (Ross *et al,* 2010). What is more, microglial and astrocyte cells are the main drivers of inflammatory signalling, which is expected to aggravate age related neurodegeneration (L'Episcopo *et al,* 2013). With an increase of the average age of the population, the risk of neurodegenerative disease rises sharply and they pose catastrophic effects on patient's quality of life, and a burden to the public health sector. Significantly, brain diseases (including neurodegeneration, psychiatric disorders and stroke) comprise 35% of the total disease burden in Europe, and it is predicted to rise further (Olesen & Leonardi, 2003). Although, the pathophysiology of neurodegenerative disorders varies greatly, a common denominator of neurodegeneration is chronic inflammation associated with the widespread presence of activated microglia and increased levels of cytokines in the cerebrospinal fluid (CSF), which can be found in amyotrophic lateral sclerosis (ALS), Parkinson's disease (PD), Alzheimer's disease (AD), multiple sclerosis (MS) and HIV-associated dementia patients (Cuadrado *et al,* 2009; Liu & Chan, 2014; Cartier *et al,* 2005). Neuroinflammation is a very complex process involving multiple cell-types, which initially act in favour of protection, but eventually become increasingly entangled in a vicious cycle of inflammation-induced damage. The Nrf2 and NF-κB transcription factors are functionally closely linked in prevention, amplification and resolution of

the inflammation, therefore understanding how they contribute to various inflammatory brain diseases is essential in designing better treatment strategies.

1.3.3. The Role of NF-κB and Nrf2 in the CNS

1.3.3.1. NF-κB

The NF-κB plays multiple roles in the nervous system and has been implicated in learning and memory, neuronal development, neurite outgrowth, calcium homeostasis, metabolism, anti-apoptotic signalling and secretion of growth factors that support neuronal viability (Ghosh *et al,* 2011; Mincheva-Tascheva & Soler, 2013; Kaldtschmidt *et al,* 2005; Figiel, 2008; Gutierrez & Davies, 2011). Importantly, as NF-κB function is cell specific, its activity is though to promote different cellular outcomes, depending on the cell type investigated. There are conflicting reports on the status of NF-κB inducible and basal activity in the neurons, as it is difficult to discriminate its cell-specific contribution (O'Neil & Kaltschmidt, 1997; Memet, 2006; Meffert & Baltimore, 2005). The resting, low level NF-κB activity in microglia and astrocytes is essential in the maintenance of robust anti-inflammatory signals, proliferation and cellular viability, however chronic inflammatory activity as a result of damage, infection or neurotransmitter extitotoxicity leads to a concatenation of the brain's inflammatory status. This eventually results in damage to the mitochondria and to formation of protein aggregates, proteasomal and autophagic dysfunction and neuronal apoptosis, which further fuels chronic inflammation (Calkins *et al,* 2009; Liu & Chan, 2014). Also, activated microglia produce large concentrations of NO, due to increased expression of iNOS, contributing to further ROS production, which is additionally augmented by an increase in NADPH oxidase activity (Bedard & Krause, 2007). The resulting high oxidative environment enhances mitochondrial damage, leading to chronic inflammation and abnormal protein deposits in neurons (Caccamo *et al,* 2005; Glass *et al*, 2010, Brown *et al,* 2010). What is more, the production of chemotactic signals by microglial and astroglial cells direct the leukocyte migration across the BBB leading to further amplification of the inflammatory burden (Brown *et al,* 2010; Liu & Chan, 2014). However it should be noted that low levels of TNFα are protective and can stimulate Nrf2 gene expression, as well as MnSOD and anti-apoptotic

signalling (Correa *et al,* 2012). The NF-κB activity is detrimental in cell survival during inflammation and therefore the inhibition of inflammatory signalling could affect normal brain function.

To conclude, the acute inflammatory signalling designed to defend the brain tissue from infection and damage, becomes compromised and hijacked during chronic inflammation and threatens the neuronal viability by fuelling progressive damage and deterioration.

1.3.3.2. The Nrf2 Pathway in the Nervous System

Neurons rely heavily on astrocytic protection against ROS, as they do not posses the ability for *de novo* synthesis of the GSH, which is necessary to maintain the correct reducing environment. The GSH is secreted to the extracellular space before being taken up as a cysteine precursor by the gamma-glytamyl transpeptidase (GGT). Once inside the neurons it can be incorporated into GSH biosynthesis for intracellular utilisation (Vargas & Johnson, 2009). The microarray studies on neuronal and astrocytic Nrf2 gene targets highlighted the differences in cell-specific Nrf2-mediated responses. The neuronal Nrf2 activity was shown to be important primarily in calcium homeostasis, ion channel and neurotransmitter receptor signalling, whereas the astrocytic ARE regulated genes are mainly involved in antioxidant responses, iron metabolism and the PPP (Lee *et al,* 2003a; Lee *et al,* 2003b). In addition, Nrf2 activation in response to H_2O_2, neuronal activity, CDDO-TFEA and tBHQ have been observed exclusively in astrocytes (Habas *et al,* 2013; Bell *et al,* 2011; Gupta *et al,* 2012), in agreement to the observation that the wild-type astrocytes were shown to rescue Nrf2 knockout neurons from mitochondrial toxin I induced apoptosis, suggesting that glial antioxidant activity is sufficient to ensure protection of the neuronal cells (Lee *et al,* 2003b). This evidence cast doubts on the existence of effective Nrf2 neuronal activity and prompted a more rigorous investigation. The study by Bell *et al,* demonstrated that the Nrf2 expression in mature neurons is inhibited by extensive promoter methylation, and therefore Nrf2 activity is not present in adult neurons. The reason for neuronal Nrf2 inactivation emerged as the high levels of ectopic Nrf2 expression inhibits neurite outgrowth. It seems like mild oxidative stress favours neuronal development and hence high

intracellular antioxidative activity could interfere with this process (Bell *et al,* 2015). Therefore, the main antioxidant potential seems to lie within astrocytes, thus highlighting the need for therapeutic compounds that are able to modulate glial activity. This is especially relevant, as the current pharmacological compounds used in the treatment of neurodegenerative disorders target neuronal physiology or neuronal-specific receptors (Calkins *et al,* 2009). What is more, astrocytes can be accessed more readily as they form direct contacts with blood vessels. Drugs such as SFN, CDDO-Me can pass the BBB and shown promise in reducing brain inflammation (Danilov *et al,* 2009; Neymotin *et al,* 2011). Neurodegeneration is frequently coupled with several pathological phenotypes linked to the inhibition of Nrf2 activity such as: the inhibition of autophagy, which is necessary to clear away the harmful inclusion bodies (Hara *et al,* 2006), the increase in free Fe^{2+} which contributes to alpha synuclein aggregation and the amyloid formation (Gan & Johnson, 2014), mitochondrial dysfunction and toxicity presence of the reactive astrocytes and microglial cells leading to high ROS levels, increased protein oxidation and the proliferation of microglia (Oberheim *et al,* 2009; Petri *et al,* 2012). It is likely that these pathological cellular phenotypes could be diminished by the reestablishment of Nrf2 gene expression by pharmacological activation of the antioxidant protection.

1.3.4. Conclusions

The inflammatory signalling that underlies aging and disease progression is a very complex process resulting from the interplay between multiple different cell types and is extremely difficult to target pharmacologically. However, the accessibility of astrocytes and their pronounced role in the protection of the brain against inflammation could facilitate the treatment of neurodegenerative disorders. In order to effectively ameliorate the chronic inflammation it is essential to understand the molecular cross talk between the Nrf2 and NF-κB pathways, which is discussed in more detail in the next section.

1.4. The Molecular Crosstalk Between NF-κB and Nrf2

1.4.1. Are the Protective Roles of p65 and Nrf2 Redundant?

The NF-κB and Nrf2 pathways are at the core of protective cellular signalling and the imbalance between their activities has been linked to many inflammatory diseases, cancer and neurodegeneration (Ben-Neriah *et al,* 2011). Nrf2 induction normally occurs in a low oxidative stress environment, thus preventing a further increase in ROS levels and to restore oxidative modifications of affected proteins. However, at a certain threshold at which ROS levels threaten cellular viability, the NF-κB responses become activated (Belleza *et al,* 2010). The NF-κB activity is also redox sensitive and has been demonstrated to respond to increase in intracellular H_2O_2 leading to the induction of the MnSOD and the anti-apoptotic genes (Vannini *et al,* 2015; Sheng *et al,* 2014; Belleza *et al*, 2010). The double knockdown of p65 and Nrf2 in mouse hepatocytes leads to severe chronic inflammation, whereas animals with single deletions exhibit much milder phenotypes (Kohler *et al,* 2013). Therefore, the balance between the Nrf2 and NF-κB activation may dictate the cellular responses, fine-tuning gene expression to resolve stress signalling (Chia *et al,* 2010).

The interplay between antioxidant and inflammatory signalling is complex and the consequences are currently not very well understood. Potential points of molecular crosstalk between Nrf2 and NF-κB are described next.

1.4.2. Nrf2 Activity is Modulated by p65

The NF-κB itself modulates the Nrf2 mediated gene expression and has pleiotropic effects on the cellular antioxidant protection. The study by Yu *et al,* demonstrated that p65 activity leads to a reduction in ARE-target gene expression by assisting in increase of nuclear Keap1 levels, subsequently targeting Nrf2 protein for degradation (Yu *et al,* 2011). Overexpression of the nuclear import facilitating protein karyopherin alpha 6 (KPNA6) leads to augmented levels of Keap1 and prompts decrease in NQO1 and HO-1 gene expression (Sun *et al*, 2011). However the exact mechanism of how p65 mediates this process has not been well defined. The best understood mechanism of NF-κB-imposed reduction in Nrf2 transcriptional activity occurs by competitive binding of the p300/CBP acetyl transferase protein, as both

the Nrf2 and NF-κB transcription factors require acetylation for efficient assembly of the transcriptional apparatus on the gene target promoters (Sun *et al,* 2009). Nrf2 interacts with CBP/p300 by the Neh4 and Neh5 domains, which leads to subsequent acetylation of the DNA binding Neh1 fragment. What is more, the p65 phosphorylation at its Ser276 residue is a pre-requisite to acetylation by CBP/p300 and overexpression of p65 its thought to impose preferential binding of the acetylase enzyme, prioritizing the expression of NF-κB target genes. Consequently, the depletion of p65 by siRNA has been shown to increase Nrf2 DNA binding by augmenting the Nrf2/CBP interaction (Liu *et al,* 2008). This competitive HAT binding can work both ways and stimulation of Nrf2 by ethyl pyruvate was shown to shift the CBP/p300 binding in favour of the ARE expression and decrease the in κB-mediated genes such as iNOS (Kim *et al*, 2013).

In addition, to competition for acetylation, the p65 has been reported to decrease the MafK acetylation by promoting HDAC3 and MafK binding, which consequently prevents it from forming a transcriptional dimer with Nrf2, which is required for antioxidant gene transcription (Liu *et al*, 2008). The well-characterised molecular crosstalk points are presented in **Figure 1.6**.

However regulation of the antioxidant signalling by NF-κB is far form simple and unidirectional, as certain cell types demonstrate increase of Nrf2 protein levels in response to pro-inflammatory TNFα cytokine. The study by Rushworth *et al,* established that *NRF*2 gene transcription is itself regulated by NF-κB transcriptional activity and the promoter of *NRF2* gene contains functional κB sites that enable inflammatory-inducted expression. Interestingly, p65 mediated Nrf2 transcription is an underlying cause for resistance of acute myeloid leukaemia to the proteasome inhibitor bortezomib, protecting the cancer cells from effective treatment (Rushworth *et al*, 2012). What is more, a study conducted in Cuadrado's lab established that LPS treatment results in Nrf2 activation and the induction of gene expression is mediated by the small RAC1 GTPase. As a result, the increase of HO-1 expression inhibits the pro-inflammatory signalling and leads to the restoration of a more reducing environment (Cuadrado *et al,* 2014).

The recent study by Zhou *et al,* demonstrated an interesting mode of regulation of Keap1 mRNA levels by the micro RNA miR-29, which blocks its translation process. Interestingly, the NF-κB has been shown to regulate miR-29 expression in a

diabetic rat model. During high glucose conditions the NF-κB activity is downregulated by activation of the Sirt1 deacetylase, leading subsequently to increased levels of Keap1 coupled with reduction in NQO1 and GCLC mRNA levels (Zhou *et al*, 2015).

1.4.3. The Proteins Linking the Nrf2 and NF-κB Pathways

The Keap1 E3 ligase alongside its canonical role in regulating the Nrf2 protein has been shown in addition to trigger IKKβ degradation through autophagy. Keap1 acts by preventing the TNFα-induced IKKβ phosphorylation, by obscuring the target residues on IKKβ and augmenting its autophagy dependent degradation. Subsequently this leads to stabilization of IKKα and inhibition of NF-κB signalling (Kim *et al*, 2010). As discussed in before the Nrf2 protein is degraded as a result of GSK-3 phosphorylation, which directs it to the Skp1/Cullin1/β-TrCP E3 ligase complex (Rada *et al*, 2011).

The GSK-3 has also been shown to modulate the p65 DNA binding and can have

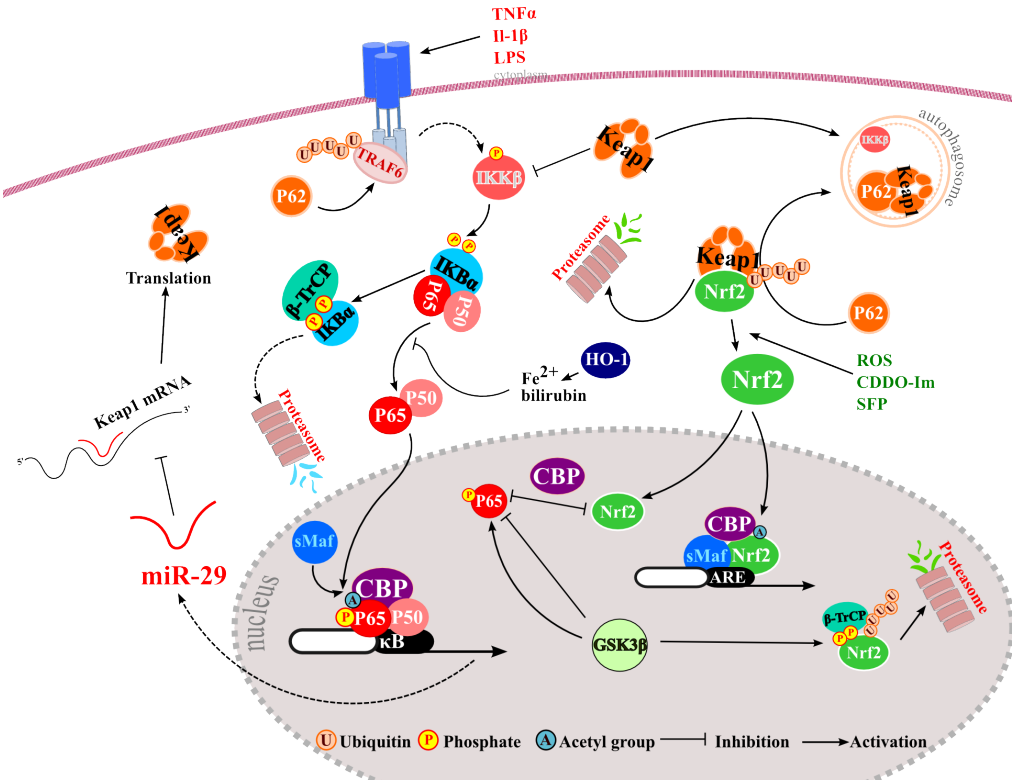

Figure 1.6 The known regulators of the Nrf2 and NF-κB molecular crosstalk. The schematic representation of some of the described common regulatory mechanisms involved in modulation of antioxidant and the inflammatory signalling. (Adapted from Wardyn *et al*, 2015)

both positive and negative effect on the κB gene expression, largely dependent on the cell type and the environment (Park *et al,* 2011). It should be noted that degradation of IKBα is also mediated by the β-TrCP adaptor protein, which highlights its dual role in potentiating NF-κB signalling and the reduction of antioxidant protection (Winston *et al,* 1999). What is more, the p62 protein aside from mediating the autophagosome dependent Keap1 depletion can prompt ubiquitin attachment on the TNFα receptor associated factor 6 (TRAF6) and augment NF-κB gene expression as a result of nerve growth factors (NGF) signalling (Wooten *et al,* 2005). **Figure 1.7** below presents the validated, common interactors of Nrf2 and p65.

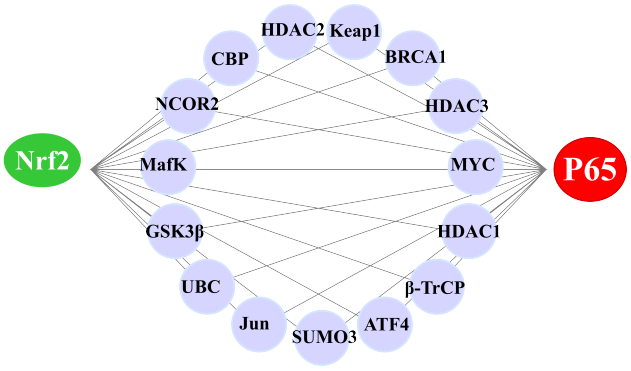

Figure 1.7 The proteins linking the antioxidant and inflammatory pathways. Data processed by Amy Ponsford (Sanderson lab) using BioGRID database. The purple nodes represent direct protein interactions. Taken from Wardyn *et al*.

1.5. Summary:

The Nrf2 and NF-κB pathways are key regulators of protective cellular responses against a wide range of stress stimuli. Crosstalk between these processes may be very complex, involving common protein partners, as well as transcriptional regulation. The mechanisms of molecular interplay provide fine-tuning points of balance between the inflammation and antioxidant signalling, ensuring effective genetic program is activated and assisting in remission into the resting state.

1.6. THESIS AIMS

The activity of Nrf2 and NF-κB transcription factors is intrinsically linked with their nuclear occupancy status. Surprisingly, even though pharmacological interventions targeting the Nrf2 pathway are already present in the clinic, the temporal Nrf2 behaviour has not been extensively studied and this contributes to the current lack of comprehensive understanding of Nrf2 regulation. Both the Nrf2 and NF-κB transcription factors have been implicated in the progression of inflammatory disorders, cancer and immune diseases however the cell type specific responses of those transcription factors, especially in mixed cells population have not been studied in detail. Lastly, the two pathways are functionally linked, however the exact mechanism of the interplay between the inflammatory and antioxidant gene expression has not been confirmed. This aim of this thesis is to generate fluorescent molecular tools to enable the tracking and dynamic localisation of the p65 subunit and Nrf2 in single cells from the mouse hippocampus and human neuroblastoma SK-N-AS models. The highlighted areas of data paucity are then addressed by using cutting edge confocal microscopy techniques providing single-cell resolution of antioxidant and inflammatory activities, coupled with functional studies of cell populations. The main focus of this thesis is to investigate the cellular responses to acute inflammatory cytokine signalling and plant derived antioxidant compounds, in order to determine how these stimuli lead to the modulation of Nrf2 and NF-κB crosstalk and provide information about the layers of molecular interplay involved in maintaining the balance between them.

2. METHODS

2.1. Generation of Fluorescent Expression Plasmids

2.1.1. Gateway Recombination Cloning

Gateway Recombination Cloning Technology (Invitrogen) was used according to manufacturer's instructions to generate plasmids for expression of fluorescent proteins fusions. Gateway cloning system allows a rapid, site-specific recombination of gene targets into multiple expression vectors (Hartley *et al,* 2000). First, the desired gene targets were amplified using high-fidelity Hot Start KOD polymerase (Merck Millipore, 71086) from plasmids encoding the genes of interest or from a cDNA library using reaction conditions and PCR program as stated in **Table 2.1**. The gene specific primers used to amplify the inserts were contained the flanking *attB* recombination sequences allowing insertion into specific sites of Gateway compatible vectors (**Table 2.2**). The amplified PCR products of correct size were recombined into pDONR223 donor vectors using Gateway BP Clonase II kit (Invitrogen, 11789-020). Briefly, 2-3µl of the PCR amplified product (~200ng) and 200ng of the pDONR223 plasmid were mixed with 2µl 5x BP Clonase™ reaction buffer and topped up with ddH_2O to 10µl, mixed and incubated overnight at 25ºC (~16h). The following morning 0.5µl of Proteinase K was added to terminate the reaction and sample was further incubated at 37ºC for 10min and placed on ice until bacterial transformation or stored at -20ºC.

KOD Reaction Mix [25ul]	KOD PCR Cycle
• Template: 10ng plasmid DNA template (or up to 200ng cDNA library) • 2.5µl dNTP (2mM stock) • 1.5µl $MGSO_4$ (25mM stock), • 0.5µl KOD Polymerase (1U/µl) • 0.5µl Forwards primer (10µM stock)	1. 95ºC 2min 2. 95ºC 30sec 3. 58-65ºC 1min 4. 70ºC 0.5-2min (extension speed 5sec/1kbp) 5. Repeat step 2 to 4, (29x) 6. 4ºC storage

• 0.5µl Reverse primer (10µM stock) • 2.5µl of 10x Reaction buffer	

Table 2.1 The KOD PCR reaction conditions and cycling parameters.

Target	Forward Primer	Reverse Primer
GFAP (promoter)	*ATCCAGTTTGGTTAAT* GTCTGTAAGCTGAAGACCT G	*TCGACTGCAGAATTCG GGTGCCCTGCCTCTGCGT*
NRF2 promoter	ATCCAGTTTGGTTAATTTT TCGGTGCTCCAGAGAAC	AGC GCT AGC GTC TAG GCT GAG GGC GGA CGC TGT GGT A
(hm)p65	gaattcacaagtttgtacaaaaaagcaggct ggATG GAC GAT CTG TTT CCC CTC	gtcgaccactttgtacaagaaagctggGT G TTA GGA GCT GAT CTG ACT C (with STOP)
		gtcgaccactttgtacaagaaagctggGT G GGA GCT GAT CTG ACT CAA AAG (w/o STOP)
5κB	ATCCAGTTTGGTTAAT CTA GGG GAC TTT CCG CTT G	TCG ACT GCA GAA TTCG TTTACCAACAGTACCGGAA TGC
LaminB1	gaattcacaagtttgtacaaaaaagcaggct ggATG GCGACTGCGACCCCCGTGC	gtcgaccactttgtacaagaaagctggGT G CATAATTGCACAGCTTCTA

Table 2.2 PCR primers used for amplification of genes of interest and incorporation using Gateway cloning system.

2.1.2. Bacterial Transformation

The Gateway BP reaction mixture was then transformed into an appropriate bacterial strain (**Table 2.3**). The chemically competent bacterial stocks were maintained at -80ºC as aliquots and were thawed on ice shortly before the transformation procedure. The appropriate amounts of reactions were added into the bacterial suspension, gently mixed and incubated on ice for 30min. The reaction was placed for 45sec at 42ºC water bath to heat shock bacterial cells and then placed back on ice for 2min. Next, 250µl of SOC media (Invitrogen) was added and sample was then placed at 37ºC into horizontal orbital shaker at 220rpm for 1h. The transformation reaction was plated onto appropriate solid selection media (**Table 2.5** and **2.6**) and cultured at 37ºC overnight to allow growth of bacterial colonies.

Transformation Substrate	Quantity Required	Bacterial Strain	Vol of bacterial suspension	Solid media and the volume of the reaction plated
BP reaction product	2µl (40ng)	Alpha-Select (Bioline, BIO-85027)	30µl	2xTY agar, 200µl
LR reaction product	2µl (~20ng)	DH5α™ (Invitrogen, 18265017)	30µl	2xTY agar, 200µl
In-Fusion reaction product	1-2ng	One shot® Stbl3™ (Invitrogen, C7373-03)	50µl	LB agar, plated 100µl
Empty pDONR223 vectors (no insert)	50ng	One shot ccdB Survival™ T1^{R} *E.coli* (Invitrogen, #A10460)	50µl	2xTY agar (+Spectinomycyn)

Fluorescent expression plasmids	10ng	DH5α or Stbl3	30µl or 50µl	2xTY or LB agar, plated 50-100µl

Table 2.3 Bacterial strains and reaction conditions used for transformation of target constructs.

2.1.3. Bacterial Colony PCR (BCPCR)

The bacteria transformed with generated clones were grown on solid selective media and screened for successful insertion of the desired DNA fragment by bacterial colony PCR (BCPCR) using BIOTAQ™ Polymerase kit (Bioline, BIO-21040) according to manufacturer's instructions and applying aseptic technique. The colonies were picked with a sterile toothpick, which was sequentially immersed in the PCR reaction mix and then in the 25µl of Luria-Bertani (LB) media containing appropriate selection antibiotic for subculture. The PCR was then run as stated in **Table 2.4.**

BIOTAQ Polymerase Reaction [10µl]	BIOTAQ Polymerase PCR Cycle
• Template: bacterial colony • 0.7µl Forward primer (10µMstock) • 0.7µl Reverse primer (10µM stock) • 0.25µl dNTP (25mM stock) • 0.4µl MgCl2 (50mM stock) • 1µl 10x NH_4 reaction buffer • 0.05µl BIOTAQ polymerase • 6.9µl ddH_2O	1. 98ºC for 5min 2. 95ºC 1min 3. 55ºC 1min 4. 72ºC 1-2min (30s/1kb extension speed) 5. Repeat steps 2-4, (34x) 6. 15ºC to finish

Table 2.4 BIOTAQ PCR reaction conditions and cycling parameters.

The PCR products were then combined with Orange G stain and run on 1% agarose gel (the concentration of agarose was adjusted to the size of expected product bands) containing 1:20000 SYBRsafe DNA stain (Life Technologies, #S33102) alongside Hyperladder 1kb (Bioline, BIO-33053), in 0.5xTBE buffer (Fisher Scientific, #10031223) at 110V for ~45min. The bacterial colony stocks from which band of correct size was amplified by PCR were propagated for further DNA amplification and DNA purification using PureYield™ Plasmid Miniprep kit (Promega, A1223) according to manufacturers instructions. The purified DNA was then sent off for sequence verification.

2.1.4. Verification of Plasmid Quality

The plasmid concentration of all obtained DNA stocks were verified using NanoDrop Lite Spectrophotometer (Thermo Fisher Scientific) at 260nm excitation. The ratio between the DNA and protein contaminants at 260nm to 280nm emissions respectively, was usually around 1.8 value indicating high plasmid purity.

2.1.5. Sequencing

Generated vectors containing desired inserted sequences were sequence verified using GATC sequencing service (GATC Biotech, Germany) using forward and reverse primers (designed to anneal 100bp upstream of gene insertion). The correct open reading frame of the insert was and aligned with known gene sequence using Nucleotide BLAST (http://blast.ncbi.nlm.nih.gov/Blast.cgi) and Clustal Omega alignment tool online (http://www.ebi.ac.uk/Tools/msa/clustalo/).
Sequence verified clones were then amplified from a single bacterial colony and their DNA purified using HiSpeed Plasmid Maxi Kit (Qjagen, 12662) according to manufacturer's instructions.

2.1.6. Preparation of Glycerol Stocks

The stocks of sequence verified clones were stored in form of purified DNA and additionally as bacterial glycerol stocks made using 80µl of 80% sterile glycerol and 200µl of appropriate bacterial suspension (aliquoted from bacteria used for DNA

extraction previously). These were briefly vortexed and kept at -80ºC. When more plasmid DNA was needed the glycerol stocks were thawed on ice and streaked out on selective solid media to obtain single colony, which was further propagated for DNA purification.

2.1.7. LR Reaction

The Entry vectors generated as a result of BP cloning contained gene targets flanked with *attL* recombination sites that could be easily flipped into the Destination expression vectors containing the *attR* sites during LR cloning reaction. For the purpose of this study Gateway compatible fluorescent Destination expression plasmids were chosen in to visualize the distribution of the proteins of interest in live cells. The Entry vectors used were either conventional mammalian expression systems (Gateway, Invitrogen) or plasmids allowing production of lentiviral particles for stable gene expression as stated in **Table 2.8**. The construction of Gateway compatible lentiviral transfer fluorescent plasmid backbones was described previously (Bagnall *et al,* 2015) and the empty Entry clones were kindly gifted by Dr. James Bagnall (Paszek lab, University of Manchester). The LR reaction was performed using Gateway LR clonase II kit (Invitrogen, 11791-100) by combining 100ng of generated pDONR223(+appropriate insert) with 100ng of appropriate fluorescent entry vector *e.g.* EGFP-Entry and 1µl of the LR clonase II mix (Invitrogen) and topped up with ddH_2O to 5µl of the final reaction volume. The mixture was then briefly mixed and incubated at 25ºC overnight and the next morning 0.5µl of Proteinase K was added and tube placed at 37ºC for 10min to terminate the reaction and deactivate the enzymes. Then the reaction mix was transformed as stated in **Table 2.3** and processed as previously (Section 2.1.2) with BCPCR (Section 2.1.3) and insert sequencing (Section 2.1.5). The lentivirus compatible vectors contain LTR regions, which are highly unstable, were amplified in *E.coli* Stbl3 cells (Invitrogen), which reduce the occurrence of viral plasmid recombination events.

2.1.8. Bacterial Media

Media for culture of bacterial trains for DNA plasmid cloning and purification were prepared using aseptic technique and prepared using components stated in **Table 2.5** and when necessary using appropriate selection antibiotic at concentration stated in **Table 2.6.**

Media	Components	Purpose
LB (liquid)	5g Tryptone 2.5g Yeast Extract 5g NaCl Top up with ddH_2O up to 500ml	Culture of bacteria transformed with viral transfer vectors
2xTY (liquid)	10g Tryptone 5g Yeast Extract 5g NaCl Top up with ddH_2O up to 500ml	Culture of bacteria transformed with Gateway compatible vectors
LB (solid)	5g Tryptone 2.5g Yeast Extract 5g NaCl 10g Agar Top up with ddH_2O up to 500ml	Selection of bacteria containing viral transfer vectors, following appropriate supplementation with antibiotics
2xTY (solid)	10g Tryptone 5g Yeast Extract 5g NaCl 10g Agar Top up with ddH_2O up	Selection of bacteria transformed with Gateway compatible vectors

	to 500ml	

Table 2.5 Growth media used for bacterial culture.

Antibiotic (stock)	Final concentration in media
Spectinomycin (50mg/ml in ddH_2O)	50µg/ml
Kanamycin (50mg/ml) in ddH_2O)	50µg/ml
Ampicillin (100mg/ml in ddH_2O)	100µg/ml

Table 2.6 The concentration of antibiotics used in selective bacterial growth media.

2.1.9. Genomic DNA Extraction

The fluorescent protein fusions encoded in lentiviral fluorescent Entry vectors were driven by high expression Human Ubiquitin C (*UBC*) promoter. For designing endogenous promoter driven mouse Nrf2 protein fusions it was necessary to amplify the *NRF2* gene promoter from the mouse genomic DNA template. The genomic DNA was extracted from primary cortical astrocytes cultured as described in Section 2.4.3, using ZR-Duet™ DNA/RNA MiniPrep kit (Zymogen, D7001) according to manufacturers instructions. The 70% confluent monolayer of astrocytes was briefly washed twice with warm DPBS and lysed in 100µl DNA/RNA lysis buffer and preceded as described in manufacturer's protocol with spin column purification steps. The genomic DNA was eluted twice using 50µl in RNAse/DNAse free water with yielding 20ng/µl (~2µg total) genomic DNA.

2.2. In-Fusion Cloning

2.2.1. Insert Amplification

The In-Fusion cloning technology was primarily used to insert specific promoter sequences into fluorescent lentiviral Entry vector backbones to report on changes in the transcriptional regulation of Nrf2 protein (*2kb*-Venus-msNrf2) or κB repeats (5xκb-Venus) or to label specifically astrocyte cell populations using glial fibrillary acidic protein (GFAP) promoter-driven fluorescent protein fusions (*GFAP*-Cyan, *GFAP*-LaminB1-Cyan) (see Supplementary Section Figure 8.2 for Maps). The insertion of promoter sequences into the *2kB*-Venus-msNrf2 and the *GFAP*-Cyan and *GFAP*-LaminB1-Cyan and 5xκB-Venus was performed by directional, seamless In-Fusion cloning technique according to the Clontech manual (Takara Bio). The *NRF2* promoter sequence was amplified from the mouse genomic DNA (genomic DNA extraction described in Section 2.1.9) to create the *2kB*-Venus-msNrf2. To amplify the *GFAP* promoter sequence the pDRIVE-ms*GFAP* plasmid was purchased from Invivogen Europe, using custom-designed primers (primer sequences in **Table 2.1**) and the NF-κB-Luc construct (**Table 2.8**) was used as a template to amplify the 5xκB repeats. The insert sequences were amplified using the Clone Amp HiFi PCR Premix (Clontech, Cat. No. 639298) using the reaction mixture and the PCR cycle as stated in **Table 2.7** below.

HiFi PCR Reaction Mix [25ml]	HiFi PCR Cycle
• Template: 1ng plasmid or 10ng murine genomic DNA • 12.5µl HiFi PCR Premix (Clontech) • F primer 0.75µl [10µM stock] • R primer 0.75µl [10µM stock] • Top up with ddH_2O	1. 98ºC for 2min (denaturation) 7. 98ºC for 10sec (denaturation) 8. 58-62ºC for 15sec(annealing) 9. 71ºC for 5-30sec (extension, HiFi speed 1kB/5sec) 10. Repeat step 2 to 4, (34x) 11. 72ºC 5min 12. 4ºC

Table 2.7 The HiFi PCR reaction conditions and cycling parameters.

The amplified PCR products were analysed on an agarose gel (Section 2.1.3) and obtained DNA bands of correct size (2kb for *NRF2* promoter, 1.6kb for the *GFAP* promoter, 120bp for 5κB repeats) were then purified directly from the PCR reaction mixture using the Nucleospin Gel & PCR Cleanup (Macherey-Nagel, #740609.50) kit accordingly to the manufacturer's protocol. The purified PCR product was then eluted in 30µl of DNAse free ddH_2O and the obtained concentration was measured using the Nanodrop spectrophotometer (Section 2.1.4).

2.2.2. Vector Linearization

The fluorescent, lentiviral transfer Entry vectors used to insert the promoter sequences were first linearized at desired sites using NEB restriction enzymes PacI and BstBI to remove the *ccdB* cassette and the *UBC* promoter (see Figure 8.2 in the Supplementary). The double digest was performed on 50µg of purified plasmid using 5µl PacI, and 8µl of the 10x Smart Cut buffer (NEB, B7204S) in total reaction volume of 80µl. The PacI digestion was performed for 1h at 37ºC and then 5µl of BstBI restriction enzyme was added and the temperature of incubation increased to 65ºC for another 1h. To purify the linearized vector, the entire reaction volume was run on 0.8% agarose gel and the obtained restriction products were illuminated in the dark room using UV platform at long wavelengths settings to minimize UV-induced DNA mutations. The band representing the correct linearized vector template was then cut out from the gel using scalpel and placed into a pre-weighted Eppendorf tube. The DNA was extracted using Nucleospin Gel & PCR Cleanup kit and the concentration of purified sample was measured using NanoDrop Lite Spectrophotometer.

2.2.3. The In-Fusion Reaction

The molar ratios of insert to vector used for the In-Fusion reaction were estimated

using In-Fusion Molar Ratio Calculator tool online: http://bioinfo.clontech.com/infusion/molarRatio.do and appropriate quantities of the purified insert and the target vector were then combined with 2µl In-Fusion HD Enzyme Premix (Clontech, 638917) in a total reaction volume of 10µl. The tube with the reaction was placed at 50ºC for 15min and then cooled on ice and used for bacterial transformation (**Table 2.3**), sequencing (Section 2.1.5) and DNA amplification and purification using Maxi/MiniPrep (Qjagen) according to the manufacturer's protocol.

2.3. List of Plasmids Used

The **Table 2.8** below provides a list of generated fluorescent protein expression plasmids using Gateway and In-Fusion cloning techniques described below. The maps main vector maps generated in this project are attached in the Supplementary Section 8.3.

Plasmids Used	LENTIVIRAL (Y/N)?	Purpose	Source/Generated By
RFP-(ms)p65	Y	Imaging	Gateway cloning
RFP-(hm)p65	Y	Imaging	Gateway cloning
Venus-(ms)Nrf2	Y	Imaging	Gateway cloning
2kb-Venus(ms)Nrf2	Y	Imaging	Gateway and In-Fusion cloning
Cyan-(ms)Keap1	Y	Imaging	Gateway cloning
5xκb-Venus	Y	Imaging	In-Fusion cloning
GFAP-Cyan	Y	Imaging	In-Fusion cloning
GFAP-LaminB1-Cyan	Y	Imaging	In-Fusion and Gateway cloning
mCherry-Keap1	N	Imaging	Amy Ponsford/Gateway cloning
p65-DsReDXP	N	Imaging	White lab (Ashall *et al*, 2002)
Venus-Nrf2	N	Imaging	Dr. Karen Dunn (previously

			Sanderson/White labs)
NF-κB-Luc	N	Luciferase assay	Stratagene (USA)
8xARE-Luc (pGL4.11)	N	Luciferase assay	Dr. Joanne Walsh, Pharmacology (Kratschmar *et al*, 2012)
pNRF2-luciferase	N	Luciferase assay	MacEwan's lab (Rushworth *et al*, 2012)
ΔκB2-luciferase	N	Luciferase assay	MacEwan's lab (Rushworth *et al*, 2012)
pDendra2-Nrf2	N	Protein stability imaging	Gateway cloning
pDendra2-MARCH5	N	Protein stability imaging	Dr. Robert Jenn
pGL4.0-Luciferase	N	Luciferase assay (control)	MacEwan's lab
FUW-EGFP-p65 (mouse p65 promoter, human p65 gene)	Y	Imaging	Dr. James Bagnall (Paszek lab) University of Manchester (Bagnall *et al*, 2015)

Table 2.8 List of plasmid used for imaging and dual luciferase experiments.

2.4. Primary Cell Culture

2.4.1. Preparing Glass Coverslips for Neuronal Culture

The immunocytochemistry of neuronal cultures required culture of cells on specially prepared glass coverslips. The coverslips used for primary culture were made by Thermo Scientific Gerhard Menzel, 16mm diameter, 0.13-0.17mm thick (Fisher Scientific, 12332138). They were extensively cleaned in concentrated 70% nitric acid (Sigma-Aldrich, 438073-500ML) in 100ml glass Duran® bottle placed overnight on a rocking platform. The next day the coverslips were transferred to ddH_2O and rinsed thoroughly until the solution reached neutral pH. The coverslips were then placed in 70% EtOH and sonicated in a plastic sterile beaker in a sonicator

water bath for 15min and stored in the fridge for up to a month. Before use they were extensively washed individually in sterile ddH_2O in a Petri dish and then placed in a second Petri dish to air dry, ready for coating with a Poly-D-lysine (PDL) substrate. The coating was performed using sterile 0.1mg/ml PDL (Sigma-Aldrich, P0899) in 50mM borate buffer (Fisher Scientific, 10638294) for 1.5h at RT (or 16h in the tissue culture (TC) incubator), about 120µl of this solution was enough to cover the surface of 16mm diameter coverslip. The coverslips were then washed four times in sterile ddH_2O and placed in 6-well plate (2 coverslips p/well) with remaining water aspirated from around the coverslip and covered with 120µl of plating medium (**Table 2.11**) and placed in the tissue culture (TC) incubator, ready for cell plating the next day.

The 35mm dishes used for live cell imaging did not need to be cleaned with nitric acid, but required coating with PDL (2ml of 0.1mg/ml per dish) and washing afterwards as described, the same applied to 6cm dishes used for culture of cells for Western Blot analysis.

2.4.2. Neuron-Astrocyte Cultures

Mixed hippocampal astrocyte-neuron cultures were prepared from embryonic E19 to postnatal P1 pups from C57BL6J mice as described by Kaech & Banker, with minor modifications (Kaech & Banker, 2006). The hippocampi were collected under light microscope into ice-cold Dissection medium (**Table 2.11**), the procedure did not usually take longer than 1h. The tissue was then placed in Dissection media containing 0.25% Trypsin (**Table 2.11**) (Life Technologies, 15090046) for up to 10min at 37ºC. The trypsin was decanted and tissue was gently washed in cold 10ml Plating medium (**Table 2.11**). The hippocampi were then transferred to 3ml of cold Plating medium and triturated with glass Pasteur pipettes with two different bore sizes. The cell suspension was passed through 100µm nylon mesh (Fisher Scientific, 11517532) to remove any cells clumps. The cell viability was assessed by trypan blue staining by mixing cell suspension with 0.4% (w/v) trypan blue dye (in PBS) at 1:1 ratio (cells to 0.4% trypan blue). Only cells that did not take up the dye were counted and the suspension was plated onto previously prepared glass or plastic surfaces. For imaging purposes the isolated cells were plated at 0.35-0.45x10^6 cell

p/ml in 35mm CELLview™ imaging dish (Greiner Bio-One, 627870 or 627860), or 120 µl (250,000 c/ml density) directly onto 16mm glass coverslip.

The cells were then allowed to attach in Plating medium containing serum (**Table 2.11**) for 16-24h to encourage some astrocyte growth. All media was always pre-equilibrated in the TC incubator to contain the right amount of CO_2 and the temperature before it was applied to primary cells. The next day the Plating media was changed to Neurobasal media (**Table 2.11**) and the cultures were fed every 4-5 days by changing half of the media following next two weeks of culture and then fed once a week with 30% media change. The imaging experiments were performed on mature neurons around 14^{th}-17^{th} day *in vitro* (DIV14-17).

For neuronal cultures with smaller astrocyte numbers, the cultures were prepared from earlier E16 embryos and the plating step with serum was shortened to only two hours.

2.4.3. Culture of Primary Astrocytes

To obtain enriched hippocampal and cortical astrocyte cultures it was important to appropriately coat all the plastic or glass surfaces in advance of the dissection or passaging procedures. The coating was performed using sterile filtered PDL stock at 0.1mg/ml as described in Section 2.4.1.

Hippocampal and cortical astrocyte cultures were obtained from C57BL6J mice or $Nrf2^{-/-}$ knockout mice at postnatal day 1-2 (P1-P2) using hippocampi or cortices as previously described by Kaech & Banker with some modifications. The Nrf2 knockout mice were kindly provided by Dr. Kitteringham's group in the Pharmacology Department (University of Liverpool); being previously generated by M. Yamamoto (Itoh *et al,* 1997). The dissection procedure was performed as described previously (Section 2.4.2). Following the digestion of isolated tissue samples in Dissection media, the tissue was placed in cold Astrofood media (**Table 2.11**) and gently rinsed by inverting the tube several times to inactivate trypsin activity. To obtain single cell suspension the tissue was further triturated 15 times using flame polished glass Pasteur pipettes and passed through 100µm nylon mesh tissue strainer. The cell suspension was then spun down at 1500rpm for 5min and re-suspended in cold 5ml Astrofood media and viable cells were counted using trypan blue staining and plated onto PDL-coated T75 flask immersed with 20ml Astrofood.

The next day, media was exchanged following vigorous tapping of the flask to remove any adherent microglial cells that usually grow on top of astrocytes and fed every 3-4 days by changing the media completely, every-time following vigorous shaking. The flask was usually fully confluent within 7-9 days.

Astrocyte culture was passaged after the cell monolayer reached about 80% confluence, up to two times for subculture for experiments. For passaging, the astrocytes were washed twice with pre-warmed DBPS (w/o Ca^{2+} and Mg^{2+}) and then the flask was filled with 10ml 0.05% Trypsin-EDTA (Invitrogen, 25300054) and 8ml was rapidly removed and the flask placed for ~5min to the TC incubator. When the cells rounded up as a result of trypsin activity, they were removed using cell scraper (Greiner Bio-One). The astrocytes attached firmly to coated surfaces and scraping dramatically increased the cell yield after passaging. The astrocytes were seeded usually at $0.5x10^6$ p/6cm dish for western blotting or directly onto glass surface of 35mm imaging dish at $0.12x10^6$ cells.

2.4.4. Viability Assay

To assess the toxicity of drug treatments on primary and cancer cell lines the cellular viability was measured using CellTiter-Glo (Promega) ATP based assay according to manufacturer's instructions. The cells were plated onto 96-well tissue culture treated white walled plate (**Table 2.12**) and cultured for at least a day before treatment with pharmacological compounds. Following desired incubation time the plate was equilibrated at RT for 30min and 120µl of CellTiter-Glo Buffer (1: 1 (v/v) reagent to cell media ratio) was added to each well using multichannel pipette and the sealed plate was shaken vigorously in an orbital shaker for 2min. The luminescence readings were then taken using GloMax-Multi Detection System (Promega) at RT and results were compared to untreated and positive control samples (0.1% Triton-X treated cells).

2.4.5. Transfection of Primary Cells

The primary astrocyte cells were transfected for live-cell imaging or for dual luciferase assays using purified plasmid stocks. For live cell imaging experiments the cells were seeded at $0.1x10^6$ cells p/35mm imaging dish and transfected when they

reached 60% confluence. The Astrofood media was changed to serum free Astrofood about 1h before the transfection, as serum was found to inhibit effective transfection in primary astrocytes (personal observations). The transfection was performed by placing desired amount of Lipofectamine2000 according to manufacturer's protocol at 1µl of reagent per 1µg of plasmid DNA into tube containing Opti-MEM medium (Invitrogen, 11058021) for 5min, then the required plasmid DNA was added and incubated for further 15min at RT. The transfection reaction was then dropped onto cells and incubated for 2h, and following the incubation period the media was changed back to full Astrofood and incubated for another 24h.

Plasmid	Purpose	Concentration
mCherry-msNrf2	Live cell imaging	2µg/ml
mCherry-UBE2D2	Live cell imaging	2µg/ml
RFP-p65 (mouse variant)	Live cell imaging	2µg/35mm dish
EGFP-p65 (mouse variant)	Live cell imaging	2µg/35mm dish
pGL4.11 ARE-Luc/NF-κB-Luc	Dual luciferase	0.5µg/well (24well format)
SV40-Renilla	Dual luciferase	0.025µg/well (24well format)
Fluorescent fusion proteins	Dual luciferase	0.5µg/well (24well format)

Table 2.9 The quantity of plasmids used for imaging and dual luciferase studies on primary cells.

2.4.6. Dual Luciferase Assay

The Dual-Luciferase Reporter assay (Promega, E1960) was used to monitor the transcriptional activity of selected gene sequences driving the expression of firefly luciferase following pharmacological treatments or transient expressions of plasmid encoding proteins, in accordance to the manufacturer's instructions.

The luciferase-based reporter plasmid expressing Firefly luciferase and Renilla luciferase (*SV40*-Renilla) transfection control were transfected as stated in **Table 2.9**. Following 24h and after desired drug incubation time the cells were processed for dual luciferase assays. The cells were gently washed twice using warm DPBS and then lysed in 100µl of 1x passive lysis buffer (PLB) and mixed at RT for 15min. The collected cell lysates were placed in Eppendorf tubes and spun down at 12,000rpm for 1min at RT. The supernatant was then transferred to a 96-well plate, sealed and frozen at -20ºC for up to a week. Before, the luciferase assay, the Luciferase Assay Reagent II (LARII) and Stop & Glo (S&G) reagents were defrosted in the dark until they reached RT (for ~1,5h) and appropriate amounts were transferred to 15ml Falcon tubes to be used in the assay. The cell lysates were also equilibrated at RT and 20µl was transferred to 96-well white plate for luminescence reading. The assay was performed in GloMax machine following cleaning of the inlet tubing that was used for dispensing the LARII and the S&G reagents. The 100µl of reagents was added p/well and the reading taken following 10s of reagent addition.

2.4.6.1. Dual Luciferase Data Analysis

The Luciferase luminescence signal was normalized to Renilla luminescence readings (from the same sample) and the average ratio from the technical triplicate measurements was then obtained, the fold change was calculated by comparing each sample to the untreated control. The mean values were then plotted using GraphPad Prizm 5 with error bars representing the standard deviation of the mean and compared using student t-test (for comparison of two means) or One-Way Anova with Tukey's post-hoc analysis (for comparison three and more means). The statistical significance of the P-values were denoted as follows: 0.01-0.05=*; 0.01-0.001=**, 0.001-0.0001=*** and P value< 0.0001=****.

2.5. Immunocytochemistry

The primary neuron-astrocyte or pure neuronal cultures were grown on glass coverslips in a 12-well or 6-well plates as described before (Section 2.4.1, 2.4.2). To visualize the cell-specific markers or the localisation of proteins of interest the

primary cells were immunostained following at least 14 days *in vitro* (DIV). The cells were gently washed twice in warm PBS (with Ca^{2+} and Mg^{2+}) and then fixed using the paraformaldehyde fixing solution (4% fresh paraformaldehyde, 3% sucrose in PBS) for 10min. Cells were briefly washed 2x with PBS and permeabilised using 0.15% Triton-X in PBS for 15min and the permeabilising solution was replaced with fresh PBS and washed three times and incubated in serum from the host of the secondary antibody to minimize the non-specific staining. The 5% goat serum was used (GIBCO) in PBS for 30-60min to block the non-specific interactions and then the primary antibody of choice was applied (**Table 2.10**) in 5% goat serum/PBS for 1h at room temperature (RT) or overnight at 4ºC in a humidified box. This was usually performed on coverslips placed on a parafilm in a sealed box with the antibody solution placed directly on top of cells (usually 80µl of diluted antibody is enough to cover 16mm diameter coverslip) in a humidified atmosphere. The primary antibody was then washed away by placing the coverslips back into the 12-well plate and replacing the PBS solution three times. The fluorescence-labelled secondary antibodies (**Table 2.7**) (Jackson ImmunoResearch) were used to visualize the primary antibody staining at 1:1000 concentration in 5% goat serum in PBS, in the dark for 45min at RT. Following the incubation, the coverslips were gently washed with fresh PBS three times and then briefly dipped into the ddH_2O and left to dry in the dark for about 20min. The coverslips were then mounted in ProLong Gold Antifade with DAPI (Invitrogen, P36931) on glass slides and left to set in the dark overnight at RT and then placed in a storage box at 4ºC until the imaging (usually within a week).

Antibody	Species/Company	Dilution	Purpose
CD11b	Rat, AbCam Ab7260, Pn	1:300	Microglial marker
GFAP	Rabbit , AbCam Ab8878, Pn	1:300	Astrocyte marker
β Tubulin III	Mouse, Promega G7121, Mn	1:1000	Neuronal marker
α Tubulin	Mouse, AbCam, ab7291, Mn	1:500	Visualization of tubulin filaments
p65/RelA	Rabbit, Santa Cruz sc-372, Pn	1:300	Visualization of p65
PML	Rabbit, Santa Cruz, sc-766, Pn	1:200	Visualization of PML

Secondary antibodies	Anti-Goat (Jackson ImmunoResearch)	1:1000	Visualisaiton of primary antibody staining

Table 2.10 The list of antibodies and their concentrations used in immunocytochemistry.

2.6. Production of Lentivial Particles

The lentiviral transfer vectors containing fluorescent protein fusions were generated using Gateway and In-Fusion cloning approaches as described previously (Section 2.2. & 2.1). All practices were carried out according to detailed health and safety rules and established standard operating procedures. The 3rd generation lentivirus packaging system was used with compatible transfer vector expressing the protein fusion of interest as described previously by Tiscornia *et al, 2006;* with minor modifications. The HEK293 cells were used for producing the lentiviral particles and for this purpose they were maintained in DMEM supplemented with P/S, sodium pyruvate, 10% FBS, GlutamaX (not older than passage 15) (**Table 2.11**). The $6x10^6$ HEK293 cells were seeded onto 15cm dishes in the late afternoon and the next day (late afternoon) the cell media was exchanged 2h before the transfection (the confluence should be around 40-50%, but for each construct should be determined empirically) The transfection reaction was made up for 5x 15cm dishes (or scaled-up equivalently) into 50ml falcon tube in the following order: 112.5µg of fluorescent transfer vector (*e.g. 2kb*-Venus-msNrf2) and packaging plasmids 39.5µg VSVG plasmid, 73µg REV plasmid, and 73µg RRE plasmids dropped into 3.3ml 0.1x TE buffer; then added 1.75ml buffered water (50ml ddH_2O with 125µl of 1M HEPES, pH 7.3, filter sterilised). Next, added 565µl of 2.5M $CaCl_2$ (9.8g $CaCl_2*2H_2O$ in 25ml ddH_2O, filter sterile, store -20ºC) and mixed by pipetting. The 5.7ml 2xHeBS (Sigma) buffer was added last and the transfection reaction vortexed thoroughly, until fine precipitate was visible. This reaction mixture was incubated at RT for 15min and 2.25ml dropped into HEK293 culture and gently mixed until the medium achieved uniform colour.

The media was collected early the next morning and replaced with 17ml of fresh DMEM, discarding the old media. The first batches of lentiviral particles were collected at ~40h post-transfection, and then second and final collection took place

again after 64h post-transfection. The media containing lentivirus was spun down at 1500rpm for 5min to remove any detached cells and additionally filtered through 0.22µm PES filter. The lentiviral media was further concentrated using ultracentrifugation so that only small volumes of stocks were used during transduction of primary cells to avoid changes in the growth medium composition. The medium containing lentiviral particles was concentrated in capped, polycarbonate thickwall ultracentrifugation tubes (Beckman Coulter, 355618), which were filled with minimum 16ml of media (capacity 26.3ml). The tubes were then balanced, as accurately as possible (within 10mg) using fine balance and next centrifuged in ultracentrifuge (Beckman Coulter) in Ti50.2 fixed angle rotor at 56,000g (25krpm) at 4ºC for 2h. The ultracentrifugation resulted in assembly of the viral particles in form of a pellet that could be harvested and re-suspended in small amount of PBS. For this purpose the media was aspirated using vacuum pump and the pellet obtained was washed off the tubes by adding 100µl sterile DPBS and gently pipetting and the tubes were gently rocked in the cold room overnight. The next morning the concentrated virus was aliquoted (5µl aliquots) flash frozen in liquid nitrogen and kept at -80ºC in sealed plastic bags, in cardboard storage boxes. Polycarbonate tubes are sensitive to UV light, EtOH, detergents and autoclaving therefore to sterilize them they were soaked in 10% H_2O_2 (Sigma-Aldrich) for 10 min and vortexed for 1min, and washed with plenty of sterile ddH_2O water, which was further aspirated and the tubes and caps were left to dry in the TC hood.

2.6.1. Transduction

The lentiviral infection took place around 5 days before (~DIV9-10) the imaging experiments (~DIV14-17), as the expression of lentivirally-transferred genes peaks following 64h from the transduction (Tiscornia *et al,* 2006), additionally this timing allowed the cells enough recovery from infection. Before the transduction procedure, the cells were fed by changing 50% media (saving the condition media in the fridge), and at the end of the day the concentrated virus (in PBS) was gently diluted in cell media and added to cells. The next morning the viral and plasmid DNA was digested using 10U of DNAse enzyme p/1µg of transfected DNA (Calbiochem, 260913) added to the cell media and incubated for 30min in the TC incubator to deactivate

any viral particles. The media was then changed to pre-conditioned media and cells cultured as previously stated.

2.7. Cell Culture Growth Media

Media name	Components	Purpose
Neurobasal (made up only 100ml at the time, kept up to 1month in the fridge)	Neurobasal (12348017) 2% (v/v) B27 Supplement (17504044) 0.5mM Glutamax (35050-061) 1x P/S (15140122)	1. Pure neuronal culture 2. Mixed astrocyte-neuronal culture
Astrofood	MEM (51200046) 10% Horse Serum, heat inactivated (26050-088) Glutamax 2mM P/S 1% 0.6% D-Glucose (20% stock in MEM stored -20ºC)	Culturing primary astrocytes WT and Nrf2 KO
Plating Media	Neurobasal media supplemented with 10% Horse serum	Plating neurons
Dissection Media	EBSS (w/o Ca^{2+} and Mg^{2+}) (14155048) 1% P/S 1% NaPyruvate (S8636-100ML) 10mM HEPES (15630056)	Dissection of hippocampus and Cortex
Trypsin Solution (Dissection)	1.5ml of 2.5% Trypsin 13.5ml of Dissection Media	Tissue digestion for single cell separation
$BAC^{Nrf2\text{-}Venus}$/SK-N-AS media	MEM 1% P/S 10% FBS (10270106) 1% Glutamax (2mM) 1% NEAA (11140035)	Culture of SKNAS and $BAC^{Nrf2\text{-}Venus}$ cells

HEK293T Medium	High glucose DMEM + NaPruvate, +Glutamax (31966047) 10% FBS 1% P/S	Culture of HEK293T cells for lentiviral production
Hepa1c7 Medium	DMEM 10% FBS 1% P/S	Culture of Hepa1c7 cells for testing anti-Nrf2 antibodies specificity

Table 2.11 Cell culture media components used for maintenance of primary and immortalized cells (all components from Invitrogen).

2.8. Cell Culture of SK-N-AS and BAC$^{Nrf2\text{-}Venus}$ Neuroblastoma Cell Lines

BAC$^{Nrf2\text{-}Venus}$ cells were generated previously by Dr. Karen Dunn (Sanderson and White lab) by stable integration of bacterial artificial chromosome (BAC) encoding Nrf2-Venus fluorescent protein fusion into neuroblastoma SK-N-AS cells, at 2 copies per cell. The wild-type SK-N-AS and BAC$^{Nrf2\text{-}Venus}$ were maintained in supplemented MEM medium (**Table 2.11**) in a humidified atmosphere at 37ºC, 5% CO_2 and passaged every 3-4 days when the cell monolayer reached 80-90% confluence. For subculture, the cells were washed twice with pre-warmed DPBS (w/o Ca^{2+} and Mg^{2+}) and 2ml of 0.25% Trypsin-EDTA (Life Technologies, 15090046) was added onto cells and placed to TC incubator ~2min to allow the cells to detach. The cells were collected by adding 8ml pre-warmed media and spun down for 3min at 200G. Cell media was then removed and pellet re-suspended in 10ml of fresh cell culture media and seeded onto desired flask/plate for further culture. The BAC$^{Nrf2\text{-}Venus}$ cells were used for up to 25 passages. The amounts of BAC$^{Nrf2\text{-}Venus}$ cells and vessels used for experiments are presented in **Table 2.12**, the SK-N-AS cells were scaled down by ~50% due to a higher growth rate.

Experiment	Vessel	Cell number	Experiment
Live cell imaging	35mm dish with glass bottom (Greiner Bio-one)	350,000 (for transfection) 500,000 (for imaging the next day)	Transfection or imaging following 24h
siRNA Live cell imaging	35mm dish with glass bottom (Greiner Bio-one)	200,000	Transfection following 24h
Immunocytochemistry	12 well plates	250,000	Fixing 24-48h later
Dual Luciferase	24 well plate	140,000	Transfection 24h later
Western Blot	6 or10cm plate	$1.2\text{-}2.4x10^6$	Drug treatment 48h later
Subculture	10 or 15cm plate	$1.5\text{-}3x10^6$	Passaging 64h later
Viability assay	96 well plate	90,000	Drug treatment next day

Table 2.12 The BAC$^{Nrf2\text{-}Venus}$ cell seeding densities used for experiments.

2.8.1. Transfections of Plasmids Encoding Fluorescent Fusion Proteins

Transient transfections were carried to introduce fluorescent protein fusions into target cells using Lipofectamine 2000 (Invitrogen) according to manufacturer's protocol. For transient expression of p65-DsRedXP construct of cells cultured in 35mm dish, 0.5μg of Maxi-prepped DNA stock was used alongside 0.5μl of Lipofectamine 2000 for imaging the next day.

2.8.2. Keap1 Gene Silencing Using siRNA

To silence the expression of the Keap1 protein, short interfering RNA (siRNA) duplexes targeting human Keap1 (siKeap1) (SMARTpool ON-TARGETplus Keap2 siRNA, Darmacon, L-012453-00-000) were transfected at 10nM final concentration alongside a scrambled control (siCTR) siGENOME Non-Targeting siRNA Pool nº 1 (Dharmacon, D-001206-13-05). For imaging experiments using 4-compartment 35mm glass bottom dishes (Greiner Bio-One, 627870) two reactions were prepared each with 50µl Optimem, 1µl of RNAiMax Lipofectamine (Invitrogen, 13778-100) and then 1µl of 10µM siRNA (siCTR or siKeap1) and incubated 5min at RT. Dropped 25µl p/chamber (each with 500µl media, feed just before the transfection) and incubated for 48h before the live cell imaging experiments.

2.8.3. Cryogenic Storage of SK-N-AS and BAC$^{Nrf2\text{-}Venus}$ Cells

To prepare frozen cell stocks, the cells were cultured in 15cm dishes to achieve 80-90% confluence and collected as described before (Section 2.8). The cell pellet was then resuspended in 7ml SK-N-AS media containing 10% dimethyl sulfoxide (DMSO) (Sigma-Aldrich, D8418-50ML) and 0.7ml of cell solution was aliquoted ($1.5x10^6$ cells) into externally threaded cryotubes (Alpha Labs, LW3532) and frozen in NAGLENE™ Cryo freezing container filled with 100% isopropanol and placed at -80ºC. Following at least 16h the cryotubes were transferred to gas phase liquid nitrogen crystore.

2.8.4. Thawing Cell Stocks

To defrost the stocks cells the cryotube with cells was placed on briefly on ice and then immersed into the water bath at 33ºC until for 1-2min (until only small ice clump was visible in the tube). The cell suspension was then gently transferred into 9ml of pre-warmed cell media and spun down at 220G for 4min. The cell pellet was then resuspended in fresh media and plated into 6cm dish. Following the 24h the cell media was then replaced with fresh media solution.

2.9. Q-PCR

2.9.1. Q-PCR Primer Preparation

The gene specific primers used for quantitative polymerase chain reaction (Q-PCR) analysis were designed using Vector NTI based on the coding sequence of the gene targets (**Table 2.13**). The following primers were generated and synthesized by Invitrogen, and kept at stock concentration of 100μM in RNAse and DNAse free diethylpyrocarbonate (DEPC)-treated and UV-treated (30min) water. The efficiency of target amplification of each primer pair was measured by Q-PCR by plotting standard curve of the Ct threshold from cDNA sample serial dilutions (1:1, 1:10, 1:100, 1:1000, 1:10000 and no-template control (NTC) and calculating the reaction efficiency from the slope of obtained standard curve. Only primer pairs with reaction efficiency of target amplification of 100% (+/-15%) were used in this study.

Target/gene bank name	F sequence (5'-3')	R sequence (5'-3')
Nrf2	GAGAGCCCAGTCTTCATTGC	TGCTCAATGTCCTGTTGCAT
HMOX-1	CCCACGCCTACACCCGCTAC	GGTGGCACTGGCAATGTTGG
NQO1	GGGCAAGTCCATCCCAACTG	GCAAGTCAGGGAAGCCTGGA
GCLC	GTCTTCAGGTGACATTCCAAGC	TGTTCTTCAATGGCTCCAGTC
SOD-2	TGCACTGAAGTTCAATGGTGG	CTTCCAGCAACTCCCCTTTG
IL-6	TGAACTCCTTCTCCACAAGCG	ATCTTCTCCTGGGGGTACTGG
IKBα	GATCCGCCAGGTGAAGGG	GCAATTTCTGGCTGGTTGG
IL-8	AGTGGACCACACTGCGCCAA	TCCACAACCCTCTGCACCCA
TRXDN	ATGTCATGTGAGGACGGTCGG	GGCCCCTATCTTTCTCTGTT

SFXN	GATCCGGGAGGACCCAGACA	CAAGGAGGCTGCTACTGCAA
BACH1	GGACACTCCTTGCCAAATGCAG	TGACCTGGTTCTGGGCTCTCAC
msNQO1	CGGCGAGAAGAGCCCTGA	GCAGCCTCCTTCATGGCGTA
msHMOX-1	CACGCCAGCCACACAGCA	ATATGCGTGGGCCACCAGCA
PML	CGCCCTGGATAACGTCTTTTT	CTCGCACTCAAAGCACCAGA
KEAP1	TACGATGTGGAAACAGAGACGTGGA	TCAACAGGTACAFTTCTGGTCAATCT
β-Actin	AGGCTGTGCTATCCCTGTACGC	ATGGGCACAGTGTGGGTGAC

Table 2.13 Primers used for Q-PCR expression measurements of selected, representative target genes

2.9.2. mRNA Extraction

The mRNA extraction was performed using RNAeasy (Qjagen) mRNA extraction kit. The cells (around $6x10^6$ cells) were collected as described previously (Section 2.8) the cell pellet was stored at -80ºC overnight. The pellets were placed on ice and re-suspended in 350µl RLT buffer and passed through a 21G syringe around 10 times. Next, 350µl of 70% EtOH was added (made up with RNAse and DNAse free water) and mixed by pipetting. The homogenate was transferred to a spin column and centrifuged at full speed for 30s. The column was washed with 350µl RW1 buffer and spun for 15sec at full speed, following this step the on-column DNAse was performed. The 80µl of the DNAse solution made of 10µl DNAse and 70µl RDD buffer (Qjagen) was dropped on top of the column and incubated for 15min at RT, then 350µl RW1 buffer was added and sample was centrifuged for 15sec at 9000rpm. The columns were washed twice with 500µl buffer RPE for 1min. The mRNA was eluted in 15µl RNAse and DNAse free water twice for 1min at max speed, the yield quantified using NanoDrop spectrophotometer and stored at -20ºC until the cDNA conversion step.

2.9.3. Converting mRNA into cDNA

The extracted mRNA was converted into cDNA using GoScript™ Reverse Transcription kit (Promega, A5000) according to manufacturer's instructions. The procedure was initiated by primer annealing using (1ul) OligodT primers and 2.5µg of mRNA sample in reaction volume of 4µl, which was further placed at 70ºC for 5min and then cooled on ice for 10min. The mRNA-OligodT primer mixture was then mixed with 15µl of GoScript reaction mix (4µl GoScript 5x Reaction Buffer, 4µl $MgCl_2$, 1µl PCR mix Nucleotide, RNAsin 0.5µl, GoScript RT 1µl and nuclease free water 4.5µl) and placed in the PCR block for the following cycles: 25ºC 5min, 42ºC 1h, 70ºC 15min. The reaction was diluted with 40µl of RNAse free water (final concentration ~320ng/µl), aliquoted (~8-10µl p/tube) and stored at -20ºC until the Q-PCR analysis.

2.9.4. Setting up Q-PCR Reaction

The Q-PCR reaction set-up was performed in specially designated Q-PCR hood with all the consumables UV-treated for 30min before the experiment. Each primer pair had a corresponding no-template control (NTC in triplicates) to test for DNA contamination of reagents. The reaction was set up using 20µl Precision MasterMix SYBR green (Primerdesign, PrecisionBlue-iC-SY), 0.8µM forward and reverse target-specific primers (2µl of 2µM stock), 2µl of target sample cDNA or 2µl of DEPC treated water (NTC) was added and topped up to a total volume of 40µl with DEPC treated ddH_2O. The reaction was performed in triplicated by aliquoting 10µl p/well of 96-well QPCR plate (BIO-RAD, HSP9645) using Bio-RAD (CFXconnect) realt-time PCR detection system. Cycling parameters are described in the **Table 2.14**.

Step	Temperature [ºC]	Duration [s]	Cycles
Denaturation	95	120	1
Amplification	95	15	2x39

(Denaturation/Annealing/ Extension)	60	60	
Denaturation	95	10	1
Annealing	65	5	1
Denaturation	95	5	1

Table 2.14 The Q-PCR cycling parameters.

2.9.5. Q-PCR Data Analysis

The Ct values obtained from Q-PCR experiment were analysed in Excel (Microsoft) using ddCT method, the data was then plotted and analysed in GraphPad Prism to measure the statistical significance. To compare the means of two groups of data the paired t-test was performed; when comparing more than two means the data One-Way Anova analysis with Tukey's Post-hoc test for pair-wise comparisons was used. The error bars were calculated using STDEV of the mean. The statistical significance of the P-values were denoted as follows: 0.01-0.05=*; 0.01-0.001=**, 0.001-0.0001=*** and P value< 0.0001=****.

2.10. Preparation of Whole Cell Lysates for Western Blotting Analysis

The cells were seeded according to **Table 2.12** and cultured until 90-100% confluence and treated with pharmacological compounds as required. The cells were washed twice with warm DPBS and placed on ice, then cold 100-120µl 1x RIPA buffer (Pierce, 8990) supplemented with 1% protease and 1% phosphatase inhibitors (Sigma-Aldrich) was dropped on the petri dish and cells were scraped thoroughly on ice using cell scraper (Greiner Bio-One).

The cell suspension was mixed by pipetting and kept on ice for 20min, during this time the samples were sonicated in icy water bath in Ultrasonic bath sonicator for 1min (to fragment the nuclear membrane and the genomic DNA) and spun down at 4ºC at 13krpm 15min, next the supernanant was transferred to a fresh, pre-cooled Eppendorf tube. The concentration of obtained samples was measured using the bicinchoninic acid (BCA) protein assay kit (Pierce, Thermo Scientific) according to manufacturer's instructions. The BCA assay was performed in 96-well plate using

10µl of sample to 200µl of working reagent. The samples were incubated at 37ºC for 30min and then left to equilibrate at RT for around 20min. The absorbance was measured at 560nm wavelength using GloMax plate reader (Promega). The background absorbance was deduced from all readings and a standard curve of BSA samples of known concentrations (25mg/ml-2000mg/ml) was plotted, next the concentration of the sample protein lysates was calculated from the slope of the obtained standard curve. The protein lysates were denatured in Novex loading buffer (70% (v/v) of 4x Novex NuPAGE LDS Sample Buffer to 30% (v/v) NuPAGE Reducing Agent, (both from Invitrogen) at 1:2 buffer to sample ratio and boiled at 95ºC for 10min. Boiled lysates were then stored at -20ºC until Western Blot analysis and spun at 13,000rpm at RT for 5min before being run on a protein gel.

2.10.1. Nuclear and Cytoplasmic Extraction

The nuclear and cytoplasmic protein samples from cultured cells were prepared for Western blot analysis using NE-PER™ Nuclear and Cytoplasmic Extraction Reagent (Pierce, Thermo Fisher Scientific) and scaled up appropriately to the collected cell pellet volumes. The cell pellet of around 15µl packed volume was usually obtained from confluent 6cm dish of $BAC^{Nrf2\text{-}Venus}$, was mixed with 150µl of cold buffer CERI (supplemented with 1% protease and 1% phosphatase inhibitor cocktail (Sigma-Aldrich) and mixed by pipetting and vigorously for 15sec and then incubated on ice for 10min. Following the incubation 8.25µl of cold CERII buffer was added and sample vortexed for 5sec and incubated on ice for further 1min. The sample was then vortexed briefly once more and spun down at 4ºC for 10min at max speed. The supernatant containing the cytoplasmic fraction was transferred to a fresh, pre-chilled Eppendorf tube and kept on ice until denaturation step. The pellet was then gently washed in ice-cold PBS to remove any cytoplasmic contaminants, with as much PBS as possible removed from the tube. The pellet containing the nuclear and insoluble protein fractions was then resuspended in 75µl of cold NER solution (with 1% proteases and phosphatases inhibitors) and pipetted until considerable fraction of pellet was dissolved. The sample was vortexed at the highest speed for 15sec and incubated on ice for 10min, these steps were repeated 4 times. During the incubation time, nuclear lysates were sonicated in icy water in Ultrasonic bath sonicator for

1min. Following the incubation and vortexing steps, the sample was spun down at 16,000rpm at 4ºC for 10min and the supernatant containing the nuclear fraction was transferred to new tube and the protein concentration quantified as described (Section 2.10).

2.11. Western Immunoblotting

Equal quantities (usually 40µg, or as stated) of whole cell lysates, cytoplasmic or nuclear fraction samples were run on 10well pre-cast NuPAGE Novex bis-tris gels (Invitrogen) alongside a BenchMark™ protein pre-stained protein ladder (Invitrogen, 10748-010). Samples were resolved in a gel tank in 1x 3-(N-morpholino) propanesulfonic acid (MOPS) buffer (Invitrogen) at 90V for 20min, followed by 160V for 70min. Separated protein samples were then transferred onto a nitrocellulose membrane (pore size 0.45µm, Gene Flow Limited, B3-0058) for 1h at 300mAmp. Once transfer was completed, the nitrocellulose membrane was briefly washed in ddH_2O and stained with Ponceou S to verify equal loading. The membrane was then washed briefly in PBS and blocked in 8% Blotting grade milk (Bio-Rad, 170-6404) in PBS-T (PBS with 0.1% Tween detergent (v/v), Sigma) for 1h at RT while gently agitating. The primary antibody (for antibodies used and dilutions see **Table 2.15**) was subsequently applied in 5% Blotting grade milk in the cold room, overnight. The next morning the nitrocellulose membrane was washed several times in PBS-Tween (PBS-T) and probed with horse radish (HRP) conjugated (1:5000) (AbCam) or fluorescently conjugated secondary antibodies (1:20,000) (LI-COR) in 5% Milk in PBS-T for 1h. Following washing in PBS-T the last wash was performed in PBS and the nitrocellulose membrane was imaged by X-ray film exposure (Section 2.11.1) (for HRP conjugated antibodies) or using infrared radiation using Odyssey (LI-COR Sa) imaging system (for fluorescently conjugated antibodies).

2.11.1. X-Ray Film for Western Blot Detection

The immunoblots probed with HRP-conjugated secondary antibodies were visualised using Clarity Western enhanced chemiluminescence substrate (Bio-Rad) for detection of HRP activity. The nitrocellulose membrane was then exposed on

Amersham Hyperfilm ECL (GE Healthcarse Life Science) and developed using Kodak developer and fixer solutions under dark room conditions.

Antibody target	Host/Dilution	Company
Nrf2 (H-300)	Rabbit/1:500	Santa Cruz (sc-13032)
Nrf2 (Proteintech)	Rabbit/1:1000	Proteintech (16396-1-AP)
RelA/p65	Rabbit/1:1000	Santa Cruz (sc-372)
Keap1	Rabbit/1:2000	Proteintech (10503-2-AP)
eGFP/Venus	Sheep/1:1000	from Prof. Ian Prior's Laboratory
Lamin B1 (H-90)	Rabbit/1:500	Santa Cruz (20682)
β-Tubulin	Mouse/1:10,000	AbCam DM1A (ab7291)

Table 2.15 Primary antibodies used for Western blotting.

2.11.2. Cytokine Stocks

The human recombinant IL-1β (Merck Millipore, IL038) and human and mouse recombinant TNFα (Merck Millipore, 654205 and GF027 respectively) stocks were made by dissolving 10μg of lyophilized proteins in sterile 1000ul PBS containing 0.1% BSA (w/v) to a stock concentration of 10μg/ml and the further diluted 1:1000 in cell media to a 10ng/ml concentration. The small aliquots were then made 10-20μl and stored at -80°C.

2.12. Stock and Working Concentrations of Compounds Used

*Viability data for the commonlu used drugs is presented in Figure 8.2 in the Supplementary Section.

Compound	Mechanism of Action	Stock Conc.	Working Conc.	Diluent	Source
Sulforaphane	Nrf2 induction	2mM	2μM	DMSO	Sigma-Aldrich

CDDO-Me	Nrf2 induction	200μM	50-100nM	DMSO	Goldring lab
Brusatol	Nrf2	100μM	100nM	DMSO	Goldring lab
CHIR99021	GSK-3 inhibitor	10mM	5-10μM	DMSO	Signal-Chem
MG132	Proteasome inhibitor	10mM	10μM	DMSO	Sigma-Aldrich
Leptomycin B	Nuclear export inhibitor	5.55μg/ml	10ng/ml	70% MeOH	Sigma-Aldrich
SB203580	p38 MAPK inhibitor	10mM	5-10μM	DMSO	Cell Signaling Technology
Trichostatin A (TSA)	HDAC inhibitor	5mM	3.3μM	DMSO	Sigma-Aldrich
C646	P300 inhibitor	10mM	10 μM	DMSO	Selleck Chemicals
MC1568	Class II HDAC inhibitor	20mM	2 μM	DMSO	Coulson lab
Mocetinostat	Class I HDAC inhibitor	20mM	1 μM	DMSO	Coulson lab
Cycloheximide	Translation inhibitor	10mg/ml	5 μg/ml	DMSO	Sigma-Aldrich
CNQX	Glutamate receptor blocker	10mM	10 μM	DMSO	Sigma-Aldrich
DL-APV	Glutamate receptor blocker	25mM	50μM	DMSO	Sigma-Aldrich

Table 2.16 List of compounds used in this project alongside their stock and working concentrations.

2.13. Live Cell Imaging

For real-time imaging of live cells, cells were seeded onto the 1 or 4 compartment

35mm glass bottom dishes (Greiner Bio-One). The 4 compartments allowed imaging of 4 different experimental conditions in parallel. The imaging experiments were performed under humidified atmosphere, at 5% CO_2 and 37ºC on two imaging systems. The primary cells expressing plasmid encoded fluorescent protein fusions were imaged on the Zeiss Axiovert 5.10 (Zeiss Germany) confocal microscope using 40x oil immersion objective with numerical aperture (NA) of 1.4. The image acquisition on this system was coupled with autofocus Marco (Ellenberg lab, EMBL), which enabled maintenance of stable Z-plane position of the imaged cells, avoiding the problems of focal drifts that can occur during the long acquisition times. The LSM 7.80 (Zeiss, Germany) system was used for monitoring low expression of fluorescent proteins, as it has superior resolution and sensitivity of detection, using 40xoil immersion objective (1.4 NA) and LSM ZEN 2010 image acquisition software (Zeiss). In both systems the image acquisition was performed, using 512x512 pixel resolution, 7 scanning speed with the pinhole diameter adjusted to the fluorescence intensity of imaged samples. The table below shows the filter and laser set up for imaging of the fluorescent proteins used in this study. The image acquisition of single fluorophore was performed by taking one acquisition frame at 8min interval in 1-20 imaging locations, and the time taken to acquire image at all selected positions did not exceed the 8min interval. When imaging two separate channels (or fluorescent probes) the image acquisition was performed every 7min at up to 16 locations. The drug treatment was usually performed following initial three fames were acquired, which served as a baseline fluorescence measurement. Both imaging protocols were carried out at various lengths of time between 2-14h, and the drug of interest was added following 3 initial frames, which were taken to establish a signal baseline.

Fluorophore	Laser	Filter Set
TagBFP	405nm Laser diode	420-470nm
EGFP	488nm Argon laser	490-554nm
Venus	514nm laser	529-539nm
AmCyan	488nm Argon laser	480-520nm
TagRFP	561nm DPSS diode	560-610nm
mCherry	561nm DPSS diode	570-630nm

dsRedXP	561nm DPSS diode	560-610nm
pDendra2	488nm Argon laser and	490-550nm
	561nm DPSS diode	560-667nm

Table 2.17 List of fluorescent protein fusions imaged throughout this project alongside their excitation source and filter settings for collection of the emission signal.

2.13.1. Lambda Scan

Lambda Scan imaging mode was used for spectral unmixing of fluorophores with overlapping fluorescence emission peaks. This mode was predominantly used to image cells exhibiting very low expression of fluorescent protein fusions such as $BAC^{Nrf2\text{-}Venus}$ or primary astrocytes transduced with *2kb*-Venus-msNrf2. The levels of Venus fluorescence in those models was close to autoflourescent signal and therefore there was a considerable autofluorescent noise being detected. The lambda scan allows collecting emission of Venus fluorophore with 514nm laser and collecting the emission at sequentially increasing (10nm interval) band-pass width such as 522nm, 531nm, 540nm, 548nm, 557nm, 565nm, 574nm, 583nm, 591nm and 600 using arsenide phosphate quasar detector. The spectral images were then combined using LSM ZEN 2010 software (Zeiss).

2.13.2. pDendra2 Imaging

The photoswitchable fluorescent protein pDendra2 was isolated from *Octocoral Dendronephthya (*Gurskaya *et al,* 2005*)*. It was previously characterized and optimized for imaging stability and redistribution of molecules and organelles (Chudakov *et al,* 2007). It matures completely at 37ºC, its pH stable and monomeric. The pDendra2 emits naturally in a green light spectrum, however UV irradiation results in irreversible transition in emission to bright and photostable red fluorescent protein (RFP) spectrum (Baker *et al,* 2010). The pDendra2-Nrf2 fusion was transiently expressed in SK-N-AS cells (3µg of plasmid p/35mm dish) 24h before the experiment as described previously (Section 2.8.1). The following parameters were used during image acquisition: Line averaging 1, scanning speed: 7, zoom 1.3x, 40x oil, 512x512 pixel resolution. To image turnover of Nrf2, four locations were

selected with each localisation treated with different compound (4 compartment dishes) and the 2 regions of interest (ROIs) were selected, each of 13x13 pixel size. The fluorescent signal was collected for the Green and the Red channels (**Table 2.17**) and following acquisition of three imaging frames, the drug was added and one more frame was collected (3min interval between acquisition). Then the photoconversion of pDendra2 was performed either by a UV lamp at 75% power for 45s and image taken following the irradiation and photoswitching the entire imaging localisation *e.g.* for imaging Nrf2 stability following pharmacological treatment. Local pDendra photoconversion was used to monitor nuclear import and export rates of pDendra2-Nrf2 and for this purpose the 405nm laser was used (400Hz, 100%, continuous wave mode) for 20x iterations, speed: 177.32μsec/pixel in the ROI1 and the collection of signal was measured in both the photoconverted ROI1 and the ROI2. The data measurements were performed using ZEN 2010 and exported and averaged using Microsoft Excel, the averaged data was exported to GraphPad Prism 5. The for calculating the protein turnover half-life and the fluorescence increase rates the changes in red fluorescence signal was analysed using nonlinear regression and using One phase association to measure the rate of fluorescent signal change. The obtained values were $-t_{1/2}$ is a measure of time it takes to achieve half maximal fluorescence change and therefore measure of equivalent import and export rates between nuclear and cytoplasmic compartments, tau (τ)- describes the time constant, and R^2 is the fit of the obtained data to the calculated curve.

2.13.3. Image Analysis

Image analysis was performed using Cell Tracker software Version 6.0 (www.dbbkgroup.org/celltracker/) (Shen *et al,* 2006). In order to select the representative cells of target cells for analysis on Cell Tracker the target cells had to fulfil several requirements such as: remain in the field of view, not undergo mitosis or apoptosis throughout the experiment, and where required, express second fluorescent protein fusion of interest. The nucleus was drawn manually and the changes in the nuclear shape adjusted on every acquired image (usually 100 per each location), either manually or automatically by cell tracker software. The data was averaged and exported as an Excel file format. It was normalized to the initial fluorescence levels and the noise was reduced by averaging the values using 3rd order

moving average (three frame smoothing). The data from cell populations was averaged between independent experiments and error bars were plotted using standard deviation of the mean. The legends of the figures contain information about the biological replicated "n" and the total cell numbers analysed "c". Please note some representative imaging experiments are recorded as an avi. file in the enclosed DVD at the back of this thesis.

2.13.4. Fluorescence Cross Correlation Spectroscopy (FCCS)

The FCCS experiments were performed at University of Manchester with kind help from Dr. James Boyd (White lab). The data collection was performed using LSM 780 with confocor 3 mounted on Axio observer Z1 microscope using oil immersion 100x lens (N.A. 1.46) and using ZEN2010 software (Zeiss). The Venus and the mCherry fluorescence were excited as stated in **Table 2.17**. The pinhole was set to 1 airy unit and the laser power was typically set to 1% laser power, adjusted to avoid photobleaching and to maximize the count per minute (cpm) fluorescent signal to minimum 0.5 kHz value. The data collection protocols were previously described by Bacia *et al,* 2006; and were carried out 10x for 10s each and the fluorescence signal of mCherry and the Venus channels was then compared using first correlation and then cross-correlation logarithms using LSM ZEN 2010B FCS function. The data was then exported to MATLAB (Mathworks) and processed by Dr. Boyd (White lab).

RESULTS CHAPTER 1:

3. Construction and Characterisation of Expression Systems to Study Dynamic Nrf2 and NF-κB Responses in Primary Mouse Neurons, Astrocytes and Human SK-N-AS Neuroblastoma Cells

3.1. CHAPTER 1 AIMS:

- **Construction of molecular tools for live cell imaging of NF-κB and Nrf2 protein localisation and activation**
- **Characterisation of inflammatory and antioxidant responses in the neurons and astrocytes from the CNS**
- **Characterisation of low expression model of Nrf2 in neuroblastoma SK-N-AS cell model under basal and stimulated conditions**

3.2. Introduction

The balance between the antioxidant and inflammatory pathways is essential for maintaining appropriate levels of protection against neurodegeneration. Neuronal cells have been at the centre of recent efforts to designing targeted therapeutic strategies to protect against neurodegeneration, however in recent years, the role of glial cells in mediating anti-oxidant defence and inflammatory responses has become increasingly more evident (Vargas & Johnson, 2009).

Both the NF-κB and the Nrf2 pathways have been highlighted as potential targets for therapeutic intervention, however there is limited comparative information on cell-type specific basal or induced dynamic responses due to the inherent limitations of traditional population level biochemical methods.

This study was designed to facilitate a comparative cell-type specific investigation of signalling responses in each pathway, using near-endogenous levels of fluorescently tagged p65/RelA (used here as a representative of the canonical NF-κB pathway activity) and Nrf2 proteins and corresponding reporters of transcriptional activity in cultured hippocampal neurons and astrocytes, either in mixed or pure culture settings. There are several types of glial cells in the brain including astrocytes,

microglia and oligodendrocytes (Section 1.3.1), however for this study, astrocytes were selected for detailed investigation since they are though to play an important role in mediating anti-inflammatory signalling.

Primary cell culture models present several challenges including detailed isolation and maintenance protocols. Previous research in the Sanderson and White labs lead to the generation of an SK-N-AS neuroblastoma cell line, which stably expresses Nrf2-Venus from a Bacterial Artificial Chromosome ($BAC^{Nrf2\text{-}Venus}$), however this cell line had not been fully validated as a model for studying Nrf2 protein dynamics. Therefore, the first aim of this study was to generate a suite of molecular tools to enable visualisation and tracking of the dynamic abundance and localisation of Nrf2 and p65 in primary astrocytes and neurons in response to acute TNFα-mediated inflammatory signalling and/or pharmacological induction of Nrf2 with CDDO-Me and SFN.

Secondly, the neuroblastoma $BAC^{Nrf2\text{-}Venus}$ cell line was further investigated to establish if the Nrf2-Venus fusion exhibits equivalent dynamic or conditional responses as observed for endogenous proteins. In order to confirm that this cell line is a suitable model for use in further live cell imaging studies.

3.3. RESULTS

3.3.1. Characterisation of dynamic NF-κB responses in Murine Neurons and Astrocytes

3.3.1.1. Primary Cell Culture Characterisation

To investigate the dynamics distribution, abundance and transcriptional activity of Nrf2 and NF-κB pathways in primary neurons and astrocytes it was necessary to establish primary, mixed neuron-astrocytes cultures. The isolation of cells was carried out as described in methods (Sections 2.4.2 & 2.4.3). To validate the cellular composition of enriched neuronal and astrocyte cultures immunostaining was performed to detect cell-type specific markers. In brief, neuronal and astrocyte cultures were fixed following 14 days *in vitro* culture (14DIV) and labelled by indirect-immunofluorescent staining for glial (GFAP), neuronal (β-Tubulin III) and microglial (CD11b) markers (Figure 3.1). Enriched hippocampal neuronal cultures

A)

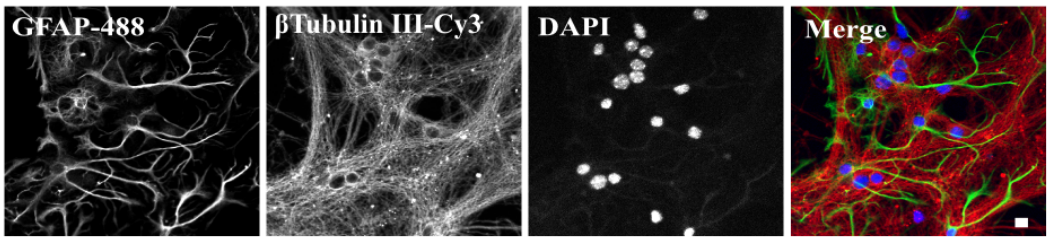

B)

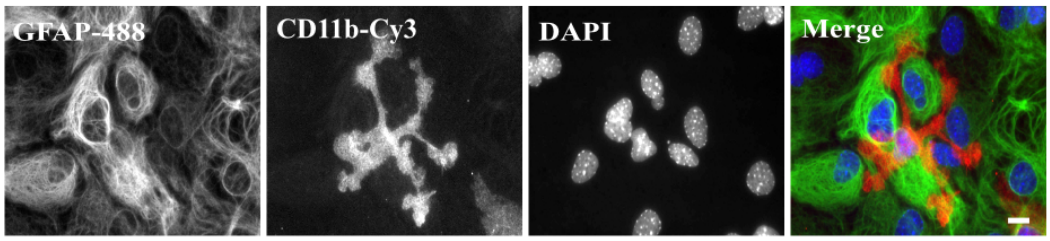

C)

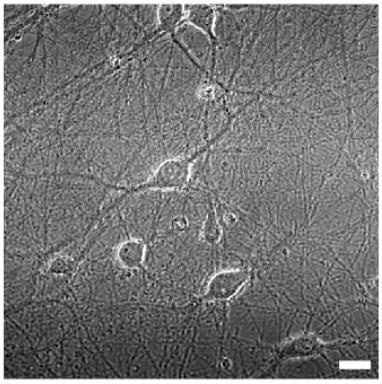

Figure 3.1 Characterisation of neural hippocampal cultures. A) Mixed neuronal/astrocyte cultures were fixed after 14 days of *in vitro* culture (14DIV), prior to staining for the astrocyte marker GFAP-488 (green) and neuronal β-tubulin III-Cy3 (red) (Methods 2.5). B) Enriched astrocyte culture showing the presence of a microglial cell, expressing the microglial marker CD11b-Cy3 (red). C) Brighfield micrograph showing phase-bright neuronal cell bodies (14DIV). Scale bar = 10μm.

showed characteristic positive staining with β-tubulin III, and exhibited densely packed neuronal connections, which were commonly wrapped around cell bodies (Figure 3.1A & C). Star-shaped astrocytes grown in the underlying layer showed strong expression of the glial marker GFAP-488 (Figure 3.1A & B). As astrocytes are essential for maintaining healthy synaptic connections, some low-level glial cell presence was allowed in neuronal cultures, in order to ensure robust neuronal growth and function. In these *in vitro* culture models, the health of neurons can easily be assessed by monitoring the shape and brightness of the cell body, which appears as a phase-bright structure, resting on top of a dense network of smooth, inter-neuronal connections (Figure 3.1C).

To compare astrocytic responses to inflammatory and antioxidant signalling in the presence or absence of neurons. Enriched astrocyte cultures isolated from either the hippocampi or cortex of P1-3 pups were grown in Astrofood media (Methods, Section 2.4.2). Indirect immunofluorescence analysis confirmed that glial cultures were predominantly composed of GFAP positive astrocytes (Figure 3.1B), with the occasional presence of low levels of microglial cells (normally less than 1% of the total cell population, as assessed by visual examination). In the absence of neurons the shape of astrocytes was observed to be generally more uniform with fewer branched protrusions, as can be seen by comparing Figure 3.1A & 3.1B.

3.3.1.2. Measuring TNFα-induced NF-κB Responses in Neural Cells

In order to define cell-specific NF-κB responses to TNFα mediated inflammatory stimulation, population level biochemical studies were first performed on pure neuronal or pure astrocyte cultures (Figure 3.2). Following treatment with murine recombinant TNFα (10ng/ml), lysates were prepared from hippocampal cell cultures at indicated time points, before being fractionated into nuclear and cytoplasmic fractions (Methods Section 2.10.1), which were then analysed by western blot to define the relative nuclear/cytoplasmic distribution of p65 (Figure 3.2A & B). Consistent with previous reports (Listwak *et al,* 2013), pure neuronal cultures did not exhibit nuclear translocation of p65 in response to TNFα, even after prolonged (16h) stimulation (Figure 3.2A). Interestingly, we observed a difference in the apparent

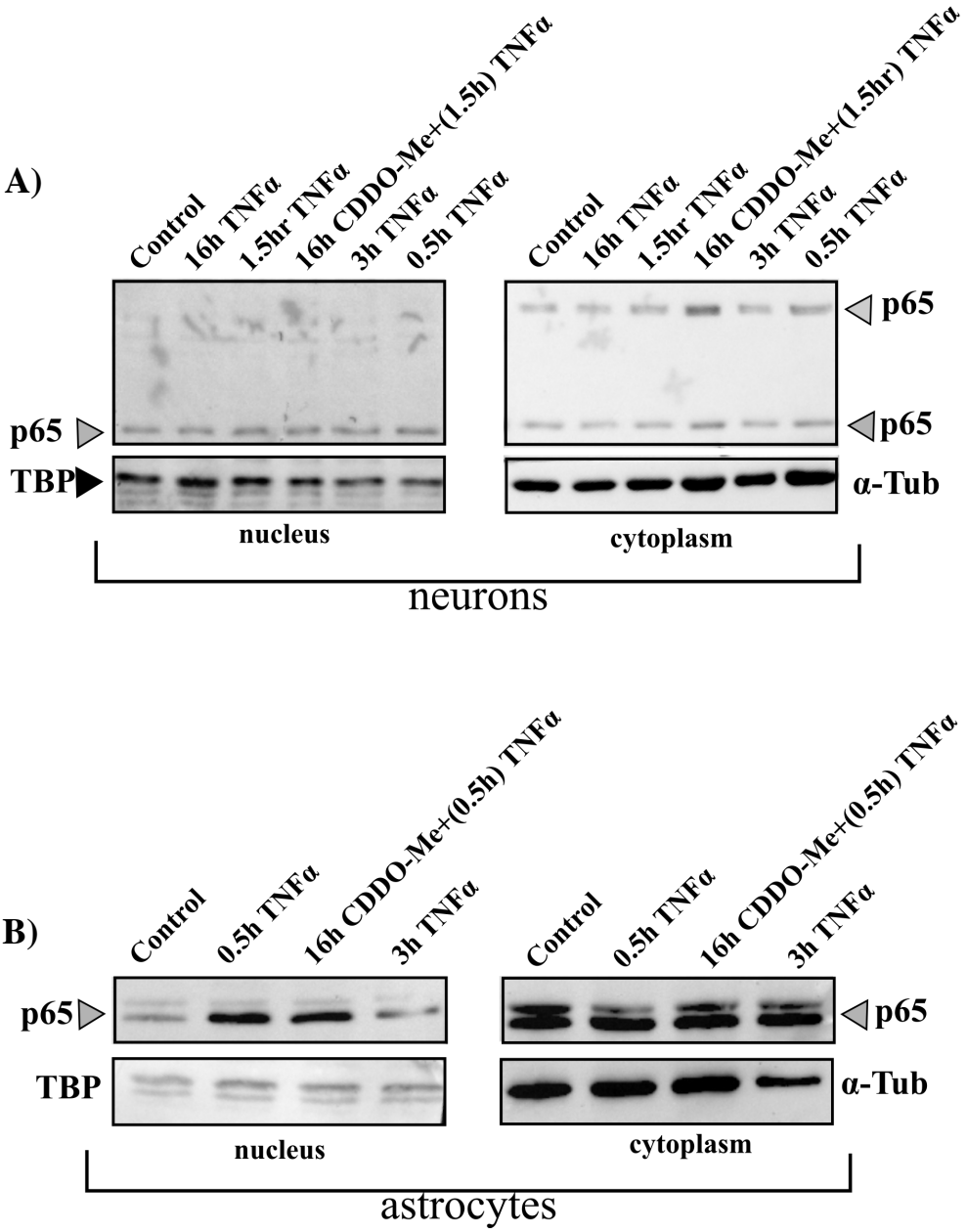

Figure 3.2 TNFα induces nuclear translocation of p65 in astrocytes. Nuclear and cytoplasmic fractions were prepared from cultures of pure neuronal cells (A), or astrocyte-enriched cultures (B), following treatment with either 10ng/ml murine TNFα alone, or 10ng/ml murine TNFα in combination with 100nM CDDO-Me, n=1. In each case western blots were performed to assess conditional changes in p65 sub-cellular distribution. TNFα induced nuclear accumulation of p65 (grey triangles) is clearly observed in astrocytes but not in neurons.

molecular weights (MW) of p65 between cytoplasmic and nuclear fractions of neuronal cells. While nuclear fractions of primary neurons contained a single 80kDa form of p65, corresponding cytoplasmic fractions also contained a higher molecular weight (~150kDa) form of p65. Significantly both forms of p65 fail do demonstrate significant responses to stimulation with TNFα or CDDO-Me.

In contrast to conditional responses observed in neurons, astrocytes displayed a pronounced TNFα induced nuclear accumulation of the 80kDa form of p65 within 30min. However, nuclear levels of p65 had declined by 3hrs post stimulation (Figure 3.2B). Co-stimulation with TNFα (10ng/ml) and the antioxidant inducer CDDO-Me (100nM) for 16h did not inhibit TNFα induced p65 nuclear translocation of p65 as a result of cytokine treatment.

3.3.1.3. Quantitative Analysis of Conditional NF-κB Transcriptional Activity in Primary Neurons, Astrocytes

To measure the degree of TNFα mediated NF-κB transcriptional activation in pure astrocyte or neuronal cultures, a quantitative dual luciferase transcription activity assay was performed, using an NF-κB-Luc plasmid in which expression of firefly luciferase is driven by 5xκB repeats, each containing a consensus NF-κB binding sequence (Nelson *et al,* 2004) (Methods 2.4.6). Using this surrogate reporter system, any increase in luciferase signal compared to control indicates a general increase in NF-κB transcriptional activity. Consistent with data from biochemical analysis of p65 nuclear/cytoplasmic distribution, 10ng/ml TNFα stimulation of astrocytes conferred a correlated conditional increase in NF-κB transcriptional activity (Figure 3.3A).

To further confirm the lack of TNFα mediated transcriptional responses in primary mouse neurons, indirect immunohistochemistry was performed on enriched neuronal cultures to investigate conditional changes in the subcellular distribution of endogenous p65 (Figure 3.3B). These studies confirmed results from our biochemical analysis showing no detectable increase in p65 nuclear translocation in response to TNFα stimulation, even after prolonged stimulation.

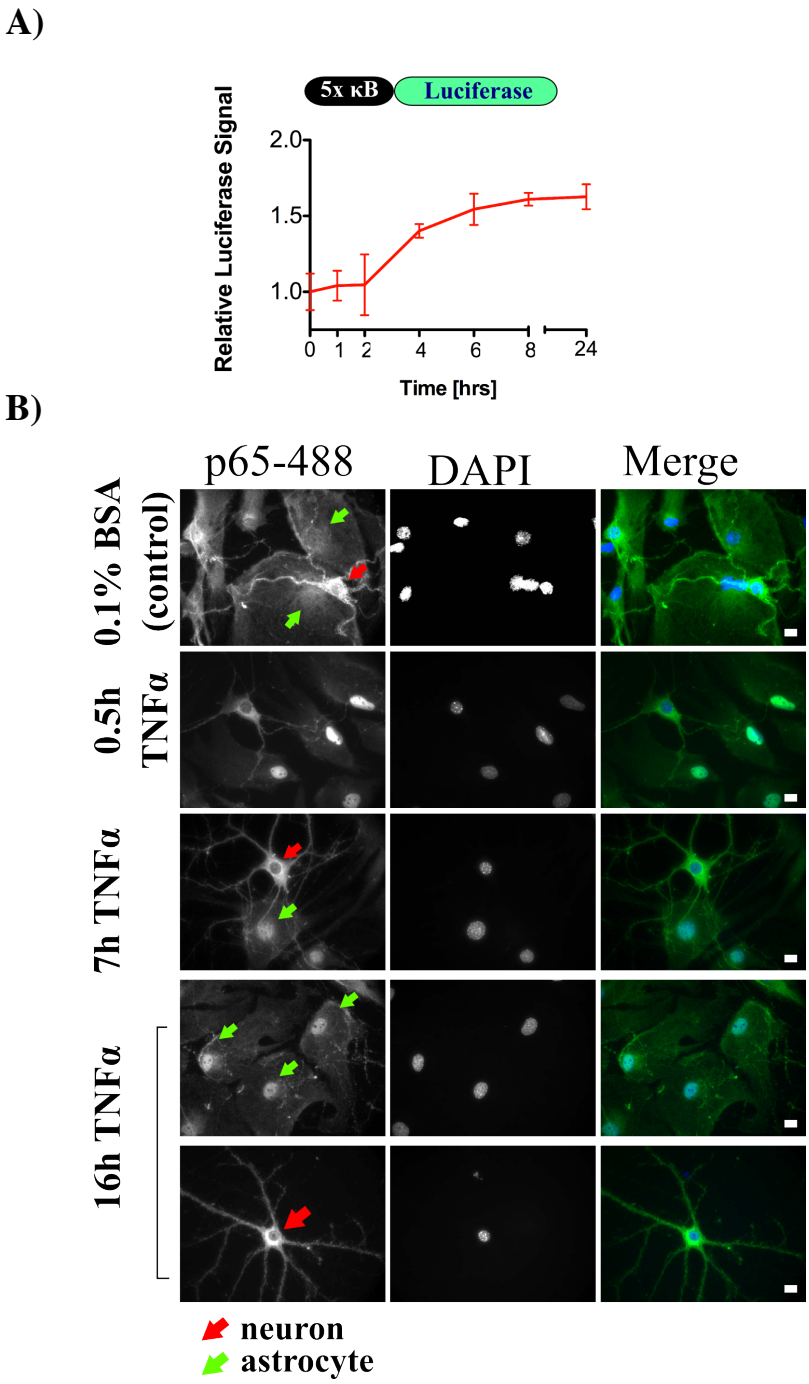

Figure 3.3 Astrocytes exhibit NF-κB activation in response to TNFα. A) Temporal changes in NF-κB transcriptional activity were measured in primary murine astrocytes following stimulation with TNFα (10ng/ml) at times specified. Increases in NF-κB–Luc luciferase reporter activity reflect temporal trends in NF-κB transcriptional activity, n=1. B) Immunofluorescent staining of p65 following TNFα treatment of mixed neuron-astrocyte cultures. It is important to note the lack of nuclear p65 accumulation in neurons compared to the positive accumulation of nuclear p65 seen in astrocytes. Error bars=STDEV, scale bar=10μm.

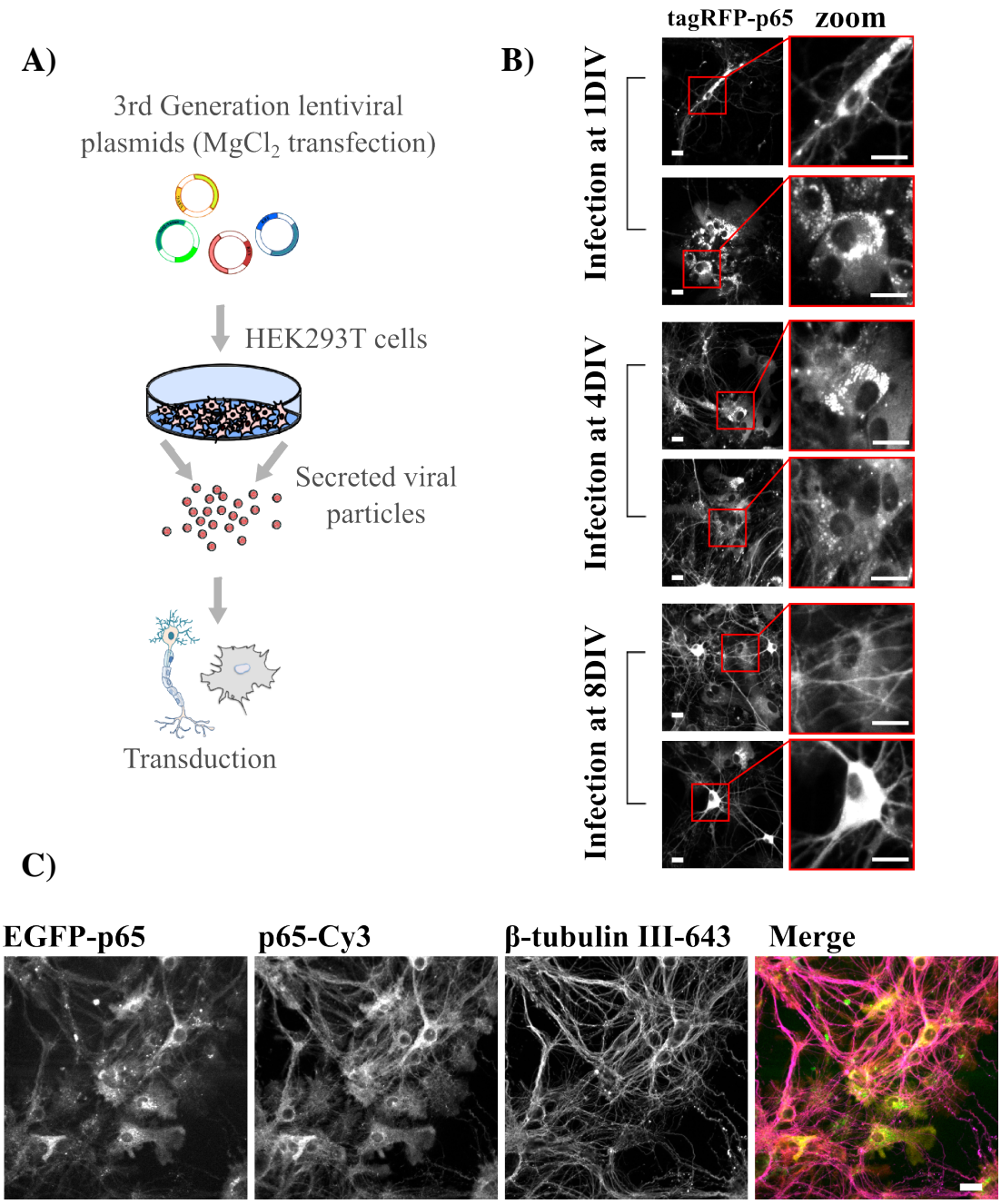

Figure 3.4. Lentiviral transduction provides an efficient method for gene delivery into primary neurons and astrocytes. A) Diagram depicting the process of lentiviral particles production. B) Optimisation of transduction of mixed cultures with tagRFP-p65 lentivirus. Transduction of cultures at earlier DIV resulted in more fluorescent protein aggregates. C) Comparative distribution of basal EGFP-p65 fusion and endogenous p65 protein showing a high degree of co-localisation in all cells. Scale bar 20μm.

In order to obtain a more detailed insight into the spatiotemporal dynamics of conditional p65 responses, a collection of molecular tools had to be developed, in order to correlate the dynamic behaviour of p65, expressed at near endogenous levels, with NF-κB transcriptional activity, in primary neuronal and astrocyte cultures. This was achieved by developing a collection of lentiviral expression vectors, which facilitate efficient delivery and low-level expression of fluorescent p65 fusions proteins and transcriptional reporter systems. The basic workflow of the lentiviral production process is shown in Figure 3.4A. In brief, the mouse p65 coding sequence was inserted into the gateway compatible lentiviral transfer vector allowing in-frame expression of p65 downstream of an N-terminal fluorescent tagRFP tag (Map in Supplementary Section 8.3) (Methods Section 2.1). A comparable EGFP-p65 plasmid encoding human p65 driven by a mouse endogenous promoter sequence was kindly provided by Dr James Bagnall (Dr Pawel Paszek group, University of Manchester). The EGFP-p65 and tagRFP-p65 lentiviral systems were found to function identically and were therefore used interchangeably throughout imaging experiments in this study. Stocks of viral particles were generated by co-transfecting fluorescent lentiviral transfer vectors with third generation lentiviral packaging vectors into HEK293T cells by $MgCl_2$ transfection (Methods Section 2.6), and the lentiviral particles were harvested after 64h.

Optimal lentiviral transduction was found to be highly dependant on the DIV stage of neuronal cultures. As later stage cultures of primary cells were found to be more optimal for transduction (Figure 3.4B).

Increased numbers of tagRFP-positive inclusions/aggregates were observed when cells were transformed at early stages of culture *in vitro* (Figure 3.4B). Therefore, DIV9 was chosen as an optimal day for lentiviral infection (Methods 2.6.1), in order to minimize the presence of fluorescent aggregates and avoid infection related stress responses when imaging at DIV14. To determine if the subcellular distribution of fluorescently labelled p65 fusion proteins appropriately mirrored that of endogenous p65 in these cells, the relative co-localisation of fluorescent constructs and endogenous p65 protein was directly compared (Figure 3.4C). Significantly, these studies also show that the process of lentiviral transduction did not confer any NF-κB activation at DIV14 when all subsequent studies were performed. Extensive co-

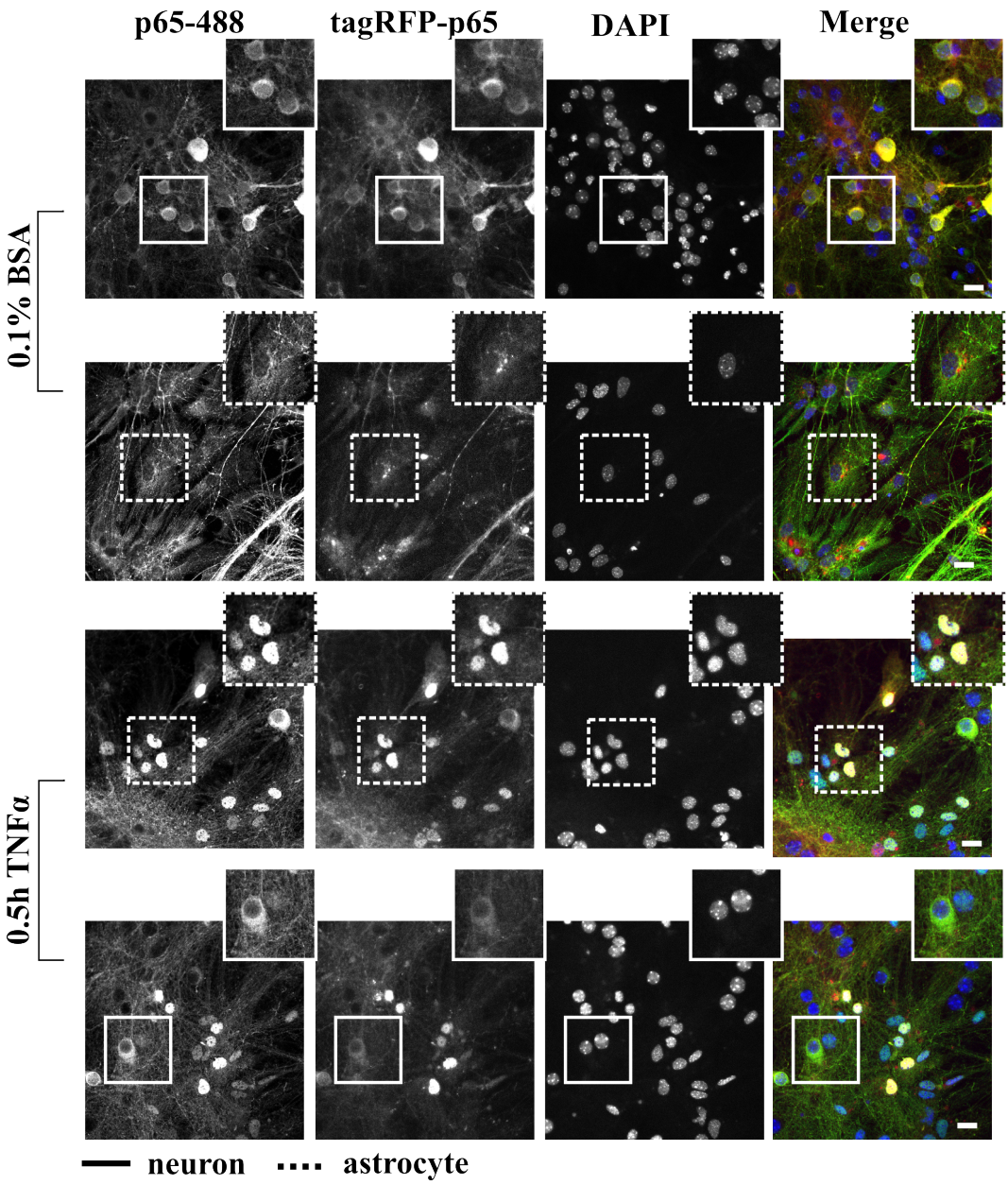

Figure 3.5 Lentivirally transduced tagRFP-p65 as a tool for monitoring p65 dynamics in primary neural cells. Mixed hippocampal cultures of neurons and astrocytes lentivirally transduced at DIV9 with tagRFP-p65 (red) virus (fixed at DIV14), show similarity with labelled endogenous p65-488 (green) protein under basal and TNFα activated conditions, n=2. Scale bar 10μm.

localisation of EGFP-p65 and p65-Cy3 (Figure 3.4C) and EGFP-p65 tagRFP-p65 (Figure 3.5), with no nuclear p65 accumulation under basal conditions indicating that the infection process itself did not elicit NF-κB activation or cell death. Prior to use in live cell imaging studies, the tagRFP-p65 construct expressed in lentivirus-transformed cells was also tested to confirm responsiveness to TNFα stimulation and co-localisation with endogenous p65 (Figure 3.5). As previously observed tagRFP-p65 fusion protein accumulated in the nucleus of astrocytes following 30min TNFα stimulation, although as in previous experiments, no nuclear accumulation of tagRFP-p65 was observed in neuronal nuclei.

3.3.1.4. Investigating Dynamic p65 Responses in Primary Mouse Neurons and Astrocytes

To gain insight into the real-time dynamics of p65 responses to TNFα stimulation in mixed neuron/astrocyte or pure astrocyte cultures, primary cells were infected with virus encoding EGFP-p65 (Methods 2.6.1) and imaged using Zeiss 7.80 confocal microscope (Figure 3.6). All cultures were maintained at 37ºC, under 5% CO_2 in a humidified atmosphere during image acquisition, which took up to 14 hours (Methods 2.13). Temporal measurements of nuclear EGFP-p65 levels showed that astrocytes display clear oscillatory nuclear shuttling in response to TNFα stimulation as measured by the normalised nuclear fluorescence (NNF) (Data normalised as described in 2.13.3) (Figure 3.6B & E). Although in this study, there also seemed to be some increase in nuclear levels of p65 in neurons (Figure 3.6C), closer inspection of these images suggest that this phenotype may simply be due to gradual shape change in the neuronal cell body, rather than a genuine nuclear accumulation (Figure 3.6G and Movie 1b). Interestingly, the dynamic profile of TNFα (10ng/ml) induced p65 oscillations was found to be dependant on whether astrocytes were cultured in the presence or absence of neurons (Figure 3.6A *vs*. 3.6D). Comparison of mean nuclear fluorescence levels show that pure astrocyte cultures (Figure 3.6A and Movie 2) maintained persistently higher amplitude of nuclear p65 oscillation in response to cytokine application, with less damping of peak amplitude after the first peak, when compared to profiles obtained when astrocytes are co-cultured in the presence of neurons.

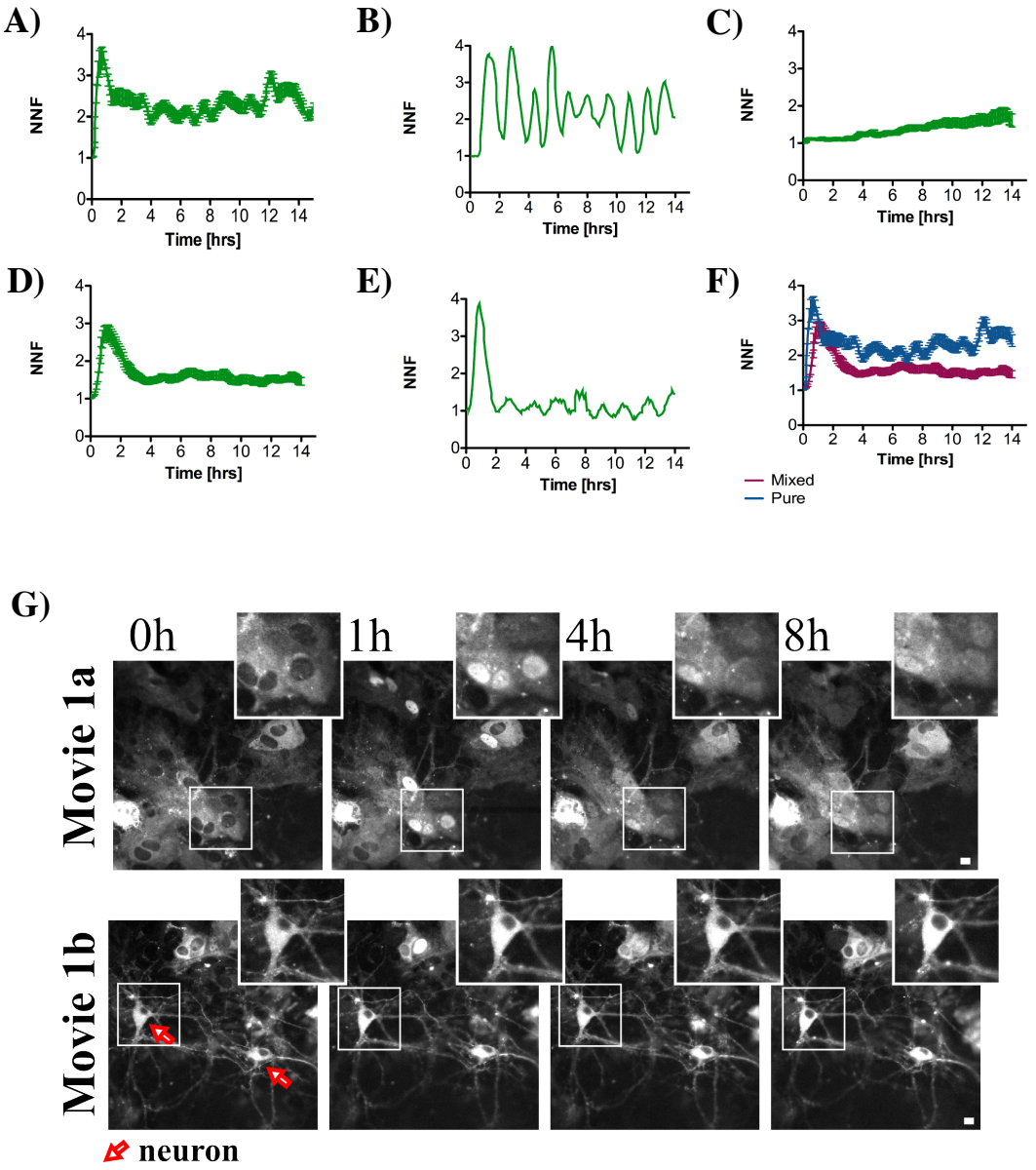

Figure 3.6 Astrocytes exhibit neuron-induced changes in EGFP-p65 nuclear oscillations in response to TNFα. The nuclear fluorescence measurements were analysed in Cell Tracker by manual labelling of the nuclear compartment throughout the acquired imaging frames (1 frame per 7min, Methods Section 2.1). A) Averaged and B) single-cell trends in nuclear EGFP-p65 levels following stimulation with 10ng/ml TNFα in pure astrocyte cultures, n=2, c=30 (Movie 2). C) Apparent changes in nuclear EGFP-p65 levels in response to TNFα stimulation in neurons, n=2, c=10 (Movie 1b). D) Averaged and E) single-cell nuclear trend in astrocytes co-cultured with neurons, n=3, c=32 (Movie 1a). F) Comparison of averaged patterns of nuclear EGFP-p65 fluorescence in astrocytes, grown in the presence and absence of neurons. G) Representative time-lapse images showing EGFP-p65 localisation in response to TNFα stimulation. NNF= Normalised Nuclear Fluorescence, Error bars=SEM, scale bar=10μm, n= independent experimental repeats, c=total cell number analysed.

Astrocytes that are co-cultured with neurons responded to TNFα with a pronounced initial accumulation of p65, followed by sustained low amplitude nuclear oscillations (Figure 3.6B, Movie 1a & 1b).

However, the apparent lack of TNFα p65 nuclear translocation in neurons, does not eliminate the possibility that other NF-κB family members could mediate a response to TNFα stimulation. To test this, hypothesis and investigate the consequences of p65 activation in more detail, a new fluorescent reporter of NF-κB transcriptional activity was developed. This reporter, which was based on the widely used NF-κB-luc reporter plasmid also encodes the 5xκB consensus repeats upstream of a TATAbox element, which was designed to drive expression of a Venus fluorescent protein sequence (Figure 3.7A, Map in Supplementary 8.3). Therefore, using this reporter system, an increase in Venus fluorescence is indicative of an increase in NF-κB transcriptional activity. The practical advantage of using this new lentiviral encoded reporter is the ability to investigate both tagRFP-p65 dynamics and relative conditional transcriptional activity in parallel in real time in primary cell cultures. The mean changes in the nuclear fluorescent signal of tagRFP-p65 and 5xκB driven Venus expression following TNFα stimulation are shown in Figure 3.7B. The Venus fluorescence accumulated gradually in parallel to tagRFP-p65 oscillations, indicating that the fluorescent reporter does respond to the cytokine induction (Figure 3.7B & C). The application of this powerful imaging tool definitively shows that in comparison to astrocytes primary mouse neuronal cells are insensitive to TNFα stimulation (Figure 3.7D, Movie 3a). As evidenced by the lack of p65 nuclear accumulation and the failure to increase by any means NF-κB transcriptional activity (Figure 3.7D). In contrast, astrocytes consistently responded to TNFα stimulation showing significant increases in 5xκB driven Venus expression, which was observed to gradually appear in the background of neuronal cells over time (Figure 3.7E, Movie 3a).

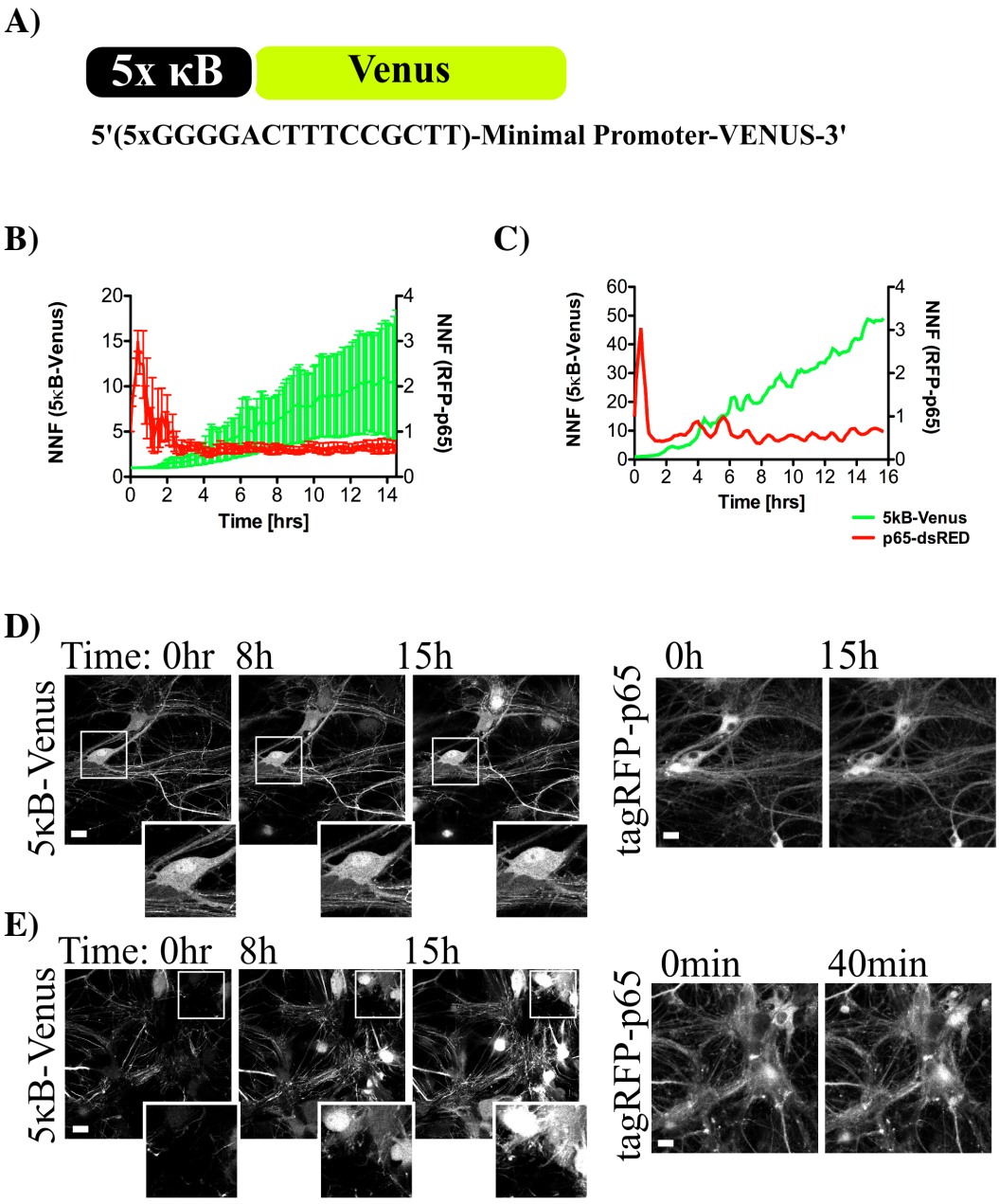

Figure 3.7 The new 5xκB-Venus reporter acts as a fluorescent activity reporter of NF-κB activity. A) Schematic representation of the 5xκB-Venus reporter of NF-κB transcriptional activity. B) Averaged levels of nuclear tagRFP-p65 and 5xκB-Venus fluorescence in astrocytes grown in mixed cultures, following stimulation with 10ng/ml TNFα (n=2, c=6). C) Representative single-cell temporal trends in p65 nuclear occupancy and NF-κB transcriptional activity. D) Time-lapse images showing mixed neuron/astrocyte co-cultures transduced with tagRFP-p65 and 5xκB-Venus following stimulation with TNFα (10ng/ml) (Movies 3a)). D) 5xκB-Venus signal remains unchanged in neurons, whereas in E) astrocytes show Venus increase in conjunction with tagRFP-p65 nuclear shuttling. Error bars=SEM, scale bar=20μm.

3.3.1.5. Astrocytes Exhibit Inherent Basal NF-κB Activity

The mixed primary culture system of neurons and astrocytes is a complex yet informative experimental model, which has the potential to provide mechanistic insight into brain physiology or potential conditional inflammatory responses *in vivo*. Having established that there are clear differences in cell-type responses to TNFα, it was necessary to determine if the basal activity of the NF-κB pathway was inherently variable in astrocyte enriched or neuron/astrocyte co-cultures. Interestingly, data from these studies show that astrocytes display spontaneous p65 nuclear translocation events, which were demonstrated by characteristic oscillatory activity in neighbouring cells (Figure 3.8, Movies 5b). To establish if these autonomous p65 oscillations correlate with an increase in transcriptional activity, the 5xκB-Venus reporter was imaged in parallel with tagRFP-p65 fluorescence (Figure 3.8C, Movie 4 & 5a). Results from these studies clearly show that autonomous nuclear translocations of tagRFP-p65 in astrocytes (grown in mixed culture) were associated with increased NF-κB transcriptional activity as demonstrated by the increase in 5xκB-Venus expression (Figure 3.8C). However, it was not clear if the observed spontaneous induction of NF-κB occurred as a result of autocrine or paracrine communication between astrocytes, or between astrocytes and neurons. The pyramidal neurons present in hippocampal cultures are known to exhibit spontaneous electrical activity as a result of glutamate signalling (Caech & Banker, 2006), and astrocytes grown in mixed cultures with neurons occasionally exhibited nuclear p65 staining detected by immunofluorescence (Figure 3.9A). To investigate the possibility that glutamate may act as an inducer of NF-κB oscillations and associated increases in transcriptional activity, mixed cultures were treated with two glutamate receptor antagonists DVLAP and CNQX (Figure 3.9B). However, blocking glutamate signalling did not prevent the spontaneous NF-κB activity as measured by nuclear fluorescence changes (NNF) of EGFP-p65. Equally, addition of 0.5mM L-Glutamate did not enhance NF-κB-luc activity in primary astrocytes (Figure 3.9C), leading instead to a reduction of luminescent signal over time. To exclude the possibility that the observed spontaneous NF-κB activity is mediated by neuronal inputs, pure astrocyte cultures infected with EGFP-p65 lentivirus were imaged in Neurobasal medium (instead of Astrofood usually used for

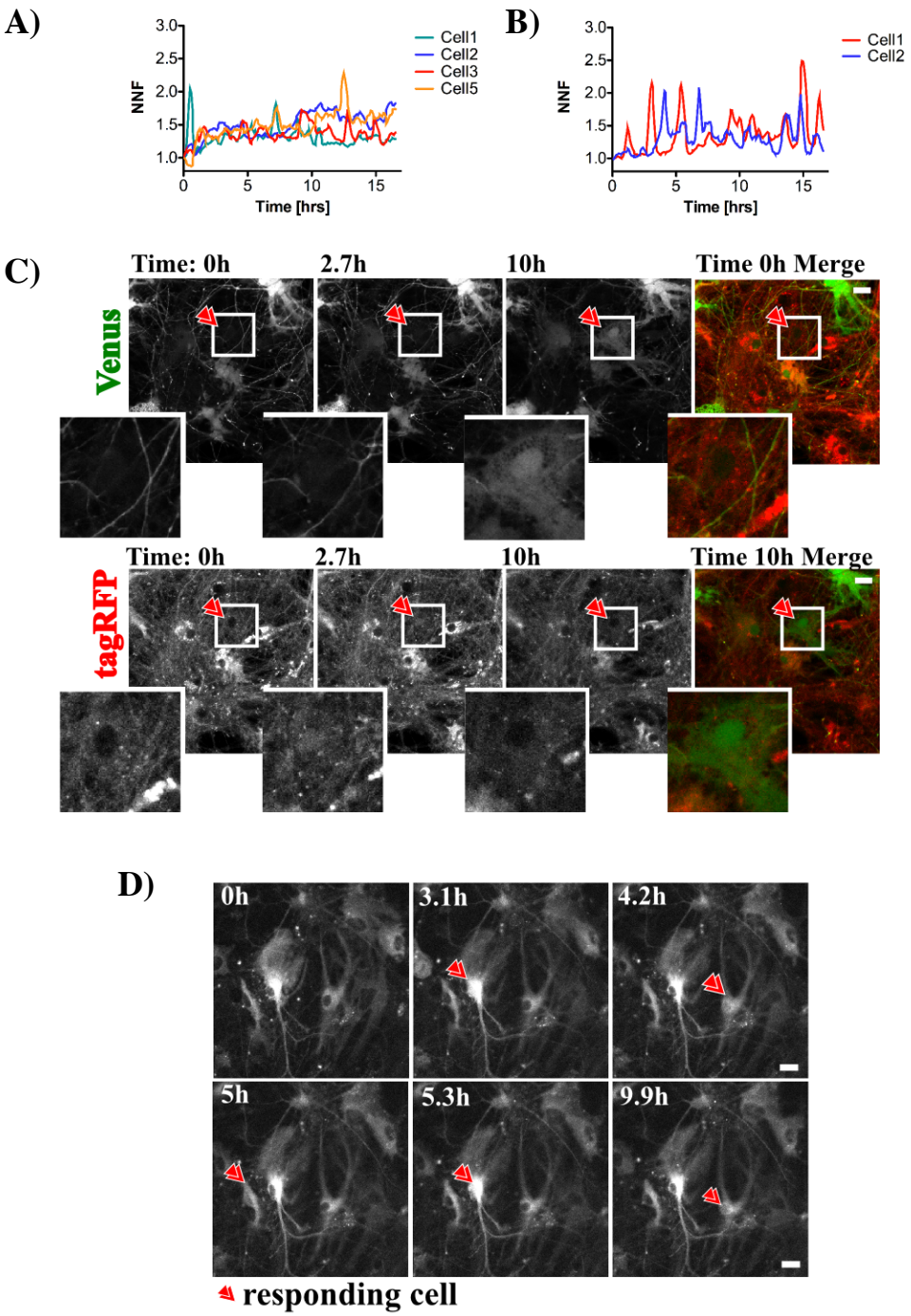

Figure 3.8 Astrocytes exhibit autonomous p65 oscillations. Panels A) & B) show example temporal traces of nuclear EGFP-p65 levels, demonstrating oscillations in nuclear p65 levels in unstimulated cells. C) Time-lapse images from astrocyte-neuron culture transduced with tagRFP-p65 and 5xκB-Venus under basal conditions. Significantly the Venus reporter signal increases in the cell showing spontaneous oscillations in nuclear tagRFP-p65 levels (Movie 4 and Movie 5b). D) Neighbouring astrocytes showing evidence of spontaneous nuclear EGFP-p65 shuttling (Movie 5a), n=3. Scale bar 20μm.

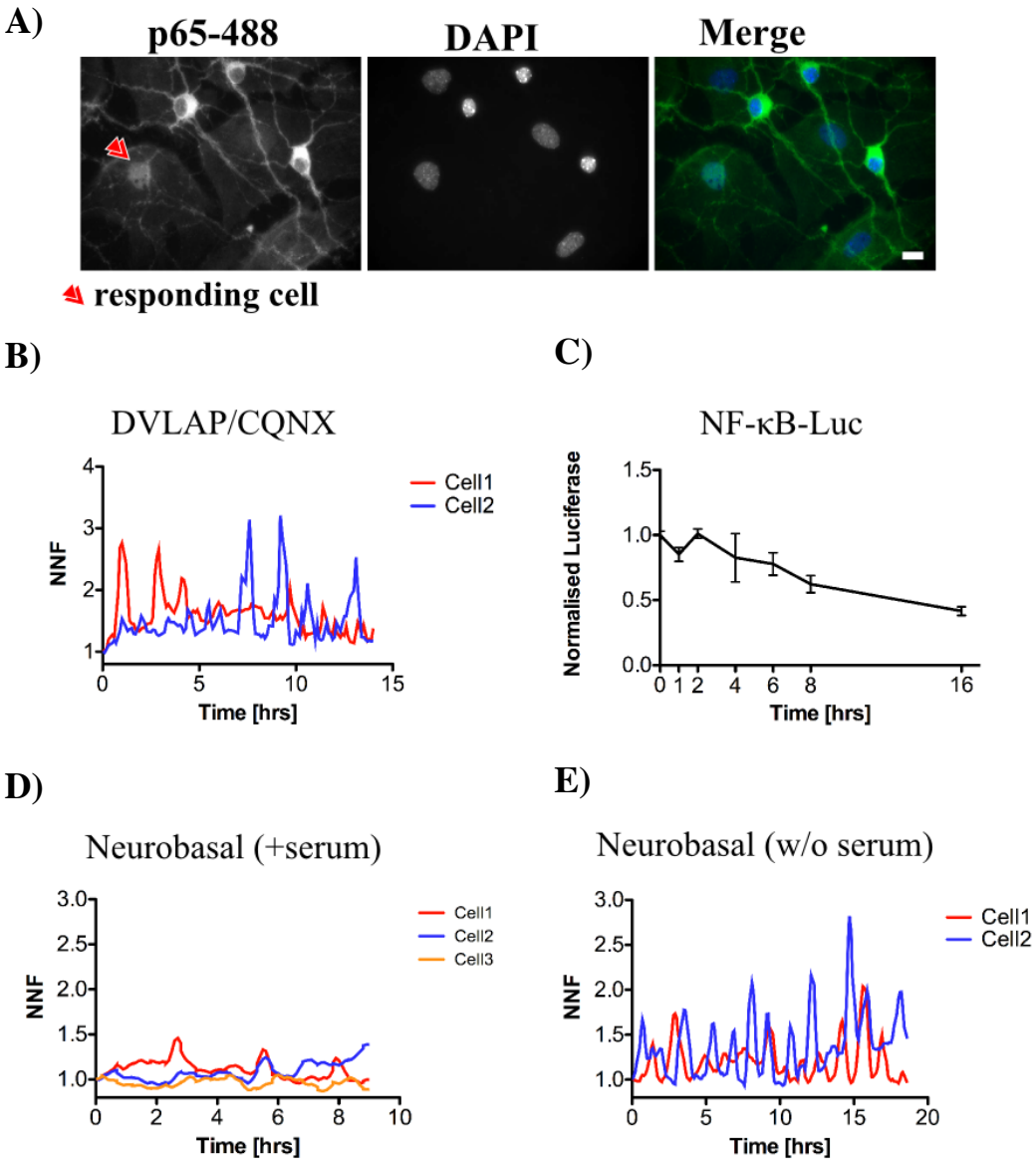

Figure 3.9 Spontaneous astrocyte p65 activity is independent of neuronal inputs. A) Indirect immunofluorescent staining of mixed neuron/astrocyte co-cultures shows evidence of p65-488 nuclear accumulation in unstimulated astrocytes. B) Spontaneous changes in nuclear EGFP-p65 fluorescence levels in mixed neuronal-astrocyte cultures imaged in the presence of glutamate receptor antagonists DVLAP (50μM) and CQNX (10μM). C) 0.5mM L-Glutamate has an inhibitory effect on NF-κB-Luc activity in pure astrocytes (n=1, in triplicates). D) Spontaneous nuclear EGFP-p65 oscillations in 5% Horse Serm (Movie 6a) are amplified and more frequent in serum-free conditions (Movie 6b) (n=1). Scale bar=10μm.

maintenance of pure astrocyte culture) with or without supplementation with horse serum (Figure 3.9D & 3.9E respectively). Although spontaneous p65 oscillations were observed in both culture conditions, they were found to be amplified and more frequent in the absence of serum (Figure 3.9E, Movie 6b *vs*. 6a). Therefore neurons are not necessary to induce the voluntary p65 activation, but the lack of serum in the Neurobasal media seems to amplify inherent NF-κB activity.

3.3.2. Constructing Molecular Tools to Image Dynamic Nrf2 Responses in Primary Hippocampal Astrocytes and Neurons.

3.3.2.1. Characterisation of Nrf2 Responses in Astrocytes and Neurons

As Nrf2 appears to be constitutively expressed at low level a broad range of cells quantification and dynamic profiling of Nrf2 by western blotting or immunofluorescence has proved challenging, in part due to the relatively poor quality of most commercially available antibodies.

To validate the tools used for detection of Nrf2 protein by western blotting (Methods Sections 2.11 & 2.15), several antibodies were tested (R&D Systems clone 383727; Santa Cruz C20 and T19, Abcam ab62352; Everest EB11042), however, in our hands only the polyclonal rabbit anti-Nrf2 (H300, Santa Cruz) successfully detected the Nrf2 protein in primary mouse cells (Figure 3.10A). However, although a specific Nrf2 band was detected with this antisera considerable levels of non-specific staining was observed in western blots. As such the anti sera was thought to be unsuitable for use in immunocytochemistry studies. Figure 3.10A presents data from western blot analysis of hippocampal astrocytes isolated from WT or $Nrf2^{-/-}$ mice. The band of about 100kDa represents Nrf2 as it was detected only in WT cells and not in cells derived from $Nrf2^{-/-}$ mice.

In addition, the identified Nrf2 specific band was shown to increase in response to induction by a single treatment with 100nM CDDO-Me, or co-treatment with CDDO-Me and the proteasome inhibitor MG132 (10μM) (Figure 3.10A). A band of the same molecular weight was also detected by western blotting in mouse hepatocellular carcinoma cells (Hepa-1c7) shown in Figure 3.10B. Therefore, we

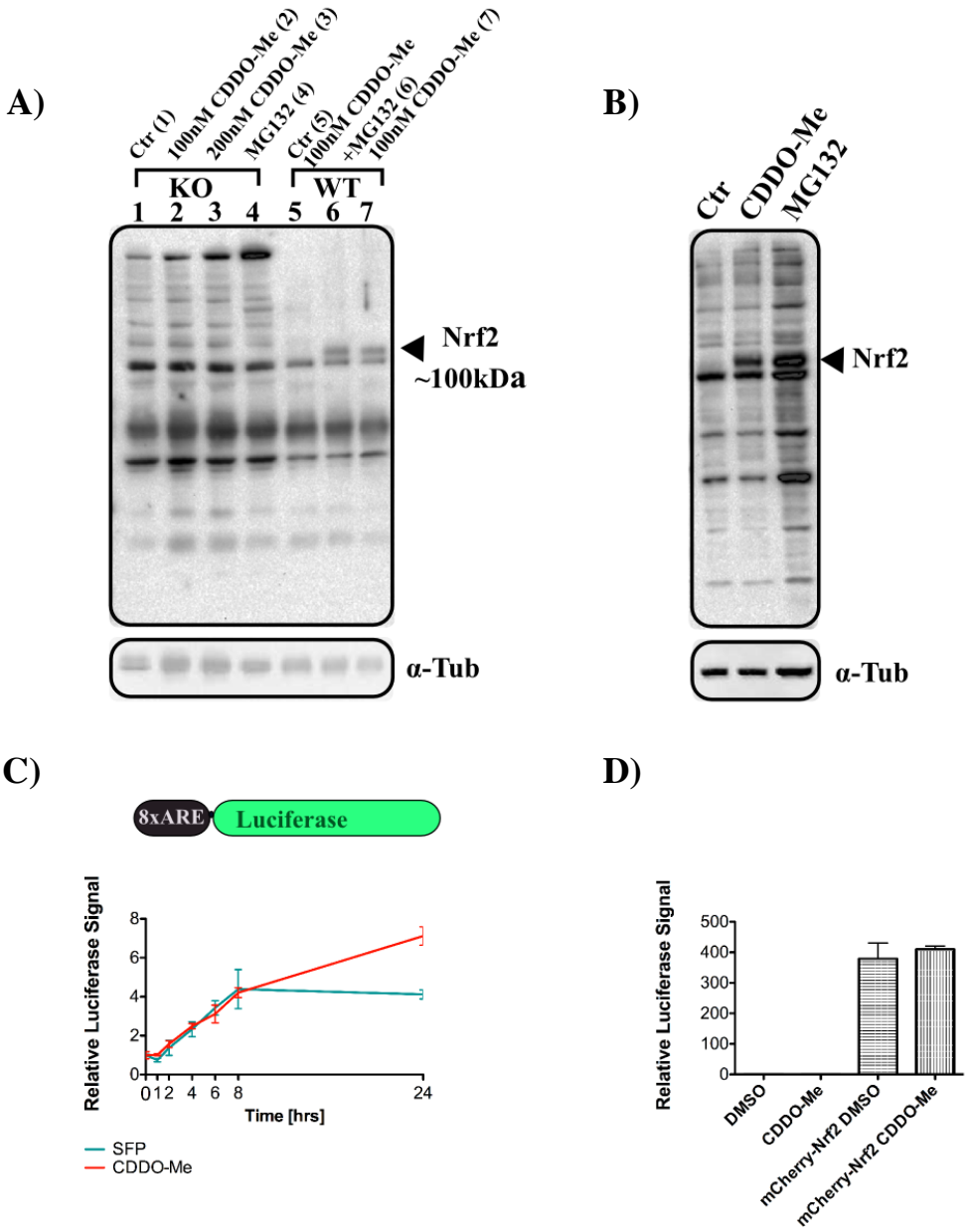

Figure 3.10 Comparison of conditional Nrf2 protein expression and transcriptional activity in astrocytes from WT or Nrf2$^{-/-}$ KO mice.
A) Western blot showing anti-Nrf2 specific staining represented by a band of ~100kDa, which is only observed in lysates prepared from WT astrocytes. B) Western blot showing changes in Nrf2 protein abundance following addition of 100nM CDDO-Me and 10μM MG132 to Hepa-1c cells. C) Relative Nrf2 transcriptional activity in WT astrocytes following addition of SFN or CDDO-Me measured in primary astrocytes using the dual luciferase assay and a reporter plasmid in which luciferase expression is driven by an 8xARE sequence in the luciferase promoter region sensitive to 2μM SFN and 100nM CDDO-Me treatment (n=1, triplicates). D) mCherry-Nrf2 protein fusion expression dramatically increases ARE-Luc activity in Nrf2 KO primary astrocytes (n=1, triplicates). Error bars=STDEV.

were confident that the H300 anti-Nrf2 antibody was suitable for use in further experiments to investigate conditional changes in Nrf2 protein levels.
In order to correlate observed trends in Nrf2 protein abundance with functional studies, with measurements of Nrf2 transcriptional activity, an ARE-Luc reporter construct (kindly provided by Dr. Joanne Walsh, University of Liverpool) was used in conjunction with the dual luciferase method (Figure 3.10C & D) to quantify conditional levels of Nrf2 transcription. Expression of luciferase in the ARE-Luc plasmid is driven by 8xARE consensus sequences based on mouse GCLC sequence (Kratschmar *et al,* 2012). All luciferase assays were performed as described in Methods Section 2.4.6.

The ARE-Luc expression was measured following addition of either 100nM CDDO-Me or 2μM SFN at indicated time points. The ARE driven luciferase activity was seen to increase in response to both Nrf2 inducing drugs (Figure 3.10C), with the CDDO-Me evoking more pro-longed activation of Nrf2 transcriptional activity. To examine the specificity of the ARE-Luc construct as a reporter for Nrf2 mediated transcriptional activity, the activity of the ARE-Luc reporter in response to CDDO-Me was also assessed in astrocytes derived from $Nrf2^{-/-}$ mice (Figure 3.10D). Significantly no increase in ARE-driven luciferase activity was observed in astrocytes derived from $Nrf2^{-/-}$ mice. Co-expression of a fluorescent mCherry-Nrf2 fusion protein restored Nrf2 activity in $Nrf2^{-/-}$ astrocytes, significantly increasing the ARE-Luc signal, however in this case addition of CDDO-Me (100nM) failed to further amplify the ARE-Luc signal.

To visualize Nrf2 dynamic responses in live cells, the mouse *NRF2* cDNA coding sequence was inserted downstream of the mCherry fluorescent tag to form a mCherry-Nrf2 protein fusion (Methods 2.1). In this vector relatively high levels of expression are driven by the human *UBC* promoter sequence. Initially, the plasmid was transiently expressed in astrocytes using Lipofectamine2000 (Methods 2.4.5) and imaged using Zeiss 5.10 confocal imaging system (Methods 2.13) (Figure 3.11A, B & D). Although transfection efficiency in primary astrocytes was found to be very low, sufficient numbers of transfected cells were obtained to perform

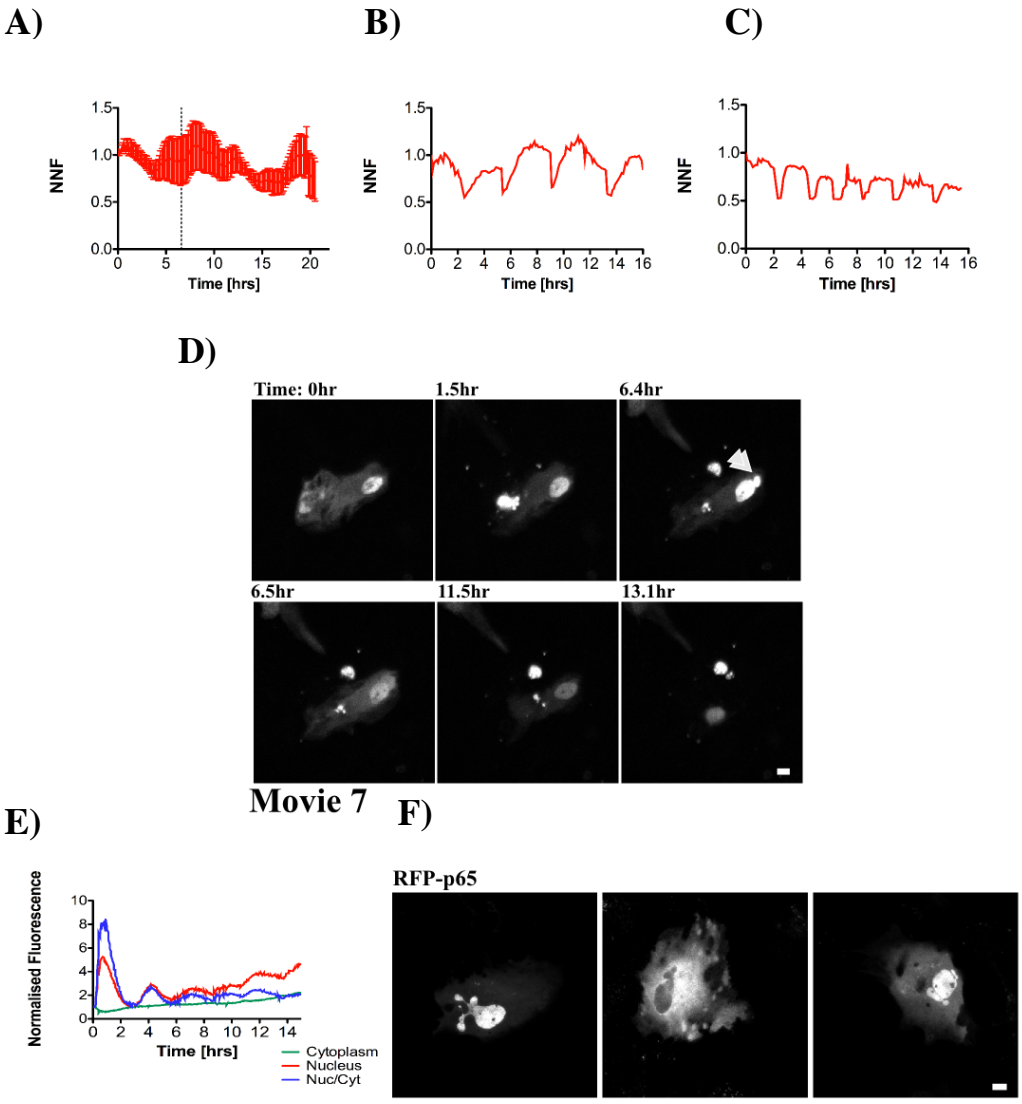

Figure 3.11 Transient expression of Nrf2 and p65 from a plasmid is associated with aberrant nuclear behaviour. A) Measuring mCherry-Nrf2 fluorescence in primary astrocytes shows no response to 100nM CDDO-Me (addition marked by a dashed line) (n=1, c=6). B) Representative trace of basal mCherry-Nrf2 levels shows nuclear oscillatory dynamics under basal conditions in astrocytes, n=3. C) Fluctuating nuclear levels of unrelated nuclear protein mCherry-UBE2D2 can also be observed under basal conditions, n=1. D) Representative images from time-lapse imaging showing nuclear breakdown events and apoptosis of astrocytes expressing mCherry-Nrf2 (Movie 7 and Movie 8). E) The transiently expressed EGFP-p65 shows appropriate oscillatory dynamics in astrocytes following TNFα. F) Transient expression of tagRFP-p65 is frequently associated with atypical nuclear morphology. Error bars=STDEV, scale bar=10μm.

planned imaging experiments. Initial time-lapse imaging studies using the mCherry-Nrf2 vector in primary astrocytes (1 image p/8min) unveiled an irregular pattern of Nrf2 nuclear fluorescence under basal conditions (Figure 3.11A & B, Movies 7 & 8), showing periodic deceases and increases in levels of mCherry-Nrf2 fluorescence (Figure 3.11B), with little or no response to the addition of CDDO-Me (Figure 3.11A & 3.10D). To test whether the observed oscillatory phenotype was specific to mCherry-Nrf2 or resulted of some deleterious artefact, another resident nuclear protein mCherry-UBE2D2 was investigated. Surprisingly the mCherry-UBE2D2 also demonstrated similar oscillatory nuclear dynamics (Figure 3.11C). As a result we concluded that the apparent oscillatory dynamics initially observed for mCherry-Nrf2 were most likely an artefact resulting from a non-specific instability, or periodic rupturing, of the nuclear membrane, as reported in other cell types (De Vos *et al,* 2011). To support this conclusion, Figure 3.11D (Movie 7) shows representative images from live cell imaging studies where high levels of mCherry-Nrf2 expression were frequently accompanied with irregular nuclear morphology characterized by the presence of a small satellite nuclear blebs (indicated by an arrow in Figure 3.11D), which are characteristic of transient nuclear rupture events. Similarly imaging p65 responses to TNFα by transient expression of EGFP-p65 plasmid demonstrated expected oscillatory behaviour (Figure 3.11F). However overexpression of p65 was associated with increased apoptosis during imaging and observation of irregularities in the nuclear shape (Figure 3.11G). Given these phenotypes we concluded that transient expression methods that result in expression of high levels of Nrf2 (or other nuclear proteins) are an inappropriate experimental system to study conditional Nrf2 dynamics as they are highly prone to experimental artefacts, which could seriously jeopardise meaningful interpretation of physiologically relevant Nrf2 responses. For this reason we developed alternate lentivirus mediated expression systems, which allow fluorescently tagged Nrf2 proteins to be expressed at near endogenous levels without the use of stress inducing transfection reagents.

3.3.2.2. Development of Lentiviral Expression System for Imaging of Dynamic Nrf2 Responses

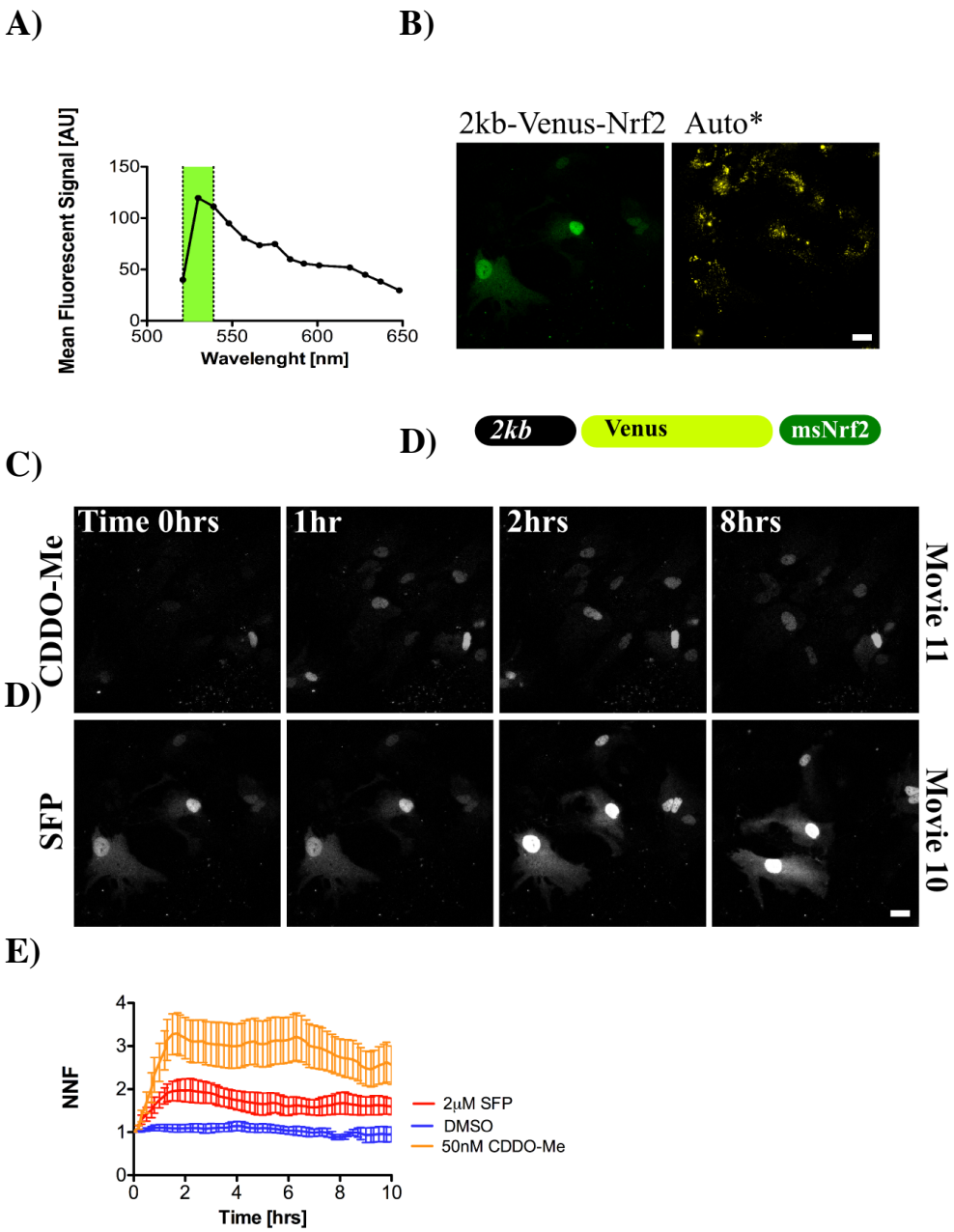

Figure 3.12 Imaging low-level expression of 2kb-Venus-Nrf2 in primary murine astrocytes. A) Spectral profile of astrocytes stably expressing Venus-Nrf2, under control of the endogenous *2kb* Nrf2 promoter region (*2kb*-Venus-Nrf2) obtained by Lambda scanning; characteristic Venus emission maxima peak is highlighted in green. B) Results of Linear unmixing showing signal from Venus the fluorescence channel (green) compared to the background autofluorescence/noise signal removed by spectral unmixing (Auto*, yellow). C) Representative time-lapse images of *2kb*-Venus-Nrf2 in primary astrocytes in response to addition of 50nM CDDO-Me or D) 2μM SFN. E) Mean nuclear fluorescence levels of *2kb*-Venus-Nrf2 in response to addition of DMSO (control) (Movie 9), 50nM CDDO-Me (Movie 11) or 2μM SFN (Movie 10) (n=2, c=4-13). Error bars=SEM, scale bar=20μm.

in

To address the problems encountered during plasmid Nrf2 expression, a lentiviral expression system was employed to allow low-level expression of the Nrf2 protein. To achieve near endogenous levels of Nrf2 expression, the *UBC* promoter sequence the *UBC*-Venus-(insert) vector was replaced by the murine proximal Nrf2 promoter sequence, including the *2kb* region directly upstream of the *NRF2* START codon (Figure 3.12D) (Methods 2.2, Map in Supplementary Section 8.3). Reassuringly, astrocytes infected with the resulting Venus-Nrf2 encoding lentivirus exhibited very low levels of *2kb*-Venus-Nrf2 fluorescence (Figure 3.12B), which was similar in intensity to levels of cellular autofluorescence. To separate the background autoflourescence signal from the *2kb*-Venus-Nrf2 fluorescence, astrocytes were imaged using the lambda scan mode on the Zeiss 7.80 confocal microscope (Methods 2.13.1). Lambda scanning allows a sequence of images to betaken by gradually increasing the wavelengths allowed to pass through the emission filter sets, while illuminating with the 514nm laser beam. It then combines the images generated and the specific fluorescence emission profile can be selected (Figure 3.12A). The astrocyte cells expressing Venus-Nrf2 showed characteristic Venus emission peak (highlighted in green Figure 3.12A), which could then be easily distinguished from background autoflourescence or noise. This approach also allowed selection of the optimal emission peak for imaging of Venus fluorescence alongside other fluorescent protein fusions.

To test whether the lentivirally expressed *2kb*-Venus-Nrf2 responds to canonical Nrf2 inducing drugs, astrocytes were imaged every 8min for at least 8hrs and the dynamic profile of the Nrf2 fusion in response to 2μM SFN, 100nM CDDO-me or the DMSO control was obtained. Representative images from this experiment are shown in Figure 3.12C & D (Movies 9, 10, 11). Measurement of Venus-Nrf2 normalised nuclear fluorescence levels (NNF), displayed clear induction profiles in response to both CDDO-Me and SFN stimulation, but remained unchanged as a result of DMSO control treatment (Figure 3.12E, Movie 9).

Finally, tagRFP-p65 and *2kb*-Venus-Nrf2 were co-transduced into mixed hippocampal neuron-astrocyte cultures in order to monitor dynamic responses to stimulation with 50nM CDDO-Me in both cell-types (Figure 3.13 and Movie 12). The experiment provided clear evidence that both astrocytes and neurons show clear

CDDO-Me induction of nuclear Venus-Nrf2. Significantly, addition of CDDO-Me did not induce nuclear translocation of tagRFP-p65 in either cell type.

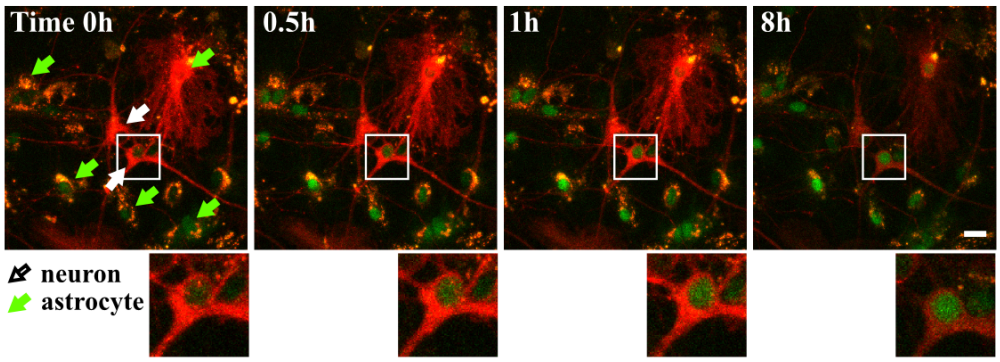

Figure 3.13 Combined temporal imaging of tagRFP-p65 and *2kb*-Venus-Nrf2 in co-cultured mouse neurons and astrocytes. Representative images taken from a mixed culture of neurons and astrocytes transduced with tagRFP-p65 and *2kb*-Venus-Nrf2. Times indicate elapsed period after addition of 50nM CDDO-Me (Movie 12), n=2. Highlighted neuronal cell shows increasing levels of nuclear *2kb*-Venus-Nrf2 expression in response to CDDO-Me treatment. Scale bar =20μm.

3.3.3. Development of an Astrocyte Specific Nuclear Marker

Unfortunately, analysis of data obtained from p65 and Nrf2 imaging experiments required tedious manual cell-by-cell analysis to define nuclear boundaries when quantifying nuclear fluorescence intensities (Methods 2.13.3). However, there was a potential that this process could be significantly automated by labelling the nuclear compartment with a stable fluorescent marker. There are several proteins that could act as a nuclear marker, however LaminB1 structural nuclear protein has frequently been used for this purpose. To avoid spectral overlap between the LaminB1 protein and tagRFP and Venus signals, a Cyan fluorescent protein was chosen to generate a fluorescent LaminB1 fusion construct for nuclear labelling. Additionally, to ensure that the measurement is indeed carried out in astrocyte cells of interest, as opposed to oligodendrocytes, microglia, neurons or epithelial cells, the LamninB1-Cyan fusion-protein was expressed under an astrocyte specific *GFAP* promoter (Figure 3.14A & C) (Map in Supplrmrntary Section 8.3). Initially, the *GFAP*-Cyan construct was tested to verify the *GFAP*-driven expression was possible in SK-N-AS and astrocytes

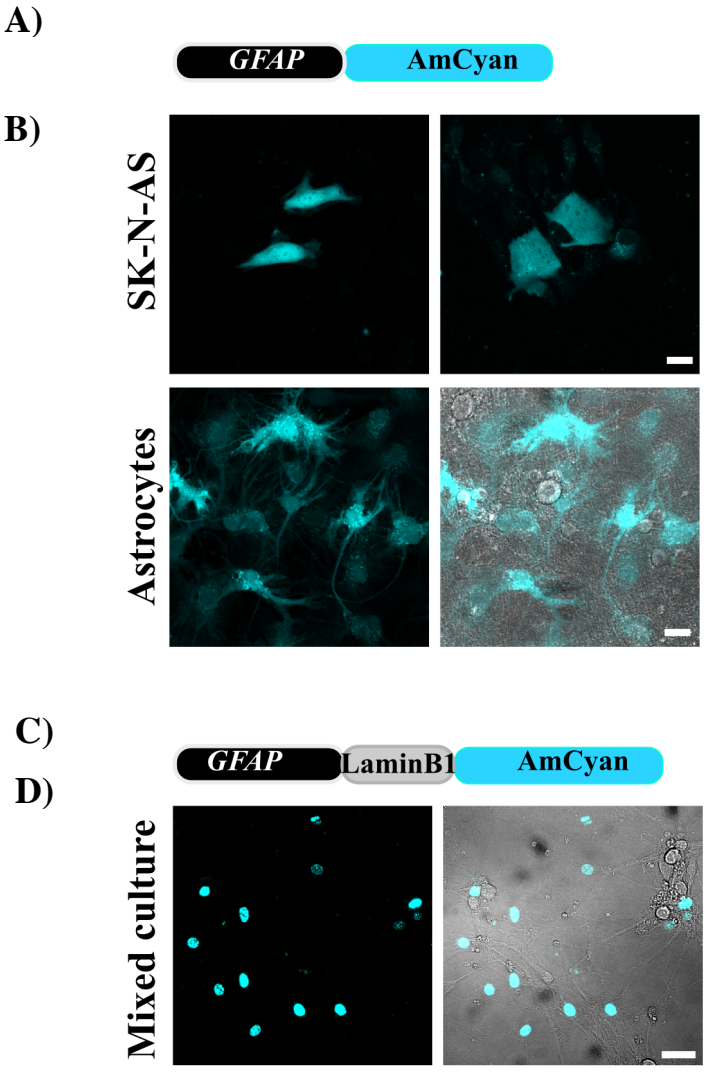

Figure 3.14 Construction of an astrocyte specific fluorescent nuclear marker GFAP-LaminB1-Cyan. A) Diagram showing the design of the Cyan fluorescent reporter under astrocyte specific *GFAP* promoter. B) Representative images of SK-N-AS neuroblastoma and primary astrocyte cells transiently transfected with *GFAP*-Cyan. C) Diagram depicting the design of *GFAP*-LaminB1-Cyan plasmid. E) Representative images of mixed astrocyte-neuronal culture showing astrocyte specific LaminB1-Cyan nuclear labelling as a result of *GFAP*-LaminB1-Cyan transduction. Scale bar=20μm.

cells (Figure 3.14 B & C). Subsequently, the *laminB1* sequence (isoform 1) was inserted downstream of the *GFAP* promoter using Gateway cloning approach (Methods 2.1) (Figure 3.14D). The mixed culture infected with *GFAP*-LaminB1-Cyan displayed nuclear staining of astrocytes, whereas phase bright neurons did not show any fluorescence (Figure 3.14E). Therefore the *GFAP*-LaminB1-Cyan lentiviral construct could be used for future studies to facilitate the automation of nuclear fluorescence intensity measurements in astrocytes. This tool has proved especially helpful in studying Nrf2 responses in astrocytes grown in mixed culture systems.

3.3.4. Characterisation of Nrf2 Dynamic Responses Using a Stable Nrf2-Venus Expressing BAC$^{Nrf2\text{-}Venus}$ Neuroblastoma Model for Live Cell Imaging

3.3.4.1. Comparison of Endogenous Nrf2 and BAC-derived Nrf2-Venus Dynamic Responses

Imaging primary neuronal and astrocyte cells is an excellent source of information about the physiological responses of cells originated form the CNS. However, limited cell numbers and the demanding nature of primary neuronal cell culture impose restrictions on large-scale multi-modal analysis of dynamic conditional signalling responses. To first establish the fundamental principles of pathway regulation and the interplay between NF-κB and Nrf2 signalling responses we chose to utilise a recently generated neuroblastoma SK-N-AS cell line, which had been engineered to stably express Nrf2-Venus in an endogenous genomic context from an integrated Bacterial Artificial Chromosome (BAC). To initiate this work it was first necessary to validate that the Nrf2-Venus BAC cells (BAC$^{Nrf2\text{-}Venus}$) were a suitable model system to use to investigate dynamic Nrf2 responses in live cells. In particular, it was important to first establish if dynamic or conditional changes in Nrf2-Venus distribution or accurately reflect expression levels and dynamic changes seen for the endogenous Nrf2 protein.

The Nrf2-Venus BAC cell line was previously generated by Dr Karen Dunn under the supervision of C.M. Sanderson (University of Liverpool) and M.White (University of Manchester). Initial fluorescence in situ hybridisation (FISH) established that the fragment of BAC expressing the Nrf2-Venus fluorescent protein

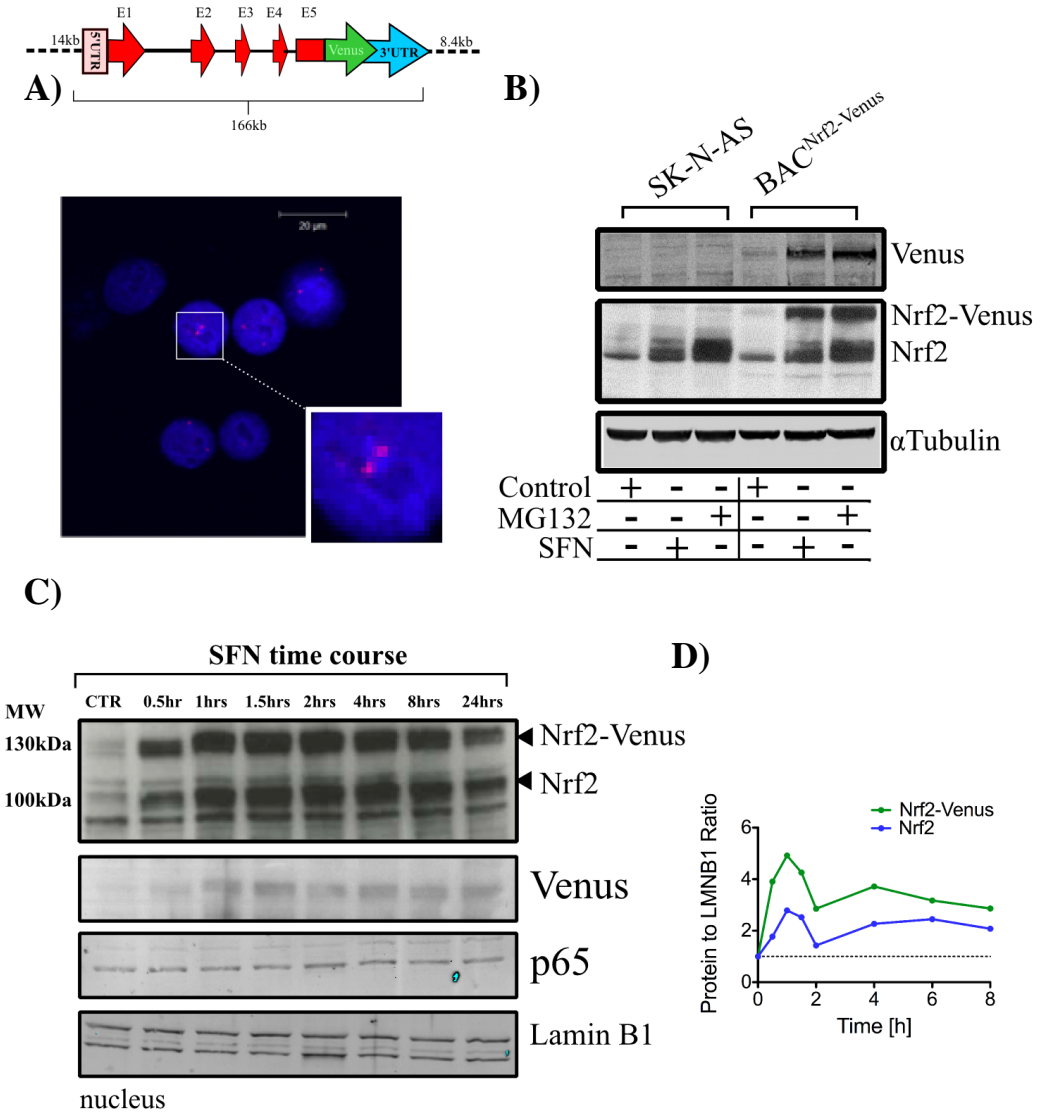

Figure 3.15 Characterisation of a neuroblastoma SK-N-AS BAC$^{Nrf2\text{-}Venus}$ cell line as model for studying dynamic Nrf2 responses at a near-endogenous level. A) Representative image from FISH analysis of BAC$^{Nrf2\text{-}Venus}$ cells (image provided by Dr Karen Dunn) showing only two sites of Nrf2-Venus encoding BAC integration in the SK-N-AS genome. B) Western blot analysis of WT SK-N-AS and SK-N-AS BAC$^{Nrf2\text{-}Venus}$ lysates showing relative levels of Nrf2 and Nrf2-Venus expression in each cell type under basal and induced conditions, n=1. C) Western blot of BAC$^{Nrf2\text{-}Venus}$ nuclear lysates, showing correlated time dependent accumulation of both endogenous Nrf2 and the BAC-encoded Nrf2-Venus protein following addition of 2μM SFN, n=2. D) Quantification of total protein levels normalised to Lamin B1 nuclear loading control, performed on ImageJ. Scale bar=20μm.

was incorporated into the SK-N-AS cells at two copies per cell (from now being referred to as $BAC^{Nrf2\text{-}Venus}$) (Figure 3.15A). A western blot analysis was then performed to assess the relative level of expression of the endogenous Nrf2 protein and Nrf2-Venus between SKNAS and $BAC^{Nrf2\text{-}Venus}$ (Figure 3.15B). As expected the higher MW band representing the Nrf2-Venus fusion protein was only observed in the $BAC^{Nrf2\text{-}Venus}$ cells (~130kDa). Importantly, the Nrf2-Venus protein and endogenous Nrf2 (100kDa) exhibited similar increases in expression levels following addition of the proteasomal inhibitor MG132 (10μM) or the Nrf2 inducer SFN (2μM) (Figure 3.15B). The western blot analysis of Nrf2 induction following time course addition of 2μM SFN displays similarity of Nrf2-Venus and endogenous Nrf2 responses and stability over 24h (Figure 3.15C & D)

Although the low levels of Nrf2-Venus are optimal, as they closely resemble levels of the endogenous protein, this poses a technical problem for live cell imaging studies. As with our previous studies using lentivirus mediated expression systems in neurons and astrocytes, visualisation of the $BAC^{Nrf2\text{-}Venus}$ cells required the use and optimisation of state of the art imaging techniques available on the 7.80 confocal system. Use of the lambda scan mode confirmed that the nuclear fluorescent signal was indeed the Venus fluorescence. The range of emission profiles acquired by 514nm illumination and the combined emission spectrum profile of Nrf2-Venus and the SK-N-AS autofluorescence are shown in Figure 3.16A & B respectively (Methods 2.13.1). From this data it is clear that imaging of the Nrf2-Venus fluorescence could be performed in two ways. Either by using the lambda scan mode, which would maximize the Venus fluorescent signal (Figure 3.16D), or by selecting the narrow Venus emission maximum (522nm-540nm), which may be preferable when imaging Nrf2 alongside other fluorescent proteins. Comparison of both methods shows the Nrf2-Venus signal is much clearer when using the linear unmixing method (Figure 3.16C).

The utility of the $BAC^{Nrf2\text{-}Venus}$ cells was further assessed by imaging live cell responses to canonical inducers of Nrf2, including 2μM SFN, 100nM CDDO-Me and 10μM MG132 (Figure 3.17A, Movies 13, 14, 15).

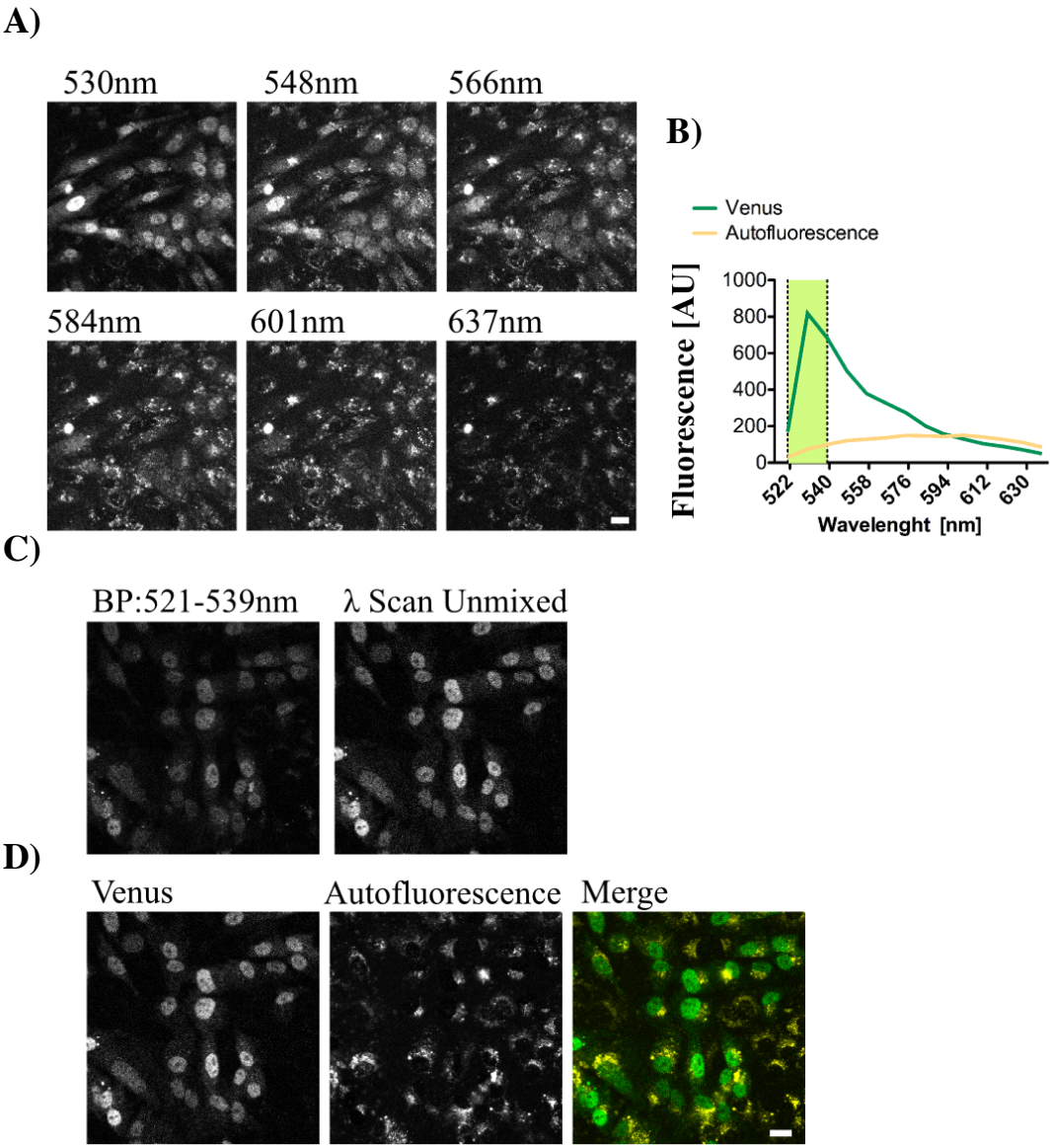

Figure 3.16 Imaging near-endogenous levels of Nrf2-Venus expression in the SK-N-AS BAC$^{Nrf2\text{-}Venus}$ cell-line using 7.80 Zeiss confocal microscope. A) Low-levels of Nrf2-Venus expression were spectrally unmixed using lambda scan mode on a 7.80 Zeiss confocal microscope. The figure shows sequential image series taken by narrow spectrum band pass filters show differences in fluorescent signal, which are dependent on detector bandwidth sensitivity. B) The emission profile of SK-N-AS BAC$^{Nrf2\text{-}Venus}$ cells following spectral unmixing to separate Venus and autofluorescence specific emission spectrum. C) Comparison of Nrf2-Venus signal taken by setting narrow detection limits on band-pass filters (set to Venus emission maximum), or by spectrally unmixing using the lambda scan method. D) Spectrally unmixed fluorescence signals of Nrf2-Venus (green) and the autofluorescence (yellow). Scale bar=20μm.

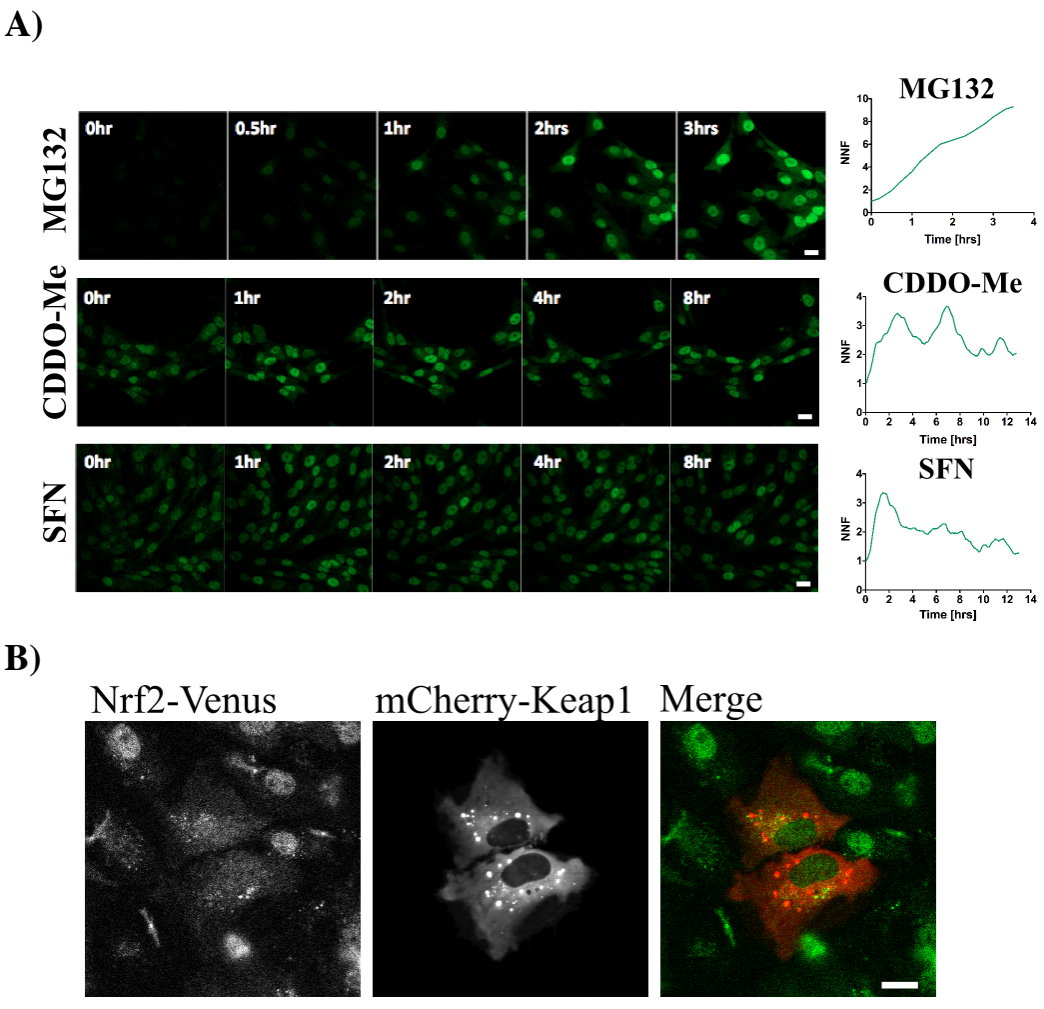

Figure 3.17 Co-expression of mCherry-Keap1 induces redistribution of Nrf2-Venus in BAC$^{Nrf2\text{-}Venus}$ cells. A) Temporal changes in Nrf2-Venus expression levels following treatments of BAC$^{Nrf2\text{-}Venus}$ cells with 10μM MG132 proteasome inhibitor (Movie 13), 2μM SFP (Movie 14) or 100nM CDDO-Me (Movie 15). B) Co-expression of mCherry-Keap1 plasmid in BAC$^{Nrf2\text{-}Venus}$ cells leads to a reduction in Nrf2-Venus expression and enhanced sequestration of Nrf2-Venus in the cytoplasm of transfected cells. Scale bar=20μm.

3.3.4.2. Measuring Keap1 and Nrf2 Interaction in Live Cells

In order to further establish that the Nrf2-Venus fusion protein was an appropriate tool to investigate functional responses in the Nrf2 pathway, it was essential to establish if the Nrf2-Venus fusion protein could associate with its primary negative regulator Keap1, in live cells. To address this point, the mCherry-Keap1 plasmid was transiently expressed in $BAC^{Nrf2\text{-}Venus}$ cells in order to define the effects of Keap1 expression on the abundance and distribution of Nrf2-Venus (Figure 3.17B). Transient over-expression of mCherry-Keap1 resulted in a dramatic depletion of nuclear Nrf2-Venus levels, with a commensurate accumulation of both mCherry-Keap1 and Nrf2-Venus in the cytoplasm of transfected cells. In contrast, Nrf2-Venus remained almost totally nuclear in neighbouring non-transfected cells (Figure 3.17B). This encouraging result prompted a more detailed study of mCherry-Keap1/Nrf2-Venus complex formation in live cells, utilising the cutting edge Fluorescence Cross-Correlation Spectroscopy technique (for which help and training were kindly provided by Dr James Boyd, Prof. M. White's group, University of Manchester). The principles of FCS and FCCS are depicted in Figure 3.18A & B and explained in Methods 2.13.4. FCCS measurements are only possible between fluorophore pairs that are spectrally well separated, and relatively photostable. However, the advantage of this technique over FRET based assays is that the two fluorescent proteins do not have to be in close proximity, they simply have to be part of the same molecular complex. The fluorescent signal of mCherry-Keap1 and Nrf2-Venus measured by the Autocorrelation function followed a steady one-phase decay, as illustrated by the FCS curves in Figure 3.18C, with the magnitude of decline being indicative of the reproducibility of diffusion behaviour. This shows that the diffusion of Nrf2 and Keap1 proteins (separately) follow a consistent pattern, *e.g.* the movement of molecules was comparable over the acquisition time. To further measure this interaction the similarity between the mCherry and Venus fluorescence signals was compared by FCCS analysis. It was expected that bound proteins would achieve a cross-correlation value greater than zero. The FCCS curve has a one-phase decay shape (as opposed to a straight line, which would signify no interaction), starting from a relatively high value of approximately 0.015 $G(\tau)$, which is indicative of the formation od a stable complex between the Nrf2-Venus and mCherry-Keap1

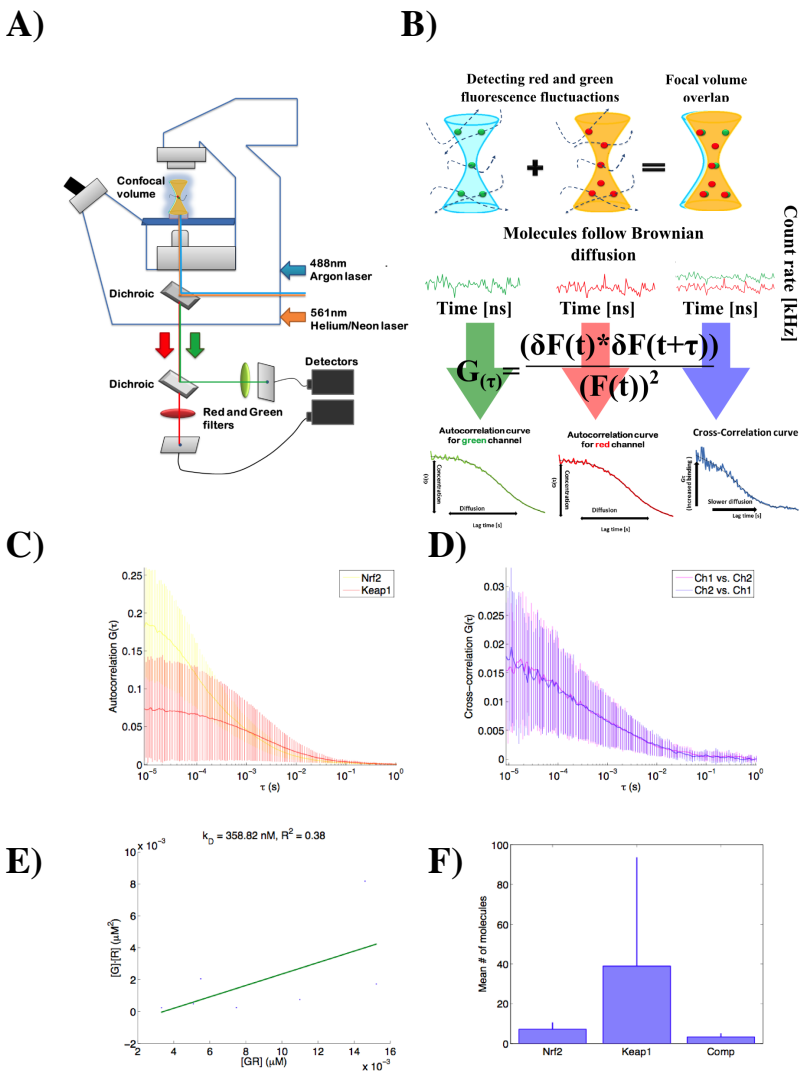

Figure 3.18 Use of FCCS microscopy to investigate the formation of Nrf2-Venus/mCherry-Keap1 complexes in cytoplasm in real-time. A & B) Diagram depicting the principles of the FCCS technique. C) Auto-correlation curves of Nrf2-Venus (yellow) and mCherry-Keap1 (red). D) Cross-correlation curves of Nrf2-Venus and mCherry-Keap1, the high correlation value indicates strong binding between the two proteins. E) The K_D constant obtained by plotting the free Nrf2-Venus [G] and mCherry-Keap1 [R] signals against Nrf2-Venus and mCherry-Keap1 complexes ([GR]), indicates strong binding between the two proteins. F) Graph showing the relative proportions of free and complexed Nrf2-Venus and mCherry-Keap1 molecules. Error bars= STDEV, n=2, c=9.

proteins (Figure 3.18D). The data obtained from FCS and FCCS measurements could be further used to assess the strength of complex formation by plotting the amount of free Venus and mCherry proteins, which diffuse much faster than proteins in larger complexes, against the values for mCherry-Venus complexes, in order to calculate a predicted dissociation constant (K_D) (Figure 3.18E). The dissociation constant calculated for the Nrf2-Venus and mCherry-Keap1 = 358.82nM K_D, representing a very strong binding. The number of free molecules in the confocal volume was calculated by substracting the amount of mCherry-Venus complexes from the total amount of Venus and mCherry proteins respectively (Figure 3.18F). As the Nrf2-Venus is expressed at near-physiological levels in $BAC^{Nrf2\text{-}Venus}$ cells, the Nrf2 molecules are out-titrated by the expression level of the transiently overexpressed mCherry-Keap1 protein, and a large proportion of Nrf2-Venus is bound in a complex with mCherry-Keap1.

3.3.4.3. Basal Nrf2 Dynamics

While it has been established that Nrf2-Venus protein responds to induction with SFN, CDDO-Me and MG132 (Figure 3.17A), it is important to note that the basal Nrf2-Venus nuclear fluorescence remained stable throughout most imaging experiments in this study (Figure 3.19A). However, there is one notable exception. There appeared to be a well-defined time-point during unstimulated imaging conditions when the Nrf2-Venus protein levels first decrease then increased in synchronised pattern in both daughter cells (Figure 3.19B & C, Movie 16). This phenotype is shown in the representative images taken during extended 14 or 24h time-lapse experiments (Figure 3.19B), showing the cell division process, which results in two, bright daughter cells. Interestingly, the Nrf2-Venus increase occurs every time cell division takes place suggesting that levels of Nrf2 expression is under cell-cycle dependent control.

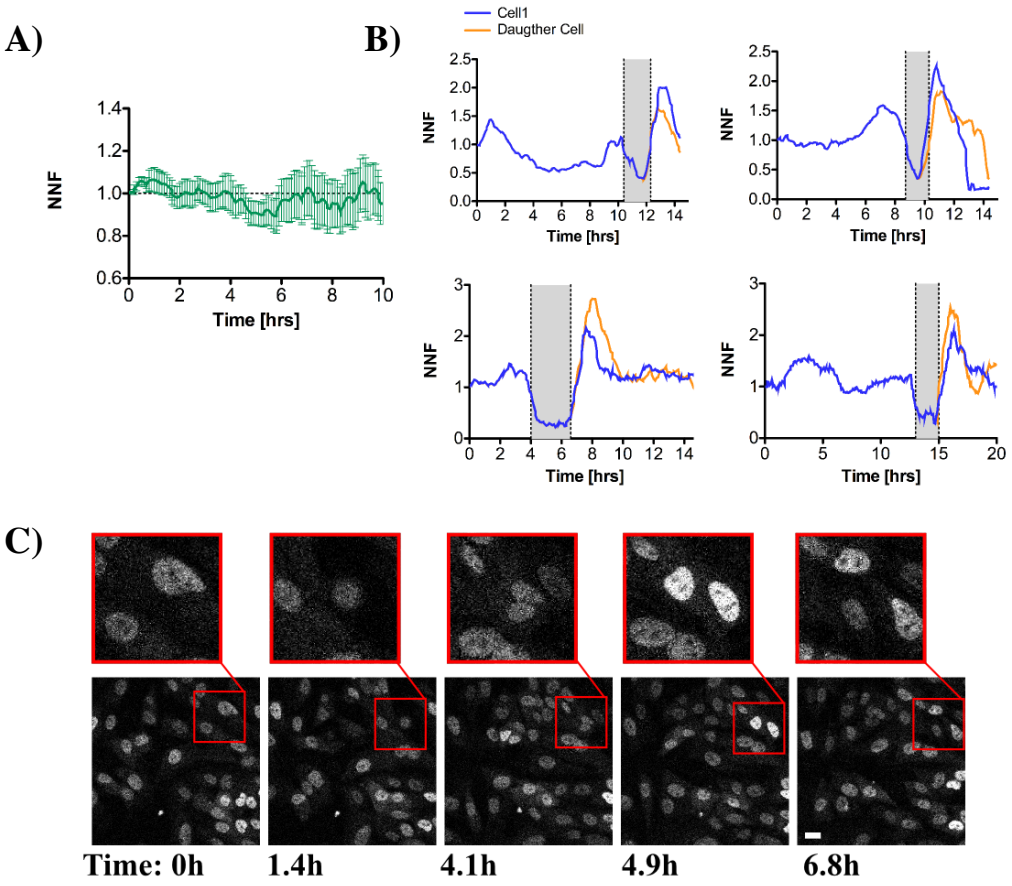

Figure 3.19 Levels of Nrf2-Venus are regulated in a cell-cycle dependent manner. A) Averaged nuclear Nrf2-Venus fluorescence under unstimulated conditions (n=2, c=6). B) Representative Nrf2-Venus fluorescence traces showing a co-ordinated dip and subsequent increase in nuclear Nrf2 levels in daughter cells following cell-division. C) Representative time-lapse images from unstimulated BAC$^{Nrf2\text{-}Venus}$ neuroblastoma cells showing a clear increase of Nrf2-Venus signals in both daughter cells following cell division (Movie 16). Scale bar 20μm.

3.4. DISCUSSION

Glial cells perform a wide array of cellular tasks in support of neighbouring neuronal cells, and are believed to be the main players involved in antioxidant protection within the brain (Vargas & Johnson, 2009). The antioxidant responses ensure appropriate resolution of acute inflammatory episodes and play a major role in the prevention of neurodegeneration (Gupta *et al,* 2012). Cellular responses to antioxidant and inflammatory stimulation are primarily mediated by the Nrf2 and NF-κB signalling cascades respectively, however their dynamic responses to physiological and pharmacological modulators in primary astrocytes and neurons have not been extensively researched. This study aimed to generate sophisticated imaging tolls to enable investigation of Nrf2 and p65 responses to TNFα, SFN and/or CDDO-Me, and to gain more insight into cellular responses that are likely to take place within the CNS.

The investigation of mixed neuronal and astrocyte cultures by live cell imaging provided an excellent approach for exploration of cell specific responses without the need to utilise large cell numbers and labour intensive biochemical studies.

3.4.1. Astrocytes Exhibit Strong Basal and TNFα-Induced NF-κB Responses

There have been mixed reports on the cell specific nature of NF-κB responses in the brain. Historically, agreement on this point was hindered by the poor quality of available antibodies used in immunofluorescent staining and western blot studies (Slotta *et al,* 2014). In this study, western blot analysis of the cytoplasmic and nuclear fractions from both astrocytes and neurons highlighted the differences in cell-type specific responses to TNFα, with neurons failing to induce nuclear p65 accumulation following cytokine treatment (Figure 3.2). Interestingly, the molecular weight of p65 detected in neurons was different between cytoplasmic and nuclear fractions. Our data shows that the quantity of nuclear p65 did not change over the time-course of TNF α treatment, and only one 82kDa band was detected (slightly higher than the predicted MW of ~69kDa, whereas two bands (82kD and ~150kDa) were detected in the cytoplasm (Figure 3.2A), to validate if the upper band represents genuine p65 staining siRNA knockdown of p65 should be performed in the future.

Lentiviral expression of the p65 subunit at near-endogenous levels as either fluorescent tagRFP-p65 or EGFP-p65 fusion proteins (Figure 3.4C and 5), allowed real-time imaging of NF-κB temporal behaviour in primary cells under basal activity (Figure 3.8 and 3.9) and following TNFα stimulation (Figure 3.5 and 3.6).

EGFP-p65 and tagRFP-p65 imaging studies performed in this study confirmed previous biochemical reports on neuronal insensitivity to TNFα stimulation. To exclude the possibility of other NF-κB subunits being involved in TNFα neuronal responses, the lentiviral 5κB-Venus reporter was imaged in mixed cultures to measure the NF-κB activity (Figure 3.7, Movie 3a). In these studies, 5κB-Venus levels only increased in astrocytes (Figure 7 B-E). However, neurons did show a strong basal expression of the 5κB-Venus signal, indicating a high basal activity of NF-κB in those cells (Figure 3.7D, Movie 3a).

Again, there are mixed reports on degree of neuronal NF-κB signalling in response to stress stimuli in the literature. Recent study by Listwak *et al*. reported that neuronal p65 responses to TNFα are minimal and testing other inputs, including LPS, ATP and Glutamate did not show significant evidence of NF-κB activation. However, the authors also argued that the NF-κB basal activity is inherently low in neurons. This conclusion is however not consistent with data from this study showing high expression from the 5xκB-Venus NF-κB reporter expression in isolated primary mouse neurons. This result is in agreement with studies by Kaltschmidt *et al*, which presented evidence of continuous activation of NF-κB in neurons, but failed to respond to inflammatory cues (Kaltschmidt *et al,* 1994). The reason for the observed insensitivity of neurons to TNFα stimulation remains unclear. TNFR1 is expressed on the surface of neurons, which were previously reported to respond to physiological levels of TNFα by enhancing neurite outgrowth in a RhoA GTPase dependent manner (Neumann *et al,* 2002). Therefore, TNFα signaling may be activating the TNFR1 signaling cascade, without triggering nuclear translocation of p65.

The neuronal NF-κB (p65) has distinct functions to the astrocyte counterpart in that it has been shown to act mainly in synapse maintenance, plasticity and GABAnergic signalling (Kaltshmidt *et al*, 2005). It is possible that the classical cytokine mediated transcriptional activation of p65 is not activated in neurons as these cells need to

maintain a stable basal activity, in order to fulfil other essential functions, with astrocyte and microglial cells being available to mediate and respond to local inflammatory signalling in the brain.

NF-κB nuclear oscillations in response to cytokine signalling have been well characterised by Ashall *et al*, in neuroblastoma SK-N-AS cells (Ashall *et al*, 2002). However, this study reports of this phenotype in primary astrocytes observed for the first time. Interestingly the amplitude of basal p65 nuclear oscillations varied significantly, depending on weather primary astrocytes were grown under the same media conditions in the presence or absence of neurons (Figure 3.6F, Movie 2 &1a). The cause of this difference has not yet been fully investigated, however the amplitude and the frequency of NF-κB oscillations have been associated with the feedback mediated by three NF-κB regulatory components including, A20, IKK, IKBα and IKBε (Paszek *et al,* 2010). Therefore, it is reasonable to hypothesise that basal neuronal paracrine communication could lead to changes in the astrocytic expression levels of those components.

3.4.2. The Autonomous NF-κB Activation

Live cell imaging of EGFP-p65 and tagRFP-p65 in astrocyte enriched and neuron/astrocyte mixed cultures provided clear evidence of autonomous p65 oscillations, which were frequently observed in neighbouring cells (Figure 3.8). Furthermore, the observed spontaneous oscillatory shuttling of p65 directly correlated with an increase in NF-κB transcriptional activity, as measured by use of the 5κB-Venus reporter construct (Figure 3.8C, Movies 4& 5b). The role of neuronal glutamate signalling in inducing this phenotype was rejected, since neither inhibition of the glutamate receptors (Figure 3.9B) nor lack of L-glutamate induced NF-κB-Luc activation (Figure 3.9C). The occurrence of spontaneous nuclear oscillations in pure astrocyte cultures (Figure 3.9D & E) also excludes this possibility. It is intriguing that sequential oscillatory behaviour was frequently observed in neighbouring cells, such that the peak of nuclear p65 in one cell was often reciprocal to transient accumulation of p65 in the other (Movie 5a). This suggests that the phenotype may be in some way controlled by short-range paracrine communication, however it is

worth noting that although, multiple neighbouring cells often exhibit this behaviour, single isolated cells can also exhibit the phenotype with no detectable consequences within the whole field of imaging (Figure 3.8D, Movie 5).

Interestingly we also found that the amplitude of the spontaneous p65 nuclear oscillations was higher when serum free Neurobasal medium was added to cells just before imaging (this media was also used for mixed cell culture), in comparison to cells maintained in 5% serum supplemented Neurobasal medium (Figure 3.9D & E, Movie 6a & 6b). Serum derived growth factors and signals could mask the effect of the signalling molecule involved in this phenomenon. Alternatively, starvation could induce stress-associated responses in cells, but in this case the occurrence of spontaneous p65 activity would be anticipated to be present more frequently, with some cells also undergoing apoptosis. Spontaneous p65 oscillations were previously observed in GFP-p65 knock-in fibroblasts, however this phenotype was not linked to an increase in κB-driven gene transcription (Zambrano *et al,* 2014). The authors hypothesised that this voluntary nuclear translocation phenotype could act as an NF-κB "resetting system", resulting from a decreased in IKBα gene transcription. Thus allowing p65 to shuttle into the nucleus; where it would then reestablish NF-κB gene target gene expression, including the synthesis of new regulatory IKBα and anti-apoptotic genes. Thus conferring sensitivity to local inflammatory cues within the cellular vicinity. In our studies this voluntary or spontaneous behavior was frequently observed in neighboring astrocytes, suggesting that there is an inherent mechanism of paracrine communication (Figure 3.8). There are several candidates that may trigger the observed pattern of voluntary p65 nuclear shuttling, such as TNFα and the chemokine SDF-1. SDF-1 secretion is induced by glutamate and its strongly chemotactic properties attract leukocytes (Han *et al,* 2001). SDF-1 has also been shown to activate the TACE enzyme, expressed on cellular membranes, which subsequently cleaves the TNFα monomer and releases it into the extracellular space. It can act either by autocrine or paracrine fashion and eventually amplify the inflammatory signaling (Han *et al,* 2001). This process was reported to be dependent on an increase in intracellular calcium concentration. Therefore, the role of SDF-1 in triggering spontaneous p65 nuclear shuttling could be validated by applying calcium chelators such as BAPTA and monitoring the effects in live cells. Nevertheless, the SDF-1 signaling relies on the release of glutamate and is expected to be enhanced in

the presence of neurons.. Taking into account the sequential behavior of these nuclear events, and the timing between the p65 nuclear peaks in proximal cells, it is quite likely that these events were triggered by paracrine TNFα signaling, which is a classical inducer of the p65 oscillatory behavior. Another argument for TNFα-mediated effects is that nuclear translocation of NF-κB can be elicited with pM concentrations of the cytokine (Turner *et al,* 2010). To validate the role of TNFα in the induction of spontaneous p65 activity, this phenotype could be targeted by using anti-TNFα antibodies, or by using TNFR1 and TNFR2 specific inhibitors to block signaling by released cytokines. Interestingly, cells undergoing senescence display high NF-κB chromatin association indicating its possible input in maintaining this phenotype. The senescent cells exhibit senescence- associated secretory phenotype (SASP), where IL-6 and IL-8 cytokines are used as means of paracrine communication between cells. Therefore, another explanation for the autonomous NF-κB signalling observed in astrocytes could be associated with paracrine senescent signalling (Chien *et al*, 2011).

The observation of this phenomenon again highlights the relevance of using single live cell imaging, as population level techniques would obscure these spontaneous nuclear p65 oscillations.

3.4.3. Low Expression Molecular Tools are Required for Optimal Imaging of Physiologically Relevant Nrf2 Dynamic Responses

Convincing detection of Nrf2 by western blots required the testing of several commercially available antibodies, eventually the rabbit anti-Nrf2 antibody (H300, Santa Cruz) was selected as it detected a clear Nrf2-specific band at a MW of around 100kDa (Figure 3.10A & B). The Nrf2 protein runs higher than its predicted MW (69kDa) and this has also been confirmed by data from other laboratories (Lau *et al,* 2013). The ARE-Luc reporter encoding 8xARE repeats, based on the sequence contained in the mouse *GCLC* promoter (Kratschmar *et al,* 2012), was effectively used for measuring Nrf2 activity by dual luciferase assay in response to pharmacological inducers (Figure 3.10C). To make the assay more sensitive to dynamic changes in the intercellular environment, the luciferase reporter protein has been destabilised by addition of a peptide degradation sequence (PEST), thus

enhancing the sensitivity of this assay to fast changes in intracellular redox conditions.

It was essential to analyse the functionality of the fluorescent Nrf2 protein fusion by measuring mCherry-Nrf2 mediated ARE-Luc expression (Figure 3.10D). The plasmid expression led to significantly higher ARE-Luc levels, however it was not sensitive to further induction by CDDO-Me (Figure 3.10D). This may be due to out-titrating the normal mechanism of Nrf2 negative regulation by Keap1. Live cell imaging experiments using mCherry-Nrf2 confirmed that expression of Nrf2 from a high activity *UBC* promoter was not only insensitive to pharmacological Nrf2 induction by CDDO-Me (Figure 3.11A), but was also frequently associated with deleterious structural nuclear defects, leading to an apparent nuclear oscillation artefact in mCherry-Nrf2 dynamic behaviour (Figure 3.11B & D). Astrocytes transfected with the mCherry-Nrf2 plasmid frequently exhibited modified nuclear morphology characterised by formation of nuclear blebs, which were prone to repetitive "bursting" events during imaging (Figure 3.11D, Movie 7 & 8). This frequently led to changes in the nuclear levels of Nrf2 and most likely other nuclear proteins, inducing a false phenotype for nuclear protein dynamics. It is unlikely that the expression of mCherry-Nrf2 plasmid was specifically causing this aberrant nuclear phenotype, as expression of mCherry-UBE2D2 had a similar effect (Figure 3.11C).

This nuclear expulsion phenotype has been observed by other labs studying other nuclear proteins, such as HIF1α (Violaine See group, University of Liverpool) and the nuclear behaviour itself has been associated with a cancer phenotype, or virus induced cellular stress (Hatch *et al,* 2013). However, it is increasingly evident that this behaviour is not exclusive to cancer related cells, since is also detected in primary cells. The frequent observations of this phenotype by expression of fluorescent nuclear protein fusions may be due to the fact that cells with weakened nuclear membrane are favoured for transfections, as plasmid expression requires the cDNA to enter the nuclear space. Therefore, as astrocyte division rate is quite slow the transfection efficiency could be enhanced by the fact that some cells exhibit the nuclear expulsion artefact permitting cDNA entry without the need of cell division.

The underlying cause of this phenotype has been associated with defective Lamin expression, and perhaps the 2D culture mode taken out of tissue context could enhance the structural stress on the nuclear envelope (De Vos *et al,* 2011). Therefore, researchers imaging nuclear fluorescent protein fusions should be cautious about this phenomenon especially if the analysed cells show clear signs of nuclear blebbing or rupture, which is associated with the nuclear expulsion phenotype. This is particularly relevant in the Nrf2 field as an oscillatory Nrf2 nuclear behaviour has been previously reported in human mammary epithelial cells (HMEC) transiently transfected with fluorescent Nrf2 protein. In this study the dynamic changes in nuclear Nrf2 levels were proposed to be a key event in the Nrf2 transcriptional cycle in response to oxidative stress (Xue *et al,* 2014).

In this study we clearly demonstrate that near-endogenous expression levels of Nrf2 did not confer any such nuclear artefacts thus enabling Nrf2 imaging of response to various pharmacological stimuli in primary cells. The *2kb*-Venus-Nrf2 fusion driven from its endogenous promoter, responded to induction with SFN and CDDO-Me and the occurrence of the spontaneous nuclear envelope breakdown was rarely observed (Figure 3.12C-E, Movies 9-11). Also, by limiting the levels of Nrf2 protein expression the potential for over-powering or out titrating Keap1 mediated regulation is much less likely to occur and hence the Nrf2 fusion protein itself will be more appropriately sensitive to Keap1 inhibition. The unequivocal benefit of lentiviral transduction is gene delivery to non-dividing cells such as neurons and the expression of fluorescently labelled Nrf2 not favoured by the cells exhibiting nuclear structure defects.

In our studies the triterpenoid CDDO-Me (50nM) proved to be a more potent inducer of Nrf2 than SFN (2μM), nearly doubling the nuclear accumulation of Nrf2 in comparison to SFN (Figure 3.12E), whereas control treatment with DMSO failed to induce Nrf2 response (Movie 12).

Finally bringing tools generated for both pathways together, the mixed cultures were transduced with both tagRFP-p65 and *2kb*-Venus-Nrf2 and treated with 50nM CDDO-Me (Figure 3.13). The drug caused a robust activation of *2kb*-Venus-Nrf2 in both astrocytes and neurons without triggering the nuclear translocation of the fluorescent p65. Significantly, as CDDO-Me is a compound that has ben shown to

cross-the BBB, it has the potential to prevent neurodegeneration (Neymotin *et al, 2011*). The *2kb*-Venus-Nrf2 expression was driven from *2kb* fragment of the mouse Nrf2 gene promoter region, which served as a good indicator of the Nrf2 promoter activity. The presence of *2kb*-Venus-Nrf2 and its activation in hippocampal neurons was promising, however it has been recently reported that the Nrf2 promoter in adult neurons is methylated and therefore inactive, so the Nrf2 activity is likely to be kept to minimal levels in adult neurons (Bell *et al,* 2015). In this study, neuronal cultures were obtained from embryonic neurons, therefore the difference in Nrf2 promoter activity could be due to the developmental stage of the animals used for the isolation of primary cells, or methylation may occur in a more upstream promoter sequence, which was not included in the *2kb* sequence used in this study.

3.4.4. *GFAP*-LaminB1-Cyan Drives Astrocyte-Specific Nuclear Marker Expression

Initial assessment of cell specific responses were performed based on the shape of the cells present in the culture, as astrocytes and neurons have quite distinct cell morphologies. However, it can be challenging to perform effective large-scale data analysis on mixed cell populations, as cultures from hippocampal region of the brain can also support growth of occasional oligodendrocytes and meningeal cells. In order to ensure the astrocyte-specific p65 dynamic behaviour was being measured, a *GFAP*-LaminB1-Cyan construct was generated (Figure 3.14C & D). The *GFAP* promoter allowed expression to be confined to astrocytes, thereby facilitating detection of astrocyte specific nuclear protein changes (Figure 3.14D). This will help to automate the analysis in future studies by providing a stable nuclear labelling by laminB1, which could be readily detected by a Cell-Tracker and other software. Unfortunately, due to time constraints, use of the construct has not been explored further in this study.

The results obtained demonstrate the lentiviral transduction system used for expression of near-endogenous proteins is a superior method of gene delivery and imaging fluorescent proteins in primary neural cells. Data generated provided novel evidence of oscillatory dynamics of p65 in astrocytes and confirm the lack of

neuronal activation of p65 by TNFα, in addition, we report the novel phenotype of autonomous, astrocytic NF-κB activity.

3.4.5. Characterisation of BAC$^{Nrf2\text{-}Venus}$

3.4.5.1. The BAC$^{Nrf2\text{-}Venus}$ is an Excellent Imaging Tool for Dissecting Nrf2 Pathway Regulation

The primary aims of this PhD project were to investigate the interplay between Nrf2 and NF-κB signalling responses and to provide further information into conditional mechanisms of transcriptional and post-transcriptional regulation of Nrf2 responses. The large number of assays required for this purpose made it challenging to base all experimental studies on primary cell cultures. Therefore, an alternative cell culture model was vital to allow easy cell manipulation and maintenance. Use of the neuroblastoma SK-N-AS BAC$^{Nrf2\text{-}Venus}$ cell line allowed many aspects of the transcriptional and post-translational regulation of dynamic Nrf2 responses to be analysed in live cells. Due to the extremely low basal level of Nrf2-Venus expression in these cells (Figure 3.15B & C) it was only possible to detect the Venus fluorescence using the state of the art Zeiss 7.80 confocal imaging system.

The imaging of the BAC$^{Nrf2\text{-}Venus}$ cells required spectral unmixing as described previously in transduced Venus-Nrf2 astrocytes (Figure 3.12A & B). The background autofluorescence was mostly present in the cytoplasm and could be separated from the genuine Venus fluorescence by utilising the lambda scan imaging mode (Figure 3.16). The live cell imaging of BAC$^{Nrf2\text{-}Venus}$ cells provided a novel spatio-temporal data on Nrf2 dynamics in response to 2 μM SFN, 10 μM MG132 and 100nM CDDO-Me, showing a distinct pattern of Nrf2 responses to different pharmacological stimulus (Figure 3.17A, Movies 13-15). This emphasised the value of BAC$^{Nrf2\text{-}Venus}$ cells in obtaining information on the temporal dynamics of Nrf2 induction and confirmed that the BAC$^{Nrf2\text{-}Venus}$ cells could be used in further study.

3.4.5.2. The mCherry-Keap1 and Nrf2-Venus Form Stable Complexes in Live Cells

The Keap1 protein acts as the main regulator of the cellular Nrf2 levels; therefore it was crucial to establish if the tag modification of Nrf2 did not interfere with Keap1

dependent degradation. This has ben verified by live cell imaging of $BAC^{Nrf2\text{-}Venus}$ cells expressing mCherry-Keap1 plasmid. As expected, the transfection of mCherry-Keap1 (*CMV* driven) led to decrease of Nrf2-Vensu fluorescence in the transiently transfected cells (Figure 3.17B).

The Fluorescence Cross-Correlation Spectroscopy (FCCS) was performed to assess mCherry-keap1 and Nrf2-Venus complex formation in live cells (Figure 3.18). The FCCS measures fluorescently labelled protein diffusion through the confocal volume and the similarity of the diffusion pattern is assessed by mathematical logarithm, and further represented by a cross-correlation curve (Methods 2.13.4). The gradient decline of the curve is a measure of complex formation with the measurements taken binned every 200ns for 10x10sec and each fluorescence signal is correlated to the previous one by mathematical function and this is then plotted as the $G\tau$ against the time (Δt) (Bacia *et al*, 2006).

The diffusion speed of proteins is slower as a complex therefore by measuring the diffusion speeds of proteins through the known confocal volume, it is possible to calculate the size and the proportion of free and complexes Nrf2-Venus and mCherry-Keap1. The mCherry-Keap1 and Nrf2-Venus form strong complex in live cells of K_D~300nM (Figure 3.18E) (protein-protein dissociation constant) and a significant proportion of Nrf2-Venus being part of a complex with mCherry-Keap1 (Figure 3.18E and F). Therefore placing the Venus tag at the C-terminus of the Nrf2 protein was unlikely to alter the Nrf2 protein interaction profile as confirmed by stable complex formation with the Keap1 E3 ligase.

3.4.5.3. Nrf2 Protein Levels are Regulated in Cell-Cycle Dependent Manner

The acquisition of long time-lapse images of live cells requires a stable experimental environment conditions and low sample irradiation, to prevent cellular damage. As Nrf2-Venus levels remained stable under unstimulated conditions even after prolonged imaging time, we can be confident that imaging conditions did not trigger Nrf2 activation (Figure 3.19A). Under these stable optimised imaging conditions we were able to identify an interesting novel pattern of Nrf2, which occurs in a cell-cycle dependent manner immediately after cell division (Figure 3.19B & C, Movie 16). This transient increase of Nrf2 nuclear levels occurred consistently with every

division process in both basal and stimulated conditions. The biological function of the transient rise in Nrf2-Venus expression was not defined, however cellular redox status is very tightly coupled to cell division and a proportion of cell-cycle regulating proteins contain highly reactive cysteine residues that can alter their activity in response to the ROS levels (Chiu & Dawes, 2012). It is therefore possible that the temporary increase of Nrf2 expression acts to sense and appropriately re-set the redox environment within the cell, in order to ensure appropriate progression of the subsequent division process. The consequence of Nrf2 activity on the cell cycle has been studied in a few laboratories and published reports show a dual effect of Nrf2 activity on cell-cycle progression. Mouse hepatocytes isolated from regenerating liver, expressing a constitutively active Nrf2 mutant displayed a diminished rate of growth (Kohler *et al,* 2014). Therefore, high levels of Nrf2 have been shown to decrease the rate of cell division in proliferating cells. On the other hand, Nrf2 KO cells showed a G2/M phase arrest, due to aggravated DNA damage, which did not allow continuing the division process (Reddy *et al,* 2008). Unfortunately, the attempts to synchronize the SK-N-AS cells in the Sanderson lab by double thymidine block or by the Nocodazole treatment to study this phenotype did not yield positive results. The effect of Nrf2 modulation could be further examined by cell-cycle analysis of the $BAC^{Nrf2\text{-}Venus}$ by FACS following application of Nrf2 inducers, such as SFN, CDDO-Me, or by addition of brusatol. It would be very interesting to investigate the effect of interruption of the post-cell division Nrf2 enhancement to clarify its functional role. In this context it is important to note that the proliferation of $BAC^{Nrf2\text{-}Venus}$ cells is greatly reduced as compared with WT SK-N-AS cells (personal observations), therefore expression of extra copies of Nrf2 also seems to be associated with a slower rate of cell proliferation. Significantly, this tendency was also observed in primary Nrf2-Venus MEF cells, which were isolated in Prof. White's laboratory (University of Manchester, personal communication).

The live cell imaging methodology provided interesting information on temporal changes in localisation of Nrf2 and NF-κB proteins. It is anticipated that changes in their nuclear localisation will correlate with responses in the target gene expression. However it is challenging to directly associate changes in dynamic protein localisation with the changes in its post-translational modification status by single

cell microscopy. Therefore additional biochemical analysis on Nrf2 activity, target DNA binding and post-translational modifications could be performed to complement this study.

To conclude the BAC$^{Nrf2\text{-}Venus}$ is a robust tool for imaging near-physiological levels of Nrf2 protein. This live cell imaging approach holds a great potential to deliver high resolution of information about real-time protein dynamics and providing new insight into regulatory networks that maintain the cellular anti-oxidant potential driven by the Nrf2 activity. The summary of the main findings from this chapter is presented in diagram in Figure 3.20 below.

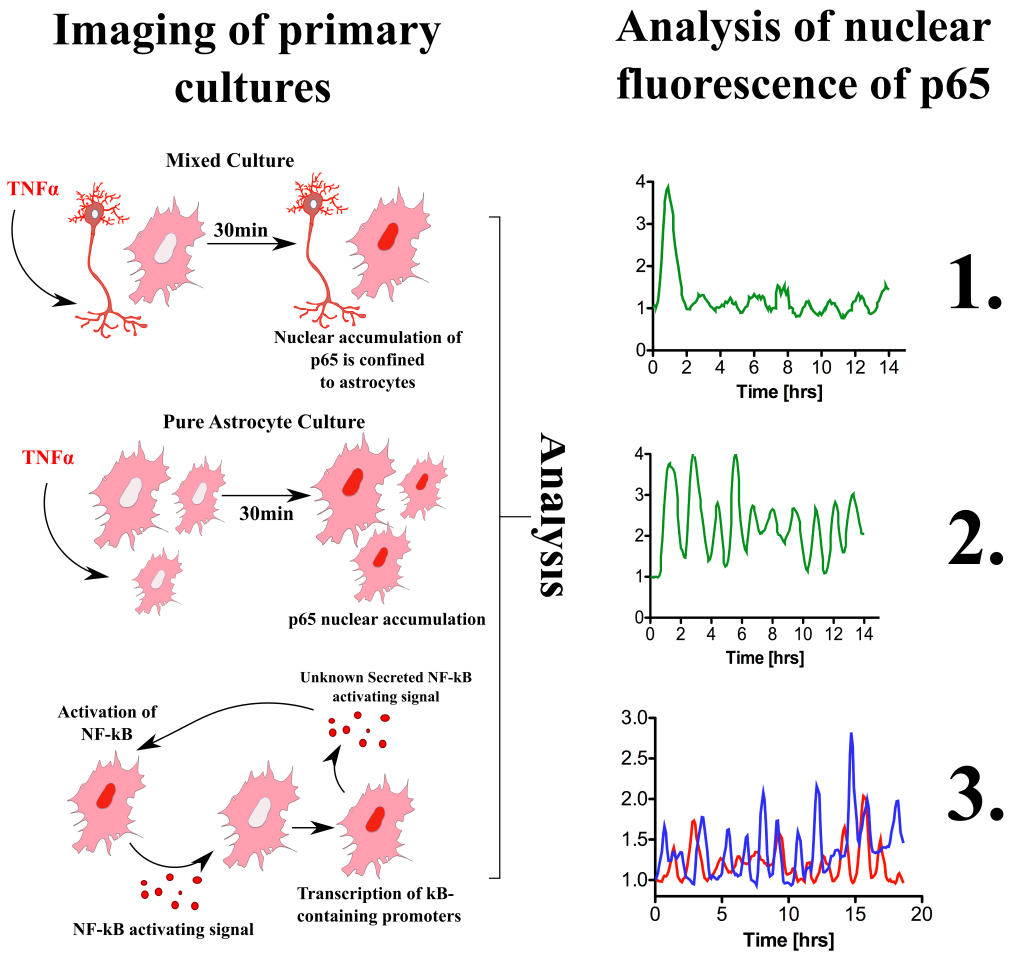

Figure 3.20 Summary of key findings from Results Chapter 1. Low expression model of p65 achieved through lentiviral transduction allowed for real-time imaging of dynamic responses of NF-κB under basal and inflammatory conditions. **1)** p65 nuclear translocation in response to TNFα is observed exclusively in astrocyte cells. The response of p65 to TNFα displays altered temporal behaviour in astrocytes grown in the presence of neurons and those observed in **2)** pure astrocytic cultures. **3)** Astrocytes demonstrate spontaneous p65 activation, which is likely to be a consequence of paracrine communication.

RESULTS CHAPTER 2

4. Investigating Dynamic Crosstalk Between Nrf2 and NF-κB Signalling Responses

4.1. CHAPTER 2 AIMS:

- **Investigating the effect of inflammation on antioxidant activityat a single-cell level**
- **Deciphering molecular interplay between Nrf2 and NF-κB**
- **Investigating the Keap1 and GSK-3 mediated regulation of Nrf2 in response to inflammation**

4.2. Introduction

As demonstrated in Results Chapter 1 the human SK-N-AS BAC$^{Nrf2\text{-}Venus}$ cell line is a physiologically relevant system to investigate dynamic conditional Nrf2 responses using both conventional biochemical and advanced live single-cell imaging techniques. The Nrf2 transcription factor is a master regulator against oxidative and chemical stress and a crucial player in resolving the potentially harmful effects of chronic inflammation. The cytoprotective effects of Nrf2 activating compounds and their potent inhibitory action on NF-κB mediated gene transcription is well characterised (Caccamo *et al,* 2005). Therefore, it is feasible that drugs that confer antioxidant protection may also provide opportunities for the treatment of a diverse group of human diseases that result from chronic inflammation. However, in comparison, the affects of NF-κB pathway activation on antioxidant defence mechanisms is much less well understood, despite numerous reports proposing points of potential cross-talk or interference between these two pathways. Finally, although there is functional evidence for imposed reciprocal effects between these pathways, the molecular mechanism of this crosstalk and key points of regulation remain unclear and may vary between cell-type or disease state.

Live cell imaging studies provide single-cell resolution of dynamic physiological processes, a major benefit of this approach is that the temporal sequence of transient or changing conditional responses can be defined with clarity. Due to the inherent

heterogeneity that exists between cells within a population, common response mechanisms may be masked simply because they are not temporally synchronised throughout the population. For this reason important spatiotemporal details of signalling pathways may only be revealed through detailed live single-cell imaging studies, as was the case for the discovery of the existence and functional importance of NF-κB oscillatory signalling responses (Hoffmann *et al,* 2002).

In this study we extended live cell imaging procedures used to define p65/RelA dynamic behaviour to assess the dynamic reciprocal consequences of Nrf2 and NF-κB pathway activation in $BAC^{Nrf2\text{-}Venus}$ cells. To facilitate these studies a p65-dsRedXP plasmid, or a lentivirally integrated tagRFP-p65 fusion-proteins were used to imaged dynamic responses to inflammatory and antioxidant signalling in parallel in real-time.

4.3. RESULTS

4.3.1. Effects of TNFα Stimulation on the Nrf2 Pathway in SK-N-AS Neuroblastoma Cells

As expected stimulation of $BAC^{Nrf2\text{-}Venus}$ cells with TNFα (10ng/ml) led to an increase in NF-κB transcriptional activity, as measured by the NF-κB-Luc dual Luciferase assay (Figure 4.1A) (Methods 2.4.6). In addition, live cell imaging of $BAC^{Nrf2\text{-}Venus}$ cells showed that TNFα (10ng/ml) modestly increased nuclear levels of Nrf2-Venus (Figure 4.1B and 4.C, Movie 17). This effect was confirmed by western blot analysis, showing a maximal peak of nuclear Nrf2 accumulation at ~2hr post-stimulation (Figure 4.1D, Quantification in Supplementary Figure 8.4). In contrast, the initial peak of nuclear p65 accumulation occurred at 30min post-stimulation, remaining higher than pre-stimulation levels for 24h (Figure 4.1D, Supplementary Figure 8.5). Significantly, no increase in cytoplasmic Nrf2 levels was observed in these studies (Figure 4.1E).

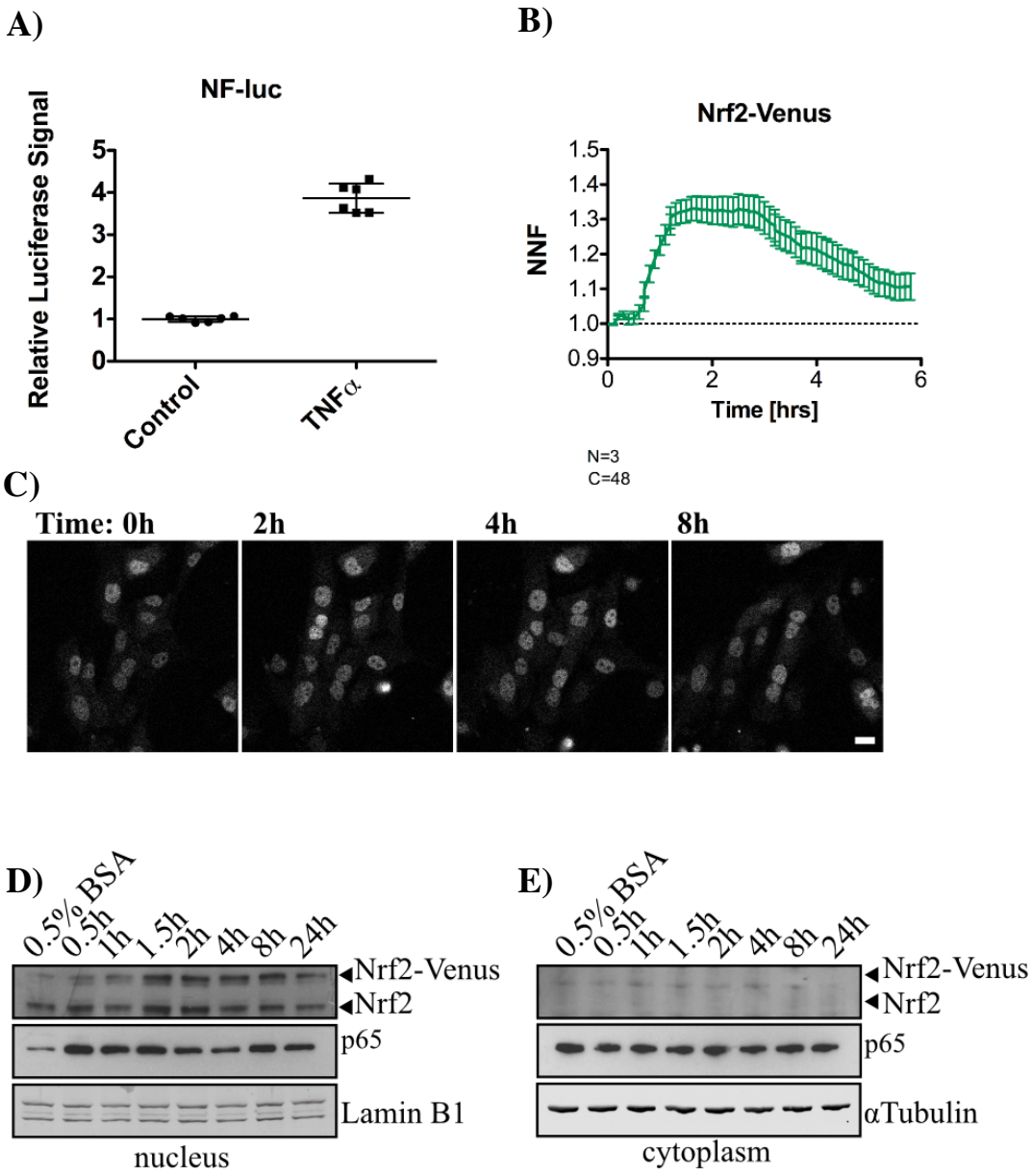

Figure 4.1. TNFα treatment increases nuclear Nrf2 levels. A) Results from NF-κB-Luc the NF-κB transcriptional reporter assay performed on lysates from BAC$^{Nrf2\text{-}Venus}$ cells, which were incubated with or without 10ng/ml TNFα for 8h (n=2, triplicates). The imaging experiments were performed in a humidified atmosphere, at 37ºC and 5% CO_2. To ensure that the imaging process itself did not trigger changes in measured proteins, three time-lapse images were taken before any drug treatment was applied (equivalent to at least 21min of imaging, for more details refer to Methods Section 2.13). B) Averaged results from live-cell imaging analysis showing a rise in nuclear Nrf2-Venus levels in response to 10ng/ml TNFα in BAC$^{Nrf2\text{-}Venus}$ cells (n=3, c=48) (Movie 17). C) Representative time-lapse images of BAC$^{Nrf2\text{-}Venus}$ cells from the experimental data presented in panel B. D) Western blot of nuclear (quantified in Supplementary Figure 8.5) and E) cytoplasmic BAC$^{Nrf2\text{-}Venus}$ lysates fractions showing changes in Nrf2 and p65 changes in response to 10ng/ml TNFα. Blots emphasize the fact that most Nrf2 is restricted to the nuclear compartment. Error bars=STDEV(luciferase)/SEM(imaging). Scale bar=20μm.

4.3.1.1. Measuring Expression of Nrf2 Target Genes

Next, it was important to verify if the increase of Nrf2 levels in response to TNFα were associated with parallel activation of ARE target genes. Before measuring the consequences of inflammatory signalling on Nrf2-mediated gene transcription, the relative induction of known Nrf2 response genes was investigated by Q-PCR (Methods 2.9) in $BAC^{Nrf2\text{-}Venus}$ cells following application of 2μM SFN for 8h (Figure 4.2). As expected SFN treatment significantly increased expression of all tested Nrf2 response genes, with the largest induction being observed with sulfiredoxin (SRXN1) (Figure 4.2E) and the smallest increase being NQO1 mRNA (Figure 4.2A). This confirmed that these target genes are responsive to Nrf2 activation in $BAC^{Nrf2\text{-}Venus}$ neuroblastoma cells and can therefore be used as markers of Nrf2 activity in further conditional studies.

To investigate if the observed TNFα–mediated rise in Nrf2 protein levels was associated with a parallel increase in Nrf2 mRNA and the expression of Nrf2 target genes, a Q-PCR analysis was performed to compare relative mRNA expression levels, under control or stimulated conditions (Figure 4.3A-F). Exposure to TNFα (10ng/ml) for 8hr led to a significant rise in *NRF2* mRNA expression in both the primary astrocytes and the $BAC^{Venus\text{-}Nrf2}$ cells (Figure 4.3G & H). Interestingly, although significant increases in NQO1, GCLC, HO-1 and Bach1 mRNA levels were also observed (Figure 4.3A, B, C, F respectively), no detectable changes in TXNRD1 or SRXN1 expression were detected (Figure 4.3D, E). To test the effect of ectopic p65 expression on *NRF2* gene transcription, the Nrf2-specific transcriptional reporter (kindly provided by Professor David MacEwan, University of Liverpool) was used, in which Luciferase expression is under transcriptional control of a 1.2kbp region of the *NRF2* proximal promoter, to generate the pNRF2-Luc plasmid (Figure 4.3I). This enabled to directly quantify the p65-mediated effect on Nrf2 gene expression.

Transfection of $BAC^{Nrf2\text{-}Venus}$ cells with p65-dsRedXP plasmid (Prof. M.White, University of Manchester) significantly increased pNRF2-Luc reporter activity in

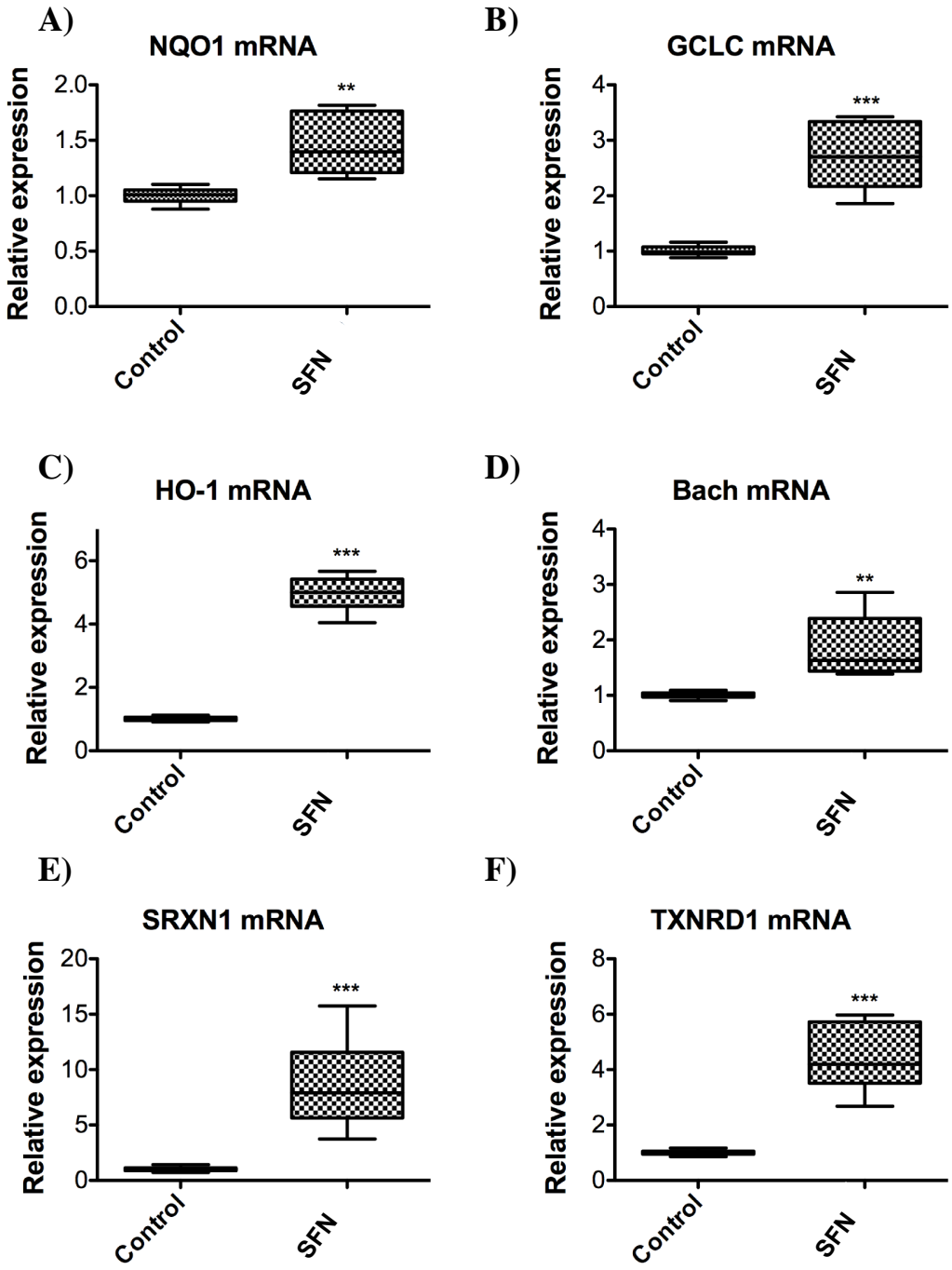

Figure 4.2 Analysis of SFN activation of Nrf2-mediated target gene expression in BAC$^{Nrf2\text{-}Venus}$ neuroblastoma cells. A-F) Relative induction of Nrf2 target gene expression in response to 8hr incubation with DMSO (Control) or 2μM SFN. In each case target mRNA levels were normalised to β-Actin mRNA levels (n=3, in triplicates). The p-values were denoted as follows: 0.01-0.05=*; 0.01-0.001=**, 0.001-0.0001=*** and p value< 0.0001=****. Error bars=Min/Max values.

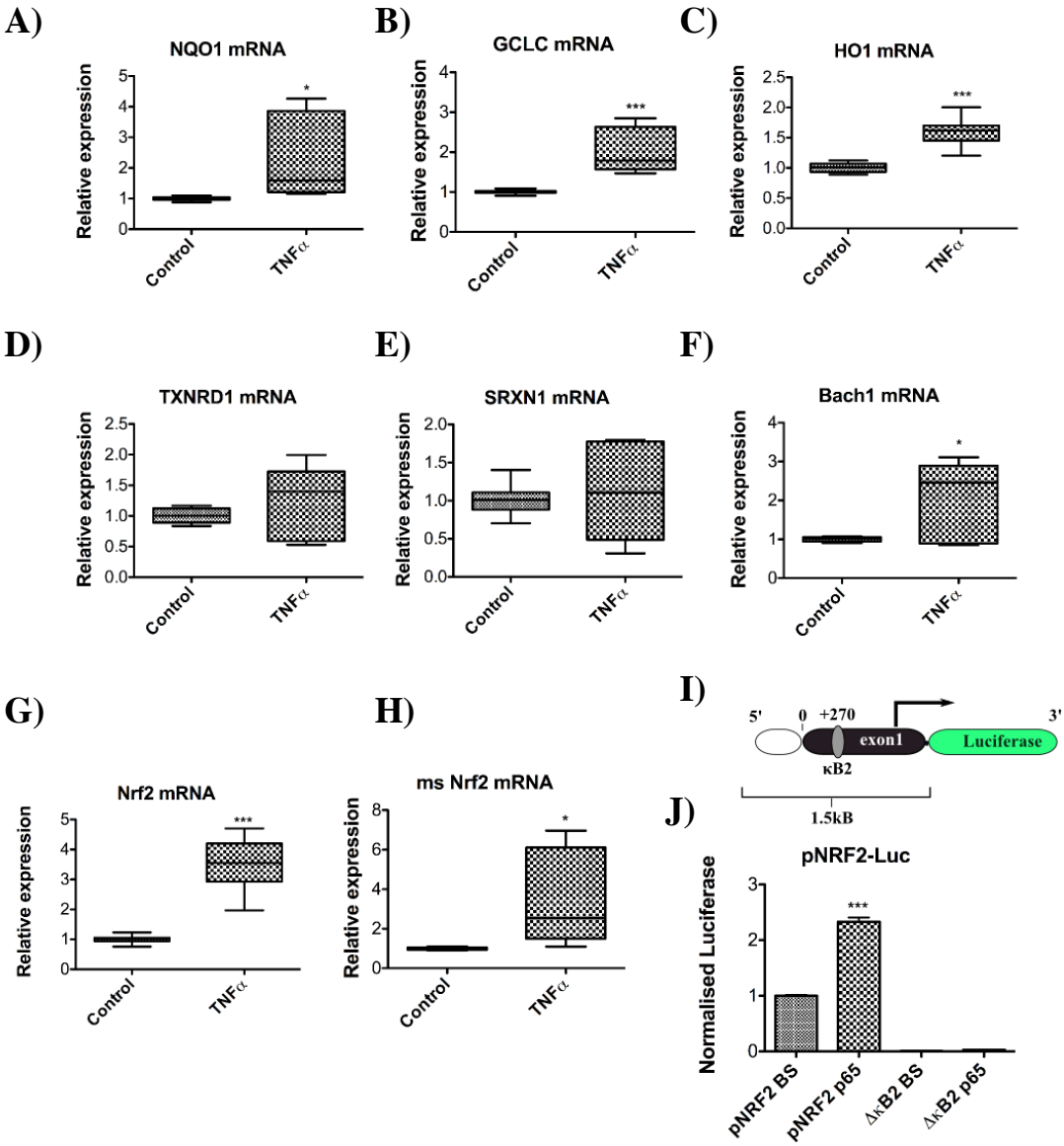

Figure 4.3 TNFα-mediated NF-κB signalling induces Nrf2 transcription leading to enhanced expression of selective Nrf2 response genes in BAC$^{Nrf2\text{-}Venus}$ cells. A-F) Relative induction of six Nrf2 target genes in response to 8hr stimulation with 10ng/ml TNFα (n=3, in triplicates). G) Relative induction of Nrf2 mRNA expression in response to 8hr exposure to 10ng/ml recombinant human TNFα in BAC$^{Nrf2\text{-}Venus}$ cells or H) stimulation of mouse cortical astrocytes with 10ng/ml murine, recombinant TNFα (n=3 in triplicates). I) Diagram showing pNRF2-Luc construct. J) Comparison of *NRF2* promoter activity following co-transfection of BAC$^{Nrf2\text{-}Venus}$ cells with pNRF2-Luc + empty Blue script vector (BS) used as a control to define endogenous Nrf2 activity, or pNrf2-Luc + p65dsRedXP to assess the effects of enhanced levels of p65 on *NRF2* transcription. Co-transfection studies using the *NRF2* promoter region in which the κB2 site has been deleted (ΔκB2) show that its activity almost totally abolished. n=3 in triplicates, Error bars=SEM(luciferase)/Min/Max values (QPCR).

response to TNFα (10ng/ml) stimulation (Figure 4.3J). Significantly, deletion of the consensus NF-κB binding sequence (κB2) in the Nrf2 promoter region greatly reduced both basal and p65 enhanced pNRF2-Luc expression (Figure 4.3J). Therefore, some part of the basal Nrf2 expression and the majority of the observed TNFα– mediated increase in nuclear Nrf2-Venus is mediated by NF-κB-mediated Nrf2 gene transcription.

4.3.1.2. Imaging Nuclear Dynamics of p65 and Nrf2 Transcription Factors in Live Cells

Having established the mild positive effect of TNFα on Nrf2 activity, next we proceeded to investigate the correlation spatio-temporal dynamics of both transcription factors. For this purpose, it was necessary to select the optimal imaging protocol to obtain an optimal specific signal for the near-endogenous levels of Nrf2-Venus fluorescence, while also allowing parallel imaging of p65-dsRedXP dynamics. As described in (Chapter 1, 3.5A) the lambda scan imaging mode provided an excellent method for resolving low-level Nrf2-Venus signals from non-specific autofluorescence. In theory, this spectral unmixing approach should enable p65-dsRedXP to be imaged alongside Venus fluorescence, as the dsRedXP excitation spectrum also includes the 514nm wavelength that is usually used for illuminating Venus (Figure 4.4A and B). Initial imaging studies showed that the Nrf2-Venus could be spectrally unmixed from both autofluorescence and p65-dsRedXP fluorescence (Figure 4.4B). However, lambda scan imaging relies on illumination with a single laser, and collection of the entire fluorescent signal with one detector set. Measurements of nuclear protein levels following TNFα in live cells using this method showed that high nuclear p65-dsRedXP levels correlated with a subsequent decrease of Nrf2-Venus signal (Figure 4.4C). To test whether this was an imaging artefact Nrf2-Venus and p65-dsRedXP signals were imaged using a stringent two channel imaging mode (Figure 4.4D), where the 514nm laser was used to illuminate the Venus signal passed through the narrow band pass filter (521-539nm) and emission signals were collected using the ChS1 detector. Alternatively, p65-dsRedXP was sequentially excited by the 561nm laser and emission signals were collected using a separate ChS detector (filter range 600nm-630nm). Using this

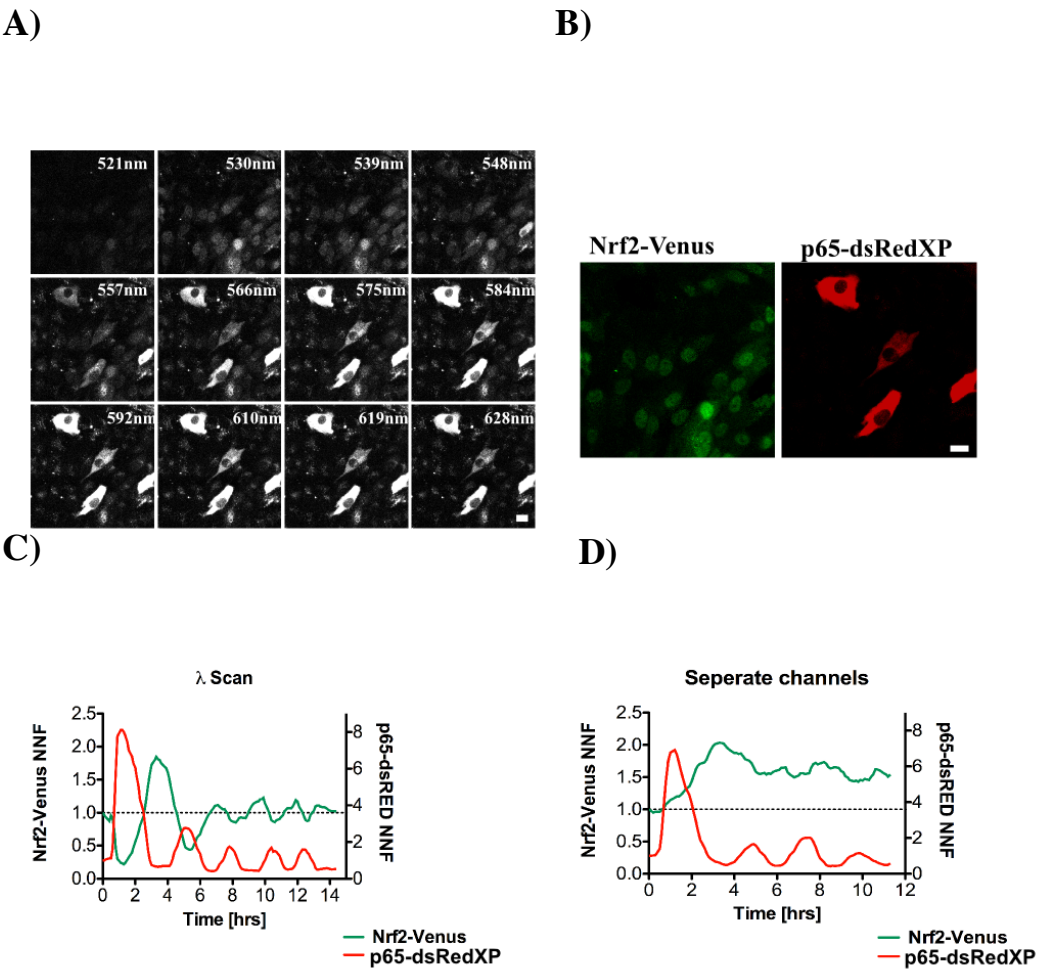

Figure 4.4 Imaging BAC$^{Nrf2\text{-}Venus}$ transfected with p65-dsRedXP construct in response to TNFα. A) Lambda scan was used to simultaneously acquire Venus and dsRedXP fluorescent signals. B) Spectrally unmixed images showing separate green (Nrf2) and red (p65) channel emission profiles. C) Combined analysis of nuclear p65dsRedXP and Nrf2-Venus fluorescence following addition of 10ng/ml TNFα (added at 21min) treatment obtained by live cell imaging using the lambda scan mode. The Nrf2-Venus signal appeared to be quenched by increase in nuclear p65-dsRedXP levels. D) Comparable p65dsRedXP and Nrf2-Venus signals obtained under identical conditions using a stringent two-channel sequential illumination method with 514nm (for Venus) and 561nm (for dsRedXP) lasers and separate detectors to record green or red fluorescence signals respectively. Scale bar=20μm.

restricted two channel imaging method, no reduction in Nrf2-Venus was observed when p65-dsRedXP levels were high (Figure 4.4D). Therefore, in lambda scan analysis it appears that disproportionately high levels of dsRedXP artificially suppressed the detected Nrf2-Venus signal, although this effect was less significant when fluorescence signals were more evenly matched. Therefore, in order to perform an accurate quantitative analysis of conditional dynamics for both p65 and Nrf2 the two-channel mode of analysis was adopted in all subsequent combined Nrf2/p65 live cell imaging studies.

One of the main aims of this study was to monitor dynamic changes in Nrf2 and p65 distribution and abundance in response to inflammatory and anti-oxidant stimuli. Two different cell models were used to investigate these phenotypes. Firstly, $BAC^{Nrf2\text{-}Venus}$ cells transiently transfected with the p65-dsRedXP plasmid, or stably transduced with tagRFP-p65 lentivirus to generate the tagRFP-p65/$BAC^{Nrf2\text{-}Venus}$ cells, (Methods), resulting in the stable integration of the tagRFP-p65 fusion (Figure 4.5A). The lysates obtained from the $BAC^{Nrf2\text{-}Venus}$ and tagRFP-p65/$BAC^{Nrf2\text{-}Venus}$ were compared by western blot confirming the presence of bands representing both endogenous p65 and a higher molecular weight form corresponding to the fluorescently tagRFP-p65 fusion (Figure 4.5A). Treatment of the $BAC^{Nrf2\text{-}Venus}$ cells with 10ng/ml TNFα triggered classic p65-dsRedXP nuclear oscillations, resulting a subsequent increase in nuclear Nrf2-Venus levels (Figure 4.5B-G, Movie 19).
Comparative Nrf2-Venus responses to stimulation with 10ng/ml TNFα are shown in Figure 4.5C, with the highest induction of nuclear Nrf2 levels being exhibited in tagRFP-p65/$BAC^{Nrf2\text{-}Venus}$ cells. Significantly, both tagRFP-p65 and p65-dsRedXP expressing cells demonstrated oscillatory p65 dynamics in response to the TNFα treatment (Figure 4.5D & E). Averaged nuclear fluorescence traces of tagRFP-p65 and p65-dsRedXP are presented in Figure 4.5H. Both model systems show comparable temporal dynamics in nuclear p65 levels in response to 10ng/ml TNFα, although nuclear levels of p65-dsRedXP were slightly higher than tagRFP-p65, possibly due to high plasmid expression as compared to lentiviral method.

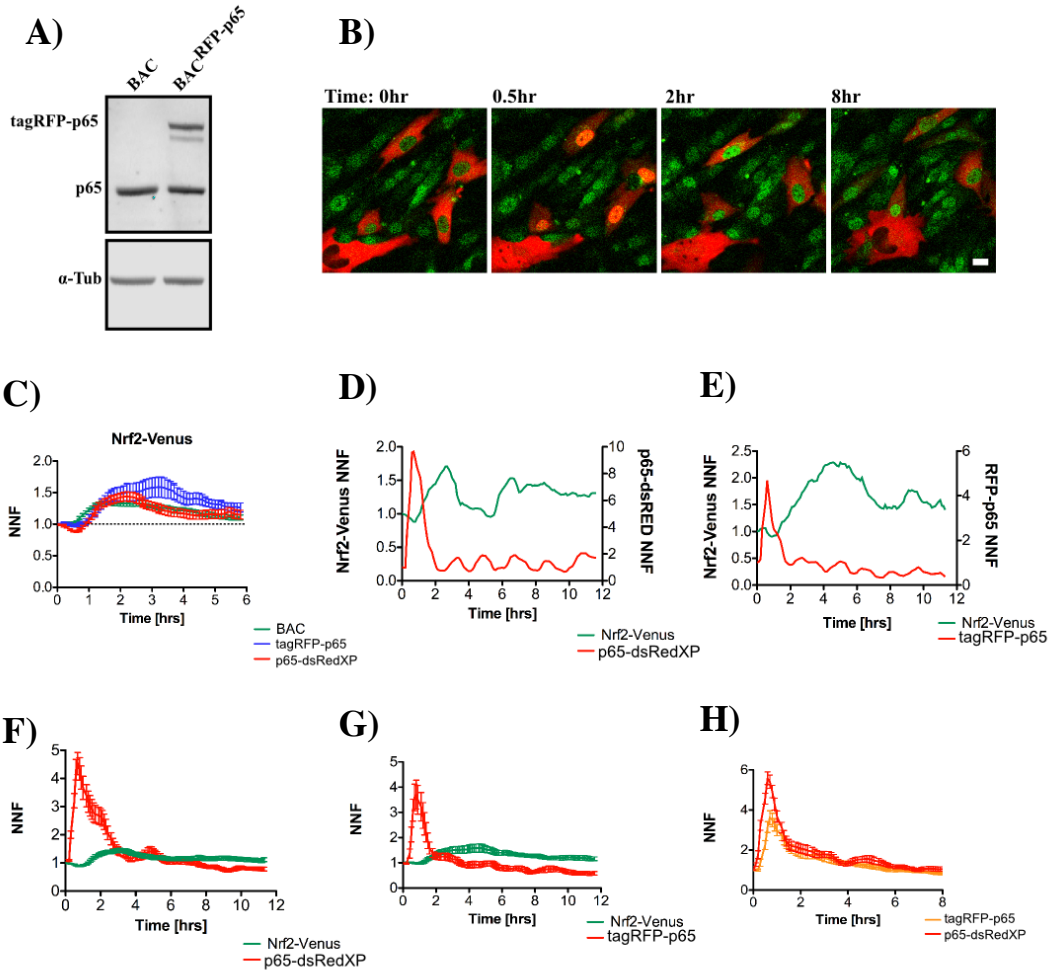

Figure 4.5 Nuclear translocation of p65 precedes increased levels of nuclear Nrf2-Venus. A) Western blot of lysates from BAC$^{Nrf2\text{-}Venus}$ cells and lentivirus transduced tagRFP-p65/BAC$^{Nrf2\text{-}Venus}$ cells, stably expressing the tagRFP-p65 fusion protein. B) Representative time-lapse images of BAC$^{Nrf2\text{-}Venus}$ cells expressing the p65-dsRedXP plasmid in response to TNFα 10ng/ml) stimulation. C) Comparison of averaged (n=3-7, c=13-46) nuclear Nrf2-Venus levels in either non-transfected BAC$^{Nrf2\text{-}Venus}$, BAC$^{Nrf2\text{-}Venus}$ transfected with p65-dsRedXP or tagRFP-p65/BAC$^{Nrf2\text{-}Venus}$ cell models in response to 10ng/ml TNFα. D) Representative single-cell traces of BAC$^{Nrf2\text{-}Venus}$ transiently expressing p65-dsRedXP (Movie 19) or E) tagRFP-p65/BAC$^{Nrf2\text{-}Venus}$ stably expressing the tagRFP-p65 fusion (Movie 18), each following stimulation with 10ng/ml TNFα. F) Average nuclear fluorescence levels of BAC$^{Nrf2\text{-}Venus}$ transfected with p65-dsRedXP in response to 10ng/ml TNFα (n=7, c=48) or G) tagRFP-p65/BAC$^{Nrf2\text{-}Venus}$ in response to 10ng/ml TNFα (n=3, c=13). H) Comparison of dynamic changes in nuclear p65-dsRedXP and tagRFP-p65 proteins following stimulation with 10ng/ml TNFα. Error bars=SEM, Scale bar=20μm.

4.3.2. Measuring the Consequences of Concerted Nrf2 and p65 Activation

To examine the consequences of combined pathway activation, $BAC^{Nrf2\text{-}Venus}$ expressing p65-dsRedXP cells were imaged following simultaneous stimulation with both 2μM SFN and 10ng/ml TNFα (Figure 4.6). Quantification of dynamic changes in nuclear Nrf2-Venus and p65 levels showed that co-administration of SFN and TNFα did not inhibit TNFα induced p65-dsRedXP nuclear accumulation (Figure 4.6A). However, co-stimulation did impose distinct changes in Nrf2 expression patterns. In addition to inducing higher overall levels of nuclear Nrf2-Venus (Figure 4.6A and B), co-stimulation with TNFα and SFN imposed periodic fluctuations in nuclear Nrf2 levels, which were frequently sequential to oscillatory increases in nuclear p65. These periodic changes were far less pronounced when cells were stimulated with either SFN alone (Figure 4.6B). However, it is significant to note that imposed periodic changes in nuclear Nrf2 were observed in both p65-dsRedXP transfected (Figure 4.6A, Movie 20) and non-transfected $BAC^{Nrf2\text{-}Venus}$ cells (Figure 4.6B). Analysis of Nrf2 transcriptional activity using the, ARE-Luc reporter confirmed that co-stimulation with TNFα and SFN enhanced Nrf2 transcriptional activity in comparison to levels observed when cells were stimulated with either TNFα or SFN alone (Figure 4.6D), which was in agreement with imaging data showing higher Nrf2 protein levels in SFN+TNFα treated cells as opposed to ones treated only with SFN compound (Figure 4.6C). This suggested that under conditions in which both pathways are activated, periodic increases in nuclear Nrf2-Venus result in increased Nrf2 transcriptional activity as a result of p65 sequential nuclear entry events.

To compare the effects of increasing p65 expression on nuclear Nrf2 induction following SFN+TNFα co-stimulation, nuclear levels of Nrf2-Venus were measured in three different conditions: (i) $BAC^{Nrf2\text{-}Venus}$ cells with endogenous levels of p65, (ii) $BAC^{Nrf2\text{-}Venus}$ cells also stably expressing near endogenous levels of tagRFP-p65, or (iii) $BAC^{Nrf2\text{-}Venus}$ cells transiently expressing higher levels of p65-dsRedXP (Figure 4.6E). Interestingly, the stable low-level tagRFP-p65 expressing $BAC^{Nrf2\text{-}Venus}$ cell line displayed the highest Nrf2 induction in response to SFN+TNFα co-stimulation, with non-transfected and p65-dsRedXP transfected $BAC^{Nrf2\text{-}Venus}$ cells exhibiting similar lower levels of Nrf2-Venus induction.

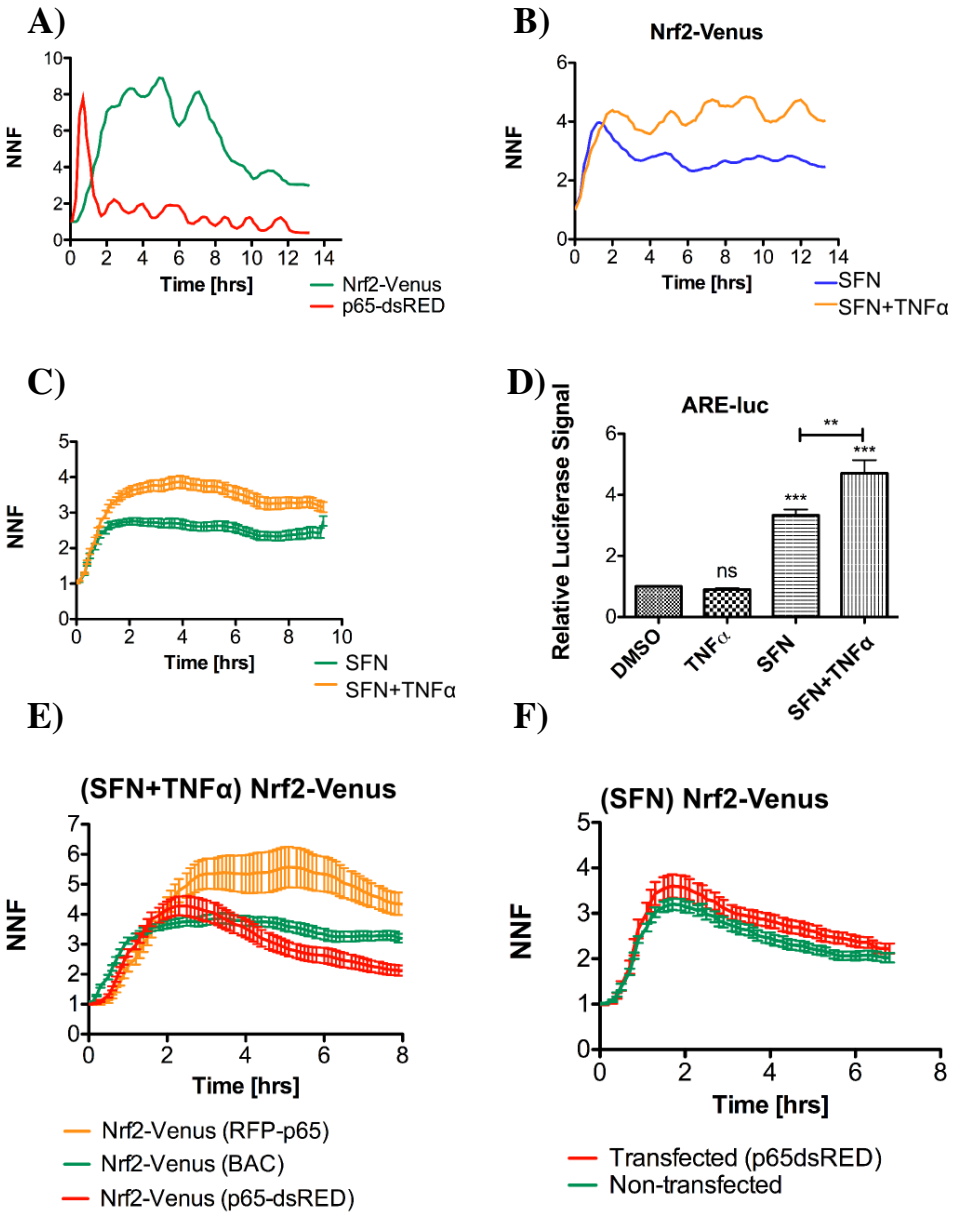

Figure 4.6 Co-stimulation with TNFα and SFN imposes sequential periodic oscillations in nuclear levels of p65-dsRedXP and Nrf2-Venus. A) Representative single-cell measurement of p65-dsRedXP and Nrf2-Venus nuclear dynamics in response to co-stimulation with TNFα (10ng/ml) and SFN (2μM) (Movie 20). B) Representative nuclear fluorescence traces of $BAC^{Nrf2\text{-}Venus}$ cells following exposure to SFN or SFN + TNFα. C) Averaged levels of nuclear Nrf2-Venus following stimulation with SFP alone or SFN+TNFα (n=4, c=31-49). D) Comparative ARE-Luc reporter activity in $BAC^{Nrf2\text{-}Venus}$ cells treated for 8hr with either DMSO, TNFα (10ng/ml), SFN (2μM) or SFN+TNFα (n=3, in triplicates). E) Comparison of mean Nrf2-Venus levels following SFN+TNFα co-stimulation in $BAC^{Nrf2\text{-}Venus}$ cells transiently expressing p65-dsRedXP or $BAC^{Nrf2\text{-}Venus}$ cells with lentivirally-integrated tagRFP-p65. F) Relative levels of nuclear Nrf2-Venus expression in $BAC^{Nrf2\text{-}Venus}$ cells following stimulation with 2μM SFN in the presence or absence of p65-dsRedXP expression (n=3, c=36-39). Error bars=SEM(imaging)/STDEV(luciferase).

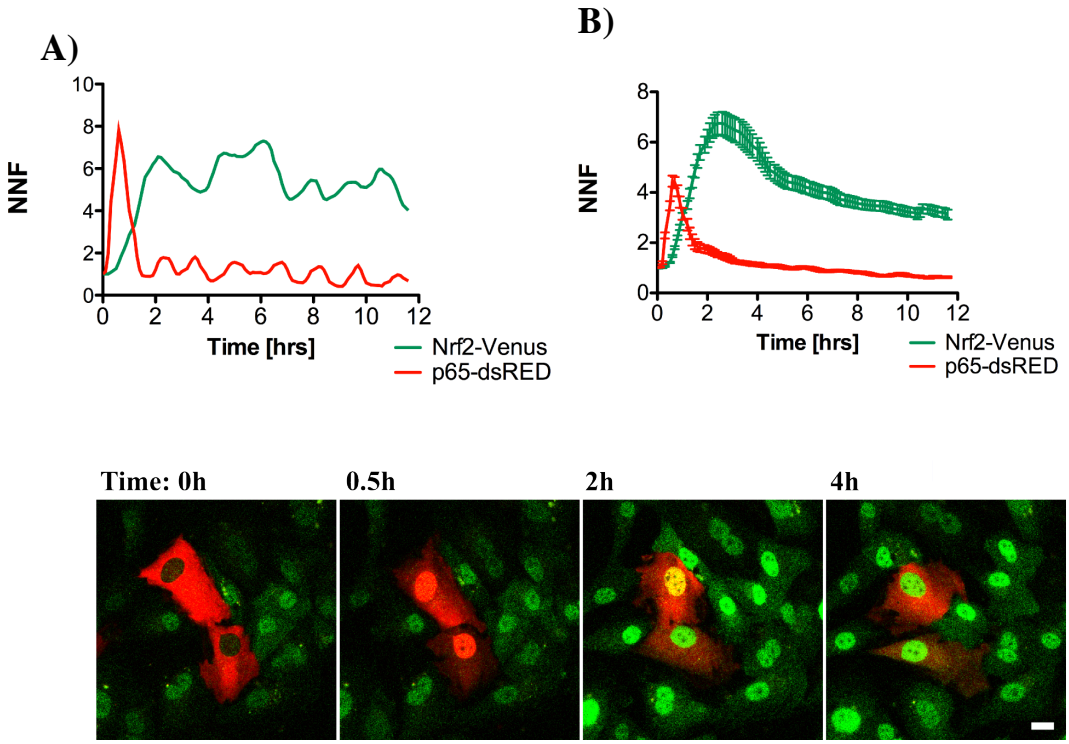

Figure. 4.7 Nuclear translocation of p65 induces subsequent increases in nuclear Nrf2 nuclear in response to combined CDDO-Me and TNFα stimulation. A) Representative and B) averaged nuclear fluorescence levels in BAC$^{Nrf2\text{-}Venus}$ cells expressing p65-dsRedXP following co-stimulation with 100nM CDDO-Me and 10ng/ml TNFα (n=4, c=49). C) Representative time-lapse images from the experiment shown in A&B. Error bars=SEM, scale bar=20μm.

To measure the effect of p65-dsRedXP expression on SFN mediated induction of Nrf2-Venus, BAC$^{Nrf2\text{-}Venus}$ cells expressing p65-dsRedXP were treated with 2μM SFN (Figure 4.6F). Comparison of transfected and non-transfected cells showed no significant difference in Nrf2-Venus induction between these experimental models, implying that expression of higher levels of p65 did not simply translate into greater levels of Nrf2-Venus expression in response to SFN activation.

To assess if p65-imposed changes in Nrf2 nuclear dynamics was unique to SFN stimulation, an alternative Nrf2 activating compound (CDDO-Me) was used instead (Figure 4.7). Co-administration of CDDO-Me+TNFα also evoked a p65-imposed increase in nuclear Nrf2-Venus expression (Figure 4.7A). In addition, application of 100nM CDDO-Me did not prevent p65-dsRedXP nuclear entry in response to TNFα

activation (Figure 4.7). Therefore, co-stimulation with TNFα and either CDDO-Me or SFN led to analogous temporal changes in Nrf2-Venus nuclear fluorescence.

4.3.3. Investigating The Effect of IL-1β on Nrf2 Signalling

To determine if TNFα induced changes in Nrf2-Venus nuclear dynamics could also be initiated by other activators of NF-κB signalling, the effects of IL-1β application on $BAC^{Nrf2\text{-}Venus}$ cells was investigated. IL-1β is known to be a potent activator of the NF-κB pathway in many cell types (Heyden & Ghosh, 2008). Measurement of NF-κb-Luc transcriptional reporter activity in $BAC^{Nrf2\text{-}Venus}$ cells showed a significant increase in 5xκB driven Luciferase activity following 8hr treatment with 10ng/ml IL-1β (Figure 4.8A).

In addition, live cell imaging studies show that 10ng/ml IL-1β triggered tagRFP-p65 nuclear/cytoplasmic oscillations in tagRFP-p65/$BAC^{Nrf2\text{-}Venus}$ cells, which in turn caused a sequential rise in Nrf2-Venus levels shortly after p65 nuclear accumulation (Figure 4.8B), leading to an almost two-fold increase in nuclear Nrf2 levels (Figure 8D, Movie 21).

Consistent with this observation, IL-1β also enhanced CDDO-Me mediated Nrf2 induction in $BAC^{Nrf2\text{-}Venus}$ cells (Figure 4.8E). Therefore, stimulation of cells with either TNFα or IL-1β trigger similar effects on the Nrf2 responses.

4.3.4. Investigating The Role of Keap1 Regulation of Nuclear Nrf2 Dynamics Under Inflammatory Conditions

The application of CDDO-Me and SFN led to transient stabilisation of p65 induced Nrf2 nuclear increases (Figure 4.6A & 4.7A) and both compounds act by inhibiting Keap1 mediated Nrf2 proteasomal degradation (Hayes & Dinkova-Kostova, 2014). Therefore, to investigate the role of Keap1 in controlling cytokine-induced nuclear Nrf2-Venus levels, Keap1 expression was knocked down by siRNA in both tagRFP-p65/$BAC^{Nrf2\text{-}Venus}$ and $BAC^{Nrf2\text{-}Venus}$ cell models (Figure 4.9). Depletion of Keap1 caused a substantial rise in levels of both endogenous and Venus labelled Nrf2 proteins as demonstrated by data from western blot analysis (Figure 4.9A).

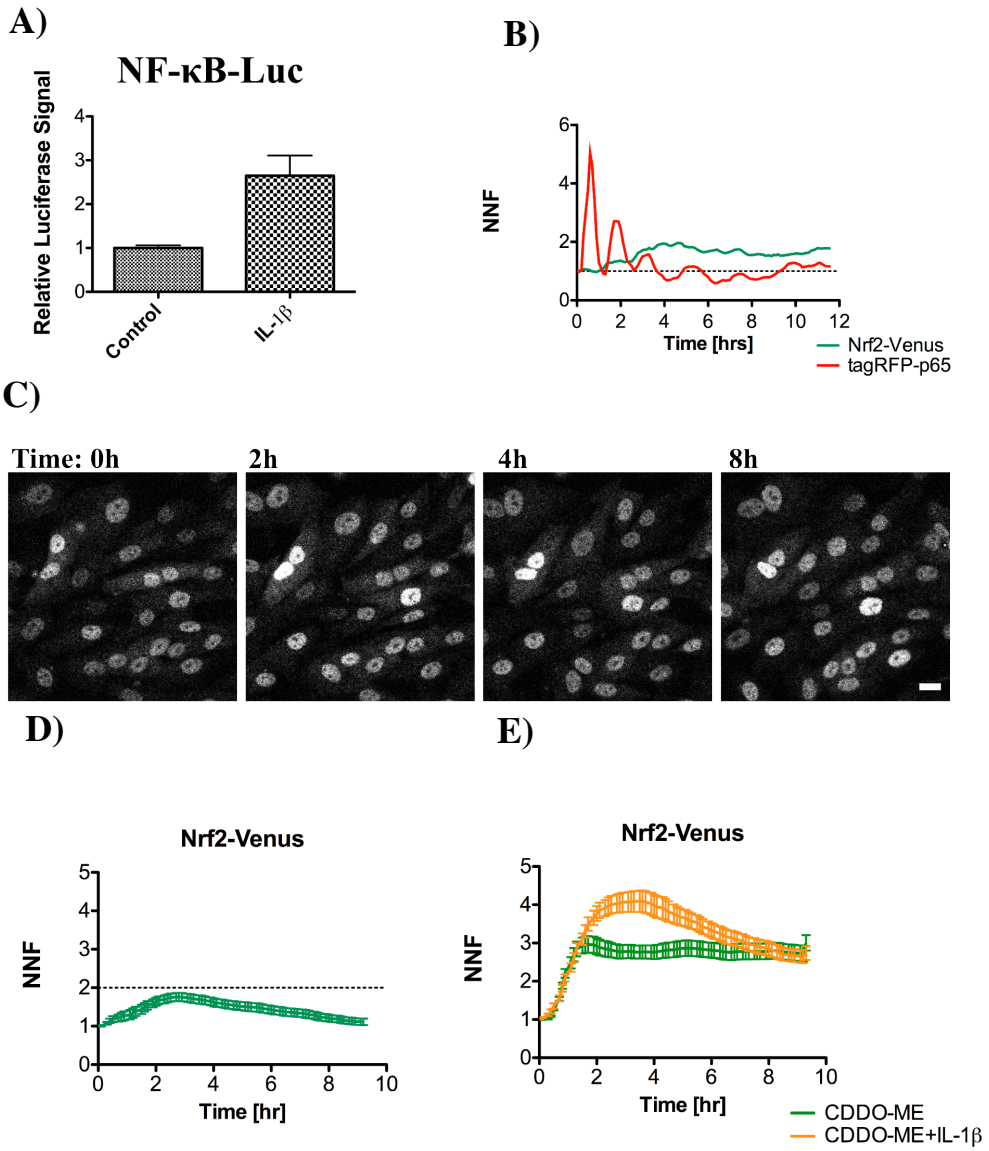

Figure 4.8 IL-1β induces the accumulation nuclear Nrf2-Venus and enhances CDDO-Me-mediated Nrf2 induction. A) NF-κb-Luc reporter activity in response to 8hr 10ng/ml IL-1β treatment in BAC$^{Nrf2\text{-}Venus}$ cells (n=1, in triplicates). B) Nuclear fluorescence levels of p65 and Nrf2 in tagRFP-p65/BAC$^{Nrf2\text{-}Venus}$ cells treated with 10ng/ml IL-1β (n=1, c=7) (Movie 21). C) Representative time-lapse images of BAC$^{Nrf2\text{-}Venus}$ cells treated with 10ng/ml IL-1β. D) Nuclear levels of Nrf2-Venus in response to 10g/ml IL-1β (n=3, c=37). E) Nrf2-Venus nuclear levels in response to 100nM CDDO-Me, or combined treatment with 100n MCDDO-Me and 10ng/ml IL-1β (n=4, c=48). Error bars=SEM, scale bar 20μM.

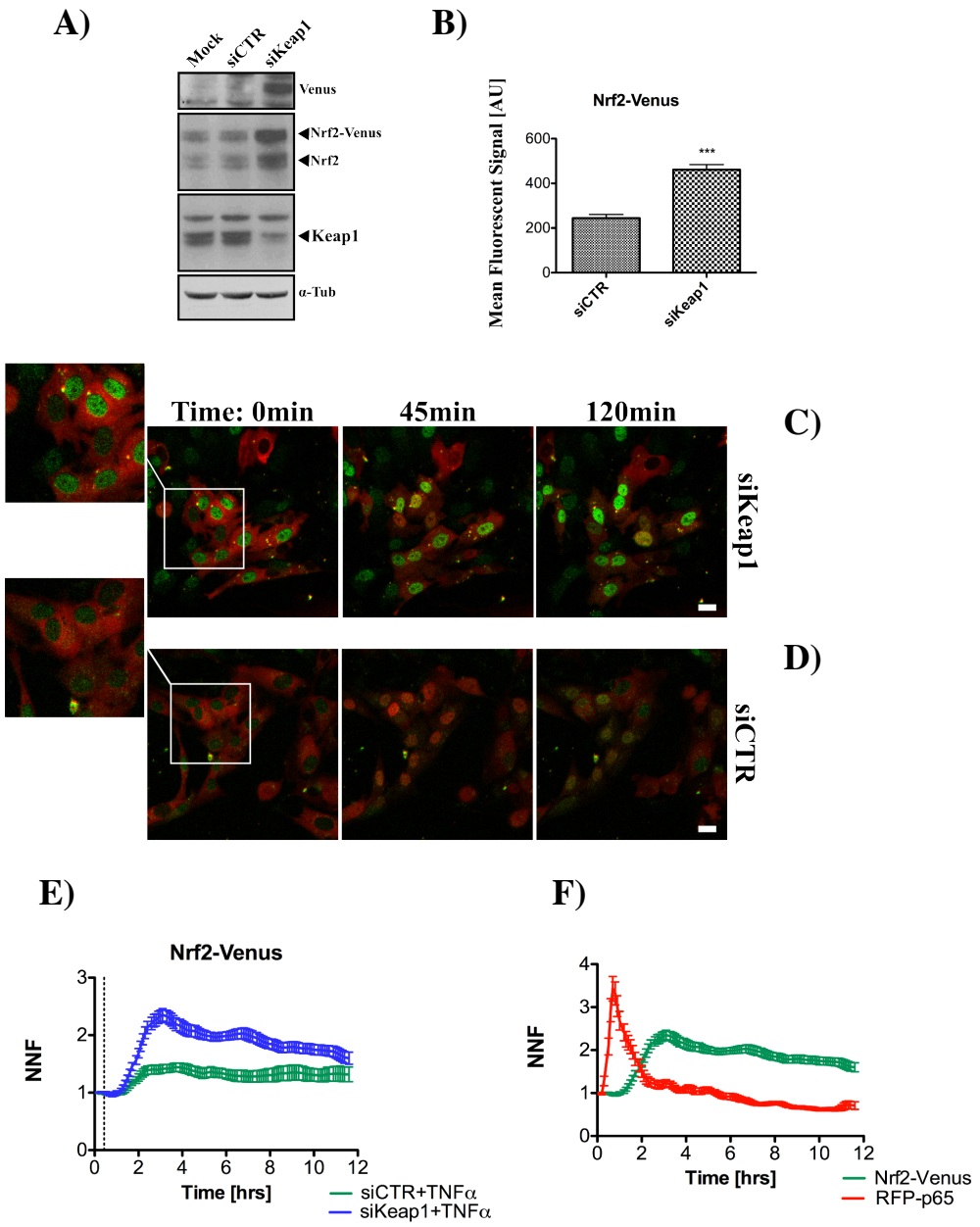

Figure 4.9 Keap1 controls the levels of newly transcribed Nrf2-Venus. A) Western blot comparing lysates from mock control, siCTR and siKeap1 transfected BAC$^{Nrf2\text{-}Venus}$ cells, following 48hr of transfection. Keap1 siRNA effectively reduces Keap1 protein levels and led to higher basal levels of Nrf2 and Nrf2-Venus proteins. B) Keap1 knockdown increased Nrf2-Venus expression in BAC$^{Nrf2\text{-}Venus}$ cells (c=40). C) Time-lapse images of tagRFP-p65/BAC$^{Nrf2\text{-}Venus}$ cells transfected with siCTR (control) (Movie 23) or D) siKeap1 (Movie 22), in both cases cells were treated with 10ng/ml TNFα and imaged over an 8h period. E) Comparison of Nrf2-Venus levels in siCTR and siKeap1 treated cells following stimulation with 10ng/ml TNFα showing higher Nrf2-Venus accumulation in cells with reduced Keap1 expression (n=3). F) Averaged nuclear tagRFP-p65 and Nrf2-Venus fluorescence in tagRFP-p65/BAC$^{Nrf2\text{-}Venus}$ cells following stimulation with 10ng/ml TNFα 48hr after Keap1 depletion (n=3, c=13-31). Error bars=SEM. Scale bar=20μm.

Imaging of unstimulated BAC$^{Nrf2\text{-}Venus}$ cells displayed a >2fold increase in nuclear fluorescence in cells treated with siKeap1 in comparison to control siCTR treated cells (Figure 4.9B). Interestingly, real-time imaging of Nrf2-Venus in response to TNFα stimulation showed that levels of nuclear Nrf2-Venus were significantly higher in Keap1 depleted tagRFP-p65/BAC$^{Nrf2\text{-}Venus}$ cells, in comparison to control siRNA transfected cells (Figure 4.9C-F). Significantly, TNFα induced robust nuclear accumulation of tagRFP-p65 in Keap1 depleted cells and this preceded a subsequent increase in nuclear Nrf2-Venus levels (Figure 4.9F, Movie 22 & 23). To summarise, Keap1 plays a significant role in regulating the inflammatory driven increase in Nrf2.

4.3.5. Investigating the GSK-3-mediated Nrf2 Regulation Following Cytokine Induced Inflammatory Stress

While Keap1 is believed to be the primary cytoplasmic regulator of Nrf2 expression levels, the GSK-3α/β kinase has been identified as a negative regulator of nuclear, Nrf2 expression (Chowdhry *et al,* 2013). To investigate the effect of GSK-3 on Nrf2 nuclear dynamics live cell imaging was performed on BAC$^{Nrf2\text{-}Venus}$ cells grown in media containing 2% or 10% serum, in the presence or absence of the GSK-3 inhibitor CHIR99021 (Figure 4.10). Cells imaged in low serum conditions showed small increase in nuclear Nrf2 levels in response to the GSK-3 inhibition (Figure 4.10A). Also, co-application of TNFα further enhanced Nrf2-Venus protein induction; although these cells exhibited a greater variability in consequent levels of Nrf2-Venus protein (Figure 4.10B). Also, stimulation with TNFα further enhanced Nrf2-Venus induction; although these cells exhibited a greater variability in levels of Nrf2-venus expression (Figure 4.10B). Comparison of the relative levels of TNFα mediated Nrf2-Venus induction, in the presence or absence of CHIR99021 showed a slight enhancement of TNFα mediated Nrf2 induction as a result of GSK-3 inhibition, and an alteration to Nrf2 nuclear dynamics (Figure 4.10C). Time-lapse imaging of TNFα induced tagRFP-p65 protein dynamics showed a greater and more rapid initial peak of p65 nuclear accumulation in tagRFP-p65/BAC$^{Nrf2\text{-}Venus}$ cells (Figure 4.10D) compared to BAC$^{Nrf2\text{-}Venus}$ cells (Figure 4.10C).

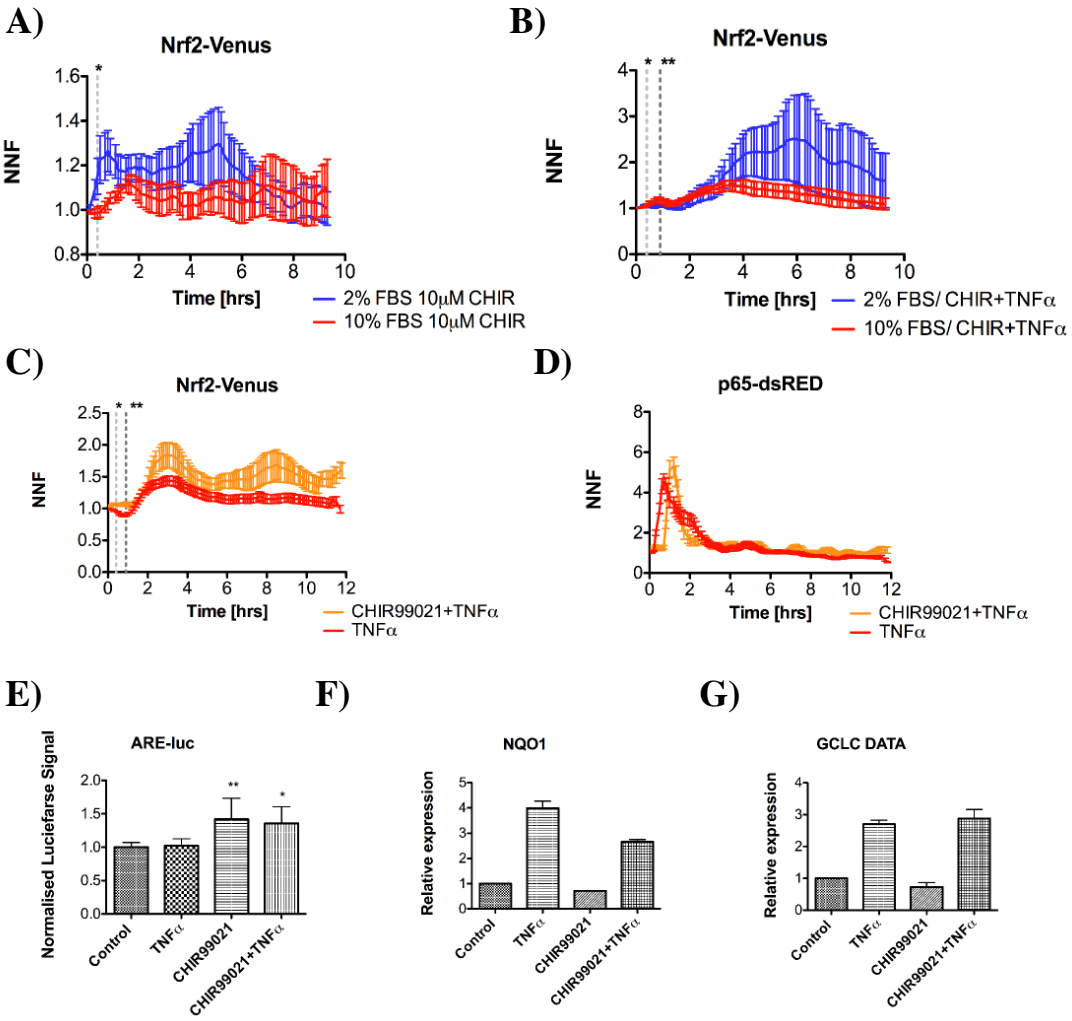

Figure 4.10 The effect of GSK-3 inhibition on the Nrf2 nuclear accumulation and activity. A) Nuclear Nrf2-Venus fluorescence was monitored in BAC$^{Nrf2\text{-}Venus}$ cells treated with 10μM CHIR99021 inhibitor in cell media supplemented with low or high serum (n=1, c=12) (inhibitor addition indicated by dashed line *). B) The BAC$^{Nrf2\text{-}Venus}$ cells treated with 10μM CHR99021 (at time indicated *) did not show significant enhanced nuclear stabilisation of Nrf2-Venus as a results of 10ng/ml TNFα stimulation (marked as **) in both, low and high serum environments (n=1, c=15). C) The Nrf2-Venus nuclear levels following GSK-3 inhibition (dashed line *) +/- 10ng/ml TNFα (dashed line **) in BAC$^{Nrf2\text{-}Venus}$ cells grown in 10% FBS containing media (n=2, c=20). D) The comparison of tagRFP-p65 nuclear dynamics following TNFα stimulation 30min after +/- addition of 10μM CHIR99021 inhibition, displayed slightly shorter nuclear accumulation event in cells pre-treated with GSK-3 inhibitor. E) The ARE-Luc expression levels following 6hr DMSO, 10μM CHIR99021, 10ng/ml TNFα or joint treatment of TNFα and CHIR99021 (n=3, in triplicates). (F-G) Relative mRNA expression of GCLC and NQO1 do not show significant changes under basal and TNFα induced (8hr) activity as a result of CHIR99021 treatment (added 30min before TNFα) (n=1, in triplicates). Error bars=SEM(imaging)/STDEV(luciferase and QPCR).

The effect of GSK-3 inhibition on Nrf2 transcriptional activity was investigated by measuring ARE-Luc reporter activity and Q-PCR was performed to quantify levels of expression of Nrf2 target genes (Figure 4.10 E-G). Inhibition of GSK-3 with 10μM CHIR99021 resulted in a slight increase in ARE-Luc activity, however neither single nor combined treatment with TNFα induced any further enhancement of this effect (Figure 4.10E). Inhibition of GSK-3 (addition of 10μM CHIR99021 for 8h) did not significantly change NQO1 or GCLC mRNA expression levels, even in combination with TNFα stimulation (Figure 4.10F & G). Therefore, it would appear that GSK-3 kinase has a negligible effect on Nrf2 transcriptional activity and did not enhance TNFα mediated gene expression.

4.3.6. Effect of Prolonged TNFα Stimulation on Nrf2 Dynamics and Transcriptional Activity

So far the experimental design focused on investigating acute inflammation by TNFα, however we were interested if chronic cytokine signalling is associated with dampening of the protective antioxidant responses. To investigate the effect of longer-term TNFα activation of NF-κB signalling on Nrf2 responses, $BAC^{Nrf2\text{-}Venus}$ cells were continuously exposed to TNFα (10ng/ml) stimulation for 64h, before measuring Nrf2 transcriptional activity and conditional changes in Nrf2 dynamics (Figure 4.11).

In contrast to short-term (8h) TNFα stimulation of $BAC^{Nrf2\text{-}Venus}$ cells, prolonged exposure to 10ng/ml TNFα significantly reduced basal ARE-Luc activity and diminished induction of Nrf2 by 2μM SFN (Figure 11A). However, live cell imaging studies showed no significant differences between cells pre-treaded with TNFα for 64hrs, compared to control (mock-stimulated) cells (Figure 4.11B & C). In each case SFN (2μM) induction led to a robust increase in levels of nuclear Nrf2-Venus (Figure 4.11B & C). Measurement of changes in gene expression for a selection of well-known Nrf2-target genes (NQO1, GCLC and HO-1) following 64hr exposure to TNFα again showed pleiotropic effects (Figure 4.11D-F). While NQO1 showed a reduced response to the SFN induction following 64h exposure to TNFα (Figure 4.11F), the levels of GCLC mRNA remained unchanged (Figure 4.11D) and HO-1 gene expression was amplified (Figure 4.11E). Therefore, from this data the

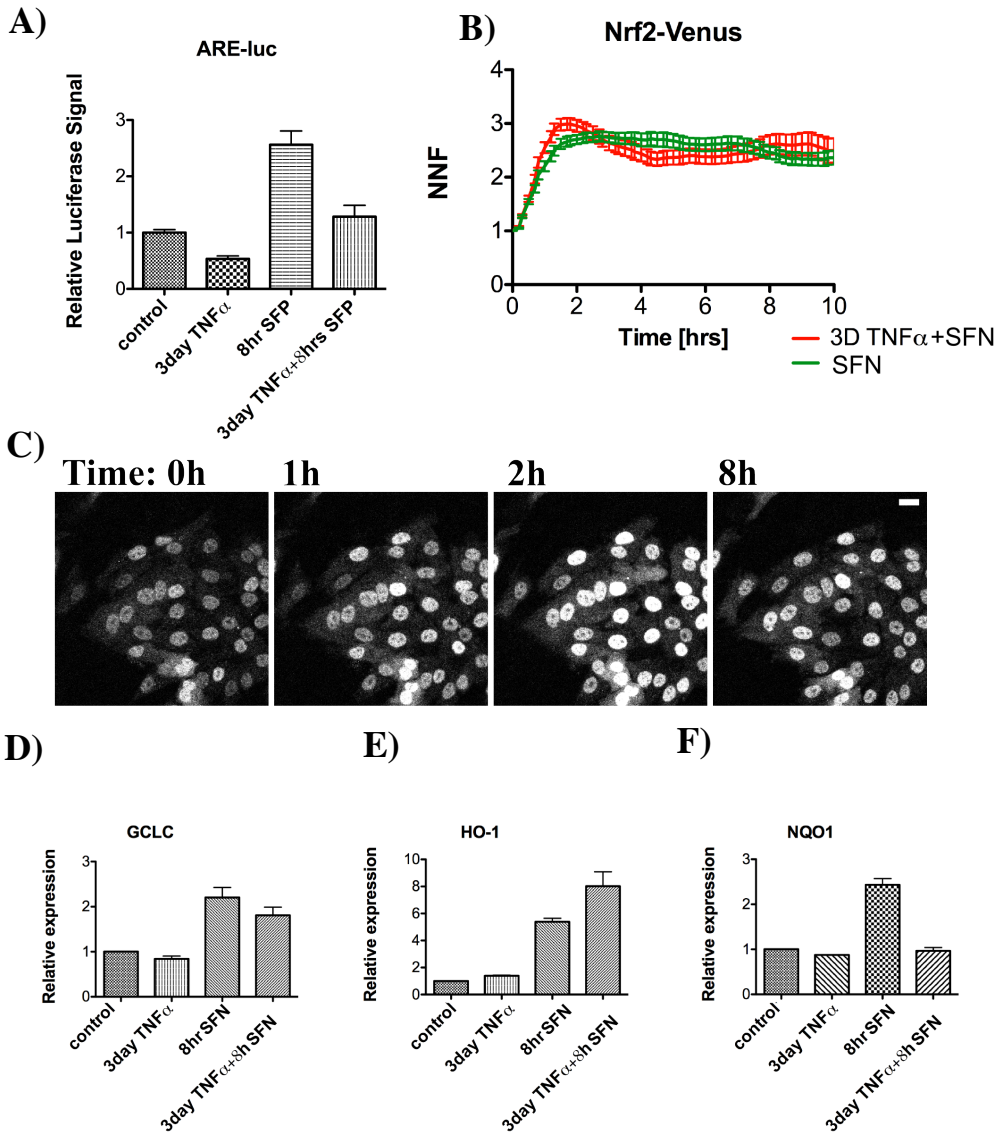

Figure 4.11 Long TNFα exposure does not prevent effective Nrf2 activation with SFN. A) ARE-Luc expression levels following 64hr 10ng/ml TNFα treatment, showing impaired induction in response to (8hr) 2μM SFN (n=2, in triplicates). B) Nrf2-Venus protein levels following the 2μM SFN treatment are not impaired by 64hr TNFα pre-treatment. C) Representative images from the experiment. D-F) Relative mRNA expression levels of GCLC, HO-1 and NQO1 following 8hr 2μM SFN induction (n=2, in triplicates). Error bars=STDEV(luciferase, QPCR)/SEM (imaging).

net effect of longer-term TNFα stimulation on cellular anti-oxidant responses remains unclear.

4.3.7. Impact of Nrf2 Activation on NF-κB Pathway Dynamic Responses

To investigate how activation of the Nrf2 pathway may modulate NF-κB transcriptional activity several canonical target genes were measures in response to TNFα or joint TNFα+SFN stimulation (Figure 4.12). Levels of IKBα, IL-6 and SOD-2 mRNA were significantly reduced in BAC$^{Nrf2\text{-}Venus}$ cells in response to SFN activation (Figure 4.12A-C). Although, IL-8 expression also followed this trend, measured differences in mRNA levels were not significant (Figure 4.12D).
As previously demonstrated (Section 4.3.1.1) transcription of the *NRF2* gene can be driven by NF-κB (p65). Therefore it is possibly not surprising that TNFα triggered expression of Nrf2 was also reduced in response to inhibitory SFN effect (Figure 4.12E) and the co-stimulation with SFN caused a significant reduction in levels of Nrf2 mRNA expression in response to acute inflammation.

Live cell imaging studies show that induction of the Nrf2 pathway by SFN or CDDO-Me did not interfere with nuclear translocations of p65 in response to TNFα. It was evident that nuclear accumulation of p65 peaked about 30min after TNFα addition, and was not affected by the co-treatments with either the SFN or CDDO-Me drugs.
In order to investigate how changes in cellular Nrf2 levels influence p65 dynamics further, Nrf2 was expressed from a high expression CMV-Venus-Nrf2 plasmid and imaged in p65-dsRedXP expressing SK-N-AS cells in response to TNFα (Figure 4.13). Nuclear fluorescence levels of Venus-Nrf2 and p65-dsRedXP demonstrate that high levels of Nrf2 inhibit nuclear accumulation of p65-dsRedXP in response to TNFα (Figure 4.13A-C). Comparison of the near-endogenous Nrf2 expression system BAC$^{Nrf2\text{-}Venus}$ with plasmid-transfected cells highlighted the fact that p65-dsRedXP accumulation was significantly inhibited in the high expression model system (Figure 4.13C). What is more, the BAC encoded Nrf2-Venus and plasmid expressed Venus-Nrf2 behaved differently in response to TNFα (Figure 13D). Specifically, the Venus-Nrf2 plasmid failed to show

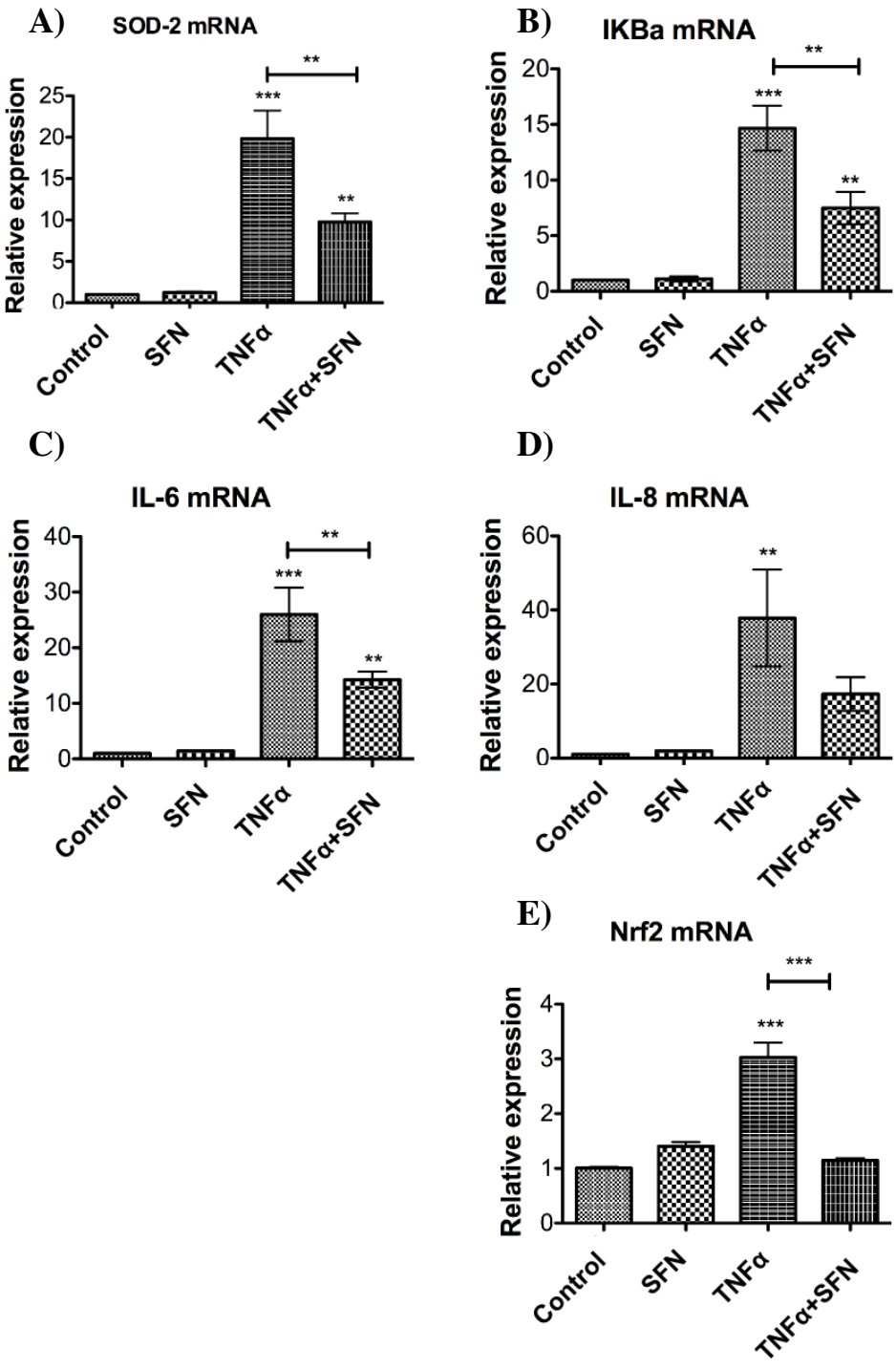

Figure 4.12 SFN reduces expression of TNFα induced NF-κB target genes. A-D) The canonical NF-κB target genes expression profiles, in response to 8hr TNFα or co-treatments with 10ng/ml TNFα and 2μM SFN, normalised to β-actin. E) Administration of SFN with TNFα led to reduction in Nrf2 mRNA expression. Error bars=STDEV, (n=3, in triplicates).

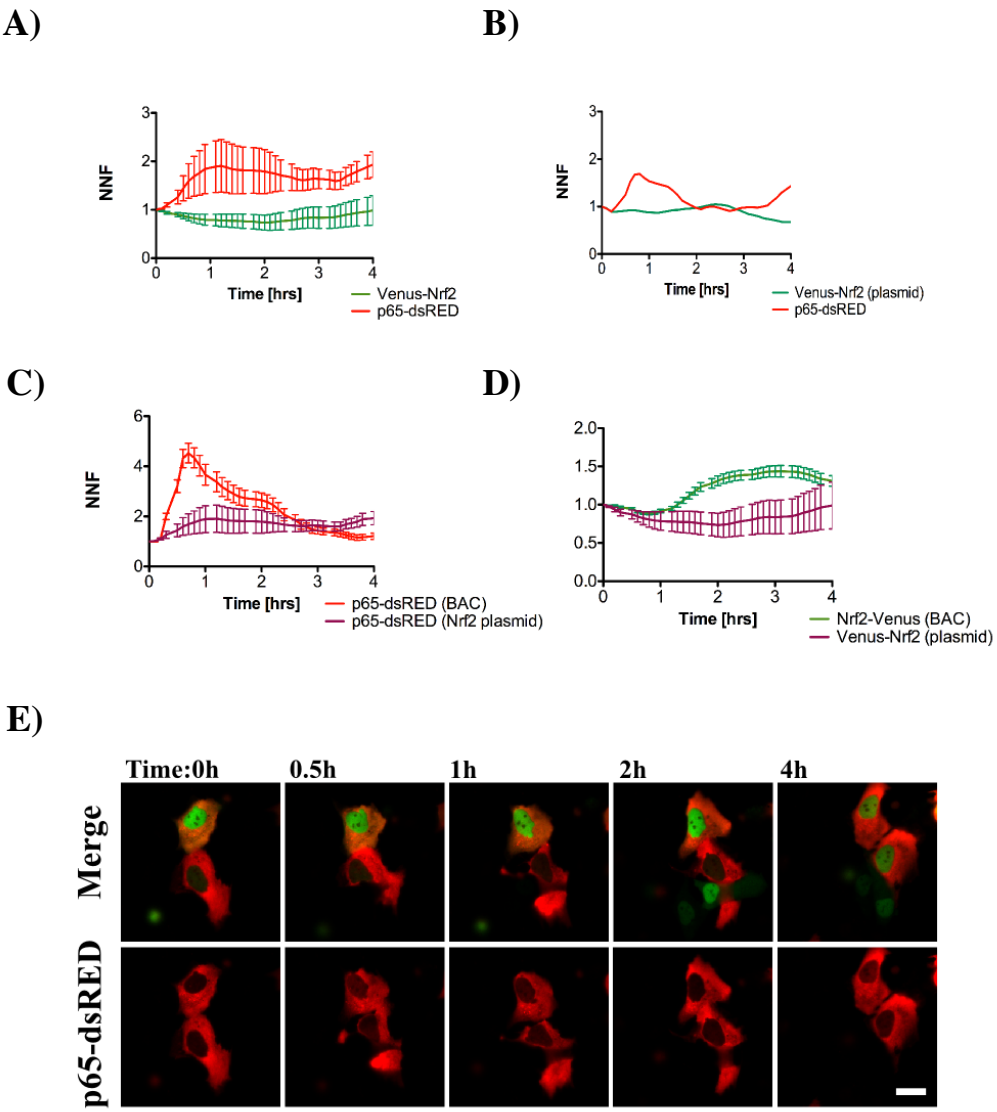

Figure 4.13 Nrf2 overexpression disrupts the p65-dsRedXP dynamics in response to inflammatory stimuli. A) Averaged nuclear fluorescence of Venus-Nrf2 (expressed from a plasmid) and p65-dsRedXP in response to 10ng/ml TNFα in SK-N-AS cells (n=3, c=17). B) Representative single cell traces. C) Comparison of p65 responses to 10ng/ml TNFα in $BAC^{Nrf2\text{-}Venus}$ and in SK-N-AS cells expressing Venus-Nrf2 plasmid, showing less effective p65 nuclear accumulation. D) Comparison of Nrf2 responses in $BAC^{Nrf2\text{-}Venus}$ and SK-N-AS cells transfected with Venus-Nrf2. E) Representative images from the experiment. Scale bar=10μM, Error bars=SEM. Scale bar=20μm.

cytokine dependant increases in nuclear levels (Figure 4.13D). Data from these experiments highlight the need for strict regulation of Nrf2 activity, as high levels can disrupt NF-κB activity in response to inflammation.

4.4. DISCUSSION

Work presented in this chapter describes the combined use of both population-level and advanced live cell imaging techniques to investigate the extent and consequence of conditional crosstalk between the NF-κB and Nrf2 response pathways.

In chapter evidence was presented to demonstrate the utility of the recently generated $BAC^{Nrf2\text{-}Venus}$ stable cell-line as a physiologically relevant model to study dynamic conditional Nrf2 responses. In this cell-line the Nrf2-Venus fusion protein is expressed from an endogenous genomic context, enabling all of the sequential stages of gene expression and protein dynamics to be investigated in real-time. Having established that the Nrf2-Venus protein is expressed at near endogenous levels and responds as predicted to canonical methods of Nrf2 pathway activation, we were interested to use the $BAC^{Nrf2\text{-}Venus}$ stable cell-line as a sensitive model system to investigate the relative conditional dominance and reciprocal affects of NF-κB and Nrf2 signalling in live cells.

The temporal dynamics of TNFα induced p65 responses have been extensively characterised in the SK-N-AS cell line, using both live cell imaging methods and NF-κb-Luc transcriptional reporter assays (Ashall *et al,* 2002; Nelson *et al,* 2004). Initial work in this study, replicated the reported oscillatory dynamics of TNFα–induced p65 nuclear/cytoplasmic shuttling (Figure 4.5D, Movie 19), and the associated rise in NF-κB transcriptional activity in the $BAC^{Nrf2\text{-}Venus}$ stable cell-line (Figure 1A) previously reported by Ashall *et al* (Ashall *et al*, 2002). Considering the reported anti-inflammatory action of the Nrf2 pathway (Chen *et al,* 2003), it is significant to note that under basal/unstimulated conditions, the extra genomic copies of Nrf2-Venus in the $BAC^{Nrf2\text{-}Venus}$ cell-line, did not impart TNFα mediated activation of the NF-κB pathway as the cytokine signalling was able to trigger nuclear

translocation of endogenous p65 and activate the transcription of target genes (Figure 4.1A & Figure 4.5).

The TNFα induced Nrf2 was previously observed in monocytes and astrocytes and in agreement with those observations it was also detected in the neuroblastoma cell model in this study (Figure 4.1B-D) (Rushwoth *et al,* 2012*;* Correa *et al,* 2012). To assess whether TNFα stimulation conferred universal, or selective, increases in Nrf2 target gene expression, the induction of a panel of Nrf2 target genes was investigated following addition of 10ng/ml TNFα and compared to effect following well-characterised Nrf2 inducer SFN. Following stimulation with SFN alone, mRNA levels of HO-1, NQO1, GCLC, SFXN1, Bach1 and TRXN1 were all significantly increased (Figure 4.2), confirming that these canonical Nrf2 response genes are responding to Nrf2 pathway stimulation in $BAC^{Nrf2\text{-}Venus}$ cells. However, when qPCR was performed on extracts prepared from cells treated for 8h with TNFα (10 ng/ml), only 4/6 tested Nrf2 response genes (GCLC, HO-1, NQO1 and Bach1) showed marked increase in transcript abundance (Figure 4.3A-C & F). With SRXN1 and TRXN1 consistently showing no significant increase in expression following TNFα stimulation (Figure 4.4D & E). Expression of NQO1 is believed to be an excellent marker of Nrf2 activity, as so far no other transcription factor binding sites have been identified in the promoter region of the *NQO1* gene (Habas *et al*, 2013). In contrast, the promoter sequence of HO-1 is complex and more promiscuous, as it also encodes κB elements upstream the start codon. Therefore, HO-1 may be jointly regulated by both NF-κB and Nrf2 response pathways (Kim *et al,* 2013).

Almost all of the selected Nrf2 regulated genes have prominent functions in antioxidant defence, with the exception of Bach1, which is atypical, as it is able to inhibit the expression of antioxidant genes. Like Nrf2, Bach1 recognises the ARE consensus sequences however, it lacks the transactivation domain, required to initiate transcription, therefore it is though to compete with Nrf2 for access to ARE-elements in the promoters of Nrf2 target genes (Jyrkkanen *et al,* 2011). Thus providing a negative regulatory loop, which may act to tune down expression of Bach-1 sensitive genes. The reason why the SFXN1 and TRXN1 genes did not respond to TNFα treatment is unclear, however it can be speculated that they are more prone to Bach1 negative feedback, which demonstrated an increase in mRNA levels following TNFα

(Figure 4.3F) or they are not favoured for transcription under conditions of inflammatory stress.

The promoter of the *SFXN1* gene was previously analysed by Harpers *et al* (Harpers *et al, 2015*) in order to study the effects of inflammation on Nrf2 activity in human hepatocytes. In this study no changes in Nrf2 transcriptional activity were observed following stimulation with TNFα (20ng/ml) . However, it should be emphasised that in the Harpers *et al* study Nrf2 transcriptional activity was assessed by measuring promoter activity of the SFXN1 gene alone. In this context, our results concur with their findings, however the broader analysis of potential Nrf2 response genes performed in this study shows that although TNFα stimulation of SK-N-AS cells increases both nuclear Nrf2, the expression profiles of ARE-containing target genes is selective. This may be due to differential epigenetic modification of ARE genes, or conditional changes in co-factor availability *etc*. Significantly, both of these scenarios may be cell type specific and in this context it should be noted that SK-N-AS cells are neuroblastoma derived and may have undergone cancer-induced changes in genes expression profiles.

Combining the results obtained from quantitative single-cell imaging studies and Q-PCR data we have established that a ~50% increase in nuclear Nrf2 levels (as measured by nuclear Nrf2-Venus fluorescence) is sufficient to trigger expression of a selective majority of ARE containing Nrf2 response genes.

As the human Nrf2 promoter region contains two NF-κB binding sites (κB1 & κB2 sites) (Rushworth *et al,* 2012) we were keen to establish whether TNFα stimulation was directly enhancing Nrf2 transcription. For this reason a new reporter of Nrf2 gene transcription p*NRF2*-Luc was generated, in which luciferase expression was under control of the endogenous 1.2kb proximal Nrf2 transcriptional promoter region (Figure 4.3I). Using this reporter it was possible to show that cells expressing a p65-dsRedXP plasmid exhibited three times more Nrf2 transcription compared to cells transfected with a Blue Script control plasmid (Figure 4.4J). Significantly, deletion of the κB2 sites in the *NRF2* promoter sequence reduced both basal and p65-dsRedXP driven Nrf2-promoter activity.

Therefore, our data is consistent with previous reports showing that Nrf2 activity in acute myeloid leukaemia (AML) is driven by NF-κB activity (Rushwort *et al*, 2012). Significantly, our data primary mouse astrocytes (Figure 4.3H) shows that TNFα mediated activation of *NRF*2 transcription is not restricted to cancer derived cells.

The fundamental aim of this study was to perform live cell imaging experiments on Nrf2 and p65 transcription factors to investigate the extent of molecular crosstalk between these processes. Therefore, it was essential to define the best imaging method to simultaneously monitor the localisation and relative abundance of fluorescently labelled proteins under investigation. The lambda scan approach was validated as a effective method for imaging low levels of Nrf2-Venus expression, leading to the enhancement of the Venus signal and reduction of the background autofluorescence (Fig 4.2. Chapter1). Therefore, this imaging mode was also initially used to monitor the combined spatio-temporal dynamics of Nrf2-Venus and p65-dsRedXP proteins in response to TNFα stimulation (Figure 4.4A). This was possible as the dsRedXP excitation spectrum includes the 514nm wavelength, which is also usually used to excite the Venus tag; therefore both fluorescent proteins could be excited by the same 514nm laser. However, after extensive profiling we became concerned that in the context of co-expression studies this approach may impose errors in Venus fluorescence values, especially when levels of the p65-dsRedXP fusion protein were relatively high. (Figure 4.4C). We believe the cause of this problem was that the acquisition of images using the lambda-scan mode relies on signal detection with a single set of detectors. These can become temporarily saturated by a very bright fluorescent signal (e.g. p65-dsRedXP nuclear accumulation), as a result they are unable to detect subtle difference in Venus and p65-dsRedXP emission spectra. This problem highlights the importance of selecting appropriate imaging parameters, especially when the protein under study needs to be expressed at very low levels. Having identified this problem, it was possible to design an alternative two-channel imaging strategy to solve this technical challenge. In this approach separate lasers and detector sets were used to sequentially illuminate and collect Venus and dsRedXP fluorescence signals (Figure 4.4D). One drawback of this approach was an inevitable loss of sensitivity in detecting the Nrf2-Venus

signal, however as it was clearly a more stringent method for the combined imaging of the two transcription factors, without the risk of introducing technical artefacts, this approach was adopted in all subsequent combined imaging studies.

The first combined imaging study focused on the simultaneous measurement of p65 and Nrf2 dynamic responses to TNFα stimulation in BAC$^{Nrf2\text{-}Venus}$ cells following transient transfection with the p65-dsRedXP plasmid, or lentiviral transduction with a tagRFP-p65 fusion protein (Figure 4.5). Despite varying levels of p65 expression (plasmid >> lentivirus > endogenous), both systems displayed comparable TNFα-imposed activation and oscillatory p65 nuclear dynamics, followed by a subsequent increase in Nrf2-Venus fluorescence (Figure 4.5A, B, F and G). Surprisingly, quantitative comparison of TNFα induced nuclear Nrf2-Venus levels showed that the highest level of Nrf2 induction was achieved in lenti-transduced tagRFP-p65/BAC$^{Nrf2\text{-}Venus}$ cells (Figure 4.5C). It is as yet unclear why a model system in which p65 is expressed at near-physiological levels imposes a more potent effect on Nrf2 induction then one in which p65 is expressed at higher, and possibly saturating levels. One possible explanation is that high expression levels of p65 could trigger formation of high proportion of p65-p65 homodimers, which are not as transcriptionally effective as the p65-p50 heterodimers (Chen *et al,* 1998). Therefore, even though more p65-dsRedXP protein is available than in tagRFP-p65 transduced cells, not all of it could be incorporated into transcriptionally superior NF-κB complex with p50.

Significantly, data from live cell imaging studies revealed a novel dynamic consequence of simultaneous pathway activation. In contrast to the single broad peak of Nrf2 induction, which was observed when BAC$^{Nrf2\text{-}Venus}$ were stimulated with SFN (Figure 4.6B); co-stimulation of p65-dsRedXP expressing BAC$^{Nrf2\text{-}Venus}$ cells induced an extended pattern of periodic changes in Nrf2 nuclear expression. Interestingly, it was possible to establish that these repetitive short-lived increases in nuclear Nrf2 levels were preceded by p65 nuclear shuttling events (Figure 4.6A & 4.7A). Given that nuclear p65 increases the levels of nuclear Nrf2 in BAC$^{Nrf2\text{-}Venus}$ cells, we proposed a model in which the observed periodic changes in nuclear Nrf2 levels result from enforced changes in the dynamic balance between Nrf2 production

and degradation. In this model, periodic increases in nuclear Nrf2 are driven by periodic TNFα–mediated increases in nuclear p65, which then drive Nrf2 transcription, thus increasing the nuclear pool of Nrf2-Venus. The magnitude of this effect is amplified by the presence of SFN, which would reduce the negative effects of Keap1 mediated Nrf2 degradation. In combination these two effects cause the observed sharp increases in nuclear Nrf2 levels that follow bursts of p65 nuclear translocation (Figure 4.6A and 4.7A). Conversely, as p65 enters the cytoplasmic phase of its oscillatory cycle, transcription of Nrf2 decreases and degradation becomes the dominant phenotype, thus leading to a decrease in nuclear Nrf2 levels, until the next cycle of p65 nuclear translocation.

Although this model explains the basic principles that we believe operate in the $BAC^{Nrf2\text{-}Venus}$ cells, several key issues remain unclear. In particular, it was not clear if imposed sequential variations in nuclear Nrf2 levels occur in response to alternate stimulation of both pathway and if they can be observed in other cell types.

To address the same issue, with respect to differential activation of NF-κB signalling, IL-1β was used as an alternate method of stimulating NF-κB signalling in $BAC^{Nrf2\text{-}Venus}$ cells. IL-1β activates NF-κB signalling via the ILR cell-surface receptor, which is distinct to that activated by TNFα (Hayden & Ghosh, 2008). (Figure 4.8 B-D). Significantly, application of IL-1β triggered an increase of ≈50% in nuclear Nrf2-venus levels, which was equivalent to the response achieved by TNFα induction (Figure 4.8D *vs*. 4.1B). As with TNFα stimulation, IL-1β also enhanced the effects of CDDO-Me induced Nrf2-Venus nuclear accumulation (Fig 4.8E). Therefore, both IL-1β and TNFα cytokines drive enhanced sequential increases in nuclear Nrf2-Venus levels and both activators of NF-κB signalling increased antioxidant responses when added in combination with Keap1 inhibiting compounds (SFN or CDDO-Me) (Figure 4.6C & 4.8E).

Both CDDO-Me and SFN exert their effects by inhibiting Keap1 mediated degradation of Nrf2. Therefore, depletion of Keap1 was expected to enhance levels of nuclear Nrf2 in response to TNFα stimulation. Our data shows that siRNA knockdown of Keap1 increases basal Nrf2-Venus nuclear fluorescence (Figure 4.9A, B, C). Interestingly, reduction of Keap1 cellular levels dramatically augmented

TNFα induced Nrf2 nuclear accumulation (Figure 4.9E, Movie) 22 & 23. This data is consistent with the idea that newly translated Nrf2 is under robust Keap1 mediated regulation in the neuroblastoma derived $BAC^{Nrf2\text{-}Venus}$ cells. However, it remains unclear whether newly translated Nrf2 is subjected to Keap1 assisted degradation in the cytoplasm directly after translation; or if nascent Nrf2 proteins are allowed to freely enter the nucleus and are then degraded, either within the nucleus, or following subsequent export into the cytoplasm. As such, further analysis of the mechanism underlying this phenotype is required, in order to facilitate the development of rational strategies to therapeutically manipulate these processes, under different conditions or disease states. These issues are addressed further in Results Chapter 3.

In the proposed model for sequential p65-driven changes in nuclear Nrf2 levels, we propose the periodic increases in nuclear Nrf2 levels are driven by p65, enhanced levels of Nrf2 transcription. However, the down phase of each period is less easily explained. The sequential periodic pattern of nuclear Nrf2 expression is most clearly seen when cells are stimulated with activators of NF-κB signalling in the presence of SFN or CDDO-Me. The transcriptional increase of Nrf2 combined with Keap-1 mediated degradation was expected to lead to a stable increase of Nrf2 levels over time. However, from our data it would appear that this trend does not operate under conditions of co-stimulation, suggesting that the primary mechanism of Nrf2 degradation occurring during the 'down-phase' of p65 driven Nrf2 nuclear fluctuations, is likely to be Keap1 independent.

An alternative mechanism of Nrf2 degradation has been reported which involves the GSK-3/β-TrCP axis, which primarily acts in the nucleus. In this case, GSK-3α/β targets Nrf2 for phosphorylation, which then acts as a signal for β-TrCP-mediated ubiquitination and target degradation (Cuadrado, 2015).
To explore the role of GSK-3-mediated Nrf2 regulation in $BAC^{Venus\text{-}Nrf2}$ cells, the effect of the GSK-3 inhibitor CHIR99021 (which effects both α and β isoforms of GSK-3) was investigated, in both low and high serum conditions (Figure 4.10A). As high-serum concentrations favour activation of PI3K, which is a potent GSK-3 inhibitor, GSK-3 activity has been shown to be higher in low-serum media (Lee &

Kim, 2007). In this study, reduction of FBS to 2% modestly enhanced the Nrf2-Venus accumulation in response to 10μM CHIR99021. However, the difference between 2% and 10% serum containing media was very small. Additionally, sequential treatment of $BAC^{Nrf2\text{-}Venus}$ cells with CHIR99021 for 30min, followed by 10ng/ml TNFα did not significantly increased TNFα imposed Nrf2-Venus nuclear accumulation (Figure 10B & C). Therefore, under these conditions it did not appear that GSK-3 was playing a significant role in regulating Nrf2 levels following TNFα stimulation.

There is also evidence in the literature that GSK-3 regulates the NF-κB pathway, although the net outcome of GSK-3 activity on inflammation is difficult to predict, as it is dependant on multiple combinatorial factors. In our studies, inhibition of GSK-3α/β before TNFα stimulation, led to a slight reduction in the timing of the initial peak of p65-dsRedXP/tagRFP-p65 nuclear accumulation, and a small increase in ARE-Luc reporter activity (Figure 4.10). In combination with TNFα, CHIR99021 did not led to significant changes in Nrf2 activity (Figure 4.10E). Equally, CHIR99021 did not increase basal or TNFα-induced expression of the Nrf2 target genes GCLC and NQO1 (Figure 10 F & G). Therefore, in the context of our model $BAC^{Nrf2\text{-}Venus}$ cells, GSK-3 appears to play a negligible role in controlling Nrf2 activity under basal or inflammatory conditions.

Prolonged acute inflammation has been associated with inhibition of the antioxidant pathway (Correa *et al,* 2012). Previous research on primary astrocytes has shown that 24hr treatment with TNFα increased Nrf2 mRNA levels and the expression of antioxidant Nrf2 target genes (Correa *et al,* 2012). In contrast, Nrf2 activity was significantly reduced following 48hr exposure to TNFα. Interestingly, this effect was then reversed by inhibition of either the p38 MAPK or GSK-3α/β kinases. Therefore the chronic inflammation underlying many diseases could potentially interfere with effective physiological and pharmacological Nrf2 activation.

To test whether long exposure to inflammatory cytokines reduced the potency of antioxidant activation, ARE-Luc expression was measured in $BAC^{Nrf2\text{-}Venus}$ neuroblastoma cells that had been pre-incubated for 64h with 10ng/ml TNFα with 2μM SFN being added for the final 8h of the experiment (Figure 4.11A). Interestingly, we found that ARE-Luc expression was reduced following prolonged

cytokine exposure, also addition of 2μM SFN did not significantly increase Nrf2 transcriptional activity (Figure 4.11A). However, further investigation by live cell imaging of BAC$^{Nrf2\text{-}Venus}$ showed that Nrf2 protein levels were induced equally well in response to SFN either with or without 64hrs exposure to TNFα (Figure 4.11B & C). Measurements of Nrf2 target gene expression, following prolonged inflammatory stimulation displayed pleiotropic effects (Figure 4.11 D-F). However this approach was sub-optimal as the half-life of TNFα in media is limited and there is an increased possibility of non-NF-κB mediated effects following prolonged cytokine application (Paszek *et al*, 2010). Therefore, it would be more appropriate to study a relevant disease model where pathogenesis is correlated with chronic inflammation. The cellular changes that occur during chronic inflammation are complex and still not well defined. Also, they may differ in the magnitude and signaling pathways involved between tissue specific microenvironments.

To summarise this data, there is conflicting evidence that long TNFα exposure has an inhibitory effect on Nrf2 transcriptional activity in the BAC$^{Nrf2\text{-}Venus}$ neuroblastoma cell line and requires more investigation.

Numerous studies have shown that Nrf2 activating compounds, such as curcumin, SFN and tBHQ inhibit NF-κB-mediated expression of inflammatory genes (Hayes & Dinkova-Kostova, 2014). This outcome is believed to be mediated by HO-1 expression, and an enhanced cellular redox status, which effectively inhibits NF-κB nuclear translocation (Lu *et al,* 2012). Evidence from this study suggests, that TNFα mediated induction of NF-κB response genes was significantly reduced when SFN was applied in parallel (Figure 4.12). This indicates that activation of both pathways at the same time may favour Nrf2 mediated responses, as joint TNFα and SFN application enhances both Nrf2 transcriptional activity and levels of Nrf2 expression (Figure 4.6). Interestingly, robust Nrf2 activation could also inhibit its own cytokine-mediated transcription (Figure 4.12E) as combined SFN/TNFα treatment reduced Nrf2 mRNA levels, in comparison to TNFα stimulation alone.

Therefore as Nrf2 activating compounds such as SFN are though to act predominantly on Keap1, it could function as an important regulator of balance between the conditional dominance of NF-κB or Nrf2 responses, as it limits the level

of Nrf2 protein available thereby ensuring levels do not reach levels at which NF-κB are inhibited, thus allowing an effective on-going response to inflammatory stress.
This hypothesis was confirmed by study of the effect of high expression model of Nrf2 protein by the (CMV driven) Venus-Nrf2 construct in SK-N-AS cells (Figure 4.13). The cells expressing the Venus-Nrf2 plasmid displayed reduction of p65-dsRedXP nuclear accumulation in response to TNFα stimulation combined with the significant inhibition of the oscillatory shuttling behaviour (Figure 13A, B & E). This experiment demonstrated that high antioxidant activity acts to limit the NF-κB inflammatory responses by modulating its spatio-temporal behaviour.
The data presented above highlights the importance of stringent Nrf2 regulation, since shifting the cellular redox balance may prevent effective inflammatory stimuli. NF-κB activity plays a vital role in anti-apoptotic signalling. It has been reported that high Nrf2 activity can trigger cell death however this phenomenon has not been studied in this investigation. Moreover, the CMV-Venus-Nrf2 plasmid does not contain an endogenous Nrf2 promoter sequence, or any other endogenous *NRF2* derived gene regulatory elements. Therefore, the fact that TNFα did not increase nuclear levels of plasmid expressed Nrf2-Venus further supports the proposed transcriptional role of NF-κB in regulating the antioxidant master regulator by driving increased transcriptional activity (Figure 4.13D).

To conclude, data presented in this chapter describe a novel pattern of sequential crosstalk between the Nrf2 and NF-κB pathways, in which inflammatory stress leads to a short sequential p65 mediated increase of Nrf2 transcription, leading to higher levels of Nrf2 protein, which is continually cleared away in the cytoplasm by Keap1-dependent degradation. This stringent regulation ensures limited Nrf2 activation, allowing the NF-κB activity to continue, while providing enough antioxidant input to dampen the effect of inflammation.
The results from this study provide new insight into the understanding of how inflammation modulates the antioxidant pathway activity and it is anticipated that it will contribute to design improved pharmacological interventions. The functional model summarising the data obtained in this chapter is presented in Figure 4.14 below.

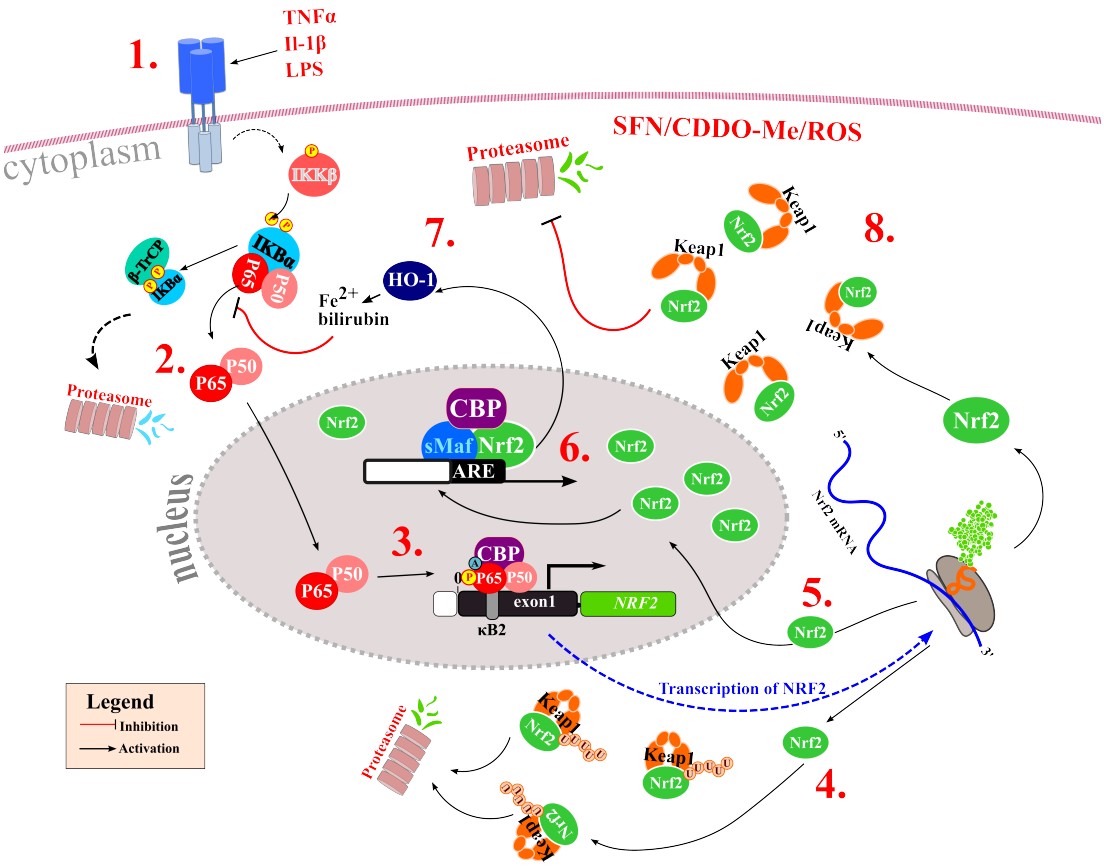

Figure 4.14 Nrf2 regulation during acute inflammatory stress. Diagram summarising the experimental findings from Results Chapter 2. **1**. Acute inflammatory signal such as TNFα triggers cascade of events, which lead to **2**. nuclear accumulation of p65. **3**. p65 binds to the κB consensus sequence within NRF2 promoter and initiates transcription. **4**. Newly synthesises Nrf2 is subjected to Keap1-mediated degradation or nuclear accumulation **5**., which leads to expression of Nrf2 target genes **6**. such as HO-1. **7**. High Nrf2 activity inhibits NF-κB function dampens inflammatory target gene expression. **8**. TNFα leads to potentiated accumulation of Nrf2 protein levels stabilised by application of CDDO-Me or SFN compounds.

Having established to physiological relevance and utility of these protein expression systems it was possible to initiate a detailed series of experiments to investigate the changes in Nrf2 nuclear levels in response to inflammatory signalling, which are presented in the following chapters.

RESULTS CHAPTER 3

5. Single-Cell Analysis of Nrf2 Dynamic Regulation in a Neuroblastoma Cell Model

5.1. CHAPTER 3 AIMS

- **Detailed characterisation of Nrf2 regulation at a single-cell level**
- **Assessment of the contribution of Keap1 and GSK-3 regulation in basal and induced antioxidant gene expression**
- **Direct measurements of nuclear import and export rates of Nrf2 to determine Nrf2 life-cycle**
- **Assessment of alternative Nrf2 post-translational regulation by acetylation**

5.2. Introduction

In order to respond effectively to changes in local environmental conditions, individual cells must maintain non-cytotoxic basal levels of Nrf2 activity. Interplay of cellular signalling cascades and redox status ensures basal regulation of antioxidant activity while allowing for rapid activation in the event of stress.
Several proteins have been identified as critical players in regulating Nrf2 protein stability, with Keap1 and GSK-3 being the most studied examples, however the conditional nature or redundancy of these two regulatory processes remains unclear. To design more effective therapeutic strategies for modulating antioxidant signalling and drug resistance, it is essential to understand the intricate dynamic control of Nrf2 in living cells. As analysis of dynamic changes in single cells can reveal insights into the molecular mechanisms that are masked by intracellular heterogeneity, when dynamic signalling responses are studied using population level techniques.

Work presented in this Chapter represents an extensive examination of conditional Nrf2 signalling responses, using both single-cell and population level techniques. Firstly, the extent of negative regulation of antioxidant responses by the cooperative

action of both Keap1 and GSK-3 is examined. Also, we present novel data relating to Nrf2 nuclear import/export dynamics obtained by using the photo-switchable pDendra2-Nrf2 fluorescent fusion. Lastly this investigation touches on the effect of Nrf2 accumulation in PML-NB nuclear structures, and the role of acetylation in modulating the antioxidant responses.

The data presented below provides new evidence of dynamic Nrf2 regulation by multiple signalling cascades at single cell resolution, which act in concert to ensure stringent control the cellular antioxidant activity.

5.3. RESULTS

5.3.1. Analysis of Single-Cell Keap1 Dependent Nrf2 Regulation

The FCCS measurements of mCherry-Keap1 and Nrf2-Venus protein diffusion in $BAC^{Nrf2\text{-}Venus}$ neuroblastoma cells provided strong evidence that the Nrf2-Venus and mCherry-Keap1 fluorescent fusions form stable complexes in the cytoplasm (Chapter 1, Figure 3.18).

ARE-Luc dual luciferase assays were performed to investigate how modulation of Keap1 expression levels impacts on Nrf2 transcriptional activity (Figure 5.1A) (Methods 2.4.6). The transient expression of the mCherry-Keap1 plasmid in $BAC^{Nrf2\text{-}Venus}$ cells reduced the basal ARE-luc activity by over 75%. Therefore, increased Keap1 protein levels were sufficient to inhibit basal Nrf2 transcriptional activity. Furthermore, live cell imaging experiments using $BAC^{Nrf2\text{-}Venus}$ cells, demonstrated that transient transfection with the mCherry-Keap1 construct led to the depletion of Nrf2-Venus fluorescence in Keap1 expressing cells (Figure 5.1B). However, the efficiency of Keap1-mediated Nrf2 clearance decreased when SK-N-AS cells were co-transfected with plasmid encoded Venus-Nrf2 (Figure 5.1C), as Venus-Nrf2 was retained in the cytoplasm. Therefore, although enhanced levels of plasmid encoded Keap1 were able to prevent nuclear entry of Venus-Nrf2, this interaction did not result in effective Nrf2 degradation (Figure 5.1C). Next, the effect of siRNA mediated Keap1 depletion on Nrf2 protein levels and localisation was measured in $BAC^{Nrf2\text{-}Venus}$ cells (Figure 5.1D). Reduction of Keap1

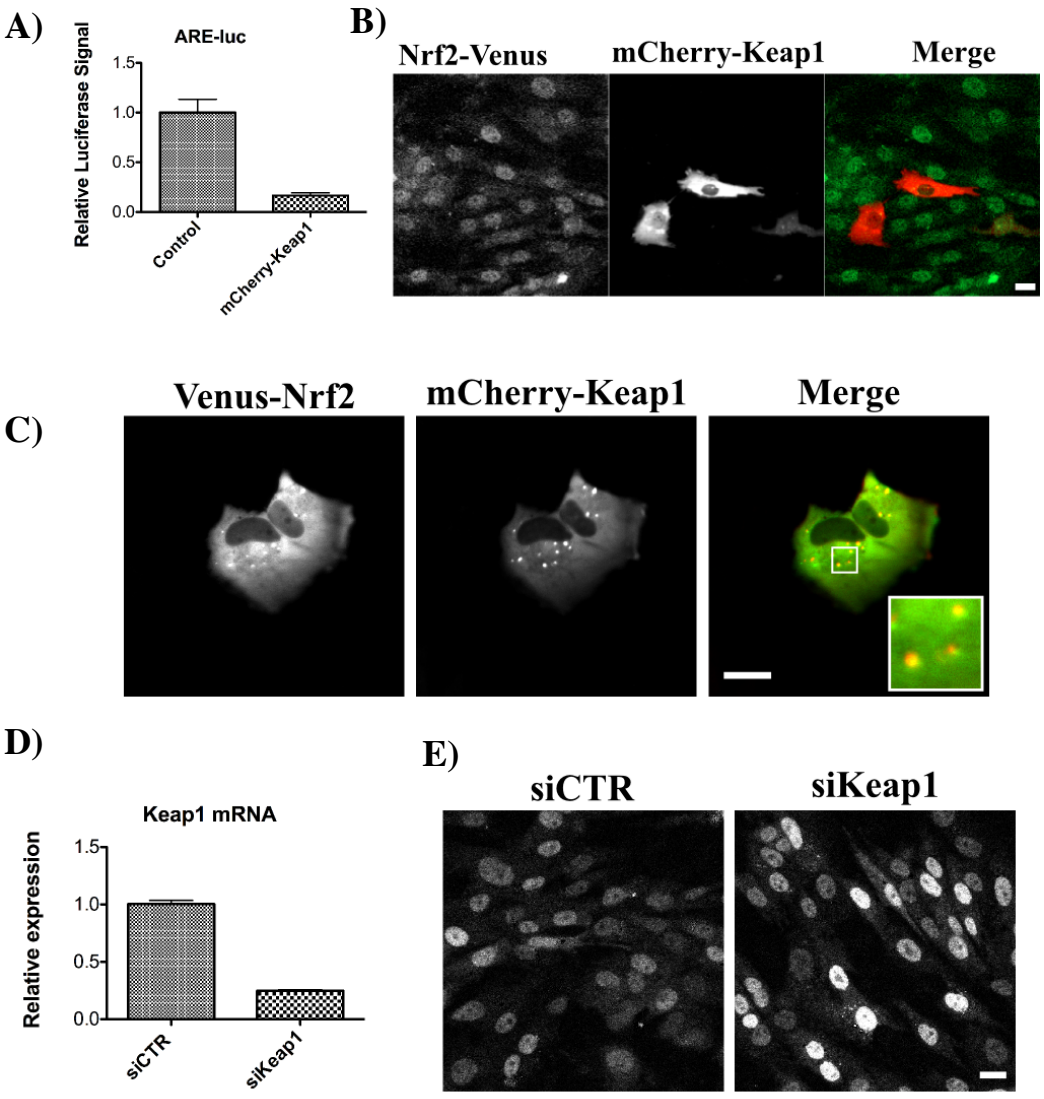

Figure 5.1 Keap1 regulates Nrf2 protein levels and activity. A) ARE-Luc reporter activity is reduced in cells transiently transfected with the mCherry-Keap1 plasmid (n=1, in triplicates). B) Representative confocal images of BAC$^{Nrf2\text{-}Venus}$ cells expressing mCherry-Keap1, showing lower Nrf2-Venus plasmid levels in transfected cells. C) Cells transiently expressing Venus-Nrf2 and mCherry-Keap1 plasmids exhibit co-localisation in SK-N-AS cells. D) Relative levels of Keap1 mRNA following 48hr knockdown with Keap1-siRNA or a control siRNA (siCTR) (n=1, in triplicates). E) BAC $^{Nrf2\text{-}Venus}$ cells show enhanced levels of nuclear Nrf2-Venus following treatment with Keap1-siRNA. Error bars=STDEV, scale bar=20μm.

mRNA by approximately 75% led to high levels of nuclear Nrf2-Venus (Figure 5.1E).

Therefore, fine-tuning of Keap1 levels ensure robust control of Nrf2 under basal cellular conditions in the SK-N-AS neuroblastoma cell model.

5.3.2. The Effect of Keap1 Overexpression on Nrf2 Localisation in Response to CDDO-Me

To understand the impact of high cellular levels of Keap1 on Nrf2-Venus dynamic responses to CDDO-Me, single-cell analysis was performed using live-cell imaging of $BAC^{Nrf2\text{-}Venus}$ following addition of 100nM CDDO-Me (Figure 5.2). The representative time-lapse images from this experiment show that Nrf2-Venus cytoplasmic accumulation is confined to cells expressing the mCherry-Keap1 plasmid (Figure 5.2A, Movie 24). In contrast, non-transfected cells, nuclear accumulation of Nrf2 was more pronounced in non-transfected cells (Figure 5.2A). Comparison of cytoplasmic and nuclear levels of Nrf2-Venus in mCherry-Keap1 transfected cells show that CDDO-Me induced accumulation of Nrf2 was more pronounced in the cytoplasmic fraction (Figure 5.2B). Measurements of relative nuclear:cytoplasmic Nrf2-Venus fluorescence provided clear evidence that cytoplasmic Nrf2 levels were far higher in cells expressing high levels of Keap1, as a result of the CDDO-Me treatment (Figure 5.2C). Therefore the mCherry-Keap1 expression greatly impeded nuclear shuttling of Nrf2-Venus in response to the CDDO-Me.

To investigate the stability of nuclear Nrf2-Venus, the nuclear export inhibitor Leptomycin B (LMB) was added in combination with the CDDO-Me.

Real-time imaging of the $BAC^{Nrf2Venus}$ cells expressing the mCherry-Keap1 show that inhibition of nuclear export with 10ng/ml LMB led to a more equal accumulation of Nrf2-Venus in the cytoplasm and nucleus in response to 100nM CDDO-Me (Figure 5.3A, Movie 25). This was trend was confirmed by quantitative analysis of nuclear and cytoplasmic levels of Nrf2-Venus (Figure 5.3B). Comparison of the nuclear:cytoplasmic ratio of Nrf2-Venus between CDDO-Me alone, or joint CDDO-Me and LMB treatments, clearly show that Nrf2-Venus nuclear accumulation was enhanced as a result of inhibiting nuclear export (Figure 5.3C). Moreover, LMB

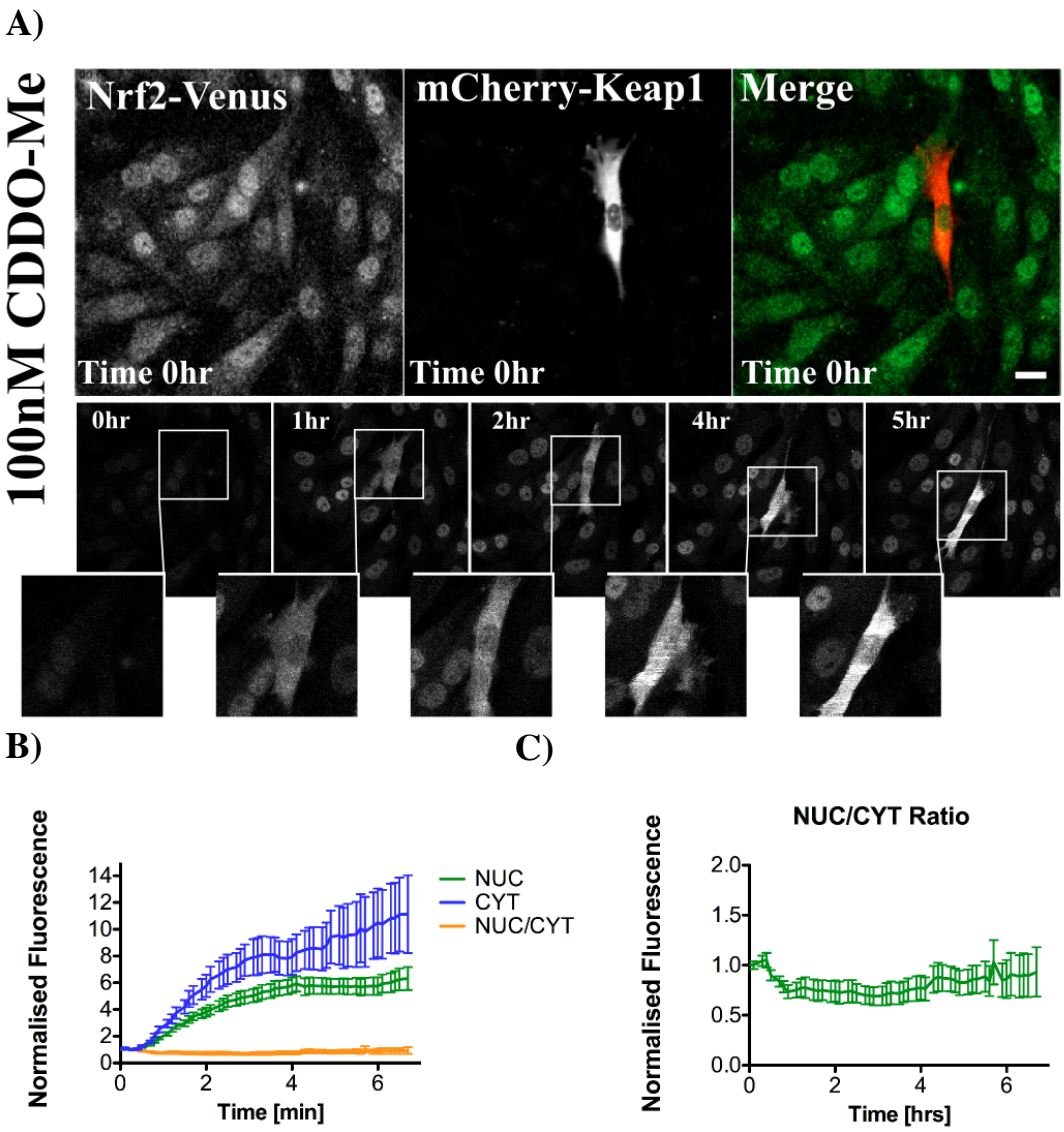

Figure 5.2 Keap1 controls cytoplasmic Nrf2-Venus levels. A) Representative time-lapse images of BAC$^{Nrf2\text{-}Venus}$ cells expressing mCherry-Keap1 in response to 100nM CDDO-Me (Movie 24). B) Nrf2-Venus accumulates more rapidly in the cytoplasm than the nucleus of mCherry-Keap1 expressing cells in response to 100nM CDDO-Me (n=5, c=19). C) Temporal profile of nuclear to cytoplasmic ratios of Nrf2-Venus in mCherry-Keap1 transfected cells following addition of 100nM CDDO-Me. Error bars=SEM. Scale bar=20μm.

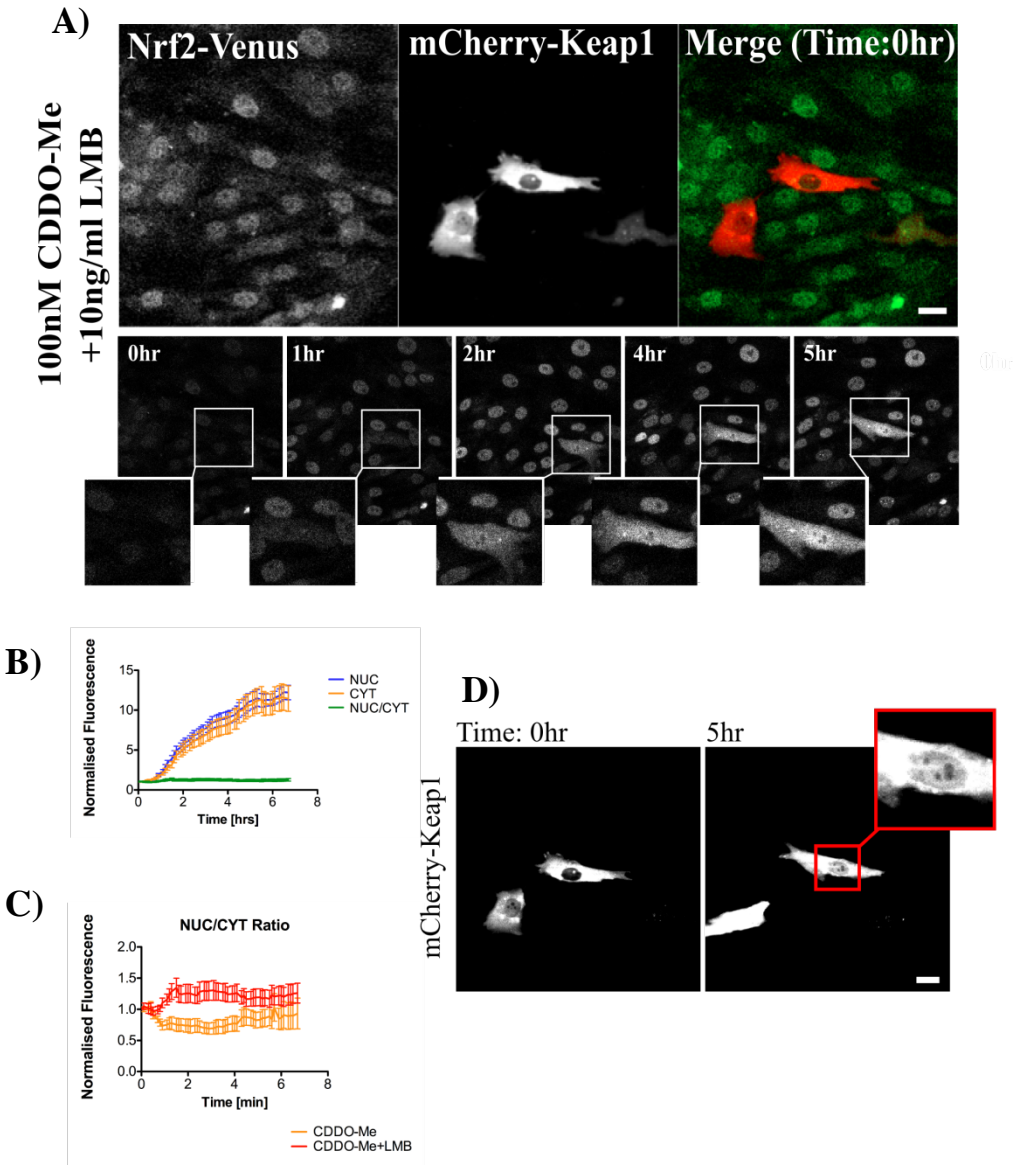

Figure 5.3 Inhibition of nuclear export enhances Nrf2-Venus accumulation in mCherry-Keap1 expressing cells following addition of CDDO-Me. A) Representative confocal images of BAC$^{Nrf2\text{-}Venus}$ neuroblastoma cells transfected with mCherry-Keap1 plasmid treated with 100nM CDDO-Me and 10ng/ml LMB (Movie 25). B) Measurements of Nrf2-Venus fluorescence in the cytoplasm and nucleus of BAC$^{Nrf2\text{-}Venus}$ cells expressing mCherry-Keap1 (n=4, c=12). C) Nuclear to cytoplasmic ratio of Nrf2-Venus fluorescence over time in cells transfected with mCherry-Keap1 following addition of 100nM CDDO-Me and 10ng/ml LMB. D) mCherry-Keap1 shows nuclear accumulation following combined treatment with 100nM CDDO-Me and 10ng/ml LMB. Error bars=SEM. Scale bar=20μm.

application also led to a significant accumulation of mCherry-Keap1 in the nuclear compartment in $BAC^{Nrf2\text{-}Venus}$ cells, following 5hr treatment with 100nM CDDO-Me and 10nM LMB as shown in Figure 5.3D. Therefore, LMB had an effect on the subcellular distribution of both proteins, suggesting that both Nrf2 and Keap1 undergo dynamic shuttling in and out of the nucleus.

5.3.3. Quantitative Live Cell Analysis of Nrf2 Nuclear Import and Export Dynamics

Currently, there is limited information about the dynamics of basal or induced Nrf2 nuclear import. The temporal stability of Nrf2 once it enters the nuclear space is also unclear. To address these points, and to clarify the role of Keap1 as a dynamic regulator of nuclear import we have utilised a sophisticated fluorescence live cell imaging approach, to measure Nrf2 nuclear import and export dynamics using the photoswitchable pDendra2 flourophore. A pDendra2-Nrf2 fusion protein was created using Gateway cloning approach (Methods 2.13.2) and the plasmid was transiently expressed in SK-N-AS neuroblastoma cells. The great benefit of using pDendra2 is that it enables quantitative real-time tracking of two distinct Nrf2 protein subpopulations. The pDendra2-Nrf2 protein is expressed as a green fluorescent fusion, however the pDendra2 fluorophore can be irreversibly photoshifted to emit light at a red fluorescence wavelength, as a result of brief irradiation with blue laser light, such as the 405nm laser or UV diode lamp (Chudakov *et al,* 2007). Therefore, following the UV-induced change in colour the decay in red fluorescence (old protein) can be imaged in real time alongside the synthesis of new green protein.

To investigate the dynamics of Nrf2 nuclear entry the pDendra2-Nrf2 was locally irradiated in the cytoplasm (ROI1) and the resulting changes in red pDendra2-Nrf2 fluorescence were measured in the nucleus (ROI2), Figure 5.4A depicts the experimental procedure employed. The representative cell shown in Figure 4B (Movie 26) demonstrates the effect of cytoplasmic UV irradiation in SK-N-AS neuroblastoma cells expressing the pDendra2-Nrf2 fusion. The green fluorescence is rapidly switched to red fluorescence following local irradiation with UV 405nm laser for 20 iterations (Methods 2.13.2). As a result, it is possible to observe the rate of red pDendra2-Nrf2 accumulation in the nucleus over time (>6min). The measurements

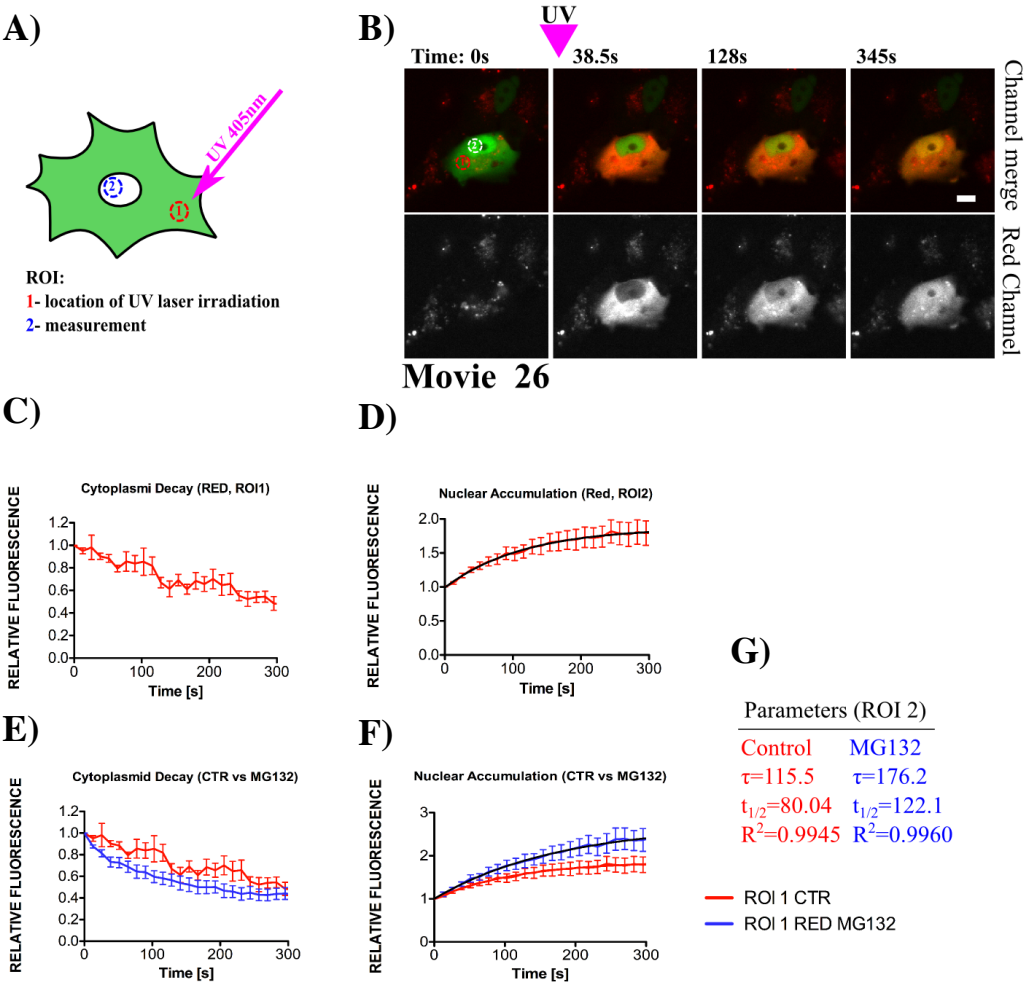

Figure 5.4 Measuring Nrf2 nuclear import dynamics in SK-N-AS cells using a photoswitchable pDendra2-Nrf2 fusion protein. A) Schematic representation of local pDendra2-Nrf2 photoconversion using the 405nm UV laser. The initial green fluorescence of pDendra2-Nrf2 was shifted to red emission by local irradiation with the 405nm laser. B) Representative time-lapse pictures, before and after UV irradiation in the cytoplasm (ROI1), showing a subsequent gradual accumulation of photoswitched red pDendra2-Nrf2 in the nucleus (ROI2) (Movie 26). C) Temporal changes in cytoplasmic photoconverted pDendra2-Nrf2. D) Corresponding rate of red nuclear pDendra2-Nrf2 accumulation (n=3, c=14). E) Treatment of cells with 10μM MG132 causes a slight increase in the rate of red pDendra2-Nrf2 cytoplasmic decay, which correlates with a higher rate of increase in nuclear accumulation of photoconverted red Dendra2-Nrf2 (n=3, c=11) (F). G) Parameters used to calculate nuclear dynamics, which were calculated by plotting changes in nuclear import and fitting the data to a non-linear regression, one phase association equation, where $t_{1/2}$ is the time required to reach half of the maximum measured fluorescence and τ represents the time constant [s]. Error bars=SEM, scale bar=10μm.

of ROI1 (cytoplasm) red fluorescence levels, exhibited a steady decay (Figure 5.4C), as the red florescence of the photoconverted pDendra2-Nrf2 accumulated in the nucleus (ROI2) (Figure 5.4D).

To measure the relative effect of proteasome mediated degradation on both populations of pDendra2-Nrf2, an equivalent experiment was performed in cells imaged in the presence of 10μM MG132. Inhibition of proteasome activity did not enhance cytoplasmic levels of photo-switched (red) pDendra2-Nrf2 (Figure 5.4E) in comparison to control (mock treated) cells. However, MG132 treatment prompted a slight increase of red pDendra2-Nrf2 in the nucleus (ROI2), in comparison to control cells (Figure 5.4F).

Quantitative data from pDendra2 imaging experiments was obtained by measuring the increase in nuclear red signal and fitting the data by non-linear regression analysis with a one-phase association equation using GraphPad Prizm (Methods 2.13.3). Measurements of red pDendra2-Nrf2 accumulation in the nucleus are plotted in Figure 5.4G. In this analysis, the half-time of nuclear fluorescence increase describes the relative dynamics of protein accumulation. The comparison between control and MG132 treated cell populations show that control cells exhibited a faster rate of Nrf2 nuclear import as evident from the nuclear accumulation rates τ (control τ=115.5s vs MG132 τ=176.2s) (Figure 5.4G).

To investigate the impact of Keap1 overexpression on the rate of Nrf2 nuclear import, pDendra2-Nrf2 was co-transfected with a plasmid encoding a tagBFP-Keap1 fluorescent fusion protein (Figure 5.5). The selection of a blue fluorescent label for Keap1 allowed simultaneous imaging of green and red pDendra2-Nrf2 fluorescence, while also being able to select cells expressing high levels of Keap1. The expression of tagBFP-Keap1 led to a rapid degradation of pDendra2-Nrf2, prior to photoshifting, therefore, to image the Nrf2 fusion it was necessary to perform the following experiment in the presence of 10μM MG132. Expression of tagBFP-Keap1 in combination with proteasomal inhibition led to enhanced cytoplasmic localisation of pDendra2-Nrf2 fusion (Figure 5.5A). As in previous experiments, cytoplasmic pDedra2-Nrf2 was subjected to brief, local-irradiation with the 405nm laser and dynamic changes in red fluorescent signal were measured in both the cytoplasm (ROI1) and nucleus (ROI2) (Figure 5.5, Movie 27). It was evident that

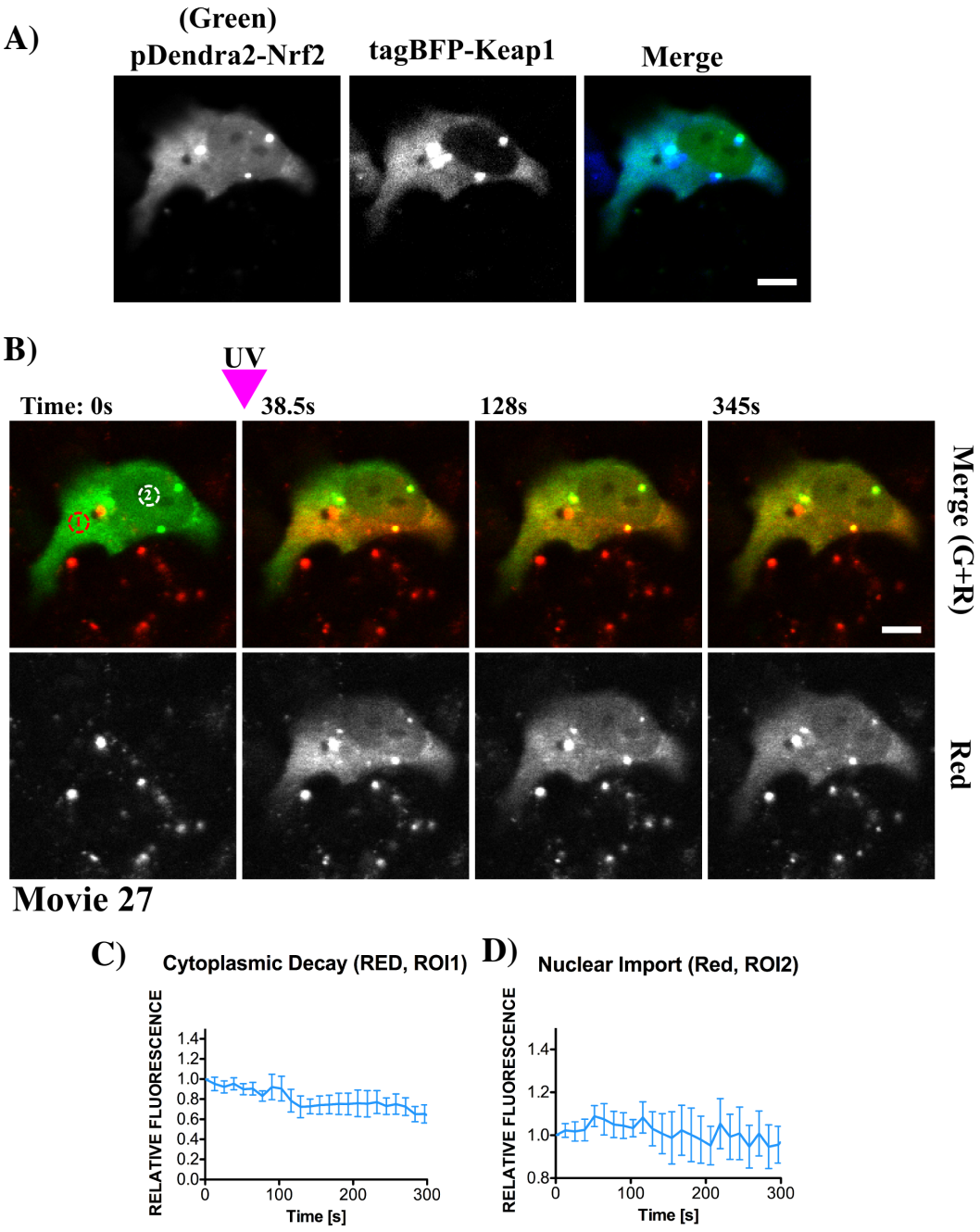

Figure 5.5 Keap1 blocks Nrf2 nuclear import even following inhibition of proteasomal degradation. A) Representative image of a cotransfected cell showing strong colocalisation of tagBFP-Keap1 and pDendra2-Nrf2 following addition of 10μM MG132 (Movie 27). B) Representative time-lapse images from the same experiment showing unchanged nuclear levels of photoconverted Nrf2. C) Measurement of the redistribution of red Dendra2-Nrf signal in the photoactivated region (ROI1) over time (n=2, c=14). D) Nuclear accumulation (ROI2) of photoactivated red Dendra2-Nrf2 originated from the cytoplasm in tagBFP-Keap1 expressing cells. Error bars=SEM, scale bar=10μM

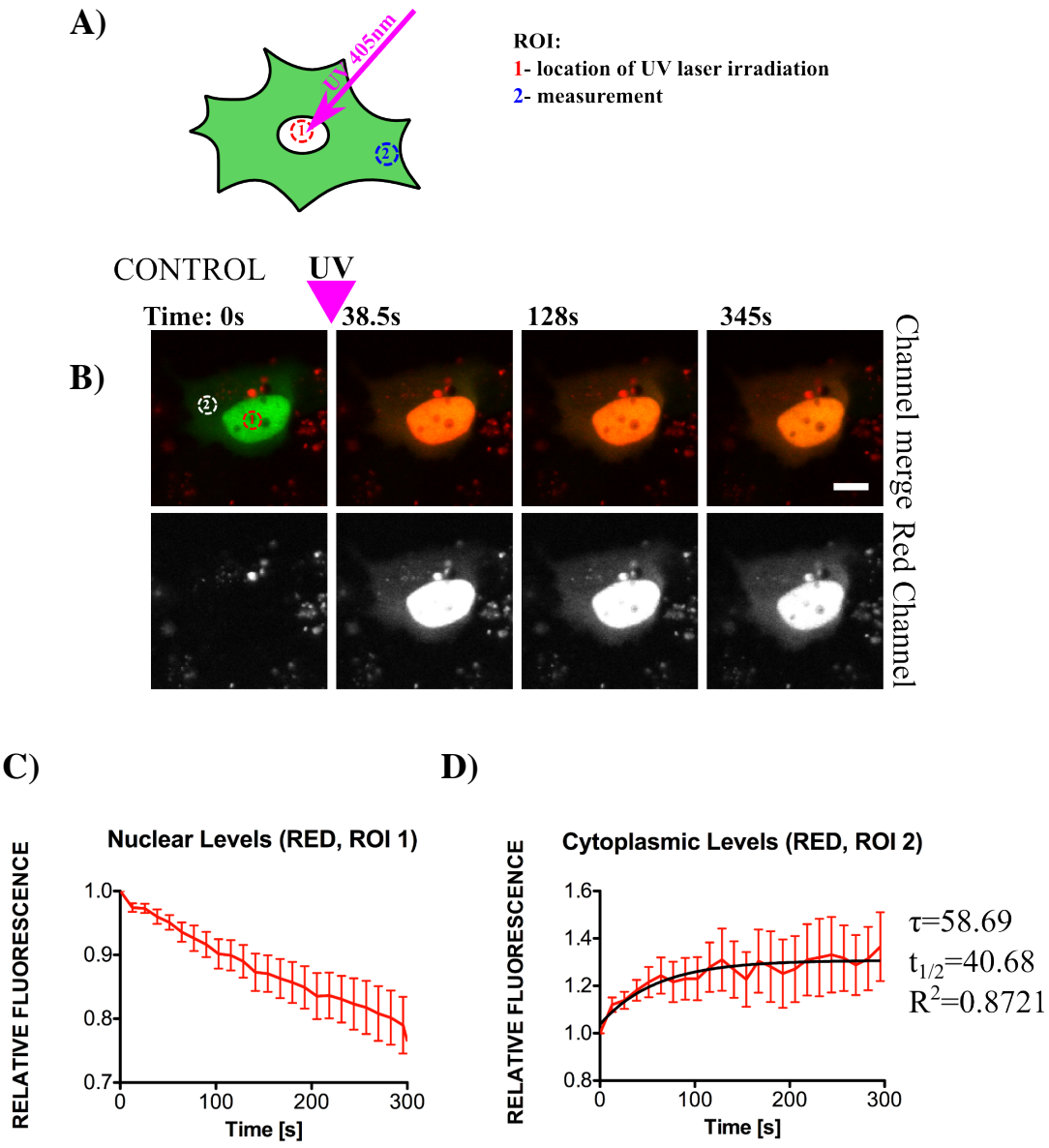

Figure 5.6 Use of Dendra2-Nrf2 to define the nuclear exported rate of Nrf2. A) Schematic representation of local nuclear pDendra2-Nrf2 photoconversion. Green pDendra2-Nrf2 is shifted to red fluorescence by brief irradiation with 405nm laser in the nucleus in (ROI1), and its accumulation in the cytoplasm is measured in the cytoplasmic in (ROI2). B) Representative time-lapse images from before and after local UV irradiation in the nucleus (ROI1) (Movie 28). C) Stable decline of photoconverted red pDendra2-Nrf2 in nuclear ROI1 of control cells. D) Measurements of cytoplasmic red Dendra2-Nrf2 show half maximal fluorescence increase at around 41s in the cytoplasmic space (n=2, c=11). Error bars=SEM, scale bar=10μm.

expression of tagBFP-Keap1 effectively prevented nuclear translocation of the photo-converted pDendra2-Nrf2 as displayed by the measurements of nuclear red Nrf2 fluorescence (Figure 5.5C), as shown in the representative images of cell from the experiment (Figure 5.5B). Therefore, in this study, high levels of Keap1 effectively prevented Nrf2 nuclear accumulation even in the presence of proteasome inhibitors.

Next, the rate of nuclear export of pDendra2-Nrf2 was investigated using a slightly modified experimental approach. To measure the accumulation of pDendra2-Nrf2 in the cytoplasmic space, SK-N-AS cells transfected with the pDendra2-Nrf2 construct were targeted by local UV irradiation in the nucleus (Figure 5.6A). This allowed the cytoplasmic influx of photoconverted pDendra2-Nrf2 from the nucleus to be measured (Figure 5.6B, Movie 28). The red fluorescent signal was quickly depleting in the nucleus (ROI1) (Figure 5.6C) and consequently the levels of photoconverted Nrf2 gradually increased in the cytoplasm, with a fluorescence half-time of ~40s (Figure 5.6D).

To measure the relative contribution of proteasomal activity and nuclear export on Nrf2 nuclear stability, SK-N-AS cells expressing the pDendra2-Nrf2 fusion were pre-treated with either DMSO, 10μM MG132 or 10ng/ml LMB for 1hr, prior to photoswitching and image acquisition (Figure 5.7, Movie 29). Representative image from this experiment (Figure 5.7A), together with measurements of cytoplasmic red fluorescence (Figure 5.7D), both strengthen the evidence that Nrf2 are exported from the nucleus when proteasome activity is inhibited. Also, blocking nuclear export with 10ng/ml LMB prevented the cytoplasmic increase of red pDendra2-Nrf2 (Figure 5.7B & D), and slightly decreased the rate of nuclear decay in comparison to MG132 treated cells (Figure 5.7C).

A summary of nuclear import measurements is presented in Figure 5.8. Comparison of nuclear import of the cytoplasmically photoconverted red pDendra2-Nrf2 was most increased in cells through stabilisation of Nrf2 protein through treatment with proteasome inhibitors, and no nuclear accumulation was observed in cells expressing the tagBFP-Keap1 (Figure 5.8B).

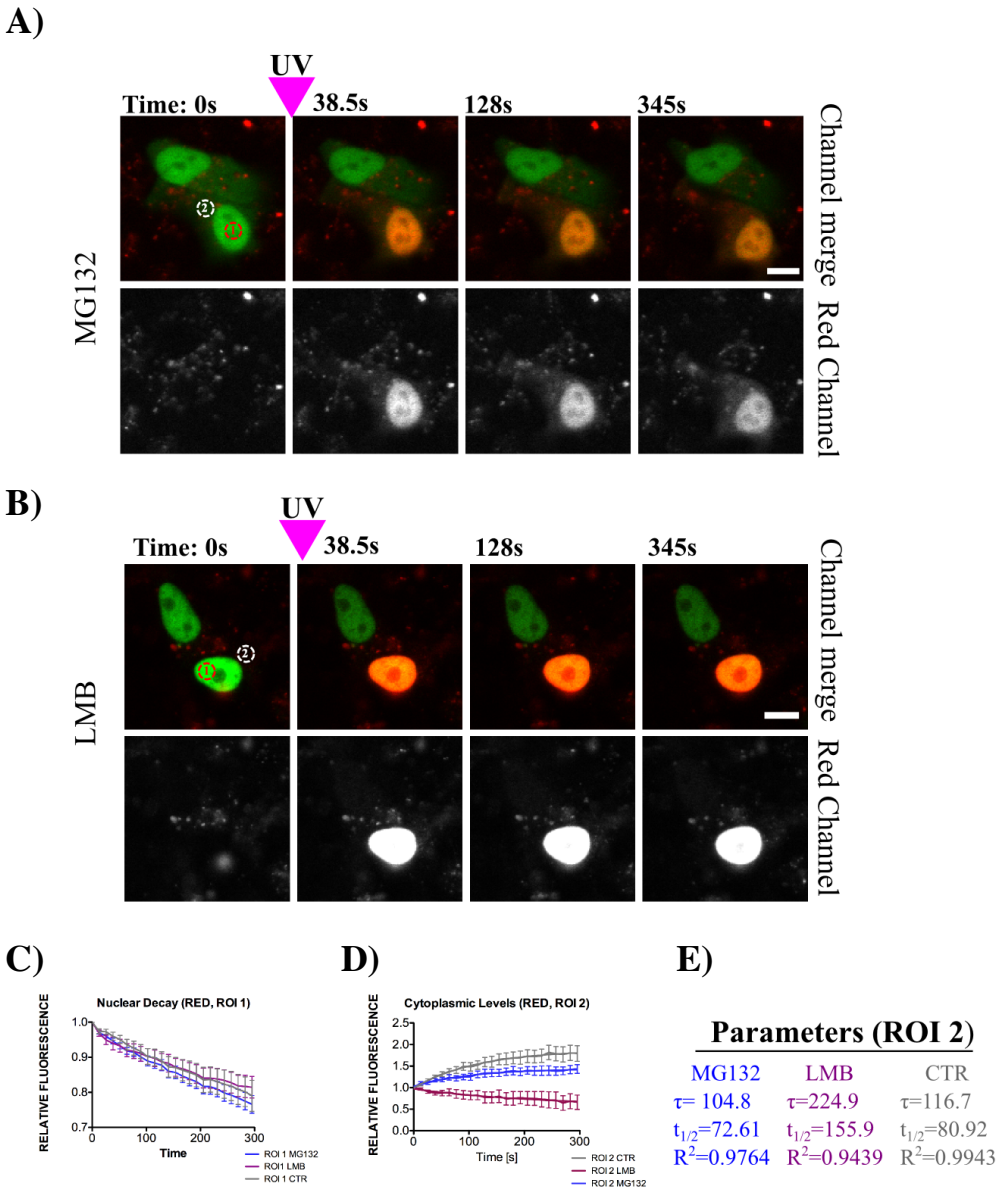

Figure 5.7 Leptomycin B blocks nuclear export of pDendra2-Nrf2. A) Representative images of 10μM MG132 treated SK-N-AS expressing pDendra-Nrf2 targeted by nuclear 405nm UV laser irradiation. Red fluorescence spreads gradually to the cellular space over time. B) 10ng/ml LMB treatment stops cytoplasmic accumulation of the red nuclear fluorescence of the photoconverted pDendra2-Nrf2 (Movie 29). C) Comparison of Nuclear and D) Cytoplasmic red fluorescent signal changes following DMSO (C=13), LMB (c=16) and MG132 treatment (c=19). LMB prevents cytoplasmic entry of the photoconverted pDendra2-Nrf2. E) Quantitative data obtained from cytoplasmic import of dynamics of pDendra2-Nrf2, fitted using non-linear regression, one-phase association function. The half-time of cytoplasmic red fluorescence increase in 10μM MG132 treated cells is equal to 72.61s. Error bars=SEM, scale bar=10μm.

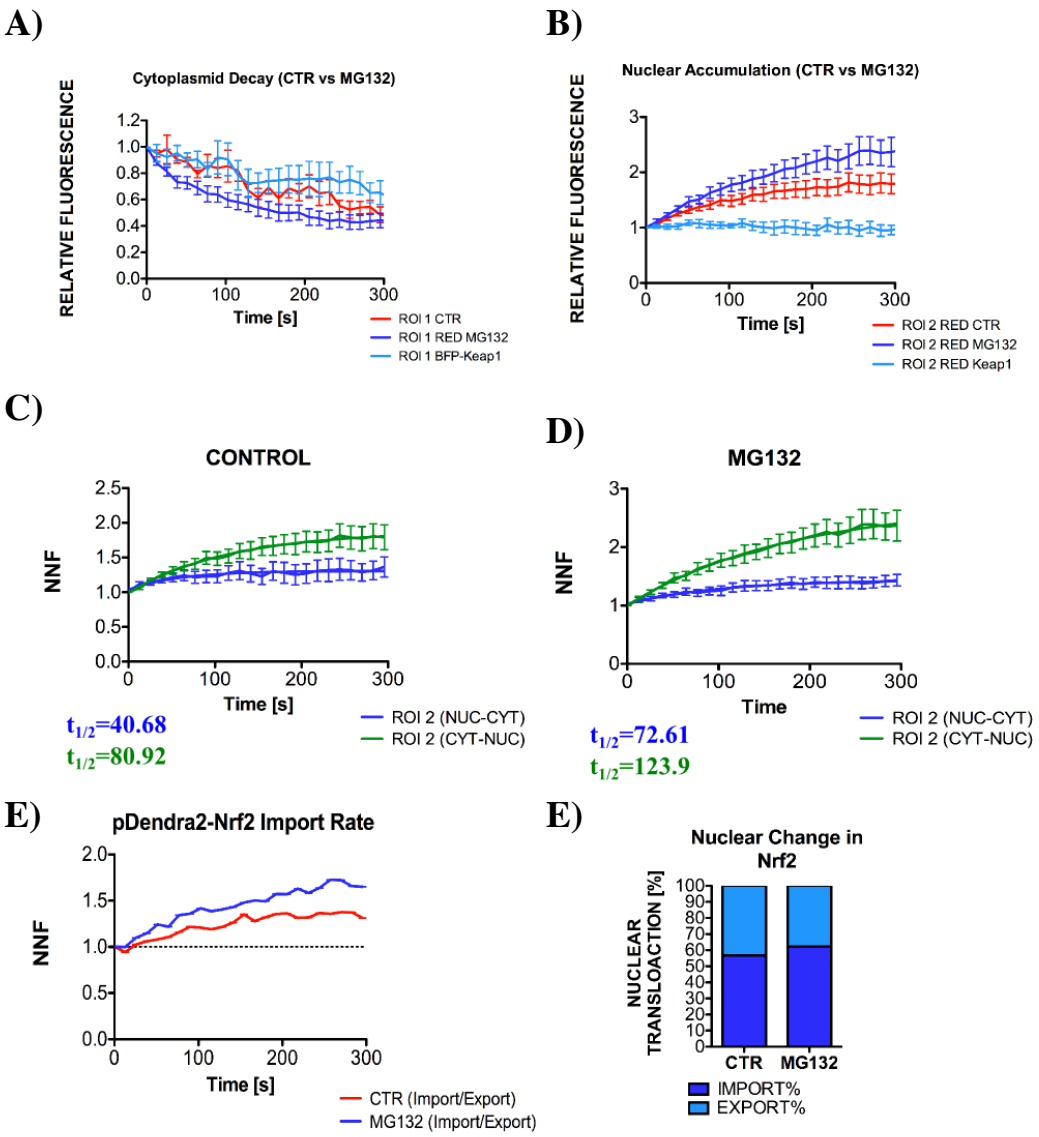

Figure 5.8 Live cell quantification of Nrf2 nuclear import and export dynamics. A) Comparison of Nrf2 cytoplasmic decay rates following local cytoplasmic photoconversion of Dendra2-Nrf2 in either control cells, cells treated with the proteasomal inhibitor MG132, or cells co-transfected with a plasmid expressing high levels of tagBFP-Keap1. B) Comparison of nuclear accumulation of photoconverted red pDendra2-Nrf2 in either control cells, cells treated with the proteosomal inhibitor MG132, or cells co-transfected with a plasmid expressing high levels of tagBFP-Keap1. C) Comparison of import and export dynamics in control cells or D) cells treated with 10μM MG132 are shown in (C&D) respectively. E) Relative balance between nuclear import and export of Dendra-Nrf2 in control or MG132 treated cells. F) Comparison of the relative levels of nuclear import and export in control cells or cells treated with 10μM MG132. Error bars=SEM.

Data presented in Figure 5.8C, E and D show a comparison of nuclear import and export dynamics in control and MG132 treated cells respectively. The calculated half-time values for increases in fluorescence were faster during nuclear export in both cases (NUC-CYT), even though the nuclear accumulation reached higher increase over time (Figure 5.8C & D). This suggests that the net ratio of protein entering the nucleus was higher overall than that which was being exported out or degraded (Figure 5.8E & F).

To investigate the impact of nuclear degradation of Nrf2 the pDendra2-Nrf2 construct was employed to measure the rate of decay of Nrf2 in the nuclear compartment, allowing defining the kinetics of the nuclear degradation in both control and LMB treated cells (Figure 5.9). For this purpose instead of locally photoconverting the green pDendra2-Nrf2 fluorescence using a 405nm laser, the UV lamp was used to irradiate the whole field of view turning all the cells in the imaging area into the photoshifted red version of pDendra2-Nrf2 (Methods 2.13.2). A schematic of this approach is shown in Figure 5.9A. Briefly, the selected cells of interest were imaged every 3min for ~3.5h. After establishing levels of baseline fluorescence, control or LMB (10ng/ml) treatment was performed and cells were then UV irradiated. Cells were effectively photoconverted from green to red fluorescence by irradiation for 1min with UV light (75% power). Representative images from the control experiment are presented in Figure 5.9B, showing effective photoconversion of the pDendra2-Nrf2 from green to red (Movie 30). Normalised measurements of nuclear red and green fluorescence are shown in Figure 9C (control) and Figure 5.9D (+10ng/ml LMB). Comparison of the level of green fluorescence detected in both experiments (Figure 5.9E) show a steady recovery over time, returning to basal levels approximately 1hr after UV irradiation. The observed decay in red signal, which could result from either degradation or photobleaching of the photoconverted pDendra2-Nrf2, followed the same dynamics in control and LMB treated cells (Figure 5.9F & G). The half-life of the pDendra2-Nrf2 can be calculated from the red fluorescence signal decay curve (Methods 2.13.2). The stability of pDendra2-Nrf2 was estimated to be around 38min in LMB treated cells and around 43min in the control cells (Figure 5.9G). Unexpectedly, inhibition of nuclear export did not significantly decrease the degradation rate of nuclear Nrf2 protein, suggesting Nrf2 degradation does not reply on nuclear export.

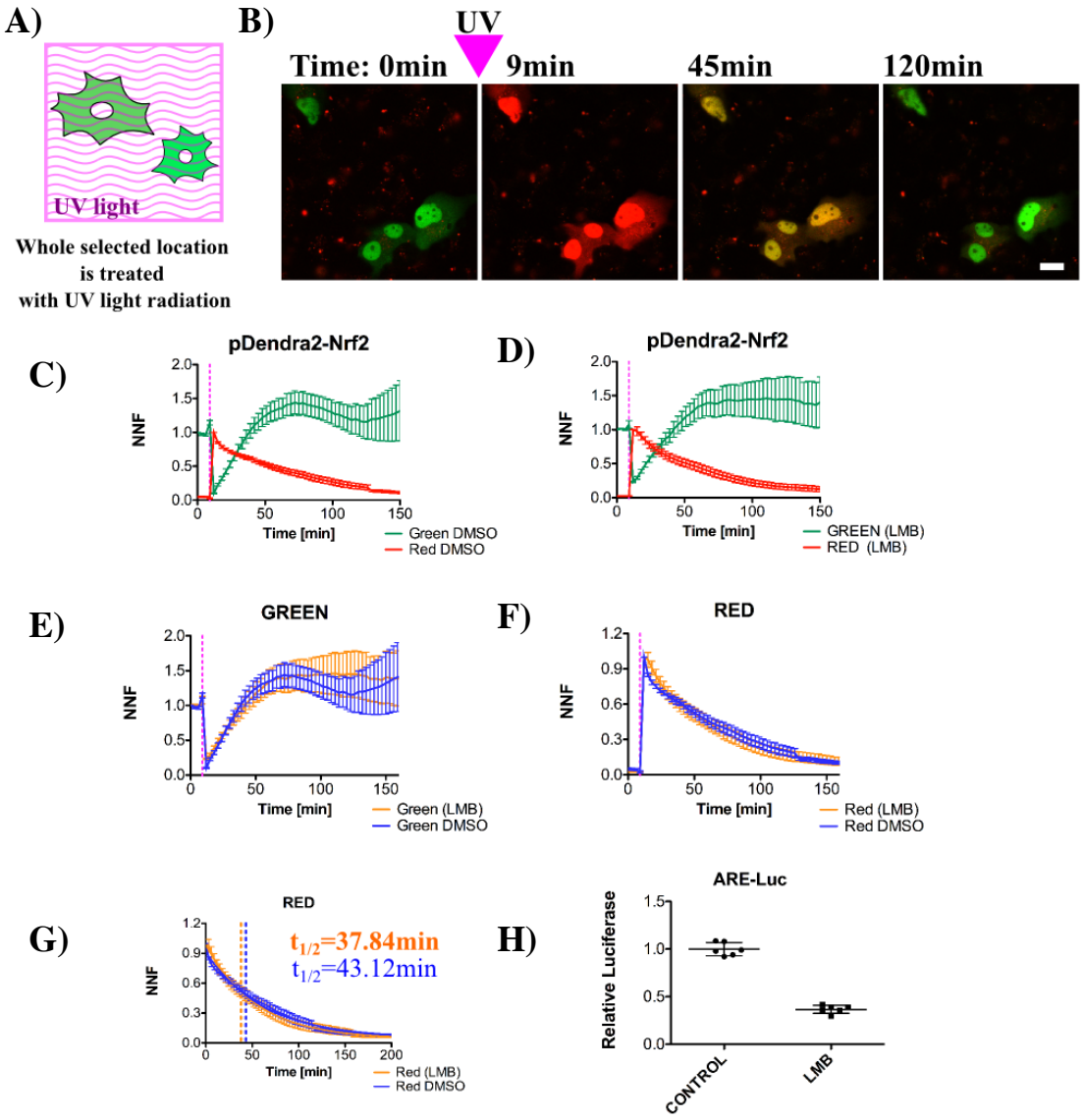

Figure 5.9. Inhibition of nuclear export does not stabilise pDendra-Nrf2 protein levels. A) Diagram depicting the experimental procedure used to perform pDendra2-Nrf2 imaging in whole cells. The UV halogen lamp was used for 45sec to photoconvert all cells in the selected imaging location. B) Representative images of control cells showing red fluorescence decay and stable accumulation of newly formed green pDendra2-Nrf2. C) Measurements of nuclear pDendra2-Nrf2 fluorescence in control cells (n=3, c=14). Red signal representing photoconverted pre-formed Nrf2 while the green signal represents newly made protein. D) Nuclear levels of red and green pDendra-Nrf2 treated with 10ng/ml LMB (n=3, c=27) (Movie 30). Comparison of green and red nuclear pDendra2-Nrf2 fluorescence in control and 10ng/ml LMB treated cells are shown respectively in (E&F). G) Reduction in photoconverted red pDendra-Nrf2 half-life in response to inhibition of nuclear export by LMB. H) LMB treatment significantly reduced ARE-Luc activity in BAC$^{Nrf2\text{-}Venus}$ cells (n=2, in triplicates). Error bars =SEM (imaging), =STDEV (dual luciferase). Scale bar=20μm.

Next, the ARE-Luc dual luciferase reporter was used as a surrogate to quantify the impact of nuclear export inhibition on Nrf2 transcriptional activity (Figure 5.9H). Basal Nrf2 driven ARE related transcriptional activity was significantly diminished following 8h incubation with 10ng/ml LMB. Therefore, it is important to note that even though the stability of the Nrf2 protein remained unmodified, Nrf2 transcriptional activity was greatly inhibited.

5.3.4. Comparing the Relative Effects of the Keap1 and GSK-3 on the Regulation of Nrf2 in Live SK-N-AS Neuroblastoma Cells

Previous data from this study indicate that Keap1 plays a more pronounced role than GSK-3 in the regulation of Nrf2 and Nrf2-mediated responses in $BAC^{Nrf2\text{-}Venus}$ neuroblastoma cells (Chapter 2, Figure 4.9 and 4.10). To measure the extent of the regulatory overlap between Keap1 and GSK-3 mediated regulation of Nrf2 expression and activity, the effect of 10μM CHIR99021 inhibition was measured under conditions of Keap1 deactivation by either siRNA or addition of SFN (Figure 5.10). Measurement of the ARE-Luc activity in $BAC^{Nrf2\text{-}Venus}$ cells highlighted that inhibition of the GSK-3 kinase had the most significant effect when combined with SFP treatment (Figure 5.10A). To confirm this result, Keap1 was depleted by siRNA knockdown (Figure 5.10B). Inhibition of GSK-3α/β by 10μM CHIR99021 (8hr) in siCTR treated cells did not lead to significant changes in ARE-Luc luciferase activity in contrast to cells transfected with Keap1 siRNA, which displayed significantly higher levels of ARE-Luc activity (Figure 5.10B). Interestingly, the highest ARE-Luc levels were detected when siKeap1 was used in combination with CHIR99021. This result was further reinforced by live cell imaging of $BAC^{Nrf2\text{-}Venus}$ cells with either Keap1 or CTR siRNA (Figure 5.10C, Movie 31a & 31b). Application of 10μM CHIR99021 significantly increased levels of nuclear Nrf2-Venus in cells with depleted Keap1. The above data suggests that the inhibition of Keap1 leads to a shift in the mechanism of Nrf2 regulation towards a GSK-3 dependent regulation.

5.3.5. The PML-Dependent Nuclear Nrf2 Regulation

Previous results from this study (Chapter 2, Figure 4.10) show that the reduction of Keap1 protein expression leads to increased accumulation of Nrf2-Venus in response

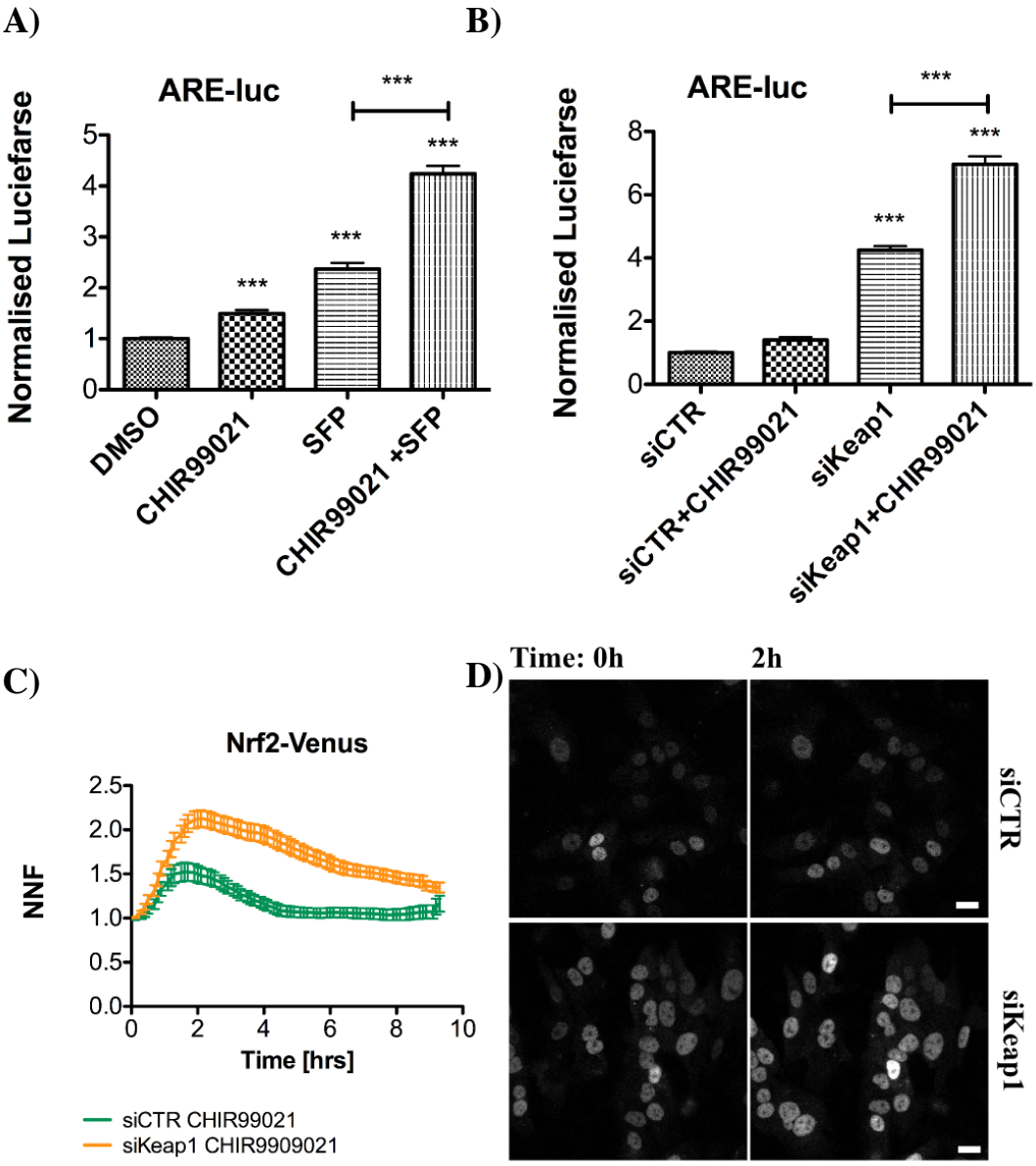

Figure 5.10 Keap1 inhibition enhances cells to negative regulation by GSK-3. A) Relative ARE-Luc activity in BAC$^{Nrf2\text{-}Venus}$ cells following 8h incubation with either 2μM SFP or 10μM CHIR99021, or both in combination (8hrs) (n=3, in triplicates). B) Relative ARE-Luc activity in BAC$^{Nrf2\text{-}Venus}$ cells transfected with Keap1 siRNA (siKeap1) (Movie 31b), or control siRNA (siCTR) (Movie 31a) following 8h incubation with DMSO or 10μM CHIR99021 (n=3, in triplicates). C) Temporal changes in Nrf2-Venus expression in BAC$^{Nrf2\text{-}Venus}$ cells transfected with siCTR or siKeap1 following addition of 10μM CHIR99021 (n=4, c=50). D) Representative images from the experiment shown in (C). Scale bar=, Error bars=SEM (imaging), STDEV (luciferase). Scale bar=20μm.

to acute inflammatory signalling. To measure the effect of downregulation of both Keap-1 and GSK-3 pathways on cytokine activated Nrf2 synthesis, BAC$^{Nrf2\text{-}Venus}$ cells were treated with 10μM CHIR99021 and siKeap1 before addition of 10ng/ml TNFα (Figure 5.11A). The extent of Nrf2-Venus induction was significantly amplified in cells treated with both siKeap1 and CHIR99021, as compared to cells treated with control siRNA and CHIR99021. However, the difference in relative nuclear Nrf2-Venus levels in cells where Keap1 and GSK-3 were both downregulated was only significantly different in a narrow temporal window approximately 3h after stimulation with TNFα (Fig. 11A). Significantly, inhibition of both of the two main Nrf2 regulators did not lead to a stable pool of Nrf2-Venus increase, even in the presence of the TNFα signalling, suggesting the possibility that an alternative degradation mechanism may also be involved in regulating cellular Nrf2 responses the antioxidant responses.

Live cell imaging of Nrf2-Venus in BAC$^{Nrf2\text{-}Venus}$ neuroblastoma cells, revealed an interesting pattern of Nrf2 accumulation, which was maximally observed following inhibition of nuclear export with Leptomycin B (LMB). However, under these conditions, only a very small increase in nuclear Nrf2-Venus was observed, suggesting a tight balance is maintained between Nrf2 nuclear import and degradation (Figure 5.11B, Movie 32). Combined addition of LMB and 10ng/ml TNFα led to only a minimal rise in nuclear Nrf2-Venus levels but this treatment was accompanied by the appearance of Nrf2-Venus positive promyelocytic leukaemia nuclear bodies (PML-NB) like structures in the nucleus (Figure 5.11B, Movie 33). Therefore, it appears that Nrf2-Venus is targeted to PML-NB-like structures under specific cellular conditions.

To measure of the effect of TNFα stimulation on the quantity of PML nuclear structures, BAC$^{Nrf2\text{-}Venus}$ cells were co-immunostained for both p65 and PML proteins after addition of 10ng/ml TNFα for 2h. This treatment increased the abundance and the mean size of nuclear PML structures suggesting a positive effect of TNFα on PML body formation (Figure 5.11C & E).

To investigate if high levels of p65 expression had a similar effect as elevated Nrf2 expression on PML body formation, theBAC$^{Nrf2\text{-}Venus}$ cells were transfected with either WT p65-dsRedXP or a transcriptionally impaired phosphorylation mutant

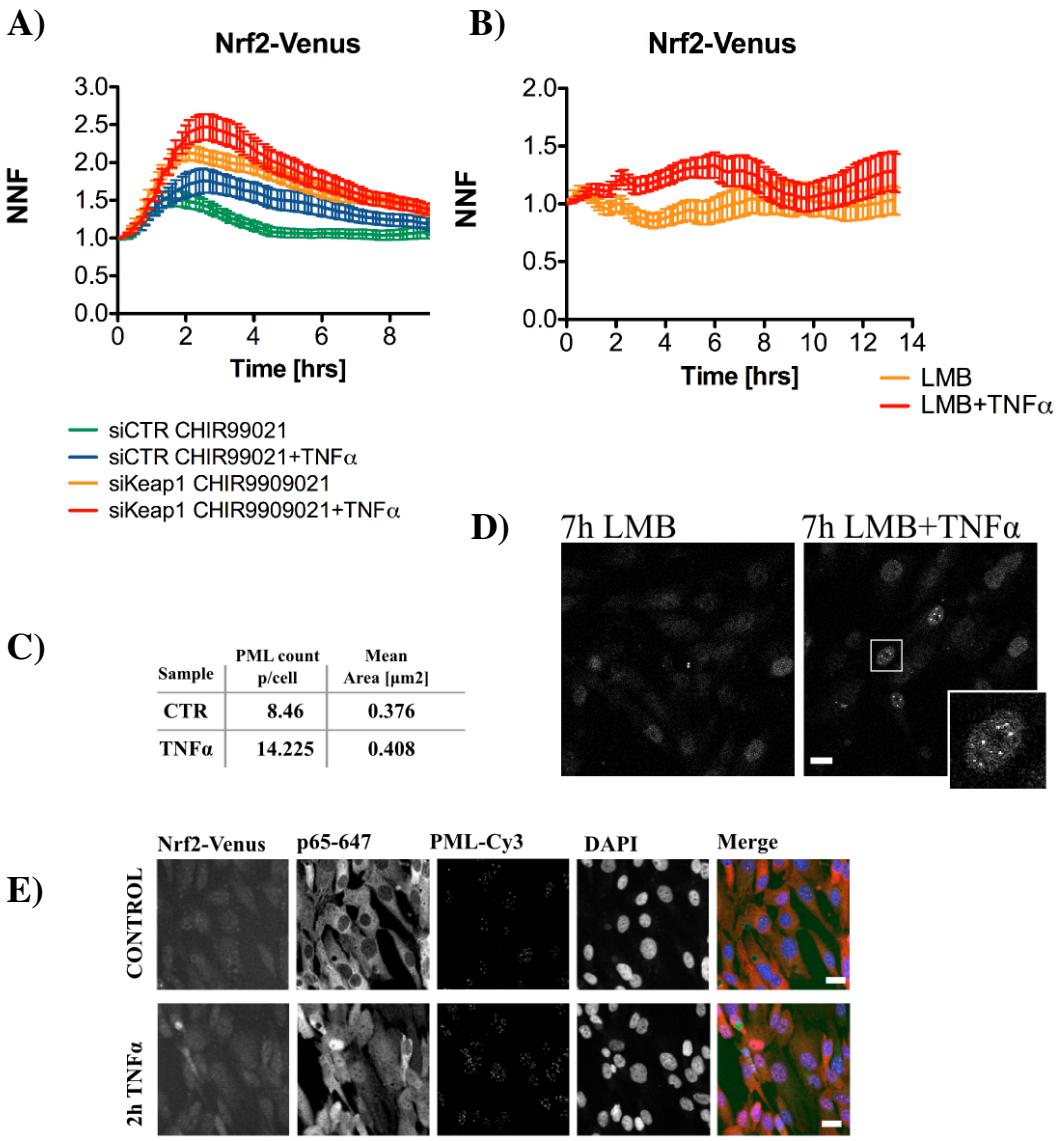

Figure 5.11 Leptomycin B augments the accumulation of Nrf2 in punctate nuclear structures. A) Relative nuclear fluorescence of Nrf2-Venus in siCTR and siKeap1 transfected cells following addition of 10µM CHIR99021 +/- for 30min before 10ng/ml TNFα (n=3). B) Dynamic changes in nuclear Nrf2-Venus levels in response to addition of 10ng/ml LMB treatment +/- TNFα (n=2, c=17-19) (Movie 32 & 33). C) Representative time lapse images of Nrf2-Venus taken 7h after addition of 10ng/ml LMB alone or 10ng/ml TNFα + 10ng/ml LMB in combination. D) Quantitative analysis of Nrf2 positive PML-like structures obtained using ImageJ of immunofluorescent images from E). E) Immunofluorescent staining of BAC$^{Nrf2\text{-}Venus}$ cells, showing PML-Cy3 and p65-488 conjugates in control or in cells treated with TNFα for 2h. Error bars=SEM. Scale bar=20µm.

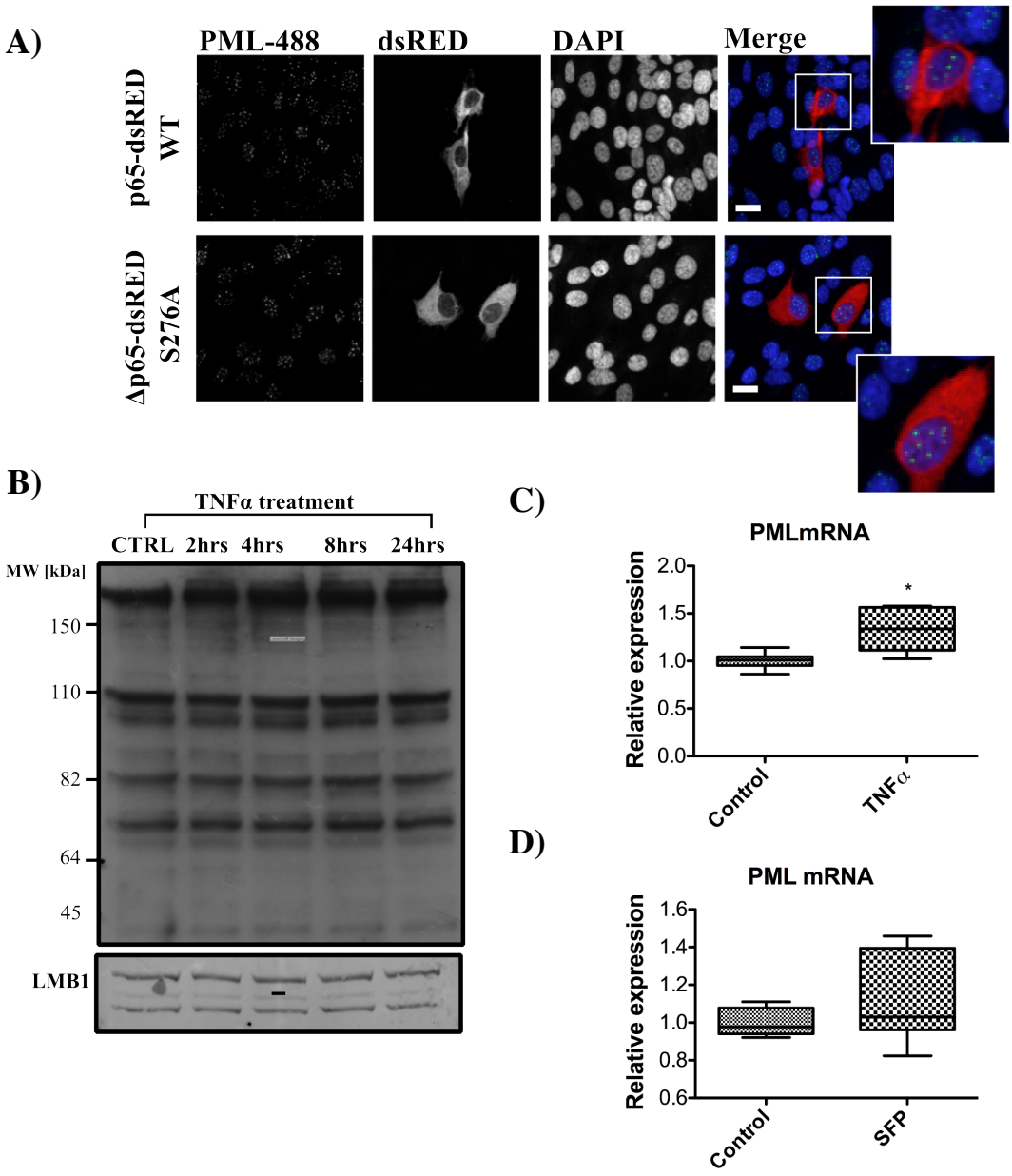

Figure 5.12 Effect of NF-κB on PML regulation. A) Immunofluorescence images of BAC$^{Nrf2\text{-}Venus}$ cells stained with PML-488 conjugates showing no change in the abundance of PML structures in cells expressing either WT p65-dsRedXP or a transcriptionally inactive mutant ΔS276A p65-dsRedXP protein. B) Western blot of BAC$^{Nrf2\text{-}Venus}$ nuclear extracts stained for the PML protein. TNFα stimulation did not cause significant changes in any of the detected bands. C) The relative level of PML mRNA increases slightly in response to 8hr stimulation with 10ng/ml TNFα. D) Addition of 2μM SFN (8hr) does not induce significant changes in PML mRNA expression (n=3, in triplicates). Error bars=STDEV. Scale bar=20μm.

ΔS276A-p65-dsRedXP (plasmid kindly gifted by Mike White's group in Manchester) (Figure 5.12A). However, the pattern of PML expression appeared very similar between mutant and WT p65-dsRedXP expressing cells, therefore we can conclude that overexpression of p65 does not have an equivalent effect as Nrf2 on PML expression or PML nuclear bodies formation.

To validate these results the $BAC^{Nrf2\text{-}Venus}$ lysates were collected at intervals during a 24h period of TNF-α stimulation. Nuclear fractions were then analysed by western blot (Figure 5.12B). Unfortunately, the PML antibody used in this study showed a lot of unspecific staining and even though PML has several isoforms between 78-97kDa, none of the bands displayed changes as a result of cytokine application (Figure 5.12B).

To test the possibility that PML expression may be regulated by either Nrf2 or NF-κB driven transcription $BAC^{Nrf2\text{-}Venus}$ cells were treated for 8hrs with either 2μM SFP or 10ng/ml TNFα and lysates were processed for Q-PCR analysis. Using primers designed to detect all 5 isoforms of PML, a significant increase in PML mRNA expression was only detected in samples treated with TNFα (Figure 5.12C and D). Therefore, evidence from this study suggests that TNFα enhances PML expression in the neuroblastoma cell model, possibly by a transcriptional mechanism.

5.3.6. The Role of Acetylation in Modulating Nrf2 Activity

Nrf2 is known to be a target for p300/CBP-mediated acetylation in the nucleus. In addition, this post-translational modification of Nrf2 is though to be essential for its transcriptional activity (Sun & Zhang, 2009). To investigate the role of acetylation in modulating Nrf2 activity, live cell imaging and ARE-Luc transcriptional reporter assays were performed to monitor the effects of inhibiting p300/CBP catalytic activity, following addition of 10μM C646 (viability assay in Supplementary 8.2C). Unexpectedly, inhibition of acetylation by C646 caused a dramatic increase in nuclear Nrf2 levels in both $BAC^{Nrf2\text{-}Venus}$ cells and primary cortical astrocytes, which stably express the *2kb*-Venus-Nrf2 fusion protein (Figure 5.13A and B) (Viability assay on C646 in Figure 8.3C).

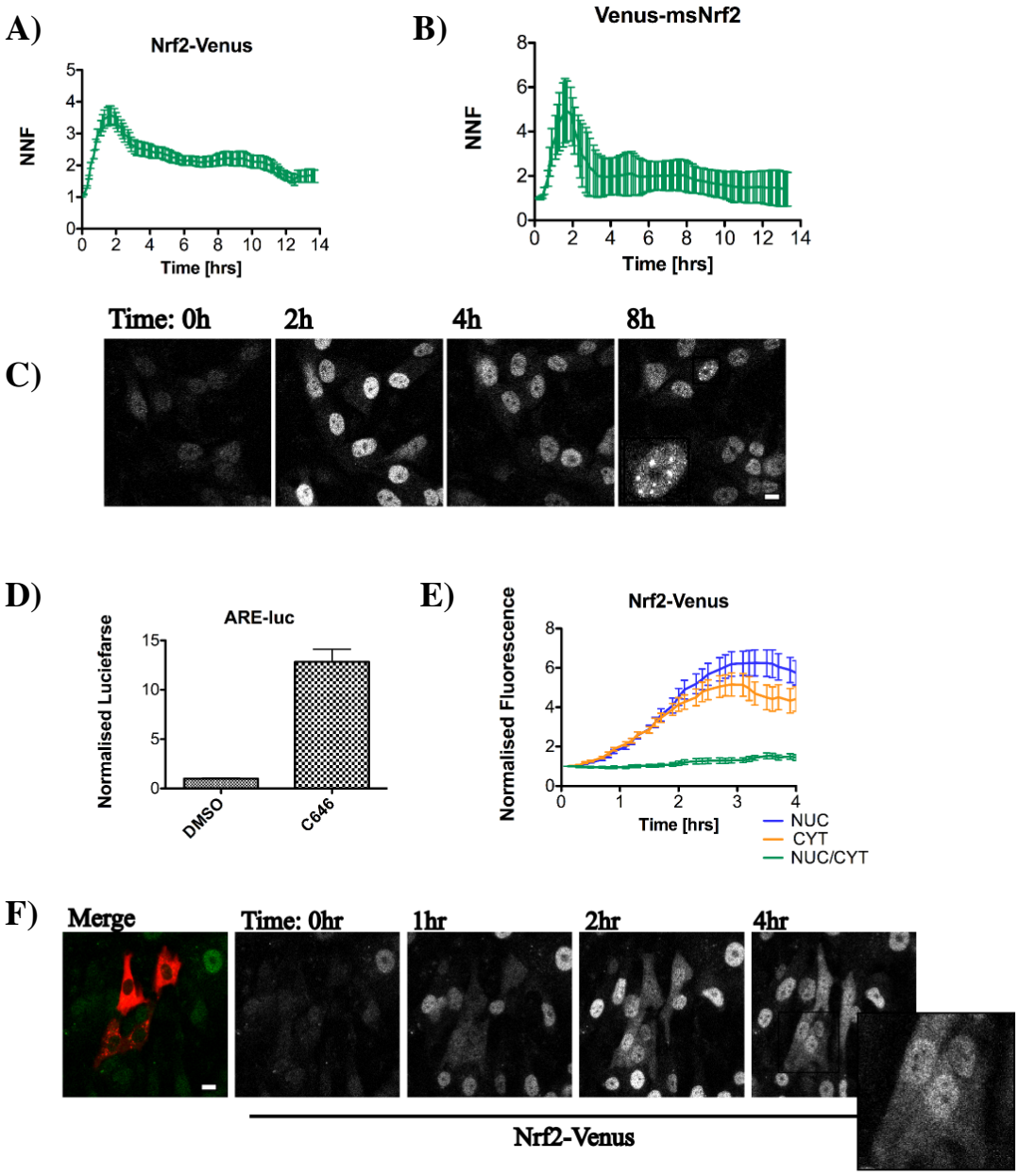

Figure 5.13 Inhibition of acetylation strongly enhances Nrf2 nuclear accumulation and transcriptional activity. A) Dynamic changes in Nrf2-Venus levels in the nuclei of BAC$^{Nrf2\text{-}Venus}$ (n=2, c=15) (Movie 34), or B) primary hippocampal astrocytes transduced with the *2kb*-Venus-Nrf2 construct (n=1, c=3), following addition of 10μM C646. C) Representative images of BAC$^{Nrf2\text{-}Venus}$ cells treated with 10μM C646, showing accumulation of Nrf2-Venus in PML-NB like nuclear structures. D) ARE-Luc activity increases in response to application of 10μM C646 for 6h (n=2, in triplicates). E) BAC$^{Nrf2\text{-}Venus}$ cells transfected with mCherry-Keap1 show a significant accumulation of nuclear Nrf2-Venus (n=3, c=13). F) Representative time-lapse images of cells from experiment (Movie 35). Error bars=SEM(imaging)/STDEV(luciferase). Scale bar=20μm.

Significantly, the C646 induced accumulation of Nrf2-Venus containing PML-NB-like structures (Figure 5.13C), was accompanied by a corresponding increase in Nrf2 transcriptional activity, as demonstrated by a significant rise in ARE-Luc activity in $BAC^{Venus\text{-}Nrf2}$ cells (Figure 5.13D). To test whether the inhibition of acetylation affected Keap1-mediated Nrf2 degradation, $BAC^{Nrf2\text{-}Venus}$ cells transiently transfected with the mCherry-Keap1 plasmid were imaged following incubation with 10μM C646 (Figure 5.13E and F). Interestingly, the inhibition of p300/CBP acetyl transferase activity led to a substantial accumulation of nuclear Nrf2-Venus even in mCherry-Keap1 expressing cells (Figure 5.13F, Movie 35).

To veryfy if the increase in protein acetylation by repressing histone deacetylatase (HDACs) activity had an opposite effect on Nrf2 transcriptional function, ARE-Luc signal was measured following application of pharmacological HDACs inhibiting compounds (Figure 5.14). Inhibition of both classes of HDACs by 3.3μM TSA caused a significant decrease in ARE-Luc activity, while selective inhibition of Class II HDACs with 2μM MC1568 led to a two-fold increase in ARE-Luc activity (8h treatments). Selective inhibition of Class I HDACs with 1μM Mocetinostat (Class I) had no effect of Nrf2 driven ARE-Luc activity (Figure 5.14). Therefore, different classes of HDAC enzymes may have differential effects on the regulation of antioxidant responses, however the nature of this regulation is largely unexplored and requires a more thorough study.

5.4. DISCUSSION

Keap1/Cullin3/Rbx1 mediated ubiquitination of Nrf2 is central to the regulation of cellular antioxidant responses. Compounds that modulate this process have been at the centre of drug design against cancer, neurodegenerative diseases, inflammatory disorders and many more (Vargas & Johnson, 2009). The first live cell imaging studies of the Keap1 and Nrf2 complex using FLIM led to the proposal of a conformational cycling model of regulation, where Nrf2 forms a closed complex with Keap1 under basal conditions (Baird *et al,* 2014). Inducers of Nrf2 activity induce a conformational change in the Keap1 protein, which shifts the Keap1:Nrf2 complex into an open state, in which bound Nrf2 cannot be degraded. In this model it is proposed that newly synthesized Nrf2 is able to translocate to the nucleus, where it

drives transcription of ARE response genes (Baird *et al,* 2013*)*. Data presented in this study supports the conformational cycling model of the Keap1:Nrf2 complex, but also provides novel insight into alternative modes of Nrf2 regulation in the nucleus.

Transient plasmid mediated-Keap1 expression was used as a mechanism to assess the effect of high Keap1 levels on basal and activated Nrf2 protein levels and transcriptional activity (Figure 4.1). Overexpression of mCherry-Keap1 expression in $BAC^{Nrf2\text{-}Venus}$ cells was sufficient to significantly diminish Nrf2-Venus fluorescence and reduce ARE dependent transcriptional activity under basal conditions (Figure 5.1A & B). However, simultaneous overexpression of both Venus-Nrf2 and mCherry-Keap1 led to the accumulation of Venus-Nrf2 in the cytoplasm. This effect may indicate that Nrf2 out-titrated Keap1 mediated degradation, even under basal conditions (Figure 5.1C). The third phenotype was observed in cells expressing high levels of mCherry-Keap1 in cells treated with CDDO-Me. In this case, induction led to a gradual accumulation of Nrf2 in the cytoplasm (Figure 5.2A). This effect may be due to the effective capture of Nrf2 in the cytoplasm by Keap1, even though subsequent degradation is blocked. Therefore, even though under these conditions, nuclear Nrf2 levels steadily increased, the cytoplasmic accumulation was dominant (Figure 5.2B & C, Movie 24). This phenotype can be explained by a model in which Keap1 can bind and sequester Nrf2 in the cytoplasm, but not as part of an active degradation complex, possibly because high levels of Keap1 out-titrate available Cullin3/Rbx1 proteins. Addition of Nrf2 activating compounds such as CDDO-Me would further enhance this effect, by inhibiting degradation of the pool of Nrf2 that is bound to Keap1 within the Cullin3/Rbx1 complexes.

In live cell imaging studies where cells were treated with a combination of both CDDO-Me and LMB, a proportion of Nrf2-Venus was seen to accumulate in the nucleus (Figure 5.3A&B). Inhibition of nuclear export led to the accumulation of Nrf2-Venus in the nucleus, showing that Nrf2 cycles through the nucleus, even when Keap1 is overexpressed. However, Nrf2 nuclear accumulation without LMB is not pronounced in CDDO-Me only treated cells (Figure 5.2) suggesting this phenotype is likely to be transient.

As depletion of Keap1 by siRNA, enhanced nuclear accumulation of Nrf2-Venus, it would appear that Keap1 protein acts like a molecular net, which not only mediates

the degradation process, but also efficiently retains Nrf2 within the cytoplasm (Figure 5.1C, 2A, Movie 25). The substantial cytoplasmic accumulation supports the evidence that the inducers do not stop Keap1:Nrf2 protein interaction, otherwise Nrf2 would accumulate in the nucleus shortly after synthesis, despite high cytoplasmic Keap1 levels. Data from this study supports the hypothesis that levels of Nrf2 must exceed levels of Keap1, in order to enter the nucleus. This requirement provides a more stringed control of Nrf2 and restricts activation of the antioxidant pathway to situations where synthesis of the new Nrf2 protein is possible.

Inhibition of nuclear export also resulted in increased mCherry-Keap1 levels in the nucleus. This highly reproducible phenotype (Figure 5.3D) is consistent with previous reports that nuclear entry of Keap1 may be essential for the removal of Nrf2 from ARE containing promoter sequences and may also assist with its nuclear export (Sun *et al,* 2011).

Levels of Nrf2 protein are very effectively regulated within the cytoplasm, which makes the measurements of dynamic changes in cytoplasmic Nrf2 levels challenging to monitor, as the rapid clearance obscures discrete fluctuations resulting from the changing balance between Nrf2 synthesis and nuclear export. The photoswitchable pDendra2-Nrf2 fusion protein provides a valuable imaging tool, which allows dynamic changes in Nrf2 protein sub-populations to be monitored in real time. The pDendra2 fluorescent protein is especially helpful in studying short-lived proteins and as Nrf2 has a very short half-life of approximately 30 minutes it was an excellent candidate for pDendra2 tagging (Belleza *et al,* 2010).

The local pDendra2-Nrf2 photoswitching experiments provided novel insight into the conditional dynamics of Nrf2 nuclear import and export, parameters that would be extremely difficult, or impossible to measure by traditional biochemical methods. Data from these studies show that the rate of Nrf2 nuclear accumulation was fastest in untreated cells (Figure 5.8B), although, the ratio of nuclear accumulation of Nrf2 was predictably highest in the presence of MG132 (Figure 5.8B). The reason for the decreased rate of nuclear import when proteasomal degradation is inhibited is unclear. Interestingly, the nuclear decay of the photoswitched red pDendra-2-Nrf2 protein was actually enhanced in cells treated with MG132, indicating that more

protein could be relocating to the nucleus as a result of proteasome inhibition, but simply being imported at a lower speed (Figure 5.8A).

Overexpression of the tagBFP-Keap1 protein neatly demonstrated the role of Keap1 as an effective cytoplasmic Nrf2 retention barrier, as the rate of Nrf2 nuclear import was dramatically decreased in the presence of high levels of Keap1 (Figure 5.5, Movie 27). Whereas, the process of Nrf2 activation has been studied in great depth the fate of Nrf2 protein once it enters the nucleus has not been clarified. The GSK-3 kinase is though to mediate both the nuclear export and/or degradation of Nrf2, with the latter being currently favoured (Cuadrado *et al,* 2015). As noted before the difficulty in analysing the role of GSK-3 in Nrf2 protein depletion is the difference in nuclear degradation and export phenotype for Nrf2, as no changes of cytoplasmic levels are detected due to robust Keap1-mediated degradation once it enters the cytoplasm. However, Dendra2-Nrf2 single-cell imaging enabled the nuclear levels of the photoswitched protein to be measured, thus providing definitive evidence for Nrf2 nuclear export (Figure 5.6). The nuclear levels of photoactivated (red) pDendra2-Nrf2 were very rapidly depleted from the nuclear space and this is likely to occur due to photobleaching, export and degradation. It was possible to distinguish between the export and the degradation processes, as the LMB treatment slowed down the decay of red nuclear fluorescent signal, even more than in MG132 treated cells (Figure 7C). Interestingly, this suggests that the rate of export is slightly faster than the rate of degradation, however the overall effect will again depend on the proportion of protein being exported *vs*. degraded. Furthermore, the red nuclear pDendra2-Nrf2 protein was stably accumulating in the cytoplasm in both control (CTR) and MG132 treated cells (Figure 5.7D), but not when nuclear export was blocked. The rate of increase of cytoplasmic Nrf2 fluorescence was higher in CTR cells with a t½ of approximately 41s, in comparison to MG132 treated cells, which show a $t_{1/2}$=72sec (Figure 5.7E). This could result from higher levels of protein leaving the nucleus as their transport is limited by the constant rate of export.

Comparison of the $t_{1/2}$ of fluorescence recovery indicates that levels of nuclear fluorescence increased faster in the cytoplasm compared to the nucleus, in both control and MG132 treated cells (Figure 5.8 C and D). This result was counterintuitive since previous results from this study (Results Ch1, 3.4.5) show that the basal Nrf2 levels were found to be constantly higher in the nucleus than in the

cytoplasm. However, comparing the relative nuclear Nrf2 movement (import *vs*. export), the proportion of protein entering the nucleus is higher than the proteins leaving it, therefore the net result is a higher net rate or import (Figure 5.8 E & F).

Measurement of nuclear pDendra2-Nrf2 stability exposed a surprising result (Figure 5.9); as the photoshifted (red) nuclear fluorescence decay of Nrf2 very closely followed the dynamics and half-life measurements in DMSO and LMB treated SK-N-AS (Figure 5.9). This data shows that Nrf2 nuclear export is not necessary for degradation to occur and importantly, LMB did not prevent the synthesis of new Nrf2 protein (Movie 30. Therefore the nuclear dynamics of newly made or 'old' pDendra2-Nrf2 follow similar dynamics in both control and LMB-treated cells (Figure 5.9E & G). The lack of change of Nrf2 protein stability suggests that nuclear degradation of Nrf2 is a very efficient process, but may not be mediated by Keap1, as current knowledge would not support its function in nuclear degradation.
However, even though the stability of Nrf2 remain unaltered as a consequence of LMB application, analysis of Nrf2 transcriptional activity displayed a significant reduction of ARE-Luc transcriptional activity, indicating that inhibition of nuclear export could potentially lead to changes in Nrf2 DNA-binding (Figure 5.9H).

Keap1 mediated regulation of Nrf2 stability is known to be sensitive to changes in intracellular redox status, whereas GSK-3α/β regulation has been proposed to differentially modulate Nrf2 responses, depending on the combinatorial activation status of different cell signalling pathways. Using the pDendra2-Nrf2 construct it was possible to investigate the regulatory potential of GSK-3 in SK-N-AS neuroblastoma cells. Previous experiments (Figure 4.10) demonstrated that GSK-3 inhibition, either alone or in combination with TNFα stimulation, did not lead to a significant increase in Nrf2-Venus levels, or transcriptional activity. However, it became clear that the inactivation of GSK-3 by 10μM CHIR99021, in combination with Keap1 inhibitor or depletion of Keap1 by siRNA knockdown, greatly enhanced the effect of GSK-3 inactivation on the Nrf2 pathway (Figure 5.10). Measurement of ARE-Luc activity confirmed that reduced Keap1-mediated Nrf2 regulation caused a significant increase in ARE-Luc activity in response to CHIR99021 application (Figure 5.10 & B). Enhanced Nrf2 transcriptional activity was also observed as a

result of Nrf2 nuclear accumulation following GSK-3 downregulation, in cells with reduced levels of Keap1 (Figure 5.10 C & D). Previously, the lack of Nrf2 responses as a result of GSK-3 inactivation in SK-N-AS cells was attributed to high levels of PI3K activity; such as when cells were maintained in serum rich growth medium (Figure 4.10). However, previous studies suggest that a strict cytoplasmic regulation of Nrf2 may limit the amount of protein that is subjected to GSK-3-mediated nuclear regulation. This would be especially relevant if, as demonstrated before, the residency of nuclear Nrf2 is only temporary, due to effective nuclear export. Therefore, depletion of Keap1 may lead to a switching of Nrf2 regulation, to a GSK-3 dependent mode. In a physiological context, Keap1 down-regulation could be associated with increased oxidative stress, or functional mutations potentiating the GSK-3/β-TrCP regulatory role. This could be particularly relevant in aging, which is associated with higher GSK-3 activity and an increasingly oxidative redox environment (Cuadrado *et al,* 2009). The GSK-3/β-TrCP axis activity is dependent on the cells metabolic status. Under normal conditions this process is inhibited by PI3K activity. Therefore, it is reasonable to presume that the negative effect of GSK-3 on the antioxidant pathway will be also be dependent on nutrient availability (Chowdhry *et al,* 2013).

The GSK-3/β-TrCP/Cullin1 and Keap1/Rbx/Cullin3 mechanisms of Nrf2 degradation may both play central, yet distinct roles in down regulation of Nrf2 signalling responses (Suzuki & Yamamoto, 2015). As such, it may be anticipated that the combined inhibition of GSK-3 and Keap1 would lead to the stable accumulation of basal Nrf2-Venus, especially in cells expressing higher levels of Nrf2 as a result of TNFα application (Figure 5.11A). However, single cell imaging experiments performed in this study, show that induction of Nrf2 is relatively short-lived (Figure 5.11A). Although it is possible that the pharmacological activity of CHIR99021 inhibitor and siRNA mediated inhibition of Keap1/GSK-3 are both transient effects, it is also possible that there are other conditional mechanisms of Nrf2 protein degradation or inhibition of Nrf2 transcriptional activity. The RNF4 E3-ubiquitin-protein ligase was previously identified as an alternative regulator of nuclear Nrf2 stability, by initiating the sequential sumoylation and ubiquitination of Nrf2, prior to degradation in PML-NBs (Malloy *et al*, 2013). It is possible, that

involvement of PML NBs in the clearance of Nrf2 could be extremely robust and completely independent of Keap1 and GSK-3 activity. In order to observe rapid Nrf2-Venus turnover within the PML-NBs it may be necessary to use more sophisticated atomic force microscopy methods, or spinning disc microscopy in future studies. The PML-NBs are very dynamic structures located predominantly in the nuclear space and can act to modulate both transcriptional activity and protein stability. The PML protein is fundamental in orchestrating the assembly of protein complexes to form the PML NBs structures, however the mechanism that leads to their formation is not simply dependent on PML protein availability, but additionally requires extensive post-translational modifications of PML, and other involved proteins (Lallemand-Breitenbach & de The, 2010).

Inhibition of nuclear export did not have a significant effect on Nrf2 nuclear accumulation, or depletion, leading to a steady state of Nrf2-Venus nuclear expression (Figure 5.11B, Movie 32). However, combined treatment with TNFα and LMB led to the formation of Nrf2-Venus containing punctate structures, which were present exclusively in the nuclear compartment (Figure 5.11D, Movie 33). As this phenotype was more evident following TNFα treatment, it was possible that NF-κB in some way controlled the expression of the PML protein, which plays a key role in the formation of the PML-NBs structures (Gao *et al,* 2008). Incubation of $BAC^{Nrf2\text{-}Venus}$ cells with 10ng/ml TNFα for 2h, increased the average number of PML punctate structures per/nucleus, as well as slightly increasing their size (Figure 5.11C & E). However, these changes cannot be considered to be statistically significant, as only two experimental replicates have so far been performed.

To investigate the possible role of p65 in the increase of PML protein, $BAC^{Nrf2\text{-}Venus}$ cells were transfected with either wild type p65-dsRedXP or a transcriptionally impaired mutant, containing a substitution of the regulatory phospho-Serine 276 residue (Figure 5.12A). However, expression of both constructs failed to changes PML nuclear staining in comparison to the non-transfected cells (Figure 5.12A). Unfortunately, analysis of nuclear PML levels by western blot was not successful, due to the low specificity of the anti-PML antibody, also none of the detected bands displayed TNFα dependant changes in expression (Figure 5.12B). TNFα stimulation augmented the expression of PML mRNA. Therefore, the increase of PML observed

by immunofluorescence could be due to the enhanced PML gene expression (Figure 5.12C). TNFα is known to enhance expression of PML mRNA levels, possibly by augmenting STAT1 transcription factor activity (Gao *et al,* 2008), consequently, increasing the quantity of nuclear speckles, which was also observed in our study (Figure 5.11).

Nevertheless, the accumulation of Nrf2 in the punctate structures may have not occurred as a result of increased net PML expression but as a result of increased Nrf2-Venus synthesis, triggered by TNFα stimulation and combined with nuclear retention, as a result of LMB treatment. Suppression, of proteasomal activity also led to the accumulation of Nrf2-Venus in discrete nuclear speckles therefore, higher levels of Nrf2 protein could lead to considerable accumulation in PML-NBs, which are otherwise too small to be observed, or are rapidly removed before accumulating into larger structures.

To reinforce the observation that Nrf2-Venus is targeted to PML-NB punctate and not similar structures; therefore the conditional co-localisation of Nrf2 and PML proteins should be investigated in more detail.

PML NBs formation requires extensive post-translational modifications including sumoylation. This modification is only possible on proteins containing specialised SIM domains that form a hydrophobic pocket allowing non-covalent attachment of the sumo tag (Nisole *et al*, 2013). Acetylation of Lys487 at the center of the SIM domain within the PML protein prevents Lys490 SUMO1 conjugation due to a change in the net charge within the SIM pocket, consequently preventing the assembly of the PML NBs. Therefore, the activity of p300 was reported to inhibit the PML NB formation by inhibition of SUMO attachment on the PML proteins (Nisole *et al,* 2013). However, the effect of Nrf2 acetylation on its degradation in the PML NBs has not been previously investigated. The application of C646 was expected to decrease ARE-Luc signaling, as p300 activity is necessary for Nrf2 transcriptional activity. In contrast, inhibition of p300/CBP by C646 in $BAC^{Nrf2\text{-}Venus}$ led to amplified relative ARE-Luc luminescence levels (Figure 5.13, Chapter 3). Furthermore, addition of C646 to both $BAC^{Nrf2\text{-}Venus}$ and primary cortical mouse astrocytes induced

a transient nuclear accumulation of Nrf2 (Figure 5.13 A & B, Movie 34). Thus suggesting that the inhibition of p300/CBP mediated acetylation may act as a potent inducer of Nrf2 responses. To test whether this effect arose as a consequence of changes in Keap1-dependent Nrf2 control, mCherry-Keap1 was over-expressed in $BAC^{Nrf2\text{-}Venus}$ cells and temporal changes in Nrf2 dynamics were measured following addition of 10μM C646 (Figure 5.13 E & F, Movie 35). In contrast to the addition of CDDO-Me, inhibition of acetylation did not promote Nrf2 accumulation in the cytoplasm, but instead led to a more substantial increase in nuclear Nrf2 (Figure 5.13F). Therefore the induced pattern of Nrf2 accumulation was more similar to that achieved with the combined application of CDDO-Me and LMB (Figure 3A). In addition, prolonged C646 treatment led to the accumulation of Nrf2-Venus into PML-NB-like structures, which was also a hallmark associated with the blocking of nuclear export by LMB (Figure 5.11D). Hypothetically, inhibition of acetylation could result in either inhibition of Keap1:Nrf2 interaction, reduced export, or suppression of PML mediated degradation. The increase of cytoplasmic Nrf2 levels in cells expressing mCherry-Keap1 following C646 application, suggest that a significant proportion of Nrf2 is still able to be retained in the cytoplasm by Keap1-mediated mechanism, therefore the inhibition of Keap1 binding is an unlikely explanation (Figure 5.13, Chapter 3). There are several possibilities of how C646 application could promote an increase in nuclear Nrf2 levels, the most likely being the inhibition of Keap1 binding, as the protein accumulates rapidly in the nucleus without a substantial rise in cytoplasmic levels.

The inhibition of acetylation was expected to have a positive effect on Nrf2 since the HAT inhibition was stimulatory on ARE gene expression (Figure 5.13).

In order to measure the effect of hyper-acetylation on Nrf2 expression or function, the removal of acetyl groups was blocked by addition of three drugs, which target different classes of HDAC proteins (Figure 5.14). Application of HDAC inhibiting compounds induced variable effects on ARE-Luc transcriptional activity, with TSA being inhibitory, while the MC1568 inhibitor augmented antioxidant gene transcription (Figure 5.14). The pleiotropic effects of HDAC inhibition on antioxidant responses has been reported in several previous studies (Chen *at el,* 2014; Kawai *et al,* 2011; Mercado *et al,* 2011). It is possible that Nrf2 activity could

be modulated by acetylation at a transcriptional level, as the canonical role of HDAC proteins is to facilitate chromatin condensation, which prevents access of the transcriptional apparatus to the DNA template. It should be noted that that we have not examined the net effect of C646 on the Nrf2 acetylation status and surprisingly no reports so far described the effect of p300/CBP inhibition on the activity of the antioxidant pathway, therefore this effect remains to be investigated in more detail.

It is evident that acetylation and de-acetylation may regulate both Nrf2 protein levels and activity. Nevertheless, pharmacological inhibition of acetylation, or de-acetylation, is a multifaceted event and hence is expected to be associated with multiple off-target effects. As such, it is not yet possible to predict what the role of acetylation may be in conditionally regulating antioxidant pathway activity, due to the complex nature of the process and time constraints of this project, however, this issue remains an interesting avenue for future exploration.

To summarise, in order to fully appreciate the potential effects of inflammatory signalling on the Nrf2 pathway, it is necessary to have a good understanding of the molecular processes that regulate basal and induced Nrf2 responses. The results of this study reinforced the proposed conformational cycling model of Keap1-Nrf2 complex formation, and provide new quantitative insight into the Nrf2 protein life cycle, in a live single-cell context (Baird *et al,* 2013). The employment of sophisticated low-level Nrf2 expression and imaging techniques and photoswitchable protein tagging has provided the first quantitative insight into the conditional dynamics of Nrf2 nuclear import and export parameters. Including the conditional sequestration of Nrf2 into discrete PML-NB like structures. This data is now being incorporated into a pertinent based mathematical model of the antioxidant pathway responses in health and disease. The functional model summarising the data obtained in this chapter is presented in Figure 5.15.

The utilisation of photoswitchable Nrf2 protein fusion provided a new insight into monitoring discrete Nrf2 protein populations. This powerful imaging tool has been further used in investigating the mechanism of action of brusatol, the results of this study are presented in the next, final chapter.

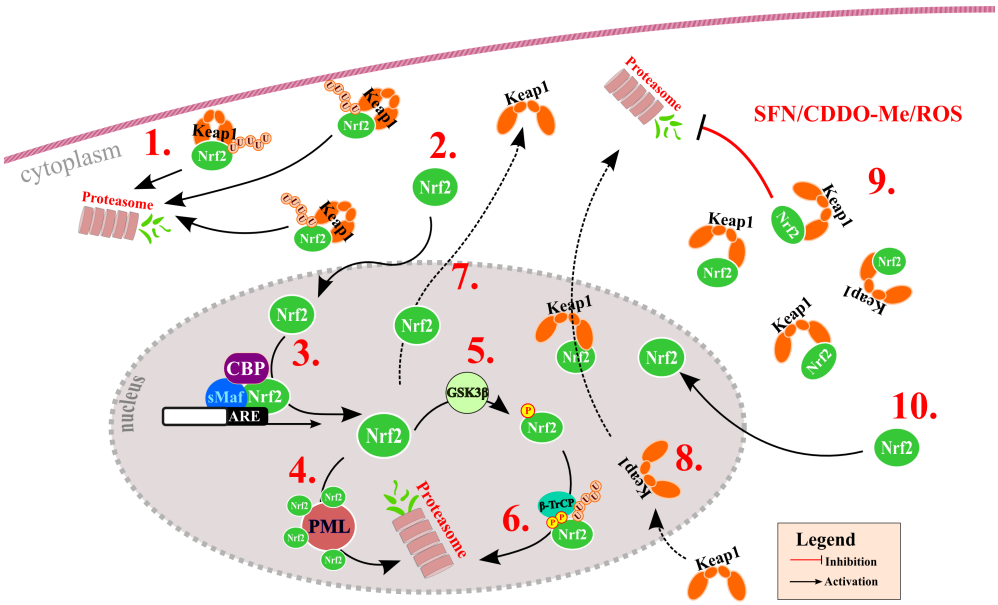

Figure 5.15 Nrf2 regulation through Keap1, GSK-3 and PML axis of degradation. 1. Keap1 mediates ubiquitination and degradation of Nrf2 within the cytoplasmic space. **2.** A small proportion of Nrf2 escapes Keap1-mediated regulation and translocates to the nucleus. **3.** In the nuclear space CBP facilitates Nrf2 association with the ARE sequences. **4.** Nrf2 can be observed in the PML-NBs where it is likely to be turnovered. **5.** GSK-3 phosphorylates Nrf2 and allows **6.** β-TrCP association and degradation of Nrf2. **7.** A proportion of Nrf2 can be exported from the nuclear space into the cytoplasm. **8.** Keap1 can enter the nuclear space and it is possible that it can serve as nuclear export facilitator for Nrf2. **9.** CDDO-Me and SFN prevent Keap1-mediated degradation, but do not dissociate Nrf2-Keap1 complex. **10.** Nrf2 out-titrates Keap1 dimers and enters the nuclear space.

RESULTS CHAPTER 4

6. Investigating the Mechanism of Action of Brusatol

6.1. CHAPTER 4 AIMS:

- **Live cell imaging of BAC$^{Nrf2\text{-}Venus}$ neuroblastoma in response to brusatol application**
- **Investigating the effect of brusatol on the NF-κB pathway**
- **Investigating the effect of brusatol on Nrf2 stability using fluorescent photoswitchable pDendra2-Nrf2 protein fusion**
- **Determining the mechanism of action of brusatol and its off-target effects**

6.2. Introduction

Expression of the Nrf2 transcription factor tightly controlled, normally being maintained at very low levels in normal tissues (Suzuki *et al,* 2013). However, high levels of expression have been observed in several types of cancer, such as pancreatic, thyroid, liver cancer and several others (http://www.proteinatlas.org) and what is more, Nrf2 has been previously identified as an important proliferative factor in neuroblastoma cells (de Miranda *et al*, 2015). This phenotype is a major obstacle to the effective treatment of these cancers as the resulting increase in expression of Nrf2 target genes contributes to resistance to both chemo- and radiotherapy. Recently, brusatol, a natural compound from the *Brucea javanica* plant was identified as a potent inhibitor of the antioxidant pathway and has been shown to sensitise cancer cells and tumours to chemotherapy, however consensus has not yet been reached on how brusatol leads to Nrf2 downregulation (Ren *et al,* 2011; Olayanju *et al,* 2015).

The following chapter describes a series of experiments that were designed to define the mechanism by which brusatol triggers Nrf2 protein depletion, using a combination of advanced live-cell imaging methods, alongside functional and quantitative studies in SK-N-AS neuroblastoma cells.

6.3. RESULTS

6.3.1. Brusatol Depletes Nrf2 Protein Levels and Transcriptional Activity in BAC$^{Nrf2\text{-}Venus}$ SK-N-AS Neuroblastoma cells

The ability of brusatol to deplete Nrf2 protein expression has been demonstrated in several cell types (Ren *et al,* 2011; Olayanju *et al,* 2015). Initial results in this study confirmed that brusatol effectively depleted Nrf2 levels in BAC$^{Nrf2\text{-}Venus}$ cells. As expected, brusatol induced depletion of Nrf2 was accompanied by a concomitant in ARE-Luc transcriptional reporter activity, which was detectable over a broad a range of brusatol concentrations from 1nM-300nM (Figure 6.1A) (viability assay in Supplementary Figure 8.2A). The 100nM concentration was selected for use in further studies, due to its potent reduction of the Nrf2 transcriptional activity and low toxicity, as demonstrated by the maintenance of cell viability, even after 24hrs of treatment (Figure 6.1B). Time course analysis of BAC$^{Nrf2\text{-}Venus}$ cells treated with 100nM brusatol revealed that Nrf2 transcriptional activity was greatly reduced, even after 2hr of drug application and appeared most potent following 8hr of treatment (Figure 6.1D). To verify the effect of brusatol on endogenous Nrf2 and Nrf2-Venus proteins, BAC$^{Nrf2\text{-}Venus}$ cells were treated with 100nM brusatol for 2h, 4h or 6h and lysates were processed for western blotting (Figure 6.1C). Both endogenous Nrf2 and Nrf2-Venus proteins showed an equivalent rapid depletion in response to the addition of brusatol, therefore modification of Nrf2 by fusion with the Venus fusion protein did not appear to significantly affect the rate of brusatol mediated degradation. Live cell imaging studies were then performed on BAC$^{Nrf2\text{-}Venus}$ cells to obtain more accurate information about Nrf2-Venus depletion kinetics (Figure 6.1E). Addition of 100nM brusatol reduced Nrf2-Venus nuclear fluorescence levels within 30min, with subsequent recovery occurring at around 8hr from the time of brusatol addition (Figure 6.1E, Movie 36).

6.3.2. Brusatol Triggers p65 Nuclear Translocation

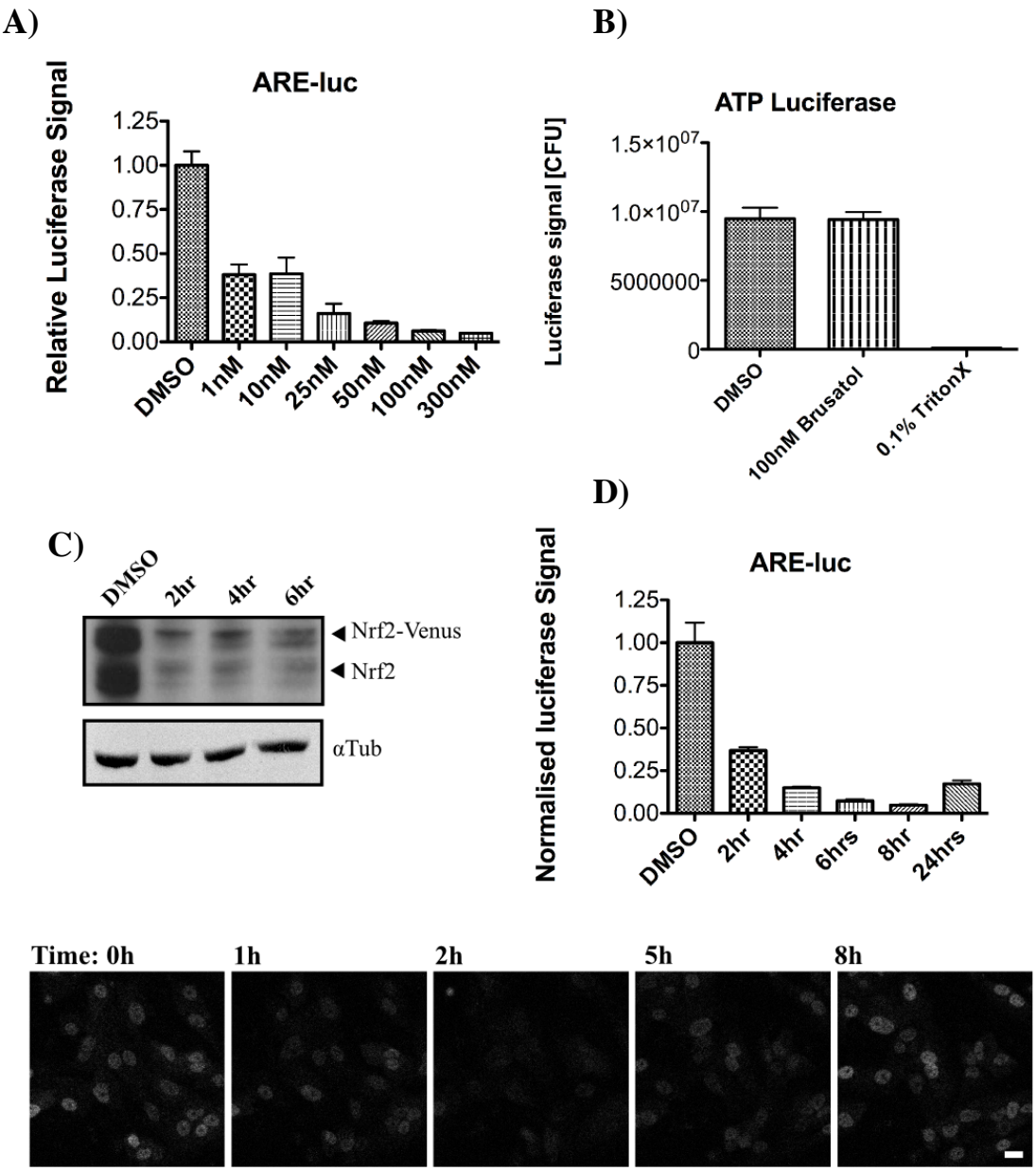

Figure 6.1 Brusatol mediated depletion of Nrf2 protein expression and inhibition of ARE-Luc transcriptional reporter activity. A) Relative effects of 1nM-300nM brusatol on ARE-Luc activity in BAC$^{Nrf2\text{-}Venus}$ neuroblastoma cells (6h treatment) (n=1, in triplicates). B) ATP-based cell viability analysis of of BAC$^{Nrf2\text{-}Venus}$ cells, following 24h treatment with DMSO, 100nM brusatol, or 0.1% Triton-X. Data shows minimal cytotoxicity of 100nM brusatol (n=2, in triplicates). C) Western blot of BAC$^{Nrf2\text{-}Venus}$ cell extracts showing comparable rates of depletion of endogenous Nrf2 and Nrf2-Venus proteins, following addition of 100nM brusatol at indicated time points. D) Changes in ARE-Luc activity following addition of 100nM brusatol in BAC$^{Nrf2\text{-}Venus}$ cells over-time (n=1, in triplicates). D) Representative time course images of BAC$^{Nrf2\text{-}Venus}$ cells following addition of 100nM brusatol (Movie 36). Error bars=SDEV, scale bar=20μm

Data presented in previous chapters established that the NF-κB and the Nrf2 pathways are closely linked. Therefore to determine if the effects of brusatol on Nrf2 also modulate NF-κB activity, p65 dynamics were imaged in parallel with Nrf2-Venus in tagRFP-p65/BAC$^{Nrf2\text{-}Venus}$ cells (Figure 6.2), and in BAC$^{Nrf2\text{-}Venus}$ cells transiently transfected with the p65-dsRedXP construct (Figure 6.2A-D). Interestingly, 100nM brusatol triggered different nuclear responses of Nrf2-Venus and p65 in both model systems (Figure 6.2A & B). Although Nrf2-Venus depletion followed the same kinetics in both systems, however the recovery phase was enhanced in cells stably expressing tagRFP-p65 (Figure 6.2C). Also, comparison of p65 responses observed with integrated tagRFP-p65, as opposed to plasmid encoded p65-dsRedXP, exposed differences in p65 responses to 100nM brusatol. In particular, p65-dsRedXP showed enhanced nuclear accumulation following addition of brusatol (Figure 6.2D). This trend was also validated by western blot analysis of nuclear lysates extracted from the BAC$^{Nrf2\text{-}Venus}$ neuroblastoma cells treated with 100nM brusatol (Figure 6.2E).

In order to measure the functional responses of Nrf2 and NF-κB to addition of 100nM brusatol in BAC$^{Nrf2\text{-}Venus}$ cells the relative expression profiles of canonical gene targets of both transcription factors were investigated by Q-PCR (Figure 6.3). The effect of brusatol-induced Nrf2 depletion was assessed by measuring relative changes in mRNA levels of four classical Nrf2 gene targets GCLC, NQO1, TRXN1, and Bach 1 (Figure 6.3A-D). Significantly, 8hr exposure to 100nM brusatol did not reduce mRNA levels of all canonical Nrf2 target genes. Surprisingly, we observed an increase in levels of GCLC (Figure 6.3B) and Bach1 mRNA (Figure 6.3D). In contrast, TRXN1 mRNA did show a decrease in response to brusatol (Figure 6.3C), whereas NQO1 did not exhibit any change in expression between control or brusatol treated cells (Figure 6.3A). Interestingly, 8hr exposure to 100nM brusatol was sufficient to evoke a potent increase in all measured NF-κB target genes including IL-6, SOD-2 and IKBα (Figure 6.3E-G), and significantly, also in the Nrf2 expression (Figure 6.3I). To further validate this result, quantification of NF-κb-Luc luciferase activity was performed following addition of 100nM brusatol for 6hrs in BAC$^{Nrf2\text{-}Venus}$ cells (Figure 6.3H). In contrast to the results obtained by Q-PCR, the

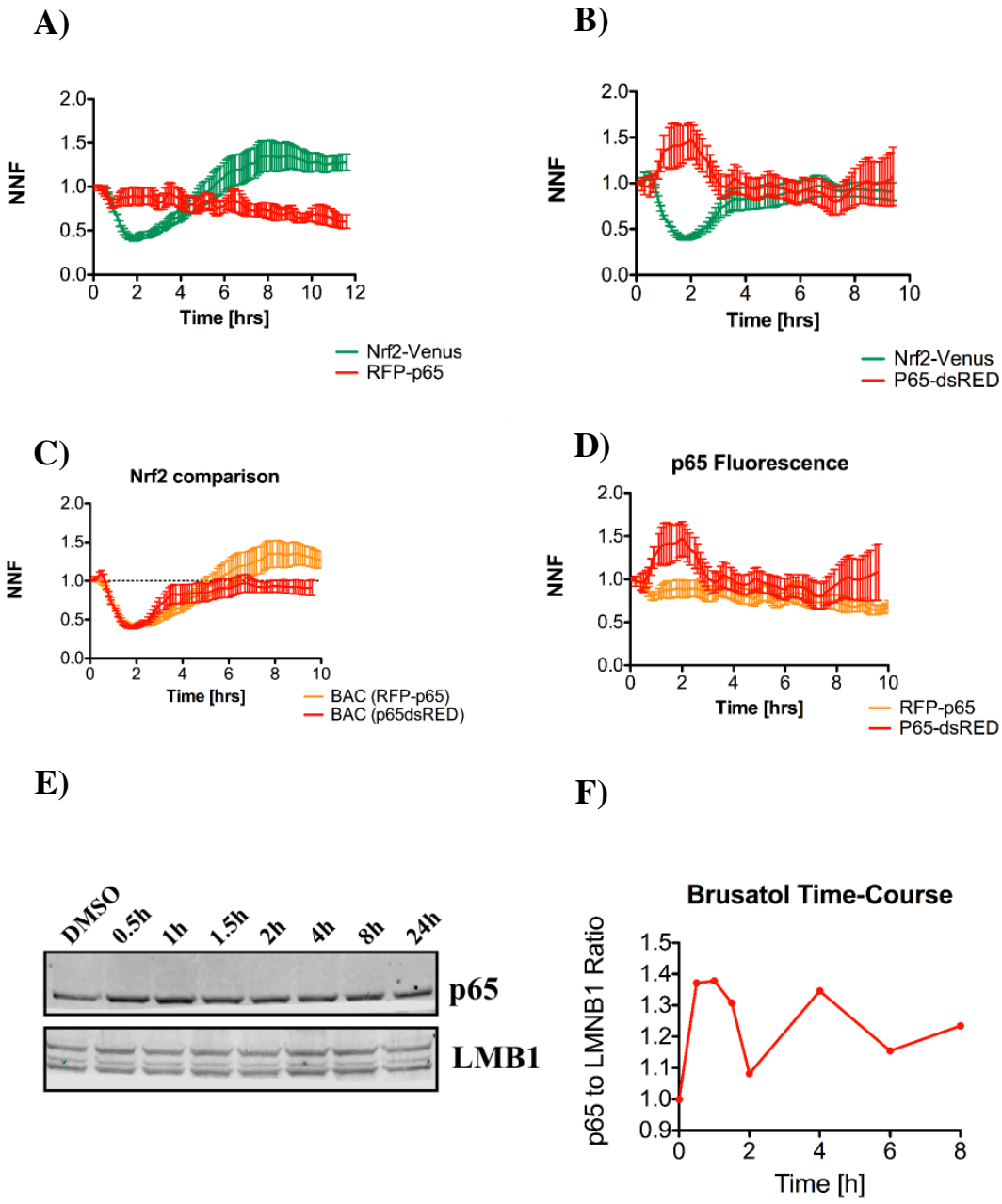

Figure 6.2 Brusatol causes changes in p65 nuclear levels. A) Imaging nuclear fluorescence levels of Nrf2-Venus and p65 in tagRFP-p65/BAC$^{Nrf2\text{-}Venus}$ (n=2, c=13) and B) BAC$^{Nrf2\text{-}Venus}$ expressing p65-dsRedXP in response to 100nM brusatol (n=1, c=8). C) Comparison of the effect of 100nM brusatol on the nuclear Nrf2-Venus depletion and recovery in BAC$^{Nrf2\text{-}Venus}$ transiently expressing p65-dsRedXP and stably transduced with tagRFP-p65. D) Comparison of the p65-dsRedXP and tagRFP-p65 nuclear dynamics in response to 100nM brusatol. E) Western Blot on nuclear BAC$^{Nrf2\text{-}Venus}$ fractions following 100nM brusatol time course showing increased nuclear translocation of p65 protein. F) Quantification of relative nuclear p65 protein changes from Western blot analysis, using ImageJ. Error bars=SEM.

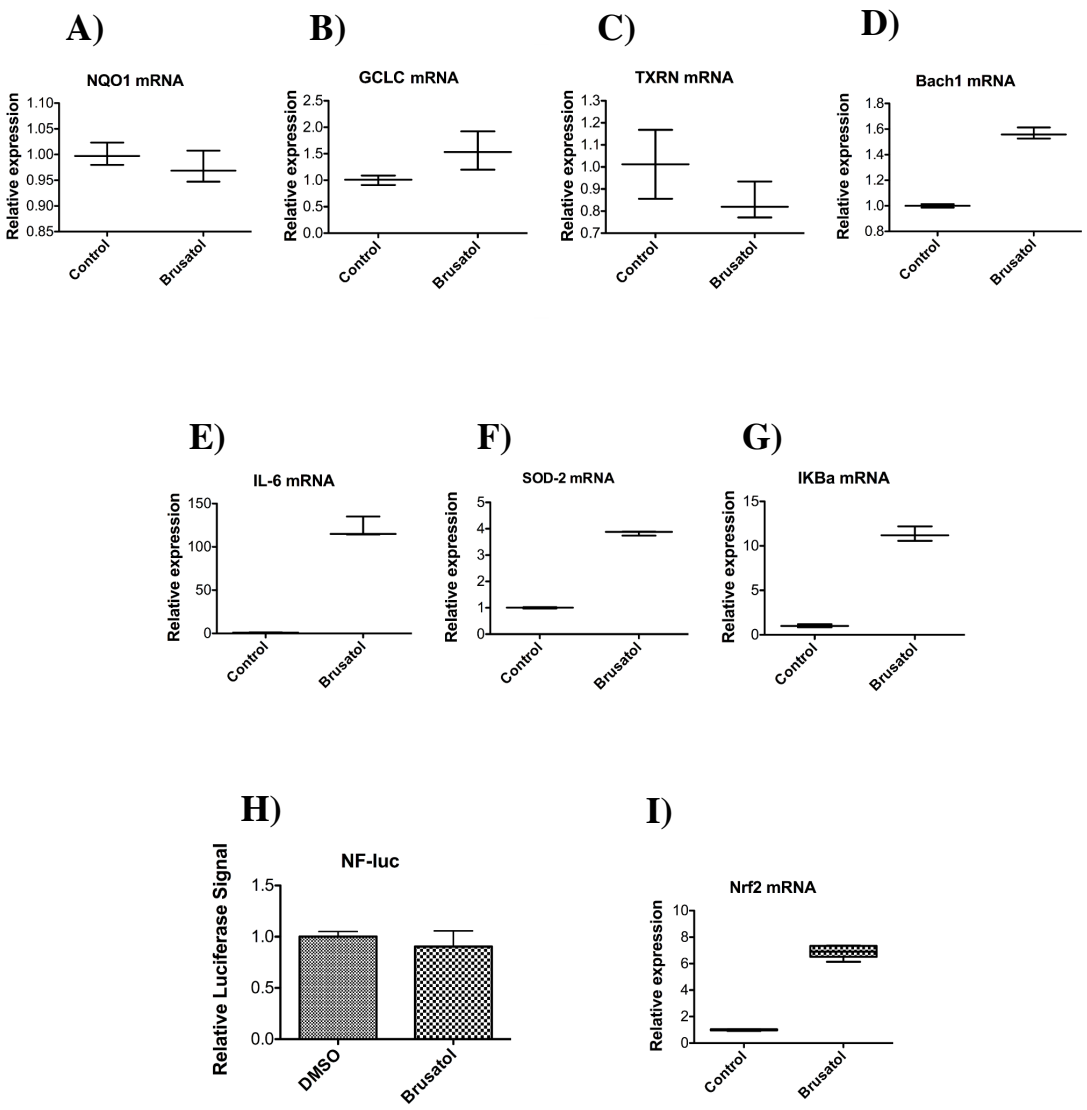

Figure 6.3 Effects of 100nM brusatol on Nrf2 and NF-κB transcriptional activity. Relative mRNA levels of A) NQO1, B) GCLC, C) TRXN1 and D) Bach1 following addition of 100nM brusatol for 8h. E-G) Relative expression of the NF-κB target genes was significantly increased by 8hr incubation with 100nM brusatol. H) NF-κB transcriptional activity was assessed by measuring the relative levels of NF-κb-Luc luminescence following 6h incubation with 100nM brusatol. I) Relative expression levels of Nrf2 mRNA following 8h incubation with 100nM brusatol. Error bars=STDEV, n=1, in triplicates.

5xκB driven luciferase reporter did not show any changes in activity as a result of brusatol application (Figure 6.3H).

6.3.3. Brusatol Does Not Inhibit N*RF2* Gene Expression

To investigate the possibility of inhibiting Nrf2 transcription, an analysis of the regulation of *NRF2* promoter activity was performed using the pNRF2-Luc transcriptional reporter construct. Results from this analysis show that transcriptional activity driven by the Nrf2 promoter sequence was significantly reduced following addition of brusatol (Figure 6.4A). To further validate this result, lentiviral transduction of SK-N-AS cells was performed with a Venus tagged mouse Nrf2 protein sequence driven by either a *UBC* or the mouse *NRF2* gene proximal (*2kb*) promoters region (Maps in Supplementary 8.3). Changes in Venus-Nrf2 nuclear fluorescence driven by either *UBC* or *2kb* sequence are shown in Figure 6.4B, which demonstrated that brusatol induces a decline in Nrf2 fluorescence regardless of the promoter sequences used to drive the Venus-Nrf2 expression (Figure 6.4B & Figure 6.4C). Therefore from this data we can conclude that brusatol does not act by inhibiting Nrf2 transcription.

6.3.4. Use of a Photoswitchable pDendra2-Nrf2 Fusion Protein to Investigate the Mechanism of Action of Brusatol on Nrf2.

To study the effect of brusatol on Nrf2 protein stability and synthesis the pDendra2-Nrf2 was used for live cell imaging experiments (Figure 6.5). In these studies, pDendra2-Nrf2 was transiently expressed in SK-N-AS cells and the imaging procedure was performed as previously described (Methods Section 2.13.2). Initially, a whole field UV illumination method was used to photoconvert the green pDendra2-Nrf2 into a red photoshifted form of pDendra2-Nrf2 in all cells
within the field of view (Figure 6.5). The nuclear levels of pDendra2-Nrf2 were investigated following UV photoconversion and treatment with DMSO (Figure 6.5A), protein translation inhibitor CHX 10μg/ml (Figure 6.5B) or 100nM brusatol (Figure 6.5C). Changes in green and red fluorescence of Dendra2-Nrf2 enabled a distinction to be made between brusatol effecting either the stability or synthesis of Nrf2. Data presented in Figure 6.5A & D shows that DMSO treatment led to a stable

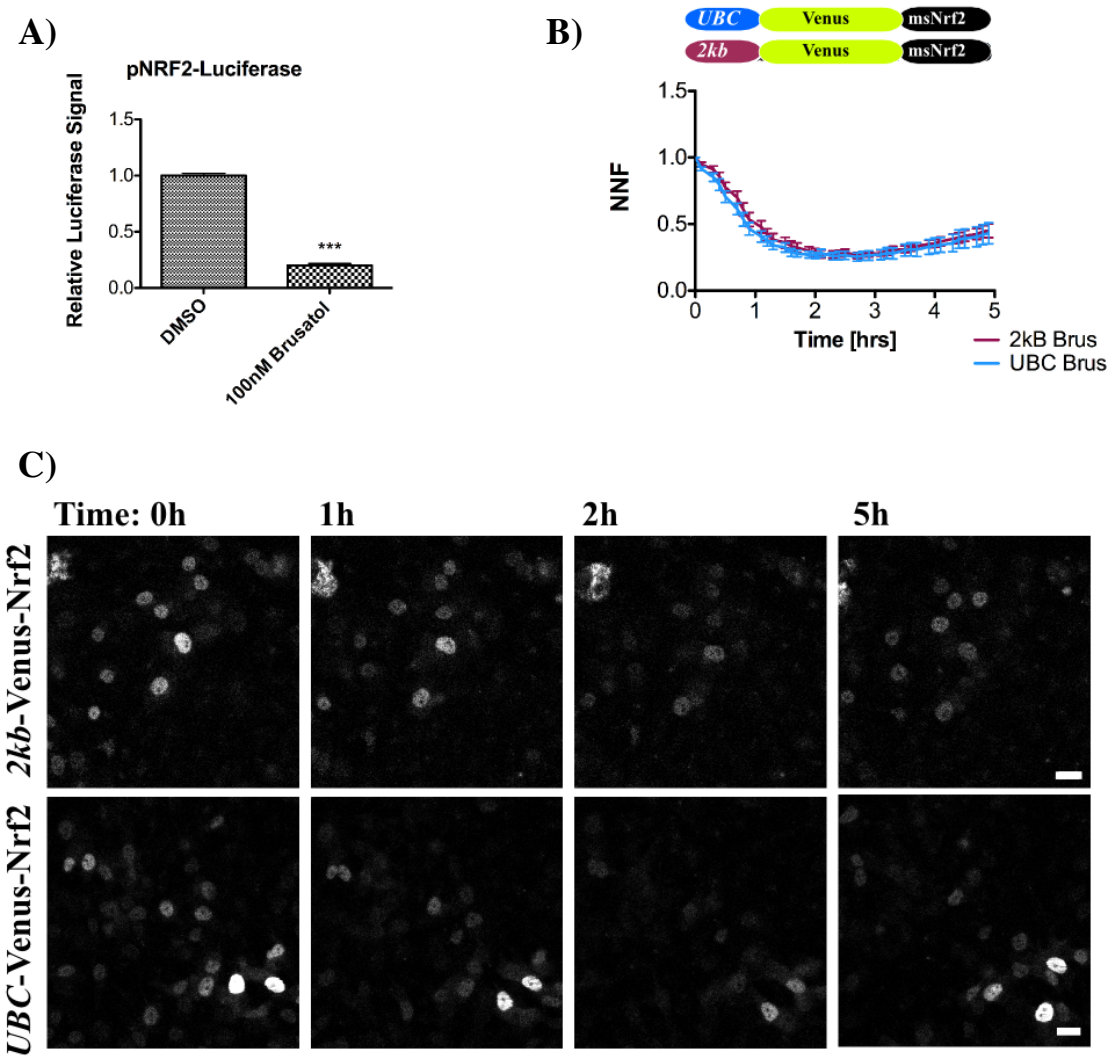

Figure 6.4 Brusatol does not regulate Nrf2 transcription. A) pNRF2-luc transcriptional reporter activity in BAC$^{Nrf2\text{-}Venus}$ cells treated with either DMSO or 100nM brusatol for 6h (n=3). B) Normalised nuclear fluorescence levels of Venus-Nrf2 measured during live-cell imaging of SK-N-AS cells transduced with lentivirus encoding either *UBC*-driven (*UBC*-Venus-msNrf2) or proximal promoter-driven (*2kb*-Venus-msNrf2) Venus-msNrf2, following addition of 100nM brusatol (c=11-14). C) Representative images from *UBC*-Venus-msNrf2 or *2kb*-Venus-msNrf2 experiments shown in C). Error bars= SEM(imaging)/STDEV(luciferase). Scale bar =20μm.

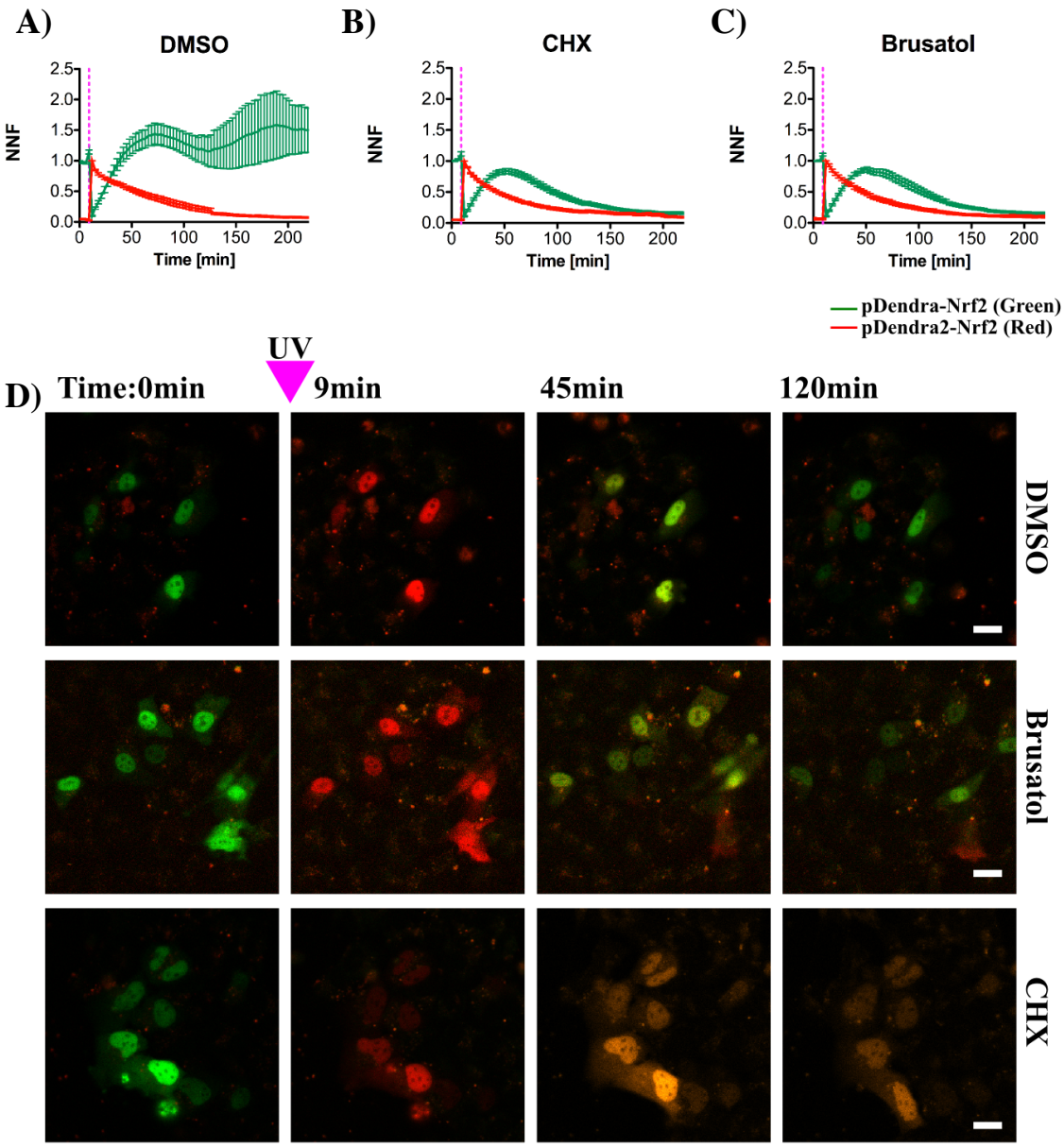

Figure 6.5 Brusatol inhibits Nrf2 protein synthesis. A) Relative nuclear fluorescence of red and green pDendra2-Nrf2 expressed in SK-N-AS cells, following addition of DMSO (n=4, c=14) (Movie 37a), B) 10µg/ml CHX (n=4, c=16) (Movie 37c) or C) 100nM brusatol (n=4, c=17) (Movie 37b). D) Representative time-lapse images from live cell imaging experiments showing green and red populations of pDendra2-Nrf2 before and after photoconversion. Drugs were applied immediately before UV light treatment (indicated by purple, dashed line). Error bars=SEM. Scale bar=20µm.

decline in photoconverted red pDendra2-Nrf2 and a parallel recovery of green pDendra2-Nrf2 signal, which eventually exceeded the initial nuclear fluorescence levels. The increase in green pDendra2-Nrf2 observed following brusatol addition, was transient and decreased rapidly after 1hr exposure to the drug. (Figure 6.5C & D). Therefore, this data shows that brusatol interferes with the production of new pDendra2-Nrf2 protein. Significantly, application of cycloheximide resulted in a very similar trend in green Dendra2-Nrf2 nuclear fluorescence, as that observed in response to brusatol (Figure 6.5B & D).

The relative nuclear fluorescence of green and red pDendra2-Nrf2 is compared in Figure 6.6. It was evident that brusatol and CHX both impair the synthesis of newly formed green pDendra2-Nrf2, which exhibited a distinct recovery pattern to that observed in DMSO treated control SK-N-AS neuroblastoma (Figure 6.6A). Half-life measurements of the red pDendra2-Nrf2 were slightly different between experimental conditions, with the most stable Nrf2 protein ($t_{1/2}$=48min) measured in control cells, while the least stable ($t_{1/2=}$29min) was observed in CHX treated cells (Figure 6.6B), however the relative nuclear fluorescence decay of the photoconverted Nrf2 protein was very similar between DMSO, brusatol and CHX samples (Figure 6.6B).

The comparable inhibition of Nrf2 protein synthesis promoted by brusatol and CHX drugs was further confirmed by measuring pDendra2-Nrf2 fluorescence following inhibition of proteasomal degradation with 10μM MG132 (Figure 6.7). MG132 treatment resulted in a gradual accumulation of newly made green pDendra2-Nrf2 over time together with an increased stability of photoconverted red pDendra2-Nrf2 (Figure 6.7A, Movie 38a). Combined application of MG132 with either 10μg/ml CHX (Figure 6.7B, Movie 38b) or 100nM brusatol (Figure 6.7C, Movie 38c) led to the stabilisation, rather than an increase in green pDendra2-Nrf2 nuclear fluorescence (Figure 6.7D). What is more, the stability of nuclear photoconverted (red) Dendra2-Nrf2 was comparable between cells treated with MG132 alone or in combination with either brusatol or CHX (Figure 5.7E).

Therefore both CHX and brusatol impaired the accumulation of newly made Dendra2-Nrf2 without affecting the stability of pre-formed Nrf2 protein.

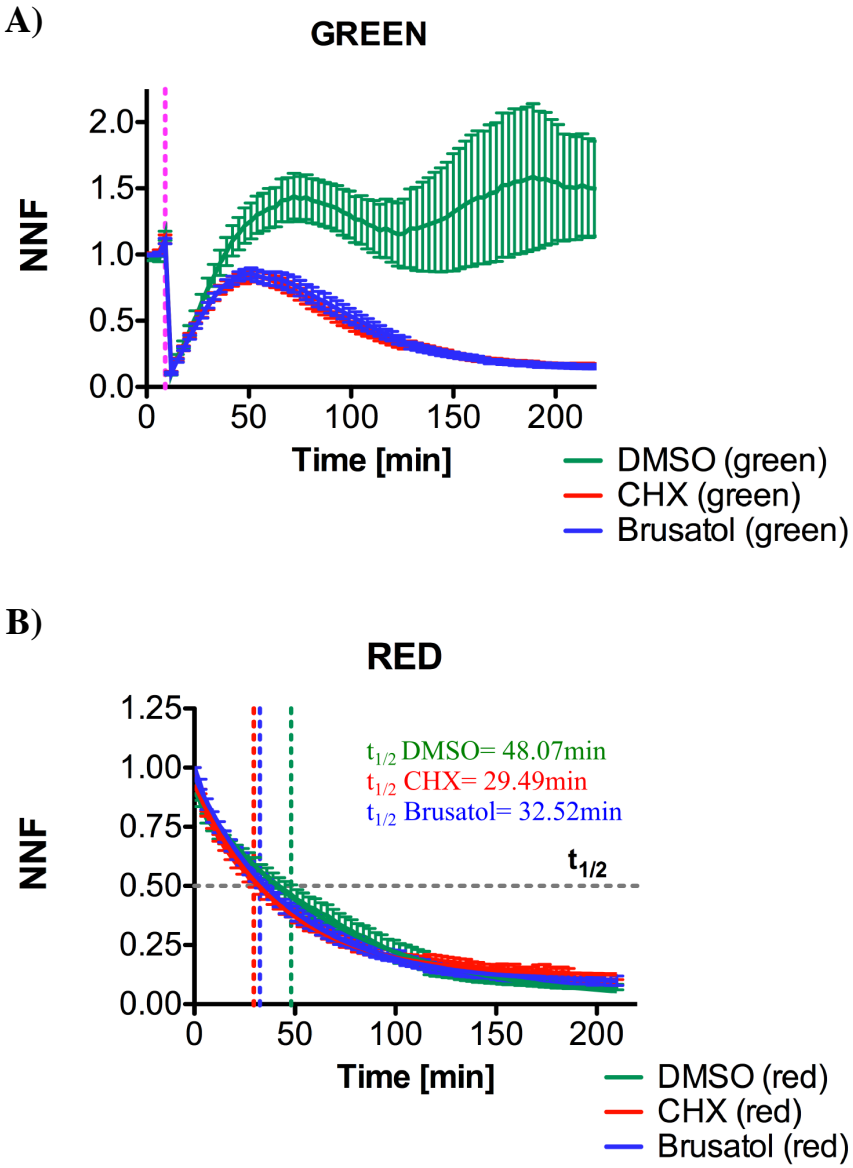

Figure 6.6 Brusatol acts by inhibiting Nrf2 translation. A) Comparison of the relative, nuclear photoconverted red pDendra2-Nrf2 or newly made green pDendra2-Nrf2 levels, in cells treated with DMSO, 10μg/ml CHX or 100nM brusatol. Comparable dynamic trends of newly made Nrf2 fluorescence (green) are observed in CHX and brusatol treated cells. Control cells maintain steady levels of new Nrf2 (green) synthesis. B) The half-life of pDendra2-Nrf2 proteins was calculated from the decay rate of red fluorescence, and did not display considerable variation between the samples. Half-life calculations were performed by fitting data to exponential non-linear regression function using a one-phase decay equation (Methods 2.13.2). Error bars=SEM.

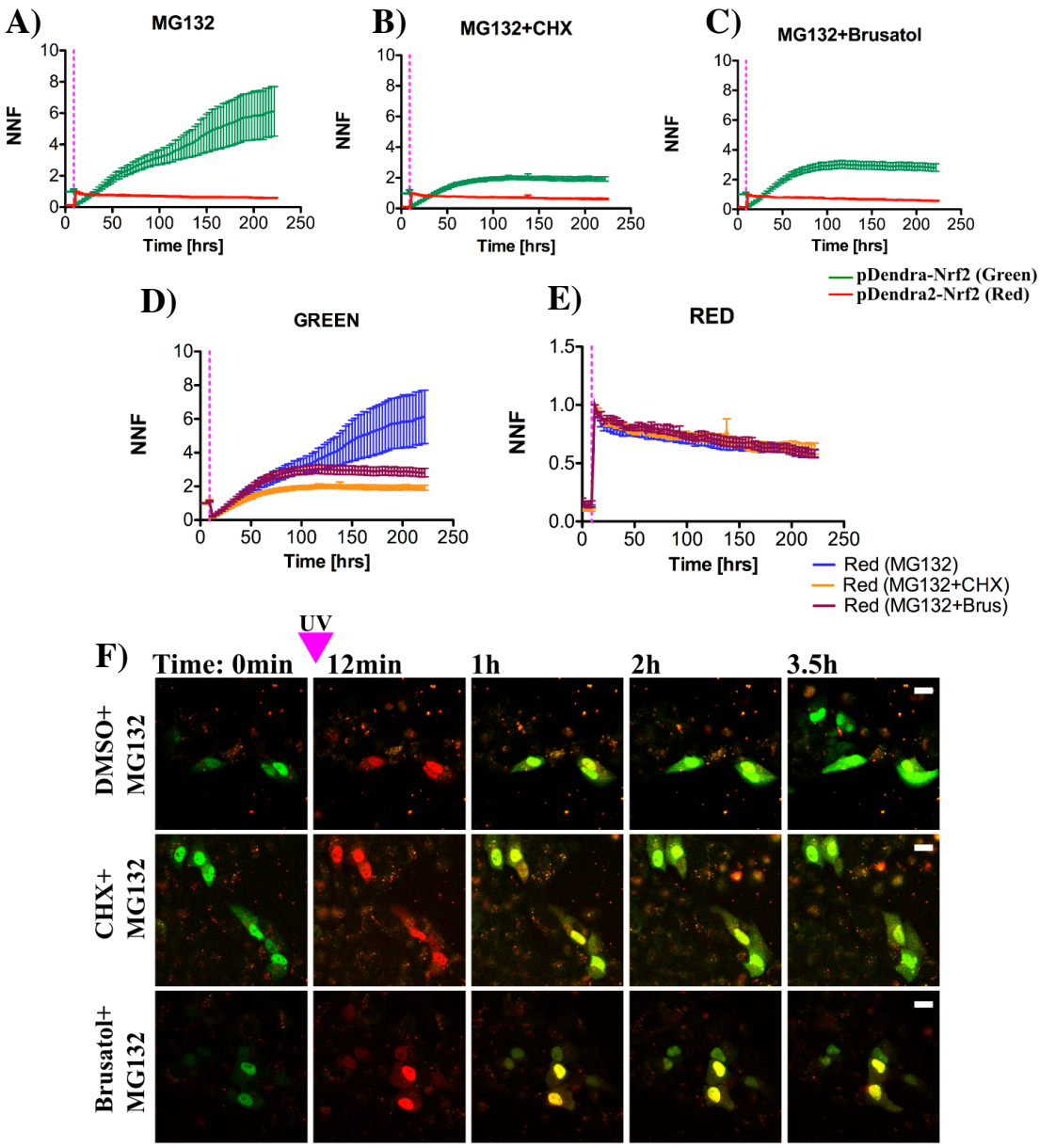

Figure 6.7 Brusatol and CHX block the gradual accumulation of Nrf2 protein following inhibition of proteasomal activity. A) Comparison of dynamic changes in green and red forms of pDendra2-Nrf2 in response to 10μM MG132 (n=6, c=21) (Movie 38a) or B) co-administration of 10μM MG132 + 10μg/ml CHX (n=4, c=14) (Movie 38b) or C) 10μM MG132 + 100nM brusatol (n=4, c=20) (Movie 38c). D) Co-administration of CHX or brusatol with MG132 stabilised pDendra2-Nrf2 fluorescence. The green fluorescence of pDendra2-Nrf2 logarithmically increased following addition of 10μM MG132 to SK-N-AS cells. E) Comparison of the photoconverted (old) pDendra2-Nrf2 protein did not show considerable differences in Nrf2 protein stability between the treatments. F) Representative images from live-cell imaging experiments. Error bars=SEM, scale bar=20μm.

A)

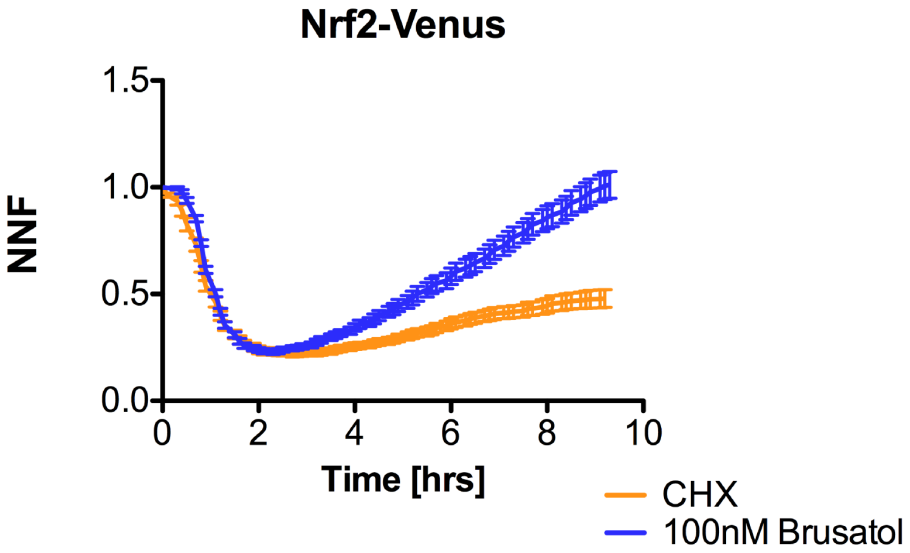

B)

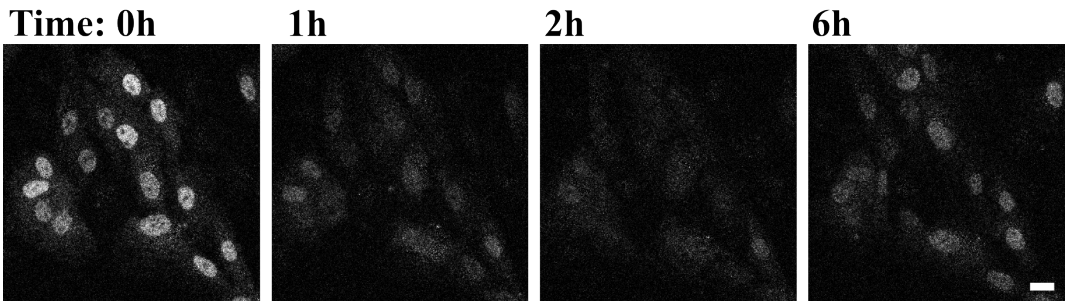

Figure 6.8 The inhibition of Nrf2 protein synthesis by brusatol is more transient than the action of CHX. A) Relative levels of nuclear Nrf2-Venus in BAC$^{Nrf2\text{-}Venus}$ cells treated with 100nM brusatol or 10µg/ml CHX measured in live cells (n=3, c=23-34). B) Representative images taken from the BAC$^{Nrf2\text{-}Venus}$ cells treated with 10µg/ml CHX (Movie 39). Scale bar=20µm.

Furthermore, live cell imaging was performed on $BAC^{Nrf2\text{-}Venus}$ neuroblastoma to compare the effect of CHX and brusatol on the kinetics of Nrf2 protein depletion (Figure 6.8, Movie 39). Measurement of the rate of depletion of nuclear Nrf2-Venus demonstrated that the speed of depletion of Nrf2 was similar between both treatments, however the recovery of Nrf2 was faster following brusatol application (Figure 6.8A).

6.3.5. Determination of brusatol target specificity

In order to verify if brusatol acts specifically on Nrf2 protein synthesis, or generally inhibits global translation, a functionally unrelated cytoplasmic protein Dendra2-MARCH5 was transiently expressed and imaged in SK-N-AS cells treated with DMSO (Figure 6.9A, Movie 40a), 10μg/ml CHX (Figure 6.9B, Movie 40c) or 100nM brusatol (Figure 6.9C, Movie 40b). The kinetics of photoconverted pDendra2-MARCH5 in control cells followed slow decay concomitantly with accumulation of the new (green) pDendra2-MARCH5 expression (Figure 5.9A). Dynamic changes in green and red Dendra2-MARCH5 following CHX and brusatol treatments are presented in Figures 6.9D & E. Comparison of the cytoplasmic fluorescence levels of pDendra2-MARCH5 between the experimental conditions exposed differences in the synthesis levels of pDendra2-MARCH5, which appeared to be reduced in both CHX and brusatol treated cells (Figure 6.9E). However, the dynamics of red pDendra2-MARCH5 fluorescence decay were closely matched in all experiments (Figure 6.9F), indicating that brusatol, may have a nonspecific effect on the synthesis of a wider array of proteins, without compromising their stability.

To further reinforce this hypothesis the SV40-Renilla (Promega) was transiently expressed in $BAC^{Nrf2\text{-}Venus}$ cells and the luminescence output was compared between 100nM brusatol treated cells treated for different time-points (Figure 6.10A). The Renilla luminescent signal was significantly reduced in brusatol treated cells with time, with the most pronounced reduction in Renilla luminescence following 24h treatment (Figure 6.10B) suggesting the drug can alter the translation of the Renilla protein itself, indicating its non-specific mode of action.

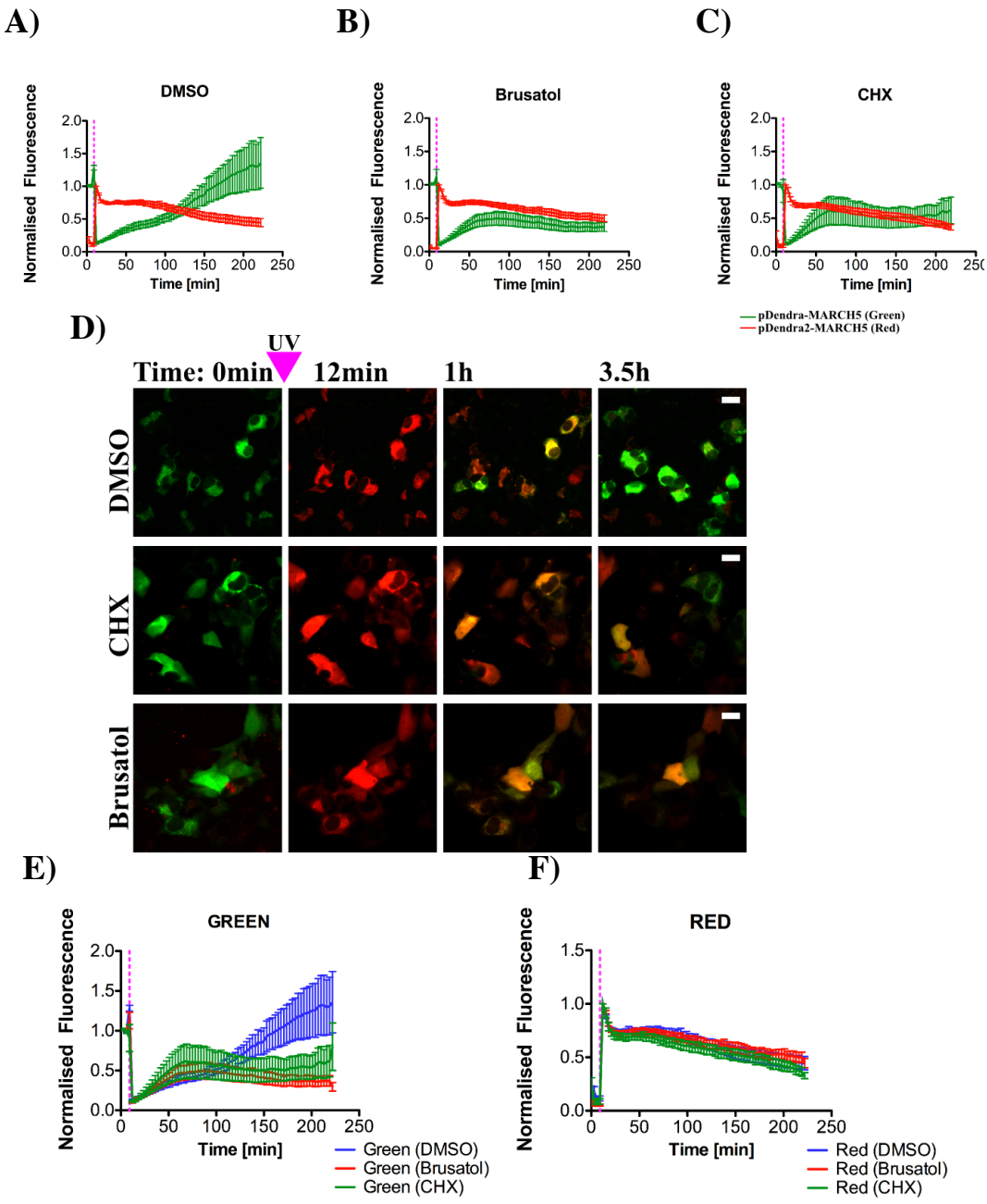

Figure 6.9 Investigating the specificity of brusatol-mediated inhibition of protein synthesis. A) pDendra2-MARCH5 was transiently expressed in SK-N-AS cells and green and red fluorescence levels were analyzed following photoconversion and treatment with either DMSO (n=2, c=21) (Movie 40a), B) 10µg/ml CHX (n=3, c=12) (Movie 40c) or C) 100nM brusatol (n=4, c=19) (Movie 40b). D) Representative images of green fluorescence taken from live cell imaging experiments shown in panels A-C (Movies 40a-c (See supplementary list)). E) Comparison of dynamic changes in newly-made green pDendra2-MARCH5 or F) photoconverted red pDendra2-MARCH5 protein dynamics. The green fluorescence levels of pDendra-MARCH5 displayed differences in the dynamic recovery profiles between control (DMSO) and 10µg/ml CHX or 100nM brusatol treated cells. Error bars=SEM.

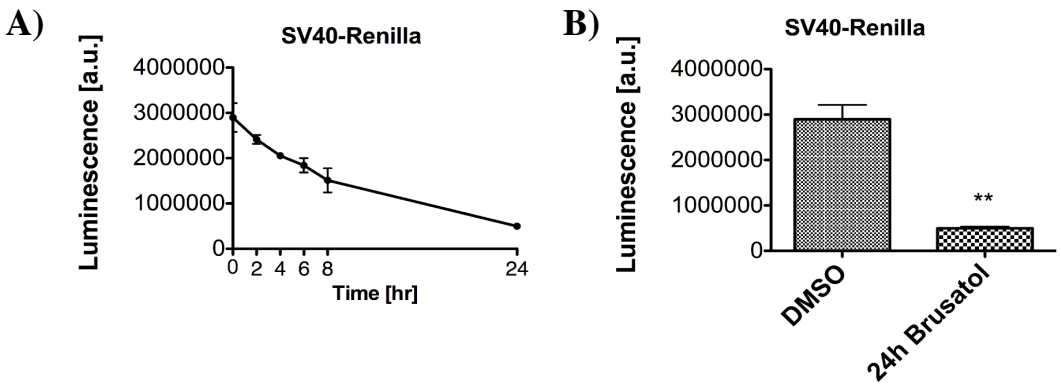

Figure 6.10 Brusatol reduces expression of Renilla luminescent signal. A) 100nM brusatol was applied for indicated time-points in BAC$^{Nrf2\text{-}Venus}$ cells transfected with SV40-Renilla. The Renilla luminescence decreases sharply with prolonged brusatol treatment, n=3 in triplicates. B) Comparison of control and Brusatol treated SV40-Renilla signal in BAC$^{Nrf2\text{-}Venus}$ cells following 24h treatment (n=3, in triplicates). Error bars=STDEV

6.4. Discussion

The Nrf2 signalling pathway acts as the double edge sword in disease, providing protection against oxidative stress, but also promoting tumourgenesis by rendering the cancer cells resistant to radio- and chemotherapy. Therefore, it is anticipated that pharmacological targeting of the Nrf2 pathway can lead to sensitisation of cancer cells to chemotherapy (Ren *et al,* 2011). Although previous studies identified brusatol as a potent inhibitor of Nrf2 antioxidant signalling however; there have been conflicting reports as to how this negative regulation is achieved (Olayanju *et al,* 2015).

Data presented in this chapter provide novel evidence into the mechanism, by which brusatol mediates the downregulation of Nrf2 protein expression, using sophisticated live-cell imaging approach combined with complementary population-level functional studies.

The BAC$^{Nrf2\text{-}Venus}$ neuroblastoma cell line provides an excellent experimental model for imaging the dynamic changes imposed by exposure to brusatol, as endogenous Nrf2 and the Venus labelled Nrf2 were shown to exhibit very similar responses to

100nM brusatol (Figure 6.1C). The inhibitory effect of brusatol on antioxidant gene expression has not been previously investigated in neuroblastoma cell lines, however we have demonstrated that even extremely low concentrations of brusatol (1nM) were sufficient to inhibit the 5xARE expression in SK-N-AS cells (Figure 6.1A).
Data presented in Result Chapters 2 and 3 demonstrate the close link between antioxidant and inflammatory pathways in neuroblastoma cells. In addition, studies by Cuendet *et al* show evidence that brusatol induced differentiation of HL-60 cells by activating NF-κB nuclear translocation and DNA binding (Cuendet *et al,* 2004). Therefore, in this context, it was important to verify if brusatol could modulate NF-κB pathway activity. Interestingly, the behaviour of p65 in response to brusatol varied between the plasmid-encoded p65-dsRedXP protein and stably expressed fluorescent tagRFP-p65 fusions (Figure 6.2A, B & D), the latter showing clear evidence of nuclear translocation. Significantly, nuclear entry of p65 was also correlated with a subsequent depletion of nuclear Nrf2-Venus, thus reinforcing evidence for the functional reciprocity between antioxidant and inflammatory signalling (Figure 6.2B). The reason for p65 activation remains unclear, however it was additionally correlated with increased transcription of a selection of canonical NF-κB target genes (Figure 6.2E). At this stage it cannot be concluded that brusatol leads to a general increase in NF-κB transcriptional activity (Figure 6.3B), as 5xκB driven luciferase expression remained unchanged (Figure 6.3C). However, in the context of our data there may be a logical explanation for these apparently dichotomous results. If, as our data suggests, brusatol acts by inhibiting protein translation but not transcription it is reasonable that mRNA levels may increase without a correlated increase in luciferase reporter expression, as this system is dependant on both transcription and translation of the luciferase reporter.

Equally, inhibition of Nrf2 by brusatol has previously been associated with a decrease in expression of Nrf2 target genes (Ren *et al,* 2011; Olayanju *et al,* 2015), however, this was not observed in SK-N-AS cells by Q-PCR (Figure 6.3A.) in contrast to results obtained with ARE-Luc transcriptional reporter assays, which was very sensitive to brusatol induced changes in Nrf2 inhibition (Figure 6.1A and D). As the reduction in Nrf2 target gene expression in A549 and Hepa-1c1c7 cells was detected after a more prolonged exposure to brusatol (12-16h), it would be

interesting to see if extending the time of brusatol application would have a more pronounced effect on antioxidant gene transcription in SK-N-AS cells (Ren *et al,* 2011; Olayanju *et al,* 2015).

Interestingly, our data shows that brusatol actually promotes the accumulation of Nrf2 mRNA (Figure 6.3D), even though the *NRF2* promoter activity was sharply reduced (Figure 6.4A), suggesting that the increase of mRNA levels was not simply associated with an increased rate of Nrf2 gene expression, as a result of increased conditional NF-κB driven transcriptional activity. Furthermore, live-cell imaging experiments using *UBC* and *2kb* driven Venus-Nrf2 fusions demonstrate that the promoter sequence did not have an effect on the sensitivity of Nrf2 expression to brusatol (Figure 6.4B and C), therefore the possibility of transcriptional inhibition of Nrf2 by brusatol was rejected.

The results from our studies confirm that brusatol induces depletion of Nrf2 protein levels, while mRNA levels remained high. This phenotype was previously described by Olanyu *et al*, who also demonstrated that the depletion of Nrf2 protein was independent of the proteasome activity (Olayanju *et al,* 2015). However, an earlier report on the mechanism of brusatol-mediated Nrf2 inhibition presented evidence that brusatol does not affect Nrf2 mRNA levels, but did enhance ubiquitin-mediated degradation (Ren *et al,* 2011).

Live-cell imaging of pDendra2-Nrf2 dynamics has provided new and definitive evidence as to the molecular mechanism of brusatol inhibition, in terms of the existing debate between the regulation of Nrf2 synthesis or degradation (Figure 6.5-6.9). The stability of pDendra2-Nrf2 was not affected in DMSO (Figure 6.5A), 10μg/ml CHX (Figure 6.5B), or 100nM brusatol (Figure 6.5C) treated samples, indicating that in neuroblastoma cells, brusatol does not compromise Nrf2 protein stability as suggested previously (Ren *et al,* 2011). The key to understanding the pharmacological effect of brusatol was the ability to measure dynamic changes in the production of new Nrf2 protein in single cells, using the pDendra2-Nrf2 construct. The relative nuclear fluorescence of newly formed green pDendra2-Nrf2 displayed a parabolic shape in cells treated with 100nM brusatol and 10μg/ml CHX, in contrast

to control cells, which exhibited a gradual increase (Figure 6.6A) in Nrf2 abundance. The comparison of CHX and brusatol treated SK-N-AS cells expressing pDendra2-Nrf2 demonstrated that both drugs exhibit comparable dynamic profiles of green Dendra2-Nrf2 depletion, reinforcing the hypothesis that brusatol acts to impede Nrf2 protein translation (Figure 6.6A).

The speed by which brusatol leads to a reduction in protein synthesis was previously estimated to occur following a lag of 2-4min at 30ºC in rabbit reticulocytes, however the concentration of drug used was 1000x higher then that applied here (Willingham *et al,* 1984). Therefore, due to the fast pharmacokinetics of brusatol the observed initial increase of green Dendra2-Nrf2 following addition of 10μg/ml CHX and 100nM brusatol treated samples was not anticipated (Figure 6.6A). However, we hypothesise that this transient increase in pDendra2-Nrf2 synthesis (following UV treatment) is caused by the post-translational folding time of the pDendra2 fluorescent tag (Chudakov *et al,* 2007). Therefore, as brusatol and CHX are expected to act at the stage of translation they will inevitably be a pool of already translated pDendra2-Nrf2, which acquires fluorescent properties after inhibition of protein synthesis (Figure 6.6A).

Stabilisation of pDendra2-Nrf2 by proteasome inhibition the direct comparison of dynamic changes in levels of newly synthesised pDendra2-Nrf2 in cells treated with MG132 alone, or in combination with brusatol or CHX (Figure 6.7). In both cases, inclusion of CHX or brusatol prevented the accumulation of newly formed protein, which was reflected by a steady decrease in nuclear green pDendra2-Nrf2. In contrast, to cells treated with MG132 alone, where protein translation was unaffected (Figure 6.7D).

Additional similarities between brusatol and CHX effects were demonstrated by live-cell imaging of $BAC^{Nrf2\text{-}Venus}$ cells, showing very similar Nrf2-Venus protein depletion dynamics (Figure 6.8B). However, the reduction of Nrf2-Venus fluorescence was more transient in brusatol treated cells compared to CHX mediated depletion. This difference may highlight key differences between the relative kinetics of drug stability or action. This observation may also reflect a more selective mode of action of brusatol compared to CHX. In this scenario a short window of inhibition, will

have a greater effect on reducing the levels of short-lived proteins, compared to those with longer half-lives.

Lastly, in order to investigate the potential specificity of brusatol action, it was important to compare the effects of brusatol on another relatively unstable with and functionally unrelated protein pDendra2-MARCH5 with half-life of around 1h, which is usually localised to the cytoplasm and mitochondria (Figure 6.9) (Nagashima *et al,* 2014). Live-cell imaging experiments show that brusatol did not exclusively affect Nrf2 or components of the antioxidant response pathway, but also had an effect on the levels of green cytoplasmic pDendra2-MARCH5 levels, which showed impaired recovery following the photoconversion process (Figure 6.9A-D). The changes in green fluorescence signal followed similar dynamics following addition of CHX or brusatol, both of which were distinct to the pattern observed in control cells (Figure 6.9E). This effect was likely to result from the fact that brusatol and CHX both act by inhibiting translation of pDendra2-MARCH5, without affecting the stability of the photoconverted red pDendra2-MARCH5 (Figure 6.9E & F). This data suggests that brusatol is likely to have a global effect on protein synthesis, which could also explain the observed non-specific action of brusatol on the NF-κB pathway. The half-life of free IKBα is reported to be <10min (Berggvist *et al*, 2009), therefore a transient enforced decrease in IKBα expression could result in a burst of p65 nuclear translocation and the subsequent activation of NF-κB target gene transcription.

What is more, the discrepancies observed between the mRNA measurements used to assess the transcriptional activity of Nrf2 and NF-κB in response to brusatol were not in agreement with results obtained by luciferase reporter assays (Figure 6.1A & 3C). However, it should be noted that as brusatol appears to have a general effect on protein translation, it would also diminish the luminescence signal of the SV40-Renilla luminescence, which was used as a transfection control (Figure 6.10). This can result in misleading measurements of transcription factor activity assays based on dual luminescence of luciferase and Renilla proteins and interpretation of results obtained with this assay should be treated with caution. This will be especially relevant in the application ARE-Luc reporter, which contains a destabilising PEST

sequence that enhances luciferase degradation process and leads to shortening the half-life of luciferase from 3h to 15min (Promega). Therefore, the dramatic inhibition of the ARE-Luc expression following very low (1nM) brusatol concentration could be caused by inhibition of both the luciferase and Renilla synthesis, rather than a decrease in transcriptional activity (Figure 6.1A). This highlights the importance of selecting appropriate methods for investigating brusatol and other compounds that may inhibit translation, as assays relying of short-lived protein tags (*e.g.* luciferase) are expected to generate different results to those obtained by measuring more stable proteins such as EGFP (half-life around 24h) or those based on the measurement of mRNA expression.

To summarise, this chapter provides essential evidence on the mechanism of action of brusatol on the Nrf2 pathway. Rather than compromising the Nrf2 protein stability as shown before by Ren *et al* (2011) brusatol actually leads to rapid depletion of Nrf2 by inhibition of protein translation, by an as yet unknown mechanism. This study emphasises the benefits of using photoswitchable fluorescent protein fusions and live cells imaging techniques to investigate the molecular mechanisms of poorly understood drug action. Nrf2 may well be particularly vulnerable to the action of brusatol due to its very short half-life, however the specificity of brusatol action remains to be defined, in order to evaluate potential off-target effects that may hinder its application in future clinical applications.

CONCLUDING DISCUSSION

The Nrf2 and NF-κB pathways are responsible for sustaining optimal cellular function, consequently deregulation of their activity precipitates the progression of a wide array of diseases. Both pathways are under intense research because of their involvement in a range of neurodegenerative disorders, such as amyotrophic lateral sclerosis, multiple sclerosis, Alzheimer's and Parkinson's diseases. To tackle these conditions it is imperative that we develop new therapeutic strategies to ameliorate the harmful consequences of chronic inflammation. With an increasing average age of the population, it is now even more important to understand how manipulation of anti-inflammatory and antioxidant pathways could contribute to the healthy aging process and ensure appropriate preventative measures.

To understand the interplay between these pathways, we performed a detailed analysis of Nrf2 and NF-κB temporal dynamics at single-cell resolution, in both murine neural cells and human SK-N-AS neuroblastoma cancer. The most significant outcomes of this study are discussed in the following paragraphs together with suggestions of future research directions. The thesis concludes with an assessment of the potential impact or utility of data generated in this study.

The function of the NF-κB pathway in the brain is not well defined, as there are conflicting reports on the stimuli that trigger cell-specific NF-κB signalling in neurons, astrocytes and microglia. It has became evident that glia play a prominent role in driving inflammatory responses in the nervous system. These cells have been shown to display a protective role, but can also drive chronic inflammation, leading to the development of neurological disorders (Vargas & Johnson, 2009). This study was initiated by investigating the NF-κB dynamics in primary cells isolated from the murine hippocampi.

The oscillatory pattern of the p65 nuclear shuttling was more prominent and prolonged in astrocytes grown in single cultures (Figure 3.6) as compared to the dampened oscillatory behavior observed in glia that were co-cultured with neurons.

It has been shown that the amplitude and frequency of NF-κB signaling defines the profile of expressed NF-κB response genes. This process is regulated by three components: IKKα, IKBα/ε and A20 (Paszek *et al,* 2010). It is possible that the observed difference in nuclear oscillatory patterns in astrocytes may occur as a result of a change in the expression of one or all of these components, which could result from neuronal paracrine signaling. This compelling result emphasizes the importance of investigating dynamic changes in simple, single culture environments, as well as in more complex experimental setups, which incorporates signaling output from different cell types. Interestingly, we also observed spontaneous p65 nuclear translocations in resting astrocytes, which were also associated with the subsequent increase of inflammatory transcription (Figure 3.8).

Surprisingly, there is a significant lack of literature addressing single cell Nrf2 responses to inducers using plasmid expression. The latest report by Xue *et al* presented evidence that addition of SFN did not cause Nrf2 nuclear accumulation, but prompted an increase in the frequency of nuclear shuttling events (Xue *et al,* 2014). However, the Nrf2 phenotype described in this study most likely results from stress related nuclear blebbing, leading to periodic nuclear rupture events, which we also observed in primary astrocytes expressing plasmid encoded mCherry-Nrf2 fusion and which have been previously well documented in the literature (De Vos *et al,* 2011; Hatch *et al,* 2013).

The tools generated for imaging the activity of the Nrf2 and NF-κB in neurons and astrocytes provided interesting and exciting insights into both pathways during basal and induced conditions (Results Chapter 1). The use of primary cells for investigating the molecular basis of cross-talk between the anti-oxidant and inflammatory pathways was very challenging and needed to be supported by an alternative cell culture model, which was more readily available for additional functional study. The human SK-N-AS $BAC^{Nrf2\text{-}Venus}$ neuroblastoma cells, which stably express Nrf2-Venus provided a perfect model for live-cell imaging of Nrf2 and p65 proteins, additionally providing information on a cancer (neuroblastoma) specific phenotype. The Venus tag had been chosen for imaging Nrf2 because of its bright fluorescence and very fast folding-time (~ 15min), which allows imaging of

newly synthesized Nrf2 without considerable delay caused by the maturation of the fluorescent protein tag. The BAC integrated Nrf2-Venus protein enables physiologically relevant changes in protein expression to be correlated with changes in native transcriptional and translational control mechanisms (Spiller *et al,* 2010). This meant that the Nrf2 dynamic behavior in response to inducers and during basal activity could be effectively correlated with dynamic changes in Nrf2-Venus nuclear fluorescence in living cells in real time.

The impact of acute and chronic inflammation on cellular antioxidant protection capacity has not been studied in detail. The first study, by Rushoworth *et al* showed that TNFα promoted the induction of Nrf2 protein levels and activity in AML cells, where the resulting high levels of Nrf2 expression confer resistant to treatment with the proteasomal inhibitor Bortezomib (Rushworth *et al,* 2011). The observed increase in Nrf2 levels in the SK-N-AS neuroblastoma cells in response to TNFα and induction was modest, but sufficient to switch on the genetic antioxidant protection program (Figure 4.3). The TNFα mediated Nrf2-Venus increase has been associated with a rise in *NRF2* gene transcription following p65-dsRedXP nuclear entry, which indicates that Nrf2 may be an early p65 gene target of p65 in neuroblastoma cells (Figure 4.5). Furthermore, Nrf2 promoter activity and Nrf2 mRNA levels both increased in response to p65 overexpression and TNFα respectively (Figure 4.3). It is possible that the speed of Nrf2 transcription could be important in determining the timing of the inflammatory signaling resolution, with being an early gene having a more immediate, negative feedback potentially leading to faster dampening of inflammation. Live-cell imaging experiments performed in this study revealed a novel trend in Nrf2 dynamics, involving a sequential accumulations of nuclear Nrf2 in response to a prior peak of p65 nuclear translocation (Figure 4.6). This is a unique example of how the temporal dynamics of one transcription factor (p65) modulates the dynamic expression of a second transcription factor (Nrf2) leading to changes in its activity. Significantly, the Venus-Nrf2 plasmid, which is driven by the constitutive *CMV* promoter did not show the TNFα mediated increase in relative Nrf2-nuclear fluorescence, indicating that this phenotype is dependent on the expression of Nrf2 being driven by its proximal promoter sequence (Figure 4.13). TNFα stimulation is associated with increased intracellular ROS levels and so it was

possible that Nrf2 may become activated as a result of TNFα-induced GSH depletion (Correa *at el,* 2012). However, this effect requires post-translational modifications of Keap1 and should also cause an increase in plasmid encoded Venus-Nrf2 levels, which has not observed in our studies (Figure 4.13).

The function of cytokine mediated Nrf2 expression is expected to be especially relevant in the context of immune cell physiology, where NF-κB mediated antioxidant signaling could facilitate the resolution of inflammatory responses and counteract the generation of ROS, which may result from increased NADPH activity during phagocytosis (Bedard & Krause, 2007). It would be interesting to measure the effect of concomitant activation of Nrf2 to validate its role in the protection of immune cells against their own weapons by dampening of the inflammatory signaling.

Both Nrf2 and NF-κB pathways are thought to have redundant roles in expression of the anti-inflammatory genes (Kohler *et al,* 2015; Buelna-Chontal & Zazueta, 2013). This has been demonstrated using knockdowns of Nrf2 and p65 in mouse liver by Kohler *et al*. The authors demonstrated that the single knockdown of either of the transcription factors did not result in dramatic changes of liver oxidative homeostasis, however double knockdown of both led to chronic inflammation and liver fibrosis, which eventually led to tumor development in female mice (Kohler *et al,* 2015). Therefore, NF-κB driven antioxidant protection could have profound effects on various aspects of health and may have a significant role in disease prevention.

Importantly, we show for the first time that the inflammatory signalling can modulate the nuclear dynamics of Nrf2 by amplifying its transcriptional activity (Figure 4.6C & D, and 4.8E). This mechanism forms an elegant functional cycle, which is initiated by an acute inflammatory response, followed by transient sequential activation of Nrf2 and a consequent dampening of the ROS signalling coupled with a concomitant decrease in NF-κB gene transcription. This in-turn leads to a reduction in Nrf2 transcription, thus eventually leading to reestablishment of resting cellular state levels of Nrf2, without inducing an apoptotic phenotype (Figure

4.6A & 4.7A, Chapter 2), which would result from unquenched elevation of cellular Nrf2 levels.

The transcribed Nrf2 protein is synthesized in the cytoplasm, where it normally rapidly interacts with Keap1. It was therefore anticipated that Keap1 would serve as the prime regulator of newly made Nrf2 protein levels. Indeed, knockdown of Keap1 expression by siRNA demonstrated an enhanced nuclear accumulation of Nrf2 in response to TNFα (Figure 4.9, Chapter 2). Therefore, the levels of Keap1 will determine the net increase in Nrf2 levels that result from inflammatory signaling. However, the magnitude of this response would be expected to vary between cell types. We have demonstrated that acute inflammatory signaling can be an effective inducer of Nrf2 protein expression, however this increase was short lived. The role of Keap1 in clearing away the newly made Nrf2 as a result of inflammation is expected to be especially relevant in cancers such as some lung cancers, which are associated with Keap1 mutations, or its suppressed expression as a result of promoter methylation. In these cases the resulting reduction of Keap1 levels could further amplify Nrf2 activity driven by the inflammatory status within the cancer tissue microenvironment, thus leading to an upregulation of antioxidant gene transcription, which in turn would selectively protect the tumor against therapeutic drug treatment.

In theory, if inflammation led to inhibition of Keap1 mediated regulation in parallel with an increase in Nrf2 synthesis, the potentiated increase of Nrf2 activity could confer anti-aging and anti-oxidant protection. However this does not occur during chronic inflammation for the following reason. Induction of Nrf2 leads to the inhibition of NF-κB transcription as shown in this study, and by other previous reports (Figure 4.12, Chapter 2) (Kim *et al,* 2013; Buelna-Chontal & Zazueta, 2013). High antioxidant activity has been shown to impede anti-apoptotic signaling following application of compounds that trigger DILI and induce Nrf2, leading to inhibition of NF-κB signaling (Harpers *et al,* 2015). Therefore, tight regulation of Nrf2 ensures that in the event of inflammation the cell is able define the balance that allows appropriate, but time limited, activation of the appropriate signaling program. It can act to withstand the insult by activating the NF-κB responses and switching on the anti-apoptotic signaling, or alternatively to protect itself from the generated ROS that leads to DNA damage. Although, the latter scenario is associated with a compromise in the anti-apoptotic signaling, and could lead to cell death. Currently, it

is unclear as to what extent the two mechanisms are mutually exclusive, but this may well depend on the relative levels of both proteins and the robustness of the regulatory networks.

The current model of Nrf2 regulation is explained by the conformational cycling model (Intro Chapter Section 1.1.2), but this does not take into account the fate of the Nrf2 protein once it enters the nucleus and accomplishes its role as a transcription factor (Baird *et al,* 2013). Keap1 has been previously demonstrated to shuttle in and out of the nucleus, however this observation remains controversial, nevertheless the nuclear accumulation of Keap1 was also observed in this study, and this was found to be highly reproducible phenotype (Figure 5.3, Chapter 3) (Sun *et al,* 2011). LMB treatment combined with CDDO-Me triggered the nuclear localisation of the mCherry-Keap1 suggesting that it can shuttle between the cytoplasm and the nucleus. The role of this phenotype has not been confirmed by our results, however Zhang *et al* speculated that nuclear shuttling of Keap1 is necessary for effective Nrf2 export from the nucleus and cessation of ARE-Luc transcription. Considering the evidence for mCherry-Keap1 nuclear shuttling it would be intriguing to validate the role of acetylation in Nrf2 nuclear export. This could be achieved by monitoring pDendra2-Nrf2 protein nuclear export in the absence of Keap1 protein, following addition of C646. It would also explain the effect of LMB inhibition on the ARE-Luc transcription, as perhaps Keap1-bound nuclear Nrf2 is not able to bind to DNA, due to the proximity of Neh1 and Neh2 domains, which are involved in DNA binding and Keap1 interaction respectively (Suzuki & Yamamoto, 2015; Smirnova *et al,* 2011). The acetyl group attachment on Nrf2 could act as a marker of completed transcriptional function, thus labeling it for more efficient nuclear clearance, in order to prevent over activation of antioxidant signaling. This possibility could also explain the increased levels of nuclear Nrf2-Venus observed following pharmacological inhibition of p300/CBP, which may block its nuclear exit. The affinity of nuclear Nrf2 for the nuclear Keap1 protein could also be investigated further by FCCS studies.

The pattern of Nrf2-Venus nuclear fluorescence following addition of LMB demonstrates that there is a homeostasis between the synthesis and nuclear degradation of Nrf2. This data presents the first example of a condition where Nrf2

protein levels are uncoupled from measured transcriptional activity (Figure 5.9, Chapter 3). Understanding the consequences of Nrf2 nuclear import will be an essential part of deciphering the complex regulation of antioxidant protection. There are limited mechanistic studies on what may happen to Nrf2 proteins after driving antioxidant gene transcription. Currently, the most extensive study of the mechanism regulating nuclear Nrf2 activity describes the GSK-3 mediated degradation of Nrf2, as well as activation of Nrf2 nuclear export by Fyn kinase, which is also linked to GSK-3 activity (Niture *et al,* 2011). However, both reports failed to provide conclusive evidence to differentiate between GSK-3 mediated Nrf2 degradation or export. By using photoswitchable Nrf2 proteins we have demonstrated that Nrf2 can be effectively transported into the cytoplasmic space under basal conditions providing the first, direct evidence of Nrf2 export (Figure 5.6, Chapter 3). There are several lines of research that could be addressed with pDendra2-Nrf2 imaging, focusing on the role of GSK-3 to discern between export and degradation. What is more, the redundancy of GSK-3 and Keap1 negative regulation could be investigated more thoroughly using pharmacological inhibitors and imaging of the pDendra-Nrf2 half-life and cytoplasmic accumulation. This will be particularly relevant in studying the nuclear degradation mechanism of Nrf2 using when Keap1 expression is depleted by siRNA knockdown, in order to validate its role in nuclear Nrf2 regulation, as results obtained in this study indicated that nuclear export is not required for efficient Nrf2 clearance (Figure 5.9, Chapter 3). This demonstrates the robustness of the regulatory loops ensuring appropriate timing/limitation of antioxidant signaling responses, to prevent deleterious interference with other pathways, especially with NF-κB responses. The relative participation of the RNF4, Keap1 and GSK-3 in Nrf2 control still remains to be addressed to verify the degree of redundancy or combinatorial action between the different mechanisms of negative regulations of cellular antioxidant responses.

Lastly, data presented in Chapter 4 provides the first definitive evidence of the mechanism of Nrf2 inhibition by anti-cancer drug, brusatol. Brusatol is a quasinoid compound isolated from the Chinese medicinal plant *Brucea javanica*, which is known for its anti-cancer properties. Pioneering studies in 1983 revealed similarities between the bruceantin compound (from *Brucea antidysenterica*) and brusatol, demonstrating that both drugs reversibly target global protein translation process in

rabbit reticulocytes, although the 100μM concentration of drugs applied in this study was extremely high (Willingham *et al,* 1981; Willingham *et al,* 1984). Donna Zhang's group were the first to describe the inhibitory effects of Brusatol on the Nrf2 pathway. However, in that study, inhibition was attributed to decreased Nrf2 stability, due to enhanced ubiquitination (Ren *et al,* 2011). This conclusion diverted attention from the potential low dose effect of the drug on protein translation. As a result, further studies have focused on investigating the mechanism of brusatol evoked Nrf2 degradation. However, so far researchers have failed to identify a brusatol-induced mechanism of proteosomal degradation (Olayanju *et al,* 2015). Classical protein turnover studies have relayed on pulse chase metabolic labelling and quantification of immunoprecipitated proteins. This approach is time consuming and does not allow protein stability changes to be measured real time in live cells (Khmelinskii *et al,* 2012).

With the help of photoswitchable pDendra2 tagging of Nrf2 we were able to discriminate between the Nrf2 protein degradation and the effect of brusatol on the newly made protein synthesis (Figure 6.5, Chapter 4). This approach led to the identification of substantial similarities between the comparative effects of brusatol and cycloheximide (CHX), as both compounds led to the inhibition of Nrf2 protein synthesis, rather than any increase in the degradation of preformed Nrf2 protein. Our data also strongly suggests that even in low therapeutic dose ranges brusatol is likely to inhibit the global translation of proteins, in contrast to reports published by Ren *et al* and Olayanju *et al* (Figure 6.9 and 6.10, Chapter 4). This hypothesis is supported by the fact that brusatol application increased NF-κB target gene transcription (possibly by decreasing IKBα levels), as well as led to reduction in Renilla luminescence and MARCH5 protein synthesis (Figure 6.10, Chapter 4). Interestingly brusatol has been previously observed to deplete c-Myc protein levels in leukemic cells, which suggest this compound is likely to have many off-target effects by inhibiting global translation process (Mata-Greenwood *et* al, 2002). Consequently, the shorter the protein half-life, the more likely it is to be affected by the transient generic inhibition of translation. It is feasible that brusatol may target a more selective portfolio of proteins than CHX, simply due to the transient nature of its action, therefore reducing cytotoxicity (Figure 6.8, Chapter 4).

At present, we can only speculate that brusatol acts by inhibiting the 80S ribosomal function, since this is the exclusive target of the 16 remaining translation protein inhibitors screened previously by Garreau de Loubresse *et al*. Compounds such as CHX, lactimidomycin, lycorine and others, were co-crystallised with the yeast 80S ribosome and the authors demonstrated that the inhibitors were primarily bound to the domain responsible for mRNA or tRNA binding on the ribosome subunits (Garreau de Loubresse *et al,* 2014). Proteomic studies to assess the specificity of action of this compound are planned for the near future in order to explore the potential therapeutic benefits of other transient inhibitors of protein synthesis.

CONCLUSIONS

Generation of sophisticated, low-level expression systems enabled physiologically relevant imaging of fluorescently labelled Nrf2 and p65 proteins. Providing real-time quantitative insight into the temporal dynamics of conditional responses in single live-cells. This approach has provided novel insights into cell specific responses to stress stimuli in mixed primary hippocampal cultures and the molecular mechanisms of crosstalk between antioxidant and inflammatory pathways in SK-N-AS BAC$^{Nrf2\text{-}Venus}$ neuroblastoma cells. The results from this study suggest that NF-κB modulates dynamic nuclear localisation of Nrf2 by driving the transcriptional regulation of the κB2 site located within the *NRF2* gene promoter. Thus resulting in a transient increase in Nrf2 expression in response to cytokines. This effect was amplified by knockdown, or inhibition, of the Keap1-mediated Nrf2 degradation axis. Implying that Keap1 fine-tunes the balance between the antioxidant Nrf2 responses and p65 mediated inflammatory signalling, by titrating cellular levels of Nrf2 and allowing effective NF-κB signalling. It acts by the retention and degradation of Nrf2 within the cytoplasm on a basal level and changes in Keap1 activity, or in the rate of Nrf2 synthesis will enable nuclear accumulation of Nrf2 to adjust the intracellular redox environment. Once Nrf2 completes its transcriptional task it can be efficiently regulated by nuclear degradation, or export to the cytoplasmic space. Live cell imaging approaches presented in this thesis facilitated investigation of Nrf2 regulation at multiple levels, including cell cycle dependant temporal changes, transcription, translation, regulation of protein stability by Keap1

and GSK-3, nuclear v/s cytoplasmic rates of degradation and nuclear import/export dynamics. We now aim to integrate the quantitative data generated in this study into a mathematical model, which will permit the *in silico* prediction of conditional Nrf2 and p65 responses to inflammatory, antioxidant and potential therapeutic compounds in order to design a more informed therapeutic approach aiming to combat diseases associated with inflammatory damage.

The summary model of Nrf2 regulation during acute inflammation is presented in Figure 7.1.

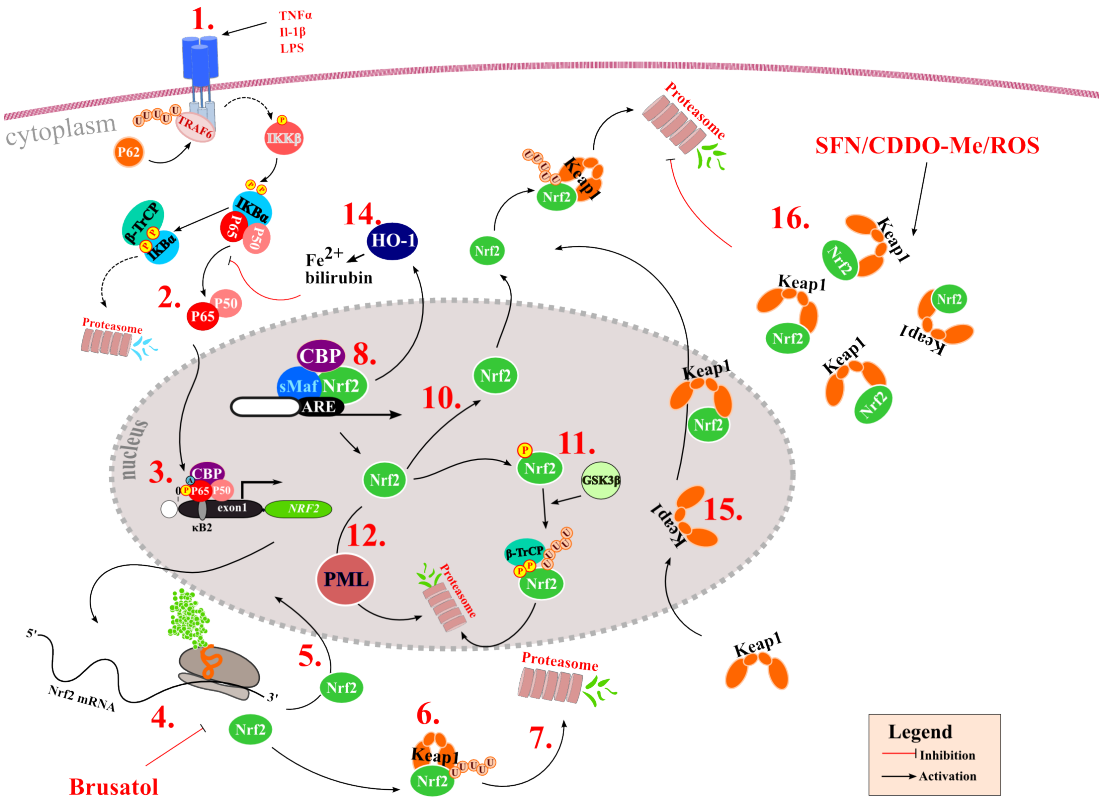

Figure 7.1 Model of Nrf2 regulation. 1. TNFα signalling triggers NF-κB signalling cascade activating IKBα phosphorylation and degradation. 2. Translocation of p50/p65 heterodimer into the nucleus. 3. Transcription of *NRF2* gene. 4. Translation of Nrf2 mRNA. 5. Nrf2 nuclear import. 6. Nrf2 binding to Keap1. 7. Nrf2 degradation by the 26S proteasome. 8. Nrf2 target gene expression. 9. Nrf2 nuclear export. 10. Nrf2 phosphorylation by GSK-3 and subsequent nuclear degradation by SCF-β-TrCP proteolysis. 11. Nrf2 accumulation into PML NBs. 12. HO-1 inhibition of the NF-κB pathway activity. 13. Keap1-mediated Nrf2 nuclear export. 14. Induction of Nrf2 levels by CDDO-Me, SFN and ROS by preventing Nrf2 degradation.

Bibliography

Ashabi G, Alamdary SZ, Ramin M, Khodagholi F (2013) Reduction of Hippocampal Apoptosis by Intracerebroventricular Administration of Extracellular Signal-Regulated Protein Kinase and/or p38 Inhibitors in Amyloid Beta Rat Model of Alzheimer's Disease: Involvement of Nuclear-Related Factor-2 and Nuclear Factor-kappa B. *Basic Clin Pharmacol Toxicol* **112:** 145-155

Ashall L, Horton CA, Nelson DE, Paszek P, Harper CV, Sillitoe K, Ryan S, Spiller DG, Unitt JF, Broomhead DS, Kell DB, Rand DA, Sée V, White MRH (2009) Pulsatile stimulation determines timing and specificity of NF-kappa B-dependent transcription. *Science (New York, NY)* **324:** 242-246

Bacia K, Kim SA, Schwille P (2006) Fluorescence cross-correlation spectroscopy in living cells. *Nat Methods* **3:** 83-89

Baggiolini M, Clark-Lewis I (1992) Interleukin-8, a chemotactic and inflammatory cytokine. *FEBS Lett* **307:** 97-101

Bagnall J, Boddington C, Boyd J, Brignall R, Rowe W, Jones NA, Schmidt L, Spiller DG, White MRH, Paszek P (2015) Quantitative dynamic imaging of immune cell signalling using lentiviral gene transfer. *J Integr Biol* **7:** 713-725

Baird L, Lleres D, Swift S, Dinkova-Kostova AT (2013) Regulatory flexibility in the Nrf2-mediated stress response is conferred by conformational cycling of the Keap1-Nrf2 protein complex. *Proceedings of the National Academy of Sciences of the United States of America* **110:** 15259-15264

Baird L, Swift S, Lleres D, Dinkova-Kostova AT (2014) Monitoring Keap1-Nrf2 interactions in single live cells. *Biotechnol Adv* **32:** 1133-1144

Baker SJ, Reddy EP (1998) Modulation of life and death by the TNF receptor superfamily. *Oncogene* **17:** 3261-3270

Baker SM, Buckheit R, Falk MM (2010) Green-to-red photoconvertible fluorescent proteins: tracking cell and protein dynamics on standard wide-field mercury arc-based microscopes. *BMC Cell Biol* **11:** 15

Bedard K, Krause KH (2007) The NOX family of ROS-generating NADPH oxidases: physiology and pathophysiology. *Physiol Rev* **87:** 245-313

Bell KF, Al-Mubarak B, Fowler JH, Baxter PS, Gupta K, Tsujita T, Chowdhry S, Patani R, Chandran S, Horsburgh K, Hayes JD, Hardingham GE (2011) Mild oxidative stress activates Nrf2 in astrocytes, which contributes to neuroprotective ischemic preconditioning. *Proceedings of the National*

Academy of Sciences of the United States of America **108:** E1-E2

Bell KF, Al-Mubarak B, Martel MA, McKay S, Wheelan N, Hasel P, Markus NM, Baxter P, Deighton RF, Serio A, Bilican B, Chowdhry S, Meakin PJ, Ashford ML, Wyllie DJ, Scannevin RH, Chandran S, Hayes JD, Hardingham GE (2015) Neuronal development is promoted by weakened intrinsic antioxidant defences due to epigenetic repression of Nrf2. *Nat Commun* **6**

Bellezza I, Mierla A, Minelli A (2010) Nrf2 and NF-κB and Their Concerted Modulation in Cancer Pathogenesis and Progression. *Cancers* **2:** 483-497

Ben-Neriah Y, Karin M (2011) Inflammation meets cancer, with NF-[kappa]B as the matchmaker. *Nat Immunol* **12:** 715-723

Bergqvist S, Alverdi V, Mengel B, Hoffmann A, Ghosh G, Komives EA (2009) Kinetic enhancement of NF-kappaBxDNA dissociation by IkappaBalpha. *Proceedings of the National Academy of Sciences of the United States of America* **106:** 19328-19333

Bezzi P, Domercq M, Brambilla L, Galli R, Schols D, De Clercq E, Vescovi A, Bagetta G, Kollias G, Meldolesi J, Volterra A (2001) CXCR4-activated astrocyte glutamate release via TNFalpha: amplification by microglia triggers neurotoxicity. *Nat Neurosci* **4:** 702-710

Bindoli A, Rigobello MP (2013) Principles in redox signaling: from chemistry to functional significance. *Antioxid Redox Signal* **18:** 1557-1593

Blakeslee WW, Wysoczynski CL, Fritz KS, Nyborg JK, Churchill ME, McKinsey TA (2014) Class I HDAC inhibition stimulates cardiac protein SUMOylation through a post-translational mechanism. *Cell Signalling* **26:** 2912-2920

Blank V (2008) Small Maf proteins in mammalian gene control: mere dimerization partners or dynamic transcriptional regulators? *J Mol Biol* **376:** 913-925

Bradl M, Lassmann H (2010) Oligodendrocytes: biology and pathology. *Acta Neuropathology* **119:** 37-53

Brown GC, Neher JJ (2010) Inflammatory neurodegeneration and mechanisms of microglial killing of neurons. *Mol Neurobiol* **41:** 242-247

Bryan HK, Olayanju A, Goldring CE, Park BK (2013) The Nrf2 cell defence pathway: Keap1-dependent and -independent mechanisms of regulation. *Biochem Pharmacol* **85:** 705-717

Buelna-Chontal M, Zazueta C (2013) Redox activation of Nrf2 & NF-kappa B: A double end sword?

Cellular Signalling **25:** 2548-2557

Caccamo D, Campisi A, Curro M, Bramanti V, Tringali M, Li Volti G, Vanella A, Ientile R (2005) Antioxidant treatment inhibited glutamate-evoked NF-kappaB activation in primary astroglial cell cultures. *Neurotoxicology* **26:** 915-921

Calkins MJ, Johnson DA, Townsend JA, Vargas MR, Dowell JA, Williamson TP, Kraft AD, Lee JM, Li J, Johnson JA (2009) The Nrf2/ARE pathway as a potential therapeutic target in neurodegenerative disease. *Antioxid Redox Signal* **11:** 497-508

Carracedo A, Pandolfi PP (2008) The PTEN-PI3K pathway: of feedbacks and cross-talks. *Oncogene* **27:** 5527-5541

Cartier L, Hartley O, Dubois-Dauphin M, Krause KH (2005) Chemokine receptors in the central nervous system: role in brain inflammation and neurodegenerative diseases. *Brain Res Rev* **48:** 16-42

Chan KM, Lu RH, Chang JC, Kan YW (1996) NRF2, a member of the NFE2 family of transcription factors, is not essential for murine erythropoiesis, growth, and development. *Proceedings of the National Academy of Sciences of the United States of America* **93:** 13943-13948

Chen FE, Huang DB, Chen YQ, Ghosh G (1998) Crystal structure of p50/p65 heterodimer of transcription factor NF-kappaB bound to DNA. *Nature* **391:** 410-413

Chen J, Chen ZJ (2013) Regulation of NF-kappaB by ubiquitination. *Curr Opin Immunol* **25:** 4-12

Chen W, Jiang T, Wang H, Tao S, Lau A, Fang D, Zhang DD (2012) Does Nrf2 contribute to p53-mediated control of cell survival and death? *Antioxid Redox Signal* **17**

Chen ZW, Ye XY, Tang NW, Shen SP, Li ZM, Niu XM, Lu S, Xu L (2014) The histone acetylranseferase hMOF acetylates Nrf2 and regulates anti-drug responses in human non-small cell lung cancer. *Br J Pharmacol* **171:** 3196-3211

Chia AJ, Goldring CE, Kitteringham NR, Wong SQ, Morgan P, Park BK (2010) Differential effect of covalent protein modification and glutathione depletion on the transcriptional response of Nrf2 and NF-kappaB. *Biochem Pharmacol* **80:** 410-421

Chien Y, Scuoppo C, Wang X, Fang X, Balgley B, Bolden JE, Premsrirut P, Luo W, Chicas A, Lee CS, Kogan SC, Lowe SW (2011) Control of the senescence-associated secretory phenotype by NF-kappaB promotes

senescence and enhances chemosensitivity. *Genes Dev* **25:** 2125-2136

Chiu J, Dawes IW (2012) Redox control of cell proliferation. *Trends Cell Biol* **22:** 592-601

Chowdhry S, Zhang Y, McMahon M, Sutherland C, Cuadrado A, Hayes JD (2013) Nrf2 is controlled by two distinct beta-TrCP recognition motifs in its Neh6 domain, one of which can be modulated by GSK-3 activity. *Oncogene* **32:** 3765-3781

Chudakov DM, S. L, Lukyanov KA (2007) Tracking intracellular protein movements using photoswitchable fluorescent proteins PS-CFP2 and Dendra2. *Nat Protoc* **2:** 2024-2032

Clarke JD, A. H, Riedl K, Bella D, Schwartz SJ, Stevens JF, Ho E (2011) Bioavailability and inter-conversion of sulforaphane and erucin in human subjects consuming broccoli sprouts or broccoli supplement in a cross-over study design. *Pharmacol Research* **64:** 456-463

Clodfelder-Miller B, De Sarno P, Zmijewska AA, Song L, Richard S, Jope RS (2005) Physiological and pathological changes in glucose regulate brain Akt and glycogen synthase kinase-3. *J Biol Chem* **280:** 39723-39731

Correa F, Mallard C, Nilsson M, Sandberg M (2012) Dual TNFalpha-induced effects on NRF2 mediated antioxidant defence in astrocyte-rich cultures: role of protein kinase activation. *Neurochem Res* **37:** 2842-2855

Cuadrado A (2015
) Structural and functional characterization of NRF2 degradation by glycogen synthase kinase 3/beta-TrCP. *Free Radic Biol Med* **88:** 147-157

Cuadrado A, Martin-Moldes Z, Ye J, Lastres-Becker I (2014) Transcription factors NRF2 and NF-kappaB are coordinated effectors of the Rho family, GTP-binding protein RAC1 during inflammation. *J Biol Chem* **289:** 15244-15258

Cuadrado A, Moreno-Murciano P, Pedraza-Chaverri J (2009) The transcription factor Nrf2 as a new therapeutic target in Parkinson's disease. *Expert Opin Ther Targets* **13:** 319-329

Cuendet M, Gills JJ, Pezzuto JM (2004) Brusatol-induced HL-60 cell differentiation involves NF-kappaB activation. *Cancer Lett* **206:** 43-50

Cullinan SB, Zhang D, Hannink M, Arvisais E, Kaufman RJ, Diehl JA (2003) Nrf2 is a direct PERK substrate and effector of PERK-dependent cell survival. *Mol Cell Biol* **23:** 7198-7209

Danilov CA, Chandrasekaran K, Racz J, Soane L, Zielke C, Fiskum G (2009)

Sulforaphane protects astrocytes against oxidative stress and delayed death caused by oxygen and glucose deprivation. *Glia* **57:** 645-656

de Miranda Ramos V, Zanotto-Filho A, de Bittencourt Pasquali MA, Klafke K, Gasparotto J, Dunkley P, Gelain DP, Moreira JC (2015) NRF2 Mediates Neuroblastoma Proliferation and Resistance to Retinoic Acid Cytotoxicity in a Model of In Vitro Neuronal Differentiation. *Mol Neurobiol*

De Vos WH, Houben F, Kamps M, Malhas A, Verheyen F, Cox J, Manders EMM, Verstraeten VLRM, van Steensel MAM, Marcelis CLM, van den Wijngaard A, Vaux DJ, Ramaekers FCS, Broers JL (2011) Repetitive disruptions of the nuclear envelope invoke temporary loss of cellular compartmentalization in laminopathies. *Hum Mol Genet* **20:** 4175-4186

Dorresteijn MJ, Paine A, Zilian E, Fenten MG, Frenzel E, Janciauskiene S, Figueiredo C, Eiz-Vesper B, Blasczyk R, Dekker D, Pennings B, Scharstuhl A, Smits P, Larmann J, Theilmeier G, van der Hoeven JG, Wagener FA, Pickkers P, Immenschuh S (2015) Cell-type-specific downregulation of heme oxygenase-1 by lipopolysaccharide via Bach1 in primary human mononuclear cells. *Free Radic Biol Med* **78:** 224-232

Dowell JA, Johnson JA (2013) Mechanisms of Nrf2 Protection in Astrocytes as Identified by Quantitative Proteomics and siRNA Screening. *PLoS One* **8**

E.A. C, Old LJ, Kassel RL, Green S, Fiore N, Williamson B (1975) An endotoxin-induced serum factor that causes necrosis of tumors. *Proceedings of the National Academy of Sciences of the United States of America* **72:** 3666-3670

Embley TM, Martin W (2006) Eukaryotic evolution, changes and challenges. *Nature* **440:** 623-630

Figiel I (2008) Pro-inflammatory cytokine TNF-alpha as a neuroprotective agent in the brain. *Acta Neurobiol Exp* **68:** 526-534

Findlay VJ, Tapiero H, Townsend DM (2005) Sulfiredoxin: a potential therapeutic agent? *Biomed Pharmacother* **59:** 374-379

Frakes AE, Ferraiuolo L, Haidet-Phillips AM, Schmelzer L, Braun L, Miranda CJ, Ladner KJ, Bevan AK, Foust KD, Godbout JP, Popovich PG, Guttridge DC, Kaspar BK (2014) Microglia induce motor neuron death via the classical NF-kappaB pathway in amyotrophic lateral sclerosis. *Neuron* **81:** 1009-1023

Fujita K, Maeda D, Xiao Q, Srinivasula SM (2011) Nrf2-mediated induction of p62 controls Toll-like receptor-4-driven aggresome-like induced structure formation and autophagic degradation. *Proceedings of the National Academy of Sciences of the United States of America* **108:** 1427-1432

Gan L, Johnson JA (2014) Oxidative damage and the Nrf2-ARE pathway in neurodegenerative diseases. *Biochim Biophys Acta Mol Basis Dis* **1842:** 1208-1218

Ganesh Yerra V, Negi G, Sharma SS, Kumar A (2013) Potential therapeutic effects of the simultaneous targeting of the Nrf2 and NF-kappaB pathways in diabetic neuropathy. *Redox Biol* **1:** 394-397

Gao C, Cheng X, Lam M, Liu Y, Liu Q, Chang KS, Kao HY (2008) Signal-dependent regulation of transcription by histone deacetylase 7 involves recruitment to promyelocytic leukemia protein nuclear bodies. *Mol Biol Cell* **19:** 3020-3027

Gardiner GJ, Deffit S, McLetchie S, Perez L, Walline CC, Blum JS (2013) A role for NADPH oxidase in antigen presentation. *Front Immunol* **4:** 295

Garreau de Loubresse N, Prokhorova I, Holtkamp W, Rodnina MV, Yusupova G, Yusupov M (2014) Structural basis for the inhibition of the eukaryotic ribosome. *Nature* **513:** 517-522

Gasper AV, Al-Janobi A, Smith JA, Bacon JR, Fortun P, Atherton C, Taylor MA, Hawkey CJ, Barrett DA, Mithen RF (2005) Glutathione S-transferase M1 polymorphism and metabolism of sulforaphane from standard and high-glucosinolate broccoli. *Am J Clin Nutr* **82:** 1283-1291

Ghosh M, Yang Y, Rothstein JD, Robinson MB (2011) Nuclear factor-kappaB contributes to neuron-dependent induction of glutamate transporter-1 expression in astrocytes. *J Neurosci* **31:** 9159-9169

Glass CK, Saijo K, Winner B, Marchetto MC, Gage FH (2010) Mechanisms Underlying Inflammation in Neurodegeneration. *Cell* **140:** 918-934

Gozzelino R, Jeney V, Soares MP (2010) Mechanisms of cell protection by heme oxygenase-1. *Annu Rev Pharmacol Toxicol* **50:** 323-354

Guan D, Lim JH, Peng L, Liu Y, Lam M, Seto E, Kao HY (2014) Deacetylation of the tumor suppressor protein PML regulates hydrogen peroxide-induced cell death. *Cell Death Dis* **5:** e1340

Guo S, Cheng X, Lim JH, Liu Y, Kao HY (2014) Control of antioxidative response by the tumor suppressor protein PML through regulating Nrf2 activity. *Mol Biol Cell* **25:** 2485-2498

Gupta K, Patani R, Baxter P, Serio A, Story D, Tsujita T, Hayes JD, Pedersen RA, Hardingham GE, Chandran S (2012) Human embryonic stem cell derived astrocytes mediate non-cell-autonomous neuroprotection through endogenous and drug-induced mechanisms. *Cell Death Differ* **19:** 779-787

Gurskaya NG, Verkhusha VV, Shcheglov AS, Staroverov DB, Chepurnykh TV, Fradkov AF, Lukyanov S, Lukyanov KA (2006) Engineering of a monomeric green-to-red photoactivatable fluorescent protein induced by blue light. *Nat Biotechnol* **24:** 461-465

Gutierrez H, Davies AM (2011) Regulation of neural process growth, elaboration and structural plasticity by NF-kappaB. *Trends Neurosci* **34:** 316-325

Habas A, Hahn J, Wang X, Margeta M (2013) Neuronal activity regulates astrocytic Nrf2 signaling. *Proceedings of the National Academy of Sciences of the United States of America* **110:** 18291-18296

Hajnoczky G, Robb-Gaspers LD, Seitz MB, Thomas AP (1995) Decoding of cytosolic calcium oscillations in the mitochondria. *Cell* **82:** 415-424

Han Y, He T, Huang DR, Pardo CA, Ransohoff RM (2001) TNF-alpha mediates SDF-1 alpha-induced NF-kappa B activation and cytotoxic effects in primary astrocytes. *J Clin Invest* **108:** 425-435

Hara T, Nakamura K, Matsui M, Yamamoto A, Nakahara Y, Suzuki-Migishima R, Yokoyama M, Mishima K, Saito I, Okano H, Mizushima N (2006) Suppression of basal autophagy in neural cells causes neurodegenerative disease in mice. *Nature* **441:** 885-889

Hartley JL, Temple GF, Brasch MA (2000) DNA cloning using in vitro site-specific recombination. *Genome Res* **10:** 1788-1795

Hatch EM, Fischer AH, Deerinck TJ, Hetzer MW (2013) Catastrophic nuclear envelope collapse in cancer cell micronuclei. *Cell* **154:** 47-60

Hayden MS, Ghosh S (2008) Shared principles in NF-kappaB signaling. *Cell* **132:** 344-362

Hayes JD, Dinkova-Kostova AT (2014) The Nrf2 regulatory network provides an interface between redox and intermediary metabolism. *Trends Biochem Sci* **39:** 199-218

Hayes JD, McMahon M (2006) The Double-Edged Sword of Nrf2: Subversion of Redox Homeostasis during the Evolution of Cancer. *Mol Cell* **21:** 732-734

Heiss EH, Schachner D, Zimmermann K, Dirsch VM (2013) Glucose availability is a decisive factor for Nrf2-mediated gene expression. *Redox Biol* **1:** 359-365

Herpers B, Wink S, Fredriksson L, Di Z, Hendriks G, Vrieling H, de Bont H, van de Water B (2015) Activation of the Nrf2 response by intrinsic

hepatotoxic drugs correlates with suppression of NF-κB activation and sensitizes toward TNFα-induced cytotoxicity. *Arch Toxicol***:** 1-17

Hirotsu Y, Katsuoka F, Funayama R, Nagashima T, Nishida Y, Nakayama K, Engel JD, Yamamoto M (2012) Nrf2-MafG heterodimers contribute globally to antioxidant and metabolic networks. *Nucleic Acids Res* **40:** 10228-10239

Hoffmann A, Levchenko A, Scott ML, Baltimore D (2002) The IkappaB-NF-kappaB signaling module: temporal control and selective gene activation. *Science* **298:** 1241-1245

Hoing S, Rudhard Y, Reinhardt P, Glatza M, Stehling M, Wu G, Peiker C, Bocker A, Parga JA, Bunk E, Schwamborn JC, Slack M, Sterneckert J, Scholer HR (2012) Discovery of inhibitors of microglial neurotoxicity acting through multiple mechanisms using a stem-cell-based phenotypic assay. *Cell Stem Cell* **11:** 620-632

Huang WC, Hung MC (2013) Beyond NF-kappaB activation: nuclear functions of IkappaB kinase alpha. *J Biomed Sci* **20:** 3

Ichimura Y, Waguri S, Sou Y, Kageyama S, Hasegawa J, Ishimura R, Saito T, Yang YJ, Kouno T, Fukutomi T, Hoshii T, Hirao A, Takagi K, Mizushima T, Motohashi H, Lee MS, Yoshimori T, Tanaka K, Yamamoto M, Komatsu M (2013) Phosphorylation of p62 Activates the Keap1-Nrf2 Pathway during Selective Autophagy. *Mol Cell* **51:** 618-631

Imayoshi I, Isomura A, Harima Y, Kawaguchi K, Kori H, Miyachi H, Fujiwara T, Ishidate F, Kageyama R (2013) Oscillatory Control of Factors Determining Multipotency and Fate in Mouse Neural Progenitors. *Science* **342:** 1203-1208

Itoh K, Chiba T, Takahashi S, Ishii T, Igarashi K, Katoh Y, Oyake T, Hayashi N, Satoh K, Hatayama I, Yamamoto M, Nabeshima Y (1997) An Nrf2/small Maf heterodimer mediates the induction of phase II detoxifying enzyme genes through antioxidant response elements. *Biochem Biophys Res Commun* **236:** 313-322

Jain AK, Jaiswal AK (2006) Phosphorylation of tyrosine 568 controls nuclear export of Nrf2. *J Biol Chem* **281:** 12132-12142

Journal of ImmunologyDeclercq W, Denecker G, Fiers W, Vandenabeele P (1998) Cooperation of both TNF receptors in inducing apoptosis: involvement of the TNF receptor-associated factor binding domain of the TNF receptor 75. *J Immunol* **161:** 390-399

Jyrkkanen HK, Kuosmanen SM, Heinaniemi M, Laitinen H, Kansanen E, Mella-Aho E, Leinonen H, Yla-Herttuala S, Levonen AL (2011) Novel insights into the regulation of antioxidant-response-element-mediated gene expression by electrophiles: induction of the transcriptional repressor BACH1

by Nrf2. *Biochem J* **440:** 167-174

Kaech S, Banker G (2006) Culturing hippocampal neurons. *Nat Protocols* **1:** 2406-2415

Kalinin S, Polak PE, Lin SX, Braun D, Guizzetti M, Zhang XL, Rubinstein I, Feinstein DL (2013) Dimethyl fumarate regulates histone deacetylase expression in astrocytes. *J Neuroimmunol* **263:** 13-19

Kaltschmidt B, Widera D, Kaltschmidt C (2005) Signaling via NF-kappaB in the nervous system. *Biochim Biophys Acta* **1745:** 287-299

Kaltschmidt C, Kaltschmidt B Fau - Neumann H, Neumann H Fau - Wekerle H, Wekerle H Fau - Baeuerle PA, Baeuerle PA (1994) Constitutive NF-kappa B activity in neurons. *Mol Cell Biol* **14:** 3981-3992

Kanezaki R, Toki T, Yokoyama M, Yomogida K, Sugiyama K, Yamamoto M, Igarashi K, Ito E (2001) Transcription factor BACH1 is recruited to the nucleus by its novel alternative spliced isoform. *J Biol Chem* **276:** 7278-7284

Kawai Y, Garduno L, Theodore M, Yang JQ, Arinze IJ (2011) Acetylation-Deacetylation of the Transcription Factor Nrf2 (Nuclear Factor Erythroid 2-related Factor 2) Regulates Its Transcriptional Activity and Nucleocytoplasmic Localization. *J Biol Chem* **286:** 7629-7640

Khmelinskii A, Keller PJ, Bartosik A, Meurer M, Barry JD, Mardin BR, Kaufmann A, Trautmann S, Wachsmuth M, Pereira G, Huber W, Schiebel E, Knop M (2012) Tandem fluorescent protein timers for in vivo analysis of protein dynamics. *Nat Biotechnol* **30:** 708-714

Kim JE, You DJ, Lee C, Ahn C, Seong JY, Hwang JI (2010) Suppression of NF-kappaB signaling by KEAP1 regulation of IKKbeta activity through autophagic degradation and inhibition of phosphorylation. *Cell Signal* **22**

Kim SW, Lee HK, Shin JH, Lee JK (2013) Up-down regulation of HO-1 and iNOS gene expressions by ethyl pyruvate via recruiting p300 to Nrf2 and depriving It from p65. *Free Radic Biol Med* **65:** 468-476

Kohler UA, Bohm F, Rolfs F, Egger M, Hornemann T, Pasparakis M, Weber A, Werner S (2015) NF-kappaB/RelA and Nrf2 cooperate to maintain hepatocyte integrity and to prevent development of hepatocellular adenoma. *J Hepatol*

Köhler UA, Kurinna S, Schwitter D, Marti A, Schäfer M, Hellerbrand C, Speicher T, Werner S (2014) Activated Nrf2 impairs liver regeneration in mice by activation of genes involved in cell-cycle control and apoptosis. *Hepatology* **60:** 670-678

Kratschmar DV, Calabrese D, Walsh J, Lister A, Birk J, Appenzeller-Herzog C, Moulin P, Goldring CE, Odermatt A (2012) Suppression of the Nrf2-dependent antioxidant response by glucocorticoids and 11beta-HSD1-mediated glucocorticoid activation in hepatic cells. *PLoS One* **7:** e36774

Krejci A (2012) Metabolic sensors and their interplay with cell signalling and transcription. *Biochem Soc Trans* **40:** 311-323

Kwak MK, Itoh K, Yamamoto M, Kensler TW (2002) Enhanced expression of the transcription factor Nrf2 by cancer chemopreventive agents: Role of antioxidant response element-like sequences in the nrf2 promoter. *Mol Cell Biol* **22:** 2883-2892

L'Episcopo F, Tirolo C, Testa N, Caniglia S, Morale MC, Impagnatiello F, Pluchino S, Marchetti B (2013) Aging-induced Nrf2-ARE pathway disruption in the subventricular zone drives neurogenic impairment in parkinsonian mice via PI3K-Wnt/beta-catenin dysregulation. *J Neurosci* **33:** 1462-1485

Lallemand-Breitenbach V, de Thé H (2010) PML Nuclear Bodies. *Cold Spring Harb Perspect Biol* **2:** a000661

Lau A, Tian W, Whitman SA, Zhang DD (2013) The Predicted Molecular Weight of Nrf2: It Is What It Is Not. *Antioxid Redox Signal* **18:** 91-93

Lee J, Kim MS (2007) The role of GSK3 in glucose homeostasis and the development of insulin resistance. *Diabetes Res Clin Pract* **77 Suppl 1:** S49-57

Lee JM, Calkins MJ, Chan K, Kan YW, Johnson JA (2003) Identification of the NF-E2-related factor-2-dependent genes conferring protection against oxidative stress in primary cortical astrocytes using oligonucleotide microarray analysis. *J Biol Chem* **278:** 12029-12038

Lee JM, Li J, Johnson DA, Stein TD, Kraft AD, Calkins MJ, Jakel RJ, Johnson JA (2005) Nrf2, a multi-organ protector? *FASEB J* **19:** 1061-1066

Lee JM, Shih AY, Murphy TH, Johnson JA (2003) NF-E2-related factor-2 mediates neuroprotection against mitochondrial complex I inhibitors and increased concentrations of intracellular calcium in primary cortical neurons. *FASEB J* **19:** 1066-1066

Lee RE, Walker SR, Savery K, Frank DA, Gaudet S (2014) Fold change of nuclear NF-kappaB determines TNF-induced transcription in single cells. *Mol Cell* **53:** 867-879

Li Q, Verma IM (2002) NF-kappaB regulation in the immune system. *Nat Rev Immunol* **2:** 725-734

Listwak SJ, Rathore P Fau - Herkenham M, Herkenham M (2013) Minimal NF-kappaB activity in neurons. *Neuroscience* **250:** 282-299

Liu C, Cui G, Zhu M, Kang X, Guo H (2014) Neuroinflammation in Alzheimer's disease: chemokines produced by astrocytes and chemokine receptors. *Int J Clin Exp Pathol* **7:** 8342-8355

Liu J, Lin A (2005) Role of JNK activation in apoptosis: A double-edged sword. *Cell Res* **15:** 36-42

Liu L, Chan C (2014) The role of inflammasome in Alzheimer's disease. *Ageing Res Rev* **15:** 6-15

Liu X, Zhang J, Li J, Volk A, Breslin P, Zhang J, Zhang Z (2014) The synergistic repressive effect of NF-kappaB and JNK inhibitor on the clonogenic capacity of Jurkat leukemia cells. *PLoS One* **9:** e115490

Losi G, Cammarota M, Carmignoto G (2012) The role of astroglia in the epileptic brain. *Front Pharmacol* **3:** 132

Lu CY, Yang YC, Li CC, Liu KL, Lii CK, Chen HW (2014) Andrographolide inhibits TNFalpha-induced ICAM-1 expression via suppression of NADPH oxidase activation and induction of HO-1 and GCLM expression through the PI3K/Akt/Nrf2 and PI3K/Akt/AP-1 pathways in human endothelial cells. *Biochem Pharmacol* **91:** 40-50

Lu X, Wang L, Yu C, Yu D, Yu G (2015) Histone Acetylation Modifiers in the Pathogenesis of Alzheimer's Disease. *Front Cell Neurosci* **9:** 226

Ludtmann MH, Angelova PR, Zhang Y, Abramov AY, Dinkova-Kostova AT (2013
) Nrf2 affects the efficiency of mitochondrial fatty acid oxidation. *Biochem J* **457:** 415-424

Malarkey EB, Parpura V (2008) Mechanisms of glutamate release from astrocytes. *Neurochem Int* **52:** 142-154

Malloy MT, McIntosh DJ, Walters TS, Flores A, Goodwin JS, Arinze IJ (2013) Trafficking of the transcription factor Nrf2 to promyelocytic leukemia-nuclear bodies: implications for degradation of NRF2 in the nucleus. *J Biol Chem* **288:** 14569-14583

Manea A, Manea SA, Gafencu AV, Raicu M (2007) Regulation of NADPH oxidase subunit p22(phox) by NF-kB in human aortic smooth muscle cells. *Arch Physiol Biochem* **113:** 163-172

Mata-Greenwood E, Cuendet M, Sher D, Gustin D, Stock W, Pezzuto JM (2002) Brusatol-mediated induction of leukemic cell differentiation and G(1)

arrest is associated with down-regulation of c-myc. *Leukemia* **16:** 2275-2284

Mauro C, Leow SC, Anso E, Rocha S, Thotakura AK, Tornatore L, Moretti M, De Smaele E, Beg AA, Tergaonkar V, Chandel NS, Franzoso G (2011) NF-kappaB controls energy homeostasis and metabolic adaptation by upregulating mitochondrial respiration. *Nat Cell Biol* **13:** 1272-1279

Meffert MK, Baltimore D (2005) Physiological functions for brain NF-kappaB. *Trends Neurosci* **28:** 37-43

Memet S (2006) NF-kappaB functions in the nervous system: from development to disease. *Biochem Pharmacol* **72:** 1180-1195

Mercado N, Thimmulappa R, Thomas CMR, Fenwick PS, Chana KK, Donnelly LE, Biswal S, Ito K, Barnes PJ (2011) Decreased histone deacetylase 2 impairs Nrf2 activation by oxidative stress. *Biochem Biophys Res Commun* **406:** 292-298

Mincheva-Tasheva S, Soler RM (2013) NF-kappaB signaling pathways: role in nervous system physiology and pathology. *Neuroscientist* **19:** 175-194

Mitsuishi Y, Motohashi H, Yamamoto M (2012) The Keap1-Nrf2 system in cancers: stress response and anabolic metabolism. *Front Oncol* **2:** 200

Mitsuishi Y, Taguchi K, Kawatani Y, Shibata T, Nukiwa T, Aburatani H, Yamamoto M, Motohashi H (2012
) Nrf2 Redirects Glucose and Glutamine into Anabolic Pathways in Metabolic Reprogramming. *Cancer Cell* **22:** 66-79

Morroni F, Tarozzi A, Sita G, Bolondi C, Zolezzi Moraga JM, Cantelli-Forti G, Hrelia P (2013) Neuroprotective effect of sulforaphane in 6-hydroxydopamine-lesioned mouse model of Parkinson's disease. *Neurotoxicology* **36:** 63-71

Nagashima S, Tokuyama T, Yonashiro R, Inatome R, Yanagi S (2014) Roles of mitochondrial ubiquitin ligase MITOL/MARCH5 in mitochondrial dynamics and diseases. *J Biochem* **155:** 273-279

Nakaso K, Yano H, Fukuhara Y, Takeshima T, Wada-Isoe K, Nakashima K (2003) PI3K is a key molecule in the Nrf2-mediated regulation of antioxidative proteins by hemin in human neuroblastoma cells. *FEBS Lett* **546:** 181-184

Nelson DE, Ihekwaba AE, Elliott M, Johnson JR, Gibney CA, Foreman BE, Nelson G, See V, Horton CA, Spiller DG, Edwards SW, McDowell HP, Unitt JF, Sullivan E, Grimley R, Benson N, Broomhead D, Kell DB, White MR (2004) Oscillations in NF-kappaB signaling control the dynamics of gene expression. *Science* **306:** 704-708

Neumann H, Schweigreiter R, Yamashita T, Rosenkranz K, Wekerle H, Barde YA (2002) Tumor necrosis factor inhibits neurite outgrowth and branching of hippocampal neurons by a rho-dependent mechanism. *J Neurosci* **22:** 854-862

Neymotin A, Calingasan NY, Wille E, Naseri N, Petri S, Damiano M, Liby KT, Risingsong R, Sporn M, Beal MF, Kiaei M (2011) Neuroprotective effect of Nrf2/ARE activators, CDDO ethylamide and CDDO trifluoroethylamide, in a mouse model of amyotrophic lateral sclerosis. *Free Radical Biol Med* **51:** 88-96

Nisole S, Maroui MA, Mascle XH, Aubry M, Chelbi-Alix MK (2013) Differential Roles of PML Isoforms. *Front Oncol* **3:** 125

Niture SK, Jain AK, Shelton PM, Jaiswal AK (2011) Src subfamily kinases regulate nuclear export and degradation of transcription factor Nrf2 to switch off Nrf2-mediated antioxidant activation of cytoprotective gene expression. *J Biol Chem* **286:** 28821-28832

O'Neill LAJ, Kaltschmidt C (1997) NF-kB: a crucial transcription factor for glial and neuronal cell function. *Trends Neurosci* **20:** 252-258

Oberheim NA, Takano T, Han X, He W, Lin JH, Wang F, Xu Q, Wyatt JD, Pilcher W, Ojemann JG, Ransom BR, Goldman SA, Nedergaard M (2009) Uniquely hominid features of adult human astrocytes. *J Neurosci* **29:** 3276-3287

Olayanju A, Copple IM, Bryan HK, Edge GT, Sison RL, Wong MW, Lai Z-Q, Lin Z-X, Dunn K, Sanderson CM, Alghanem AF, Cross MJ, Ellis EC, Ingelman-Sundberg M, Malik HZ, Kitteringham NR, Goldring CE, Park BK (2015) Brusatol provokes a rapid and transient inhibition of Nrf2 signaling and sensitizes mammalian cells to chemical toxicity—implications for therapeutic targeting of Nrf2. *Free Radical Biol Med* **78:** 202-212

Olesen J, Leonardi M (2003) The burden of brain diseases in Europe. *Eur J Neurol* **10:** 471-477

Pahl HL (1999) Activators and target genes of Rel/NF-kappaB transcription factors. *Oncogene* **18:** 6853-6866

Pajares M, Jimenez-Moreno N, Dias IH, Debelec B, Vucetic M, Fladmark KE, Basaga H, Ribaric S, Milisav I, Cuadrado A (2015) Redox control of protein degradation. *Redox Biol* **6:** 409-420

Papp D, Lenti K, Módos D, Fazekas D, Dúl Z, Türei D, Földvári-Nagy L, Nussinov R, Csermely P, Korcsmáros T (2012) The NRF2-related interactome and regulome contain multifunctional proteins and fine-tuned autoregulatory loops. *FEBS Lett* **586:** 1795-1802

Park SH, Park-Min KH, Chen J, Hu X, Ivashkiv LB (2011) Tumor necrosis factor induces GSK3 kinase-mediated cross-tolerance to endotoxin in macrophages. *Nat Immunol* **12:** 607-615

Paszek P, Ryan S, Ashall L, Sillitoe K-, Harper CV, Spiller DG, Rand DA, White MR (2010) Population robustness arising from cellular heterogeneity. *Proceedings of the National Academy of Sciences of the United States of America* **107:** 11644-11649

Pellerin L, Magistretti PJ (1994) Glutamate Uptake into Astrocytes Stimulates Aerobic Glycolysis - a Mechanism Coupling Neuronal-Activity to Glucose-Utilization. *Proceedings of the National Academy of Sciences of the United States of America* **91:** 10625-10629

Perkins ND, Gilmore TD (2006) Good cop, bad cop: the different faces of NF-[kappa]B. *Cell Death Differ* **13:** 759-772

Petri S, Korner S, Kiaei M (2012) Nrf2/ARE Signaling Pathway: Key Mediator in Oxidative Stress and Potential Therapeutic Target in ALS. *Neurol Res Int* **2012:** 878030

Pfrieger FW, Slezak M (2012) Genetic approaches to study glial cells in the rodent brain. *Glia* **60:** 681-701

Rada P, Rojo AI, Chowdhry S, McMahon M, Hayes JD, Cuadrado A (2011) SCF/{beta}-TrCP promotes glycogen synthase kinase 3-dependent degradation of the Nrf2 transcription factor in a Keap1-independent manner. *Mol Cell Biol* **31:** 1121-1133

Reddy NM, Kleeberger SR, Bream JH, Fallon PG, Kensler TW, Yamamoto M, Reddy SP (2008) Genetic disruption of the Nrf2 compromises cell-cycle progression by impairing GSH-induced redox signaling. *Oncogene* **27:** 5821-5832

Ren DM, Villeneuve NF, Jiang T, Wu TD, Lau A, Toppin HA, Zhang DD (2011) Brusatol enhances the efficacy of chemotherapy by inhibiting the Nrf2-mediated defense mechanism. *Proceedings of the National Academy of Sciences of the United States of America* **108:** 1433-1438

Rojo AI, Medina-Campos ON, Rada P, Zuniga-Toala A, Lopez-Gazcon A, Espada S, Pedraza-Chaverri J, Cuadrado A (2012) Signaling pathways activated by the phytochemical nordihydroguaiaretic acid contribute to a Keap1-independent regulation of Nrf2 stability: Role of glycogen synthase kinase-3. *Free Radical Biol Med* **52:** 473-487

Rojo AI, Rada P, Mendiola M, Ortega-Molina A, Wojdyla K, Rogowska-Wrzesinska A, Hardisson D, Serrano M, Cuadrado A (2014) The PTEN/NRF2

axis promotes human carcinogenesis. *Antioxid Redox Signal* **21:** 2498-2514

Ross JM, Oberg J, Brene S, Coppotelli G, Terzioglu M, Pernold K, Goiny M, Sitnikov R, Kehr J, Trifunovic A, Larsson N-G, Hoffer BJ, Olson L (2010) High brain lactate is a hallmark of aging and caused by a shift in the lactate dehydrogenase A/B ratio. *Proceedings of the National Academy of Sciences of the United States of America* **107:** 20087-20092

Rushworth SA, Bowles KM, MacEwan DJ (2011) High basal nuclear levels of Nrf2 in acute myeloid leukemia reduces sensitivity to proteasome inhibitors. *Cancer Res* **71:** 1999-2009

Rushworth SA, Zaitseva L, Murray MY, Shah NM, Bowles KM, MacEwan DJ (2012) The high Nrf2 expression in human acute myeloid leukemia is driven by NF-kappaB and underlies its chemo-resistance. *Blood* **120:** 5188-5198

Sakamoto K, Iwasaki K, Sugiyama H, Tsuji Y (2009) Role of the tumor suppressor PTEN in antioxidant responsive element-mediated transcription and associated histone modifications. *Mol Biol Cell* **20:** 1606-1617

Sakurai H, Suzuki S, Kawasaki N, Nakano H, Okazaki T, Chino A, Doi T, Saiki I (2003) Tumor necrosis factor-alpha-induced IKK phosphorylation of NF-kappaB p65 on serine 536 is mediated through the TRAF2, TRAF5, and TAK1 signaling pathway. *J Biol Chem* **278:** 36916-36923

Saleh A, Schapansky J, Smith DR, Young N, Odero GL, Aulston B, Fernyhough P, Glazner GW (2013) Normalization of NF-kappaB activity in dorsal root ganglia neurons cultured from diabetic rats reverses neuropathy-linked markers of cellular pathology. *Exp Neurol* **241:** 169-178

Scheller J, Chalaris A, Schmidt-Arras D, Rose-John S (2011) The pro- and anti-inflammatory properties of the cytokine interleukin-6. *Biochim Biophys Acta* **1813:** 878-888

Sen R, Baltimore D (1986) Inducibility of kappa immunoglobulin enhancer-binding protein Nf-kappa B by a posttranslational mechanism. *Cell* **47:** 921-928

Shen H, Nelson G, Nelson DE, Kennedy S, Spiller DG, Griffiths T, Paton N, Oliver SG, White MRH, Kell DB (2006) Automated tracking of gene expression in individual cells and cell compartments. *J R Soc Interface* **3:** 787-794

Sheng Y, Abreu IA, Cabelli DE, Maroney MJ, Miller A-F, Teixeira M, Valentine JS (2014) Superoxide Dismutases and Superoxide Reductases. *Chem Rev* **114:** 3854-3918

Slotta C, Müller J, Tran L, Hauser S, Widera D, Kaltschmidt B, Kaltschmidt C

(2014) An Investigation of the Specificity of Research Antibodies against NF-κB-subunit p65. *J Histochem Cytochem* **62:** 157-161

Smale ST (2011) Hierarchies of NF-κB target gene regulation. *Nat Immunol* **12:** 689-694

Smirnova NA, Haskew-Layton RE, Basso M, Hushpulian DM, Payappilly JB, Speer RE, Ahn YH, Rakhman I, Cole PA, Pinto JT, Ratan RR, Gazaryan IG (2011) Development of Neh2-Luciferase Reporter and Its Application for High Throughput Screening and Real-Time Monitoring of Nrf2 Activators. *Chem Biol* **18:** 752-765

Soares MP, Seldon MP, Gregoire IP, Vassilevskaia T, Berberat PO, Yu J, Tsui TY, Bach FH (2004) Heme oxygenase-1 modulates the expression of adhesion molecules associated with endothelial cell activation. *J Immunol* **172:** 3553-3563

Spiller DG, Wood CD, Rand DA, White MR (2010) Measurement of single-cell dynamics. *Nature* **465:** 736-745

Sporn MB, Liby KT (2012) NRF2 and cancer: the good, the bad and the importance of context. *Nat Rev Cancer* **12:** 564-571

Stepkowski TM, Kruszewski MK (2011) Molecular cross-talk between the NRF2/KEAP1 signaling pathway, autophagy, and apoptosis. *Free Radic Biol Med* **50**

Stobart JL, Anderson CM (2013) Multifunctional role of astrocytes as gatekeepers of neuronal energy supply. *Front Cell Neurosci* **7**

Suh JH, Shenvi SV, Dixon BM, Liu H, Jaiswal AK, Liu RM, Hagen TM (2004) Decline in transcriptional activity of Nrf2 causes age-related loss of glutathione synthesis, which is reversible with lipoic acid. *Proceedings of the National Academy of Sciences of the United States of America* **101:** 3381-3386

Sun Z, Chin YE, Zhang DD (2009) Acetylation of Nrf2 by p300/CBP Augments Promoter-Specific DNA Binding of Nrf2 during the Antioxidant Response. *Mol Cell Biol* **29:** 2658-2672

Sun Z, Wu TD, Zhao F, Lau A, Birch CM, Zhang DD (2011) KPNA6 (Importin alpha 7)-Mediated Nuclear Import of Keap1 Represses the Nrf2-Dependent Antioxidant Response. *Mol Cell Biol* **31:** 1800-1811

Sundararajan S, Jiang Q, Heneka M, Landreth G (2006) PPARγ as a therapeutic target in central nervous system diseases. *Neurochem Int* **49:** 136-144

Suzuki T, Takaya K, Shiraishi K, Kohno T, Kunitoh H, Tsuta K, Furuta K, Goto K, Hosoda F, Sakamoto H, Motohashi H, Yamamoto M (2013) Regulatory nexus of synthesis and degradation deciphers cellular Nrf2 expression levels. *Mol Cell Biol* **33:** 2402-2412

Suzuki T, Yamamoto M (2015) Molecular basis of the Keap1-Nrf2 system. *Free Radic Biol Med* **88:** 93-100

Taguchi K, Komatsu M, Ishii T, Unno M, Akaike T, Motohashi H, Yamamoto M (2012) Keap1 degradation by autophagy for the maintenance of redox homeostasis. *Proceedings of the National Academy of Sciences of the United States of America* **109:** 13561-13566

Takahashi S, Izawa Y, Suzuki N (2012) Astrogliopathy as a loss of astroglial protective function against glycoxidative stress under hyperglycemia. *Rinsho Shinkeigaku* **52:** 41-51

Tang T, Lin X, Yang H, Zhou L, Wang Z, Shan G, Guo Z (2010) Overexpression of antioxidant enzymes upregulates aryl hydrocarbon receptor expression via increased Sp1 DNA-binding activity. *Free Radic Biol Med* **49:** 487-492

Tanji K, Maruyama A, Odagiri S, Mori F, Itoh K, Kakita A, Takahashi H, Wakabayashi K (2013) Keap1 Is Localized in Neuronal and Glial Cytoplasmic Inclusions in Various Neurodegenerative Diseases. *J Neuropathol Exp Neurol* **72:** 18-28

Thimmulappa RK, Mai KH, Srisuma S, Kensler TW, Yamamoto M, Biswal S (2002) Identification of Nrf2-regulated genes induced by the chemopreventive agent sulforaphane by oligonucleotide microarray. *Cancer Res* **62:** 5196-5203

Tiscornia G, Singer O, Verma IM (2006) Production and purification of lentiviral vectors. *Nat Protocols* **1:** 241-245

Tsacopoulos M, Magistretti PJ (1996) Metabolic coupling between glia and neurons. *J Neurosci* **16:** 877-885

Tufekci KU, Civi Bayin E, Genc S, Genc K (2011) The Nrf2/ARE Pathway: A Promising Target to Counteract Mitochondrial Dysfunction in Parkinson's Disease. *Parkinsons Dis*

Turner DA, Paszek P, Woodcock DJ, Nelson DE, Horton CA, Wang Y, Spiller DG, Rand DA, White MRH, Harper CV (2010) Physiological levels of TNFalpha stimulation induce stochastic dynamics of NF-kappaB responses in single living cells. *J Cell Sci* **123:** 2834-2843

Vannini F, Kashfi K, Nath N (2015) The dual role of iNOS in cancer. *Redox*

Biol **6:** 334-343

Vargas MR, Johnson JA (2009) The Nrf2-ARE cytoprotective pathway in astrocytes. *Expert Rev Mol Med* **11:** e17

Wakabayashi N, Slocum SL, Skoko JJ, Shin S, Kensler TW (2010) When NRF2 talks, who's listening? *Antioxid Redox Signal* **13:** 1649-1663

Wang B, Zhu XL, Kim Y, Li J, Huang SY, Saleem S, Li RC, Xu Y, Dore S, Cao WS (2012) Histone deacetylase inhibition activates transcription factor Nrf2 and protects against cerebral ischemic damage. *Free Radical Biol Med* **52:** 928-936

Wang T, Takikawa Y, Sawara K, Yoshida Y, Suzuki K (2012) Negative regulation of human astrocytes by interferon (IFN) alpha in relation to growth inhibition and impaired glucose utilization. *Neurochem Res* **37:** 1898-1905

Wang XJ, Hayes JD, Higgins LG, Wolf' CR, Dinkova-Kostova AT (2010) Activation of the NRF2 Signaling Pathway by Copper-Mediated Redox Cycling of Para- and Ortho-Hydroquinones. *Chem Biol* **17:** 75-85

Wang XW, Tan NS, Ho B, Ding JL (2006) Evidence for the ancient origin of the NF-kappaB/IkappaB cascade: its archaic role in pathogen infection and immunity. *Proceedings of the National Academy of Sciences of the United States of America* **103:** 4204-4209

Wardyn JD, Ponsford AH, Sanderson CM (2015) Dissecting molecular cross-talk between Nrf2 and NF-κB response pathways. *Biochem Soc Trans* **43:** 621-626

Wertz IE, O'Rourke KM, Zhou H, Eby M, Aravind L, Seshagiri S, Wu P, Wiesmann C, Baker R, Boone DL, Ma A, Koonin EV, Dixit VM (2004) De-ubiquitination and ubiquitin ligase domains of A20 downregulate NF-kappaB signalling. *Nature* **430:** 694-699

Willingham W, Tobias Considine R, Chaney SG, Lee K-H, Hall IH (1984) Reversibility of protein synthesis inhibition by quassinoid antineoplastic agents in a rabbit reticulocyte system. *Biochem Pharmacol* **33:** 330-333

Willingham WJR, Stafford EA, Reynolds SH, Chaney SG, Lee KH, Okano M, Hall IH (1981) Mechanism of eukaryotic protein synthesis inhibition by brusatol. *Biochim Biophys Acta* **654:** 169-174

Winston JT, Strack P, Beer-Romero P, Chu CY, Elledge SJ, Harper JW (1999) The SCFbeta-TRCP-ubiquitin ligase complex associates specifically with phosphorylated destruction motifs in IkappaBalpha and beta-catenin and stimulates IkappaBalpha ubiquitination in vitro. *Genes Dev* **13:** 270-283

Winyard PG, Moody CJ, Jacob C (2005) Oxidative activation of antioxidant defence. *Trends Biochem Sci* **30:** 453-461

Wooten MW, Geetha T, Seibenhener ML, Babu JR, Diaz-Meco MT, Moscat J (2005) The p62 scaffold regulates nerve growth factor-induced NF-kappaB activation by influencing TRAF6 polyubiquitination. *J Biol Chem* **280:** 35625-35629

Wu KC, Cui JY, Klaassen CD (2011) Beneficial role of Nrf2 in regulating NADPH generation and consumption. *Toxicol Sci* **123:** 590-600

Xue M, Momiji H, Rabbani N, Barker G, Bretschneider T, Shmygol A, Rand DA, Thornalley PJ (2014) Frequency Modulated Translocational Oscillations of Nrf2 Mediate the Antioxidant Response Element Cytoprotective Transcriptional Response. *Antioxid Redox Signal* **23:** 613-629

Yu MA, Li H, Liu QM, Liu F, Tang LJ, Li CY, Yuan YZ, Zhan YQ, Xu WX, Li W, Chen H, Ge CH, Wang JA, Yang XM (2011) Nuclear factor p65 interacts with Keap1 to repress the Nrf2-ARE pathway. *Cell Signal* **23:** 883-892

Zambrano S, Bianchi ME, Agresti A (2014) High-Throughput Analysis of NF-κB Dynamics in Single Cells Reveals Basal Nuclear Localization of NF-κB and Spontaneous Activation of Oscillations. *PLoS One* **9:** e90104

Zhang JM, An J (2007) Cytokines, inflammation, and pain. *Int Anesthesiol Clin* **45:** 27-37

Zhang Y, Talalay P, Cho CG, Posner GH (1992) A major inducer of anticarcinogenic protective enzymes from broccoli: isolation and elucidation of structure. *Proceedings of the National Academy of Sciences of the United States of America* **89:** 2399-2403

Zhong H, May MJ, Jimi E, Ghosh S (2002) The Phosphorylation Status of Nuclear NF-KB Determines Its Association with CBP/p300 or HDAC-1. *Mol Cell* **9:** 625-636

Zhou L, Xu DY, Sha WG, Shen L, Lu GY, Yin X, Wang MJ (2015) High glucose induces renal tubular epithelial injury via Sirt1/NF-kappaB/microR-29/Keap1 signal pathway. *J Transl Med* **13:** 352

Zonta M, Angulo MC, Gobbo S, Rosengarten B, Hossmann KA, Pozzan T, Carmignoto G (2003) Neuron-to-astrocyte signaling is central to the dynamic control of brain microcirculation. *Nat Neurosc* **6:** 43-50

Supplementary Information

8. Supplementary Movies (attached)

8.1. List of Movies (avi. format)

(Open in QuickTime Player 7 or other compatible software)

Movie	Title
Movie 1a	Mixed Culture Astrocytes TNFα (EGFP-p65/GREEN)
Movie 1b	Mixed Culture Neurons TNFα (EGFP-p65/GREEN)
Movie 2	Pure Astrocytes TNFα (EGFP-p65/GREEN)
Movie 3a	5xκB-Venus in Neurons +TNFα (Mixed culture transduced eith tagRFP-P65/RED and 5xκB-Venus/GREEN)
Movie 4	Spontaneous p65 Oscillations in Mixed Culture (tagRFP-p65/RED and 5xκB-Venus/GREEN)
Movie 5a	Spontaneous Oscillations Mixed Culture (tagRFP-p65/RED and 5xκB-Venus/GREEN)
Movie 5b	Spontaneous Oscillations Mixed Culture 2 (tagRFP-p65/RED and 5xκB-Venus/GREEN)
Movie 6a	Spontaneous Oscillations Pure Astrocytes 5% Horse Serum (EGFP-p65/GREEN)
Movie 6b	Spontaneous Oscillations Pure Astrocytes Serum Free (EGFP-p65/GREEN)
Movie 7	Nuclear Envelope Breakdown, Nrf2 plasmid (mCherry-Nrf2/RED)
Movie 8	Nuclear Envelope Breakdown, Nrf2 plasmid (mCherry-Nrf2/RED)

Movie 9	Pure Astrocytes DMSO (2kb-Venus-Nrf2/GREEN)
Movie 10	Pure Astrocytes SFN Treatment (2kb-Venus-Nrf2/GREEN)
Movie 11	Pure Astrocytes CDDO-Me Treatment (2kb-Venus-Nrf2/GREEN)
Movie 12	Mixed Culture CDDO-Me (tagRFP-p65/RED and 2kb-Venus-Nrf2
Movie 13	$BAC^{Nrf2\text{-}Venus}$ MG132
Movie 14	$BAC^{Nrf2\text{-}Venus}$ SFN
Movie 15	$BAC^{Nrf2\text{-}Venus}$ CDDO-Me
Movie 16	$BAC^{Nrf2\text{-}Venus}$ Dividing Cells (Untreated)
Movie 17	$BAC^{Nrf2\text{-}Venus}$ TNFα
Movie 18	tagRFP-p65/$BAC^{Nrf2\text{-}Venus}$ with TNFα
Movie 19	$BAC^{Nrf2\text{-}Venus}$ p65dsRedXP with TNFα
Movie 20	$BAC^{Nrf2\text{-}Venus}$ p65dsRedXP TNFα and SFN
Movie 21	$BAC^{Nrf2\text{-}Venus}$ with IL-1β
Movie 22	tagRFP/$BAC^{Nrf2\text{-}Venus}$ siKeap1 with TNFα
Movie 23	tagRFP/$BAC^{Nrf2\text{-}Venus}$ siCTR with TNFα
Movie 24	$BAC^{Nrf2\text{-}Venus}$ and mCherry-Keap1(RED) with CDDO-Me
Movie 25	$BAC^{Nrf2\text{-}Venus}$ and mCherry-Keap1(RED) with CDDO-Me and LMB
Movie 26	pDendra2-Nrf2 Nuclear Import Control
Movie 27	pDendra2-Nrf2 expressing tagBFP-Keap1
Movie 28	pDendra-Nrf2 Nuclear Export CTR
Movie 29	pDendra-Nrf2 Nuclear Export after LMB
Movie 30	pDendra-Nrf2 with LMB
Movie 31a	$BAC^{Nrf2\text{-}Venus}$ siCTR with CHIR99021
Movie 31b	$BAC^{Nrf2\text{-}Venus}$ siKeap1 with CHIR99021
Movie 32	$BAC^{Nrf2\text{-}Venus}$ with LMB

Movie 33	$BAC^{Nrf2\text{-}Venus}$ with LMB and TNFα
Movie 34	$BAC^{Nrf2\text{-}Venus}$ with C646
Movie 35	$BAC^{Nrf2\text{-}Venus}$ C646 expressing mCherry-Keap1 (RED)
Movie 36	$BAC^{Nrf2\text{-}Venus}$ with Brusatol
Movie 37a	pDendra2-Nrf2 with DMSO
Movie 37b	pDendra2-Nrf2 with Brusatol
Movie 37c	pDendra2-Nrf2 with CHX
Movie 38a	pDendra2-Nrf2 with MG132
Movie 38b	pDendra2-Nrf2 with MG132 and CHX
Movie 38c	pDendra2-Nrf2 with MG132 and Brusatol
Movie 39	$BAC^{Nrf2\text{-}Venus}$ with CHX
Movie 40a	pDendra2-MARCH5 with DMSO
Movie 40b	pDendra2-MARCH5 with Brusatol
Movie 40c	pDendra2-MARCH5 with CHX

8.2. Viability Assays on BAC$^{Nrf2\text{-}Venus}$

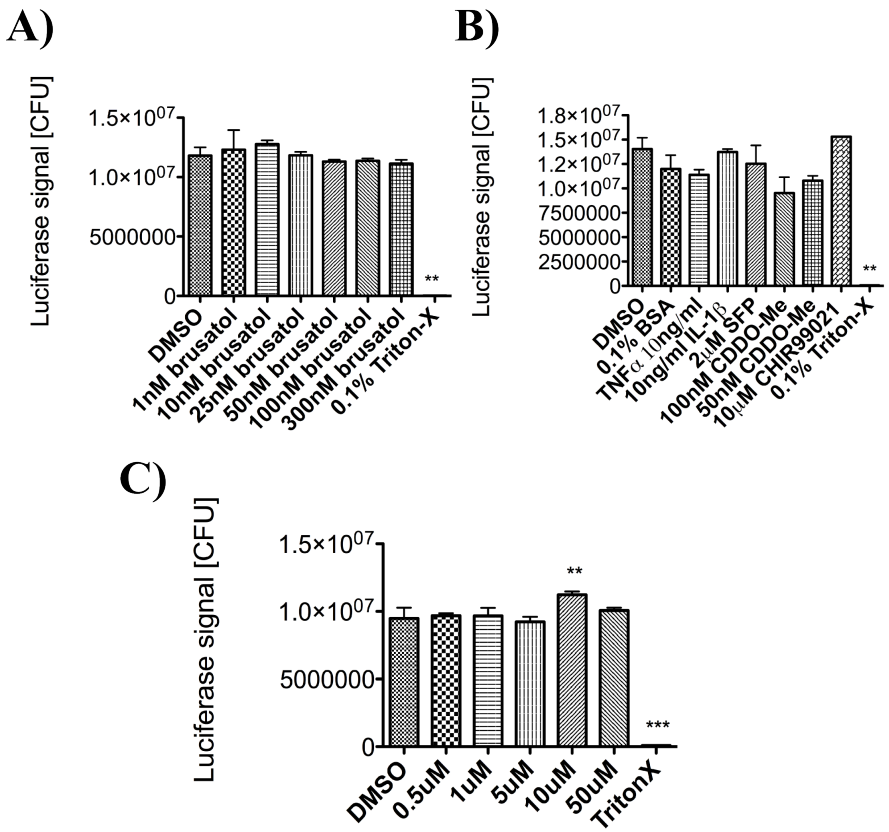

Figure 8.2 ATP-based viability assays on BAC$^{Nrf2\text{-}Venus}$ cells (Methods Section) in response to 8hr treatments of various compounds used throughout the project. A) Viability assay of various brusatol concentrations. B) Viability assay on drugs commonly used throughout the project. C) Viability assay following 24h treatment with various concentrations of C646. Error bars=STDEV

8.3. Vector Maps of Generated Constructs (Figure 8.3 and 8.4)

1. *2kb*-Venus-(ms)Nrf2
2. *UBC*-Venus-(ms)Nrf2
3. *UBC*-tagRFP-(hm)p65
4. *UBC*-tagRFP-(ms)p65
5. *GFAP*-Cyan
6. *GFAP*-LaminB1-Cyan
7. *5xkB*-Venus
8. pDendra2-(hm)Nrf2

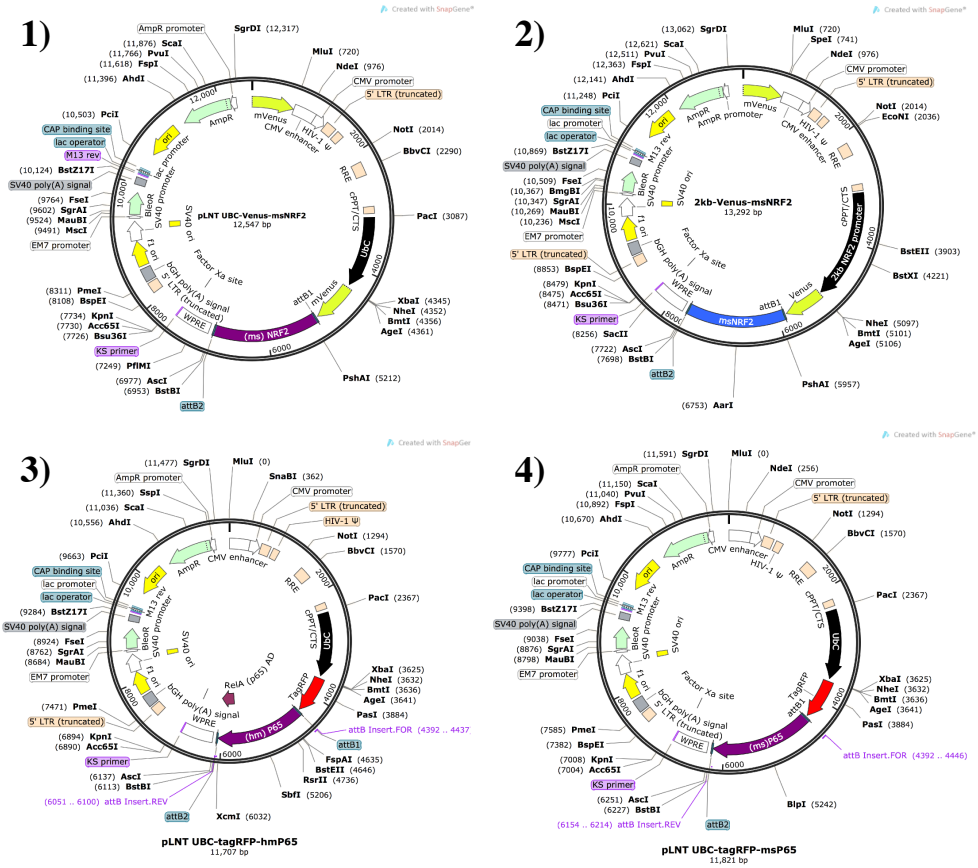

Figure 8.3 Vector maps of the lentiviral expression constructs.
1) *2kb*-Venus-(ms)Nrf2, **2)** *UBC*-Venus-(ms)Nrf2, **3)** *UBC*-tagRFP-(hm)p65, **4)** *UBC*-tagRFP-(ms)p65.

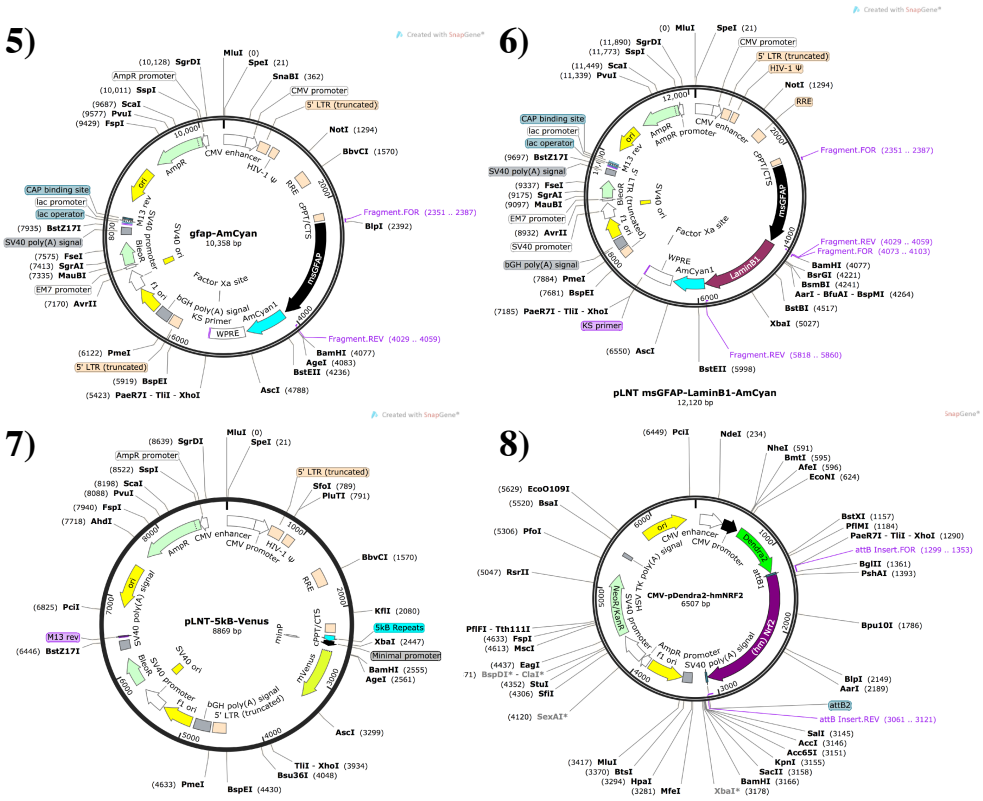

Figure 8.4 Vector maps of the lentiviral expression constructs. 5) *GFAP*-Cyan, 6) *GFAP*-LaminB1-Cyan, 7) *5xκB*-Venus, 8) pDendra2-(hm)Nrf2.

8.4. Quantification of Protein Levels from Western Blot Analysis

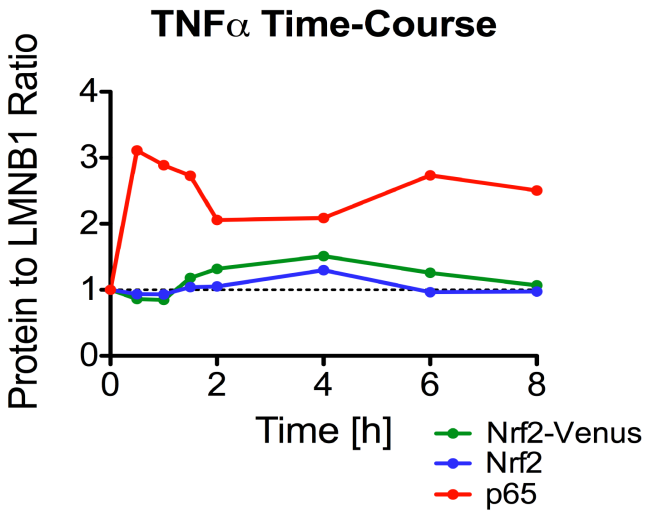

Figure 8.5 Quantification of Western Blot Figure 1 from Results Chapter 2